



# Beta/gamma-Peptide manifolds designed as alpha-helix mimetics

Claire Grison

## ► To cite this version:

Claire Grison. Beta/gamma-Peptide manifolds designed as alpha-helix mimetics. Organic chemistry. Université Paris Saclay (COMUE), 2015. English. NNT : 2015SACLS128 . tel-01527127

**HAL Id: tel-01527127**

**<https://theses.hal.science/tel-01527127>**

Submitted on 24 May 2017

**HAL** is a multi-disciplinary open access archive for the deposit and dissemination of scientific research documents, whether they are published or not. The documents may come from teaching and research institutions in France or abroad, or from public or private research centers.

L'archive ouverte pluridisciplinaire **HAL**, est destinée au dépôt et à la diffusion de documents scientifiques de niveau recherche, publiés ou non, émanant des établissements d'enseignement et de recherche français ou étrangers, des laboratoires publics ou privés.

NNT = 2015SACLS128

THESE DE DOCTORAT  
DE L'UNIVERSITE PARIS-SACLAY,  
préparée à l'Université Paris Sud

ÉCOLE DOCTORALE N° 571

Sciences chimiques : molécules, matériaux, instrumentation et biosystèmes

Spécialité de doctorat : Chimie

Par

**Claire M. Grison**

$\beta/\gamma$ -Peptide manifolds designed as  $\alpha$ -helix mimetics

**Thèse présentée et soutenue à Orsay, le 23 Novembre 2015 :**

**Composition du Jury :**

M. Merlet Denis	Professeur, Université Paris Sud	Président
M. Clayden Jonathan	Professeur, University of Bristol	Rapporteur
M. Wilson Andrew	Professeur, University of Leeds	Rapporteur
M. Martinez Jean	Professeur, Université de Montpellier	Examineur
M. Aitken David	Professeur, Université Paris Sud	Directeur de thèse
Mme Robin Sylvie	Maître de Conférence, Université Paris Sud	Encadrante









# Acknowledgements

First, I would like to thank Prof Andrew J. Wilson and Prof Jonathan Clayden to be reporters for my PhD thesis, and Prof Jean Martinez and Prof Denis Merlet to be members of my jury.

The biggest thank goes to my PhD supervisor, Prof David J. Aitken for believing in me in that famous skype interview in April 2012, for giving me the most challenging and best project ever!

I thank you for the fantastic work we have done together during these three years. Thank you for sharing your scientific passion with me during an uncountable number of fascinating discussions. Thank you for your precious guidances, your never-ending support and for always finding the time to help me, even when you do not have the time! Thank you for giving me the opportunity to represent the group in many congresses and for giving me the chance to develop other axes of my thesis. Thank you for all the apéros, the babercues, for teaching us Scottish dances among others and the discovery of new protic solvents!

I would like to thank sincerely Dr. Sylvie Robin for accepting to mentore me. Thank you for trusting me in the development of my thesis. Thank you for giving me the possibility of taking initiatives in the different approaches of my subject. Thank you for the encouragement and support throughout these three years.

A special thank goes to Prof Andrew J. Wilson for the opportunity to let me work as a member of your group. Thank you for your enthusiastic guidance and your support during this intense month!

Many thanks to Dr. Gilles Guichard for giving me the chance to work on cyclobutane ureas and welcoming me in your group.

Un grand merci à toute l'équipe de RMN pour leur aide précieuse et toujours sans faille. En particulier merci à José-Enrique Herbert-Pucheta et Denis Merlet pour leurs conseils indispensables en modélisation moléculaire (entres autres !), merci à Jonathan Farjon pour m'avoir permis de travailler sur cet incroyable 950 MHz (et de faire des carbones en 10 secondes). Un énorme merci à Jean-Pierre Baltaze pour avoir toujours su trouver pleins de créneaux, pour toujours être là à mon secours et pour m'avoir tant appris et aidé au cours de ces trois années.

Je tiens à remercier très chaleureusement tous les permanents de notre équipe, pour leurs qualités humaines, leur humour et tous ces bons moments que je n'oublierai pas! Merci à Marie-Christine et Isabelle pour essayer de nous rendre un peu plus verts; merci aux anciens, Jean et Luis, pour leurs conseils avisés (surtout ceux de Jean pour la sécurité !); en parlant de sécurité... un merci

tout particulier à Florence et Virginie pour améliorer notre quotidien au labo et à l'Institut; merci à Valérie pour tous ses conseils et son support informatique sans faille; merci à Sandrine pour son soutien, sa générosité et son enthousiasme; et enfin merci à Thomas pour sa gentillesse, sa grande implication dans l'équipe, sa bonne humeur toujours au rendez-vous et... biensûr son humour (je reste toujours ta première fan, fightung!) !!

Je remercie également les membres des autres équipes de l'Institut, en particulier toute l'équipe MSMT; merci à Antoine et Nicolas pour les bons moments partagés dans le labo 3! Un grand merci à mon ptit Rodolphe, Natasha, Terry et Vincent pour la bonne ambiance qu'ils apportent à cet Institut. Merci également à Didier pour sa générosité et son humour internationalement connu (à ceux qui les montent et à celles qui les descendent)! Et je remercie infiniment ma Paupau (mon doudou, mon poulpe, pllllll!) pour tous les délires, toutes les soirées et tous ces incroyables moments au labo et en dehors!

Un grand merci à Bastien (ma ptite Michelette), à Kévin (Mr. ICMMO), à Maxime et son cubi, à mon ptit roux P.A. pour illuminer nos soirées. Un merci tout particulier à mon incroyable Ольга, tu es mon кролик préféré. Я очень рада, что тебя встретила et cette fois-ci je peux te dire ça sans que tu me dises : mais non c'est moi!!!!.

Света, Саша, Ліна, Діма, Мороз, Катя, Пилипко і Руслан, Я дуже рада, що Андрій нас познайомив і дуже дякую за ці круті три роки. І ще, дякую, що ви говорили зі мною французькою, а не так як хлопці! Я вас обожнюю!!!

Je porterais une mention toute spéciale pour tous les étudiants de notre équipe du LSOM puis du CP3A. Un grand merci aux anciennes, Amandine pour m'avoir montré le chemin, tu as été un véritable modèle, et Hawraà pour ton soutien, toutes nos discussions, ton ouverture d'esprit et ta bonne humeur.

Merci à mes trois graçons préférés, Flo, Rémy et Mathieu! Je suis très heureuse d'avoir partagé ces trois années intenses avec vous. Merci pour tous nos délires, tous ces incroyables moments, et tout votre amour ! Merci à mon parasite paki pour avoir apporté ton entrain naturel, ta bonne humeur débordante et ta "connerie" toujours prête à sortir pour nous faire rire ! Cette année à tes côtés est passée beaucoup trop vite, je n'ai pas eu le temps de me venger de toutes tes bêtises ! Je te souhaite plein de courage pour la fin de ta thèse et n'oublie pas qu'on sera là pour te mettre la misère. Merci à Kikette pour avoir partagé ce labo 3 avec moi et tous les potins qui vont avec ! On a vraiment bien ri, fait beaucoup de batailles d'eau (Thomas, on t'aura un jour !), bien redécoré notre labo, mais aussi beaucoup mais beaucoup discuté, euh pardon travaillé aussi... Merci pour ta gentillesse démesurée et d'avoir été mon confident pendant ces deux ans. Enfin merci à mon ptit Flo, pour toute ta générosité, pour ton soutien sans faille durant toutes ses heures passées au labo, pour ton aide jusqu'au bout de la

nuît, pour toutes ces conversations skype, pour tous ces nombreux trajets à refaire le monde, pour toutes ces soirées magiques auxquelles tu as toujours été présents, et ces fameux tours de l'ICMMO!

Je tiens à remercier très sincèrement mes gros Вонючки d'amour, Mariia et Geoffrey. Merci pour tout votre soutien, tous ces incroyables moments, en Normandie, à Nantes, au Luxembourg, à Kiev, à Lviv (surtout à Lviv...!), et en Breizh (vive la pizza requin !), et en avant pour de nouvelles aventures (je suis désolée d'avance pour ta cave Geoffroy) ! Наталя і Василь, дякую вам за моральну підтримку і за чудові дні проведені в Україні.

J'aimerais remercier mes deux coupines, mes meilleures amies, mes BFF, ma Tif Touf et mon Hélène d'amour ainsi que leurs copains extraordinaires Amotrou et Barrychéri. Cela fait maintenant six ans que nous nous sommes rencontrées et on a vécu tellement de moments inoubliables toutes les trois, pendant nos années complètement folles à l'INSA (dans les magnifiques bâtiments roses des R5 et R6, les projets de fous, les cours d'Uri, les booms, les potins, notre chef-d'oeuvre "sausages to the slaughter" (j'en ris encore en écrivant), vos deux pieds !!, Linköping, Lund et notre nuit mémorable à Kopenhagen, les virées nocturnes à Lyon, les férias et notre tour d'Irlande) et celles qui suivent (à Nantes, aux férias encore et toujours, à Wrexham et Chester, dans les Lofoten, à Malaga, au fin fond de l'Ecosse, à Paris et Leeds). Merci pour ces magnifiques aventures qui ne font que commencer !

Enfin je souhaiterais remercier cette fameuse boule de neige qui a changée ma vie. Дякую мій Андрій від усього серця за незмінну підтримку, твої позитивізм, твою радість до життя, твої любові і найбільший твої красивим акцентом можна. твоя посмішка висвітлює моє життя. Я тебе кохаю!

Pour terminer, je ne remercierais jamais assez ma Maman pour m'avoir donné tout son amour, pour m'avoir tout appris, pour avoir toujours cru en moi, et surtout pour m'avoir supportée (dans tous les sens du terme !) pendant ces vingt-cinq ans. Merci de m'avoir donné le goût de la chimie organique bien malgré toi, mais en même temps me faire changer des tubes de chromatographie à cinq ans, il fallait s'y attendre ! Sans toi je n'y serai jamais arrivée. Simplement merci !



# TABLE OF CONTENTS

<b>TABLE OF CONTENTS.....</b>	<b>8</b>
<b>PART I. INTRODUCTION.....</b>	<b>1</b>
<b>1. The <math>\alpha</math>-helix in native proteins .....</b>	<b>3</b>
1.1 The four-step structural organisation in proteins .....	3
1.2 Different types of helix in proteins .....	3
1.3 The $\alpha$ -helix - a bioactive region of proteins .....	6
1.3.1. The p53/hDM2 interaction.....	7
1.3.2. The Bcl-2 family interactions.....	8
1.3.1. The co-activator/estrogen receptor interaction.....	10
<b>2. Mimetics of the <math>\alpha</math>-helix - State of the art.....</b>	<b>11</b>
2.1 Enhanced stabilisation of native $\alpha$ -helices.....	12
2.1.1. Helix-breaking and helix-promoting natural amino acids.....	12
2.1.1. N-terminal and C-terminal capping residues .....	12
2.1.2. Stabilisation by weak interactions between the side chains of natural amino acids .....	13
2.1.2.1. Hydrogen bonds .....	13
2.1.2.2. Salt bridges .....	13
2.1.2.3. Cation- $\pi$ and $\pi$ - $\pi$ interactions .....	14
2.1.2.4. Metal ion chelation.....	14
2.2 Type II mimetics.....	15
2.3 Type III mimetics.....	18
2.3.1. Pioneering work.....	18
2.3.1.1. Indane scaffold.....	18
2.3.1.2. Terphenyl derivatives.....	19
2.3.2. Hydrophilic backbones.....	20
2.3.3. Oligoarylamide derivatives .....	22
2.3.4. Multifacial mimicries.....	25
2.3.5. Polysaccharides as $\alpha$ -helix mimetics.....	26
2.4 Type I mimetics .....	27
2.4.1. Stabilisation of $\alpha$ -helical structure with unnatural amino acids.....	28
2.4.1.1. Related unnatural $\alpha$ -amino acids bearing alkyl side-chains.....	28
2.4.1.2. $\alpha,\alpha$ -Disubstituted $\alpha$ -amino acids .....	28
2.4.1.3. $\alpha$ -Helix initiators.....	29
2.4.2. Stabilisation of $\alpha$ -helical structure through covalent interaction: stapled peptides.....	31
2.4.2.1. Disulfide bridges .....	31
2.4.2.2. Lactam bridges.....	32

2.4.2.3. Hydrocarbon stapling .....	33
2.4.2.4. Hydrogen Bond Surrogate .....	34
2.4.2.5. Photocontrolled helicity .....	35
2.4.2.6. Porphyrin-peptide conjugate .....	36
2.4.3. Use of non-helical peptides.....	37
2.5 Use of helical peptide foldamers as $\alpha$ -helix mimetics .....	38
2.5.1. $\beta$ -Peptides .....	39
2.5.1.1. Helical diversity adopted by $\beta$ -peptides .....	39
2.5.1.2. Helical $\beta$ -peptides mimicking the $\alpha$ -helix .....	45
2.5.2. $\gamma$ -Peptides.....	48
2.5.2.1. Helical diversity adopted by $\gamma$ -peptides.....	48
2.5.2.2. Applications of helical $\gamma$ -peptides .....	51
2.5.3. Hybrid $\alpha/\beta$ -peptides .....	53
2.5.3.1. Helical diversity adopted by $\alpha/\beta$ -peptides.....	53
2.5.3.2. Applications of $\alpha/\beta$ -peptides mimicking the $\alpha$ -helix.....	55
2.5.4. Hybrid $\alpha/\gamma$ -peptides.....	56
2.5.5. Hybrid $\beta/\gamma$ -peptides .....	59
<b>3. Aim of this project – <i>trans</i>-ACBC-based <math>\beta/\gamma</math>-peptide manifolds as <math>\alpha</math>-helix mimetics.....</b>	<b>63</b>
<b>PART II. RESULTS AND DISCUSSION.....</b>	<b>65</b>
<b>1. Synthesis and structural studies of <math>\beta/\gamma</math>-peptides alternating <i>trans</i>-ACBC and GABA: a robust 9/8-ribbon.....</b>	<b>67</b>
1.1 The constrained $\beta$ -amino acid <i>trans</i> -ACBC.....	67
1.1.1. Presentation of ACBC .....	67
1.1.2. Synthesis of <i>trans</i> -ACBC in enantiomerically pure form .....	69
1.2 Synthesis of peptides alternating <i>trans</i> -ACBC and GABA [9]-[14] .....	71
1.2.1. Linear synthesis of peptides with <i>trans</i> -ACBC as the N-terminal residue [9]-[11] .....	72
1.2.1.1. Activation of <i>trans</i> -ACBC and synthesis of Boc-AG-OBn [9].....	72
1.2.1.2. When 2+2 = 3.....	73
1.2.1.3. Synthesis of peptides [10] and [11] .....	75
1.2.2. Convergent synthesis of peptides with GABA as the N-terminal residue [12]-[14].....	77
1.3 Structural analyses of the peptides in solution-state.....	78
1.3.1. General procedures for solution-state structural analyses .....	78
1.3.2. Complete characterisation in chloroform .....	80
1.3.2.1. Titration of DMSO- $d_6$ by 1D $^1H$ NMR.....	80
1.3.2.2. ROESY experiments by 2D $^1H$ - $^1H$ NMR.....	81
1.3.2.3. Infrared studies .....	83
1.3.2.4. Molecular modelling.....	84
1.3.2.5. Partial characterisation in protic solvent.....	91

1.3.2.6. Conclusion.....	93
<b>2. Synthesis and structural studies of <math>\beta/\gamma</math>-peptides alternating <i>trans</i>-ACBC and <math>\gamma^4</math>-amino acids: a robust 13-helix .....</b>	<b>95</b>
2.1 Peptide selection.....	95
2.2 Synthesis of $\beta/\gamma$ -peptides alternating <i>trans</i> -ACBC and $\gamma^4$ -amino acids [23]-[34] .....	96
2.2.1. Synthesis of peptides with $\gamma^4$ -amino acids at the N-terminal [23]-[28].....	96
2.2.2. Synthesis of peptides with <i>trans</i> -ACBC at the N-terminal [29]-[34] .....	100
2.3 Structural studies and molecular modelling of the peptides.....	104
2.3.1. Titration of DMSO- $d_6$ by 1D $^1H$ NMR .....	104
2.3.2. 2D $^1H$ - $^1H$ ROESY experiments and characteristic ROEs.....	105
2.3.3. Infrared studies .....	113
2.3.4. Molecular Modelling .....	114
2.3.4.1. Hybrid Monte Carlo Multiple Minima calculations .....	114
2.3.4.2. DFT optimization: Gibbs energy and Boltzmann distribution .....	116
2.3.5. Circular Dichroism .....	118
2.4 Conclusion .....	121
<b>3. Design of inhibitors of <math>\alpha</math>-helix-mediated PPIs containing <i>trans</i>-ACBC and <math>\gamma^4</math>-amino acids .....</b>	<b>122</b>
3.1 $\alpha/\beta/\gamma$ -Peptides designed as the helical segment (19-26) of p53 mimetics.....	122
3.2 Synthesis of the designed $\alpha/\beta/\gamma$ -peptides.....	127
3.2.1. Synthesis of $\alpha/\beta/\gamma$ -peptides bearing $\gamma^4$ -hTrp [42], [43], [46], [47] .....	127
3.2.2. Synthesis of $\alpha/\beta/\gamma$ -peptides bearing $\gamma^4$ -hPhe [44], [45], [48], [49] .....	130
3.3 Structural studies of the $\alpha/\beta/\gamma$ -peptides .....	132
3.3.1. DMSO- $d_6$ titration .....	132
3.3.2. 2D $^1H$ - $^1H$ ROESY experiments .....	133
3.3.1. Infrared analysis.....	135
3.3.2. Circular Dichroism .....	136
3.4 Biophysical analyses of the $\alpha/\beta/\gamma$ -peptides proposed as $\alpha$ -helix mimetics.....	137
3.4.1. Proteolytic studies.....	137
3.4.2. Fluorescence anisotropy (FA) competition assays for inhibition of PPIs .....	141
3.4.2.1. Presentation of the technique .....	141
3.4.2.2. FA directed against p53/hDM2 interaction .....	142
3.4.2.3. Test of selectivity: FA directed against Bak/Bcl- $x_L$ and NOXA B/Mcl-1 interactions.....	144
3.4.3. $^1H$ - $^{15}N$ HSQC NMR study of the $\alpha$ -helix p53 mimetics in complex with hDM2 .....	145
3.5 Conclusion .....	148
<b>CONCLUSION .....</b>	<b>151</b>
<b>PART III. EXPERIMENTAL PART .....</b>	<b>153</b>

<b>1. Synthesis of <i>trans</i>-ACBC.....</b>	<b>156</b>
<b>2. Synthesis of peptides .....</b>	<b>162</b>
2.1 Peptides alternating (1 <i>R</i> ,2 <i>R</i> )-ACBC and GABA .....	163
2.2 Peptides alternating (1 <i>S</i> ,2 <i>S</i> )-ACBC and ( <i>R</i> )- $\gamma^4$ -homologous amino acids.....	173
2.3 Peptides containing (1 <i>S</i> ,2 <i>S</i> )-ACBC, ( <i>R</i> )- $\gamma^4$ -homologous amino acids and $\alpha$ -amino acids .....	195
<b>3. Biological assays .....</b>	<b>211</b>
3.1 Protein expression .....	211
3.2 Fluorescence anisotropy .....	212
3.3 Proteolytic studies .....	213
3.4 $^1\text{H}$ - $^{15}\text{N}$ HSQC studies .....	213
<b>BIBLIOGRAPHY .....</b>	<b>217</b>
<b>RESUME SUBSTANTIEL EN FRANÇAIS .....</b>	<b>232</b>





# **PART I. INTRODUCTION**



## **1. The $\alpha$ -helix in native proteins**

### **1.1 The four-step structural organisation in proteins**

The breadth of structure and function displayed by the molecules of biology is remarkable. There are four classes of biomolecules: proteins, lipids, carbohydrates and ribonucleic acids. Most of the interesting functions carried out by biomacromolecules within living organism, such as molecular recognition, molecular transport and catalysis of metabolic reactions, are performed by proteins.

The structure of proteins can be divided in four classes. Proteins are composed of L-amino acids linked to each other through amide bonds in a specific order that constitutes their primary structures. Certain parts of the sequence of amino acids are organised in secondary structures: helices, strands and loops. Other parts may be not organised and form random coils. Because of the spatial proximity of specific amino acids due to the secondary structures, proteins can fold into tertiary structures stabilised by hydrophobic interactions, salt bridges, hydrogen bonds and disulphide bonds. The tertiary structures of proteins can be spontaneously formed in the native state or can be induced by chaperones. Quaternary structures can be observed for some proteins when they interact with other proteins forming a multi-subunit complex.

### **1.2 Different types of helix in proteins**

In natural proteins, helices are formed by the repeated display of particular backbone dihedral angles  $\phi$  and  $\psi$ . The dihedral angle  $\phi$  is defined by the plane formed by the four atoms  $\text{CO}(i-1)$ – $\text{N}(i)$ – $\text{C}\alpha(i)$ – $\text{CO}(i)$  and  $\psi$  is defined by the plane formed by the four atoms  $\text{N}(i)$ – $\text{C}\alpha(i)$ – $\text{CO}(i)$ – $\text{N}(i+1)$ . Helices are the most common secondary structures found in globular proteins.<sup>1</sup> A helix is characterised by the number of atoms per turn ( $n$ ) and by the number of residues per turn ( $p$ ); and it is called a  $p(n)$ -helix. Different pairs of dihedral angles, which promote three types of helices, are conformationally accessible, as illustrated on a Ramachandran plot (see Figure 1).

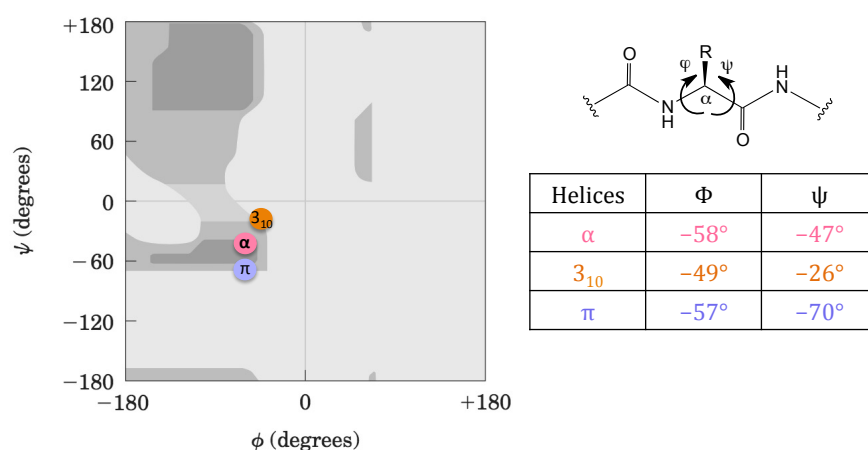


Figure 1. Theoretical Ramachandran plot for all residues (except glycine) with accessible dihedral angles (in dark grey)<sup>2</sup> promoting the different types of helices (points) in proteins.

The three types of helix (see Figure 2) are populated differently in proteins:<sup>1,2</sup>

- the right-handed  $\alpha$ -helix or 3.6(13)-helix was first characterised by the Branson group in 1951.<sup>3</sup> It is the most abundant helix in proteins, accounting for over one-third of all residues (32-38%).
- the  $3_{10}$ -helix or 3.0(10)-helix is rare in proteins; 3.4% of all residues are involved in  $3_{10}$ -helices. They are very short helices: 96% of  $3_{10}$ -helices contain no more than 4 residues.  $\alpha$ -Helices sometimes begin or end with a single turn of a  $3_{10}$ -helix.
- the  $\pi$ -helix or 4.4(16)-helix is an extremely rare secondary structure. The existence of this type of helix remained a hypothesis for a long time, but it was recently discovered at the ends of certain  $\alpha$ -helices.<sup>4</sup>

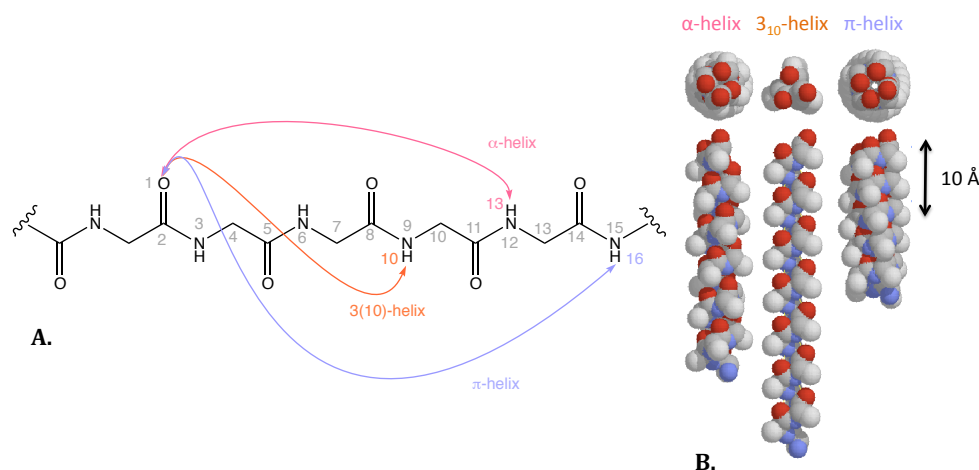


Figure 2. A: Hydrogen bonds which are at the basis of the three types of helix. B: Side and top views of the three helical models.

Other types of helices were predicted: a left-handed  $\alpha$ -helix composed of L-amino acids and 2.2(7), 4.3(14) and 4.4(16)-helices.<sup>5</sup> However, they have never been observed in proteins.

The abundance of the  $\alpha$ -helix compared to the other helices can be rationalised as follows:<sup>6</sup>

- the  $\phi$  and  $\psi$  angles lie in the centre of a minimum energy region of the Ramachandran plot (see the dark grey region in Figure 1).
- the hydrogen-bonding backbone atoms, carbonyl and amines, are in near perfect alignment.
- the radius of the helix allows favourable and stabilising van der Waals interactions of the main-chain atoms with each other and with the side-chain atoms.
- side chains are well staggered, thus minimizing steric interference.

These features make the  $\alpha$ -helix the lowest energy conformer among all predicted or observed helices.

As its name indicates, the  $\alpha$ -helix or 3.6(13)-helix completes one rotation per 3.6 residues; each residue has ideal backbone dihedral angles of  $\phi = -58^\circ$  and  $\psi = -47^\circ$  (see Figure 3 C).<sup>1</sup> The helix has a rise of 5.4 Å per turn (see Figure 3 B). The backbone of the helix is primarily stabilised by a network of hydrogen bonds between the carbonyl oxygen of residue  $i$  and the amide hydrogen of residue  $i+4$ . The hydrogen bond network is comprised of a series of 13 membered-hydrogen bonded rings (see Figure 3 D). For this reason the  **$\alpha$ -helix** can be classified as a **13-helix**. The amides are all oriented in the same direction leading to a macro-dipole along the  $\alpha$ -helix axis (see Figure 3 A). The positive end of the dipole is located at the N-terminus and the negative end at the C-terminus.

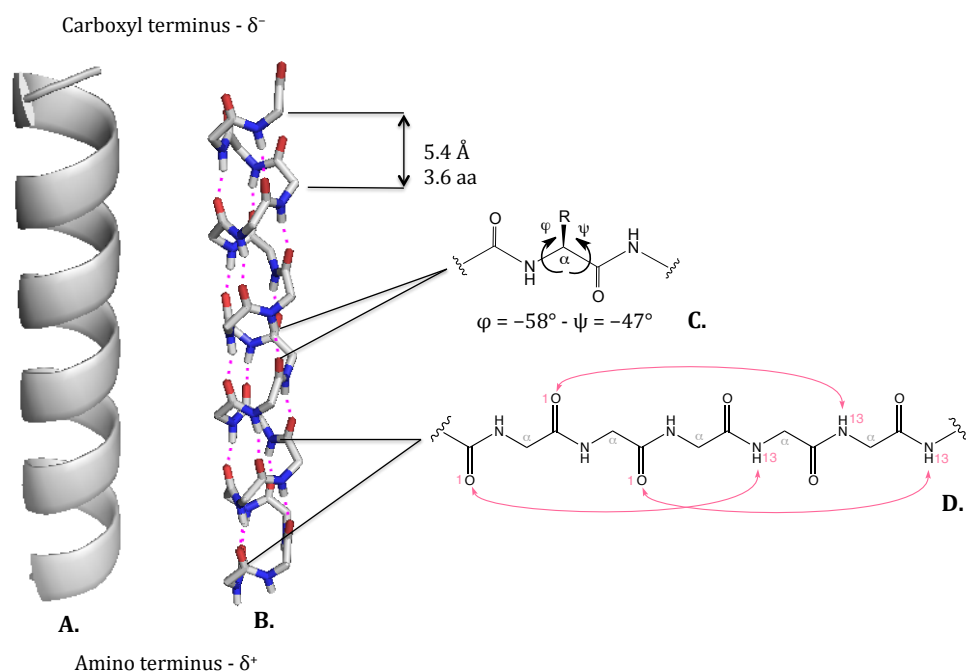


Figure 3. A: Ribbon diagram representing  $\alpha$ -helix. B: Backbone with hydrogen-bonding network (in pink) of an  $\alpha$ -helix. C: Amide backbone showing the dihedral angles. D: 13-Membered hydrogen-bonded rings (in pink).

The  $\alpha$ -helix places its amino acid side-chains along its surface on three distinct faces, as is illustrated in Figure 4 A and B. The accurate position of the side-chains are crucial to assure the  $\alpha$ -helix function. The cartoon of Figure 4 C representing the top view of the  $\alpha$ -helix will serve in this manuscript to illustrate the three faces mimicked by the  $\alpha$ -helix mimetics considered during this work.

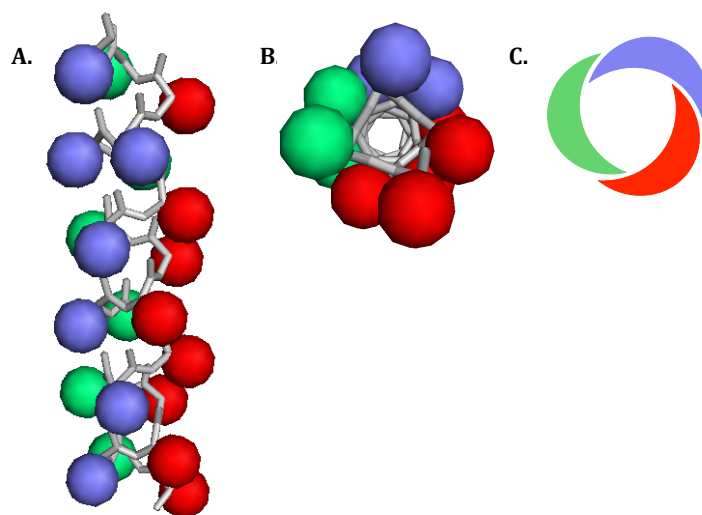


Figure 4. A: Side view of an  $\alpha$ -helix where side chains are displayed by spheres. B: Top view of an  $\alpha$ -helix where side chains are displayed by spheres. C: Top view of an  $\alpha$ -helix with a cartoon representation showing the three faces.

### 1.3 The $\alpha$ -helix - a bioactive region of proteins

The structure of the  $\alpha$ -helix plays a prevalent role in structural biology making it a central topic of interest.

When buried in the hydrophobic core of a protein, the  $\alpha$ -helix plays a **structural role** and serves to stabilise the tertiary structure.

However, when exposed or partially exposed on the surface of proteins,  $\alpha$ -helices play **critical roles in protein interactions** with other biological molecules. A binding process with a biomolecule directly occurs through three to four key side-chain residues, that are called the **hot-spot residues**, located along one face of the helix in 60% of cases.<sup>7</sup> When displayed on one face of the helix, they correspond to the residues at the  $i$ ,  $i+4$ ,  $i+7$  and often  $i+11$  positions in the peptide sequence. The side-chains displayed by the other faces interact with the solvent or/and even with the target. These residues of apparently little significance to binding affinity show changes in enthalpy and entropy of association upon mutation.<sup>8</sup> They have properties like hydrophilicity, hydrophobicity, electrostatic or ionic charges and can favour the interaction by orienting the  $\alpha$ -helix or stabilising the binding complex.

$\alpha$ -Helices are found to mediate many protein-peptide, protein-protein, protein-DNA, protein-RNA and protein-membrane interactions.<sup>9</sup> Examples of such interactions that have been considered in this thesis are given in Table 1.

Table 1. Examples of proteins displaying bioactive  $\alpha$ -helices

Name	Function	Target	Receptor nature
p53	Transcription factor	Promoter of gene encoding for p53	DNA
<i>hDM2</i>	Apoptosis regulator	p53	protein
NOXA B	Cell differentiation	Mcl-1	protein
Bak	Apoptosis regulator	Bcl-x <sub>L</sub>	protein

In addition to being bioactive regions of proteins,  $\alpha$ -helices can be implicated in other biological activities such as antibiotics or drug vectors.

More than 400 amphiphilic helical  $\alpha$ -peptides were reported to have antimicrobial properties<sup>10</sup> and to target and kill cancer cells.<sup>11</sup> Their mechanism of action is still not fully clear at the physicochemical and molecular level but helical  $\alpha$ -peptides appeared to be able to disrupt the cell membrane by various models: disordered toroidal pore model, aggregate model and carpet model.

The cellular internalisation of drugs still remains the main limitation for their clinical use. Several peptide families were identified to possess the ability to cross the cell membranes. These peptides are called CPPs for Cell Penetrating Peptides. The  $\alpha$ -helical conformation of CPPs was found to play a major role in stabilising their interactions with membranes and promoting their cellular uptake which allowed the delivery of various cargoes into the cytoplasm or even the nucleus.<sup>12</sup>

### 1.3.1. The p53/*hDM2* interaction

p53 ('p' for protein and '53' for the apparent molecular weight of 53 kDa) is a transcription factor that targets the transcriptional activity of a large number of genes.

When a cell is stressed, p53 is activated by a kinase transducing stress signal that phosphorylates its N-terminal domain. It becomes able to recruit DNA repair proteins when DNA has sustained damages. In that case, p53 is also able to arrest the cell cycle allowing DNA repair proteins to fix the damage. However, when the damage proves to be irreparable, p53 can initiate apoptosis to eliminate the damaged cell from the replicative pool.<sup>13</sup>

In unstressed cells, the pool of p53 is maintained low through a continuous degradation mediated by the human double minute 2 protein (*hDM2*). *hDM2* binds to the transactivation domain near the N-terminus of p53. The protein-protein interaction (PPI) between a fragment of p53 and the murine analogue of *hDM2*, *mDM2*, has been mapped (see Figure 5). The N-terminus of p53 forms an amphipathic helix (19-26 aa) in which three residues are crucial for the PPI: Phe 19 (*i*), Trp 23 (*i+4*) and Leu 26 (*i+7*). The side chains of these three hot-spot residues lie on a hydrophobic side and are nestled into a deep hydrophobic pocket formed by two  $\alpha$ -helices on the *mDM2* surface.<sup>14</sup> The hydrophobic contacts are augmented by only two hydrogen bonds: one between the Phe 19



carboxamide hydrogen of p53 and the carbonyl of the Gln 72 side chain of *mDM2*, and another between the Trp 23 indole NH of p53 and the Leu 54 carbonyl of *mDM2*.<sup>15</sup>

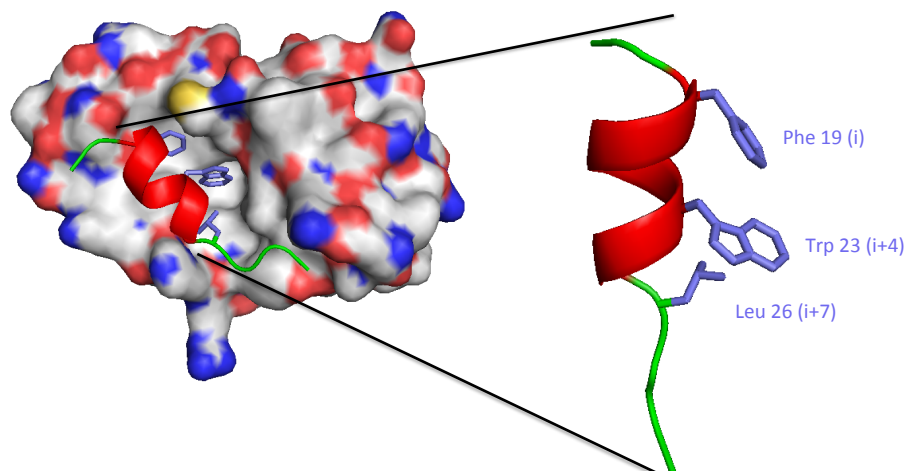


Figure 5. *p53/mDM2* interaction (PDB ID: 1YCR)<sup>16</sup> showing the key residues of p53.

The interaction between p53 and *hDM2* prevents the transcriptional activity of p53 by blocking its fixation to DNA. More importantly, when bound to p53, *hDM2* acts as a E3 ligase that ubiquitinates and transports p53 from the nucleus to the cytosol for degradation by the 26S proteasome.<sup>15,17</sup>

Overexpression of *hDM2* inhibits activation of the p53 pathway, leading to uncontrolled cell proliferation and tumour development.

Therefore, disruption of the deleterious interaction between p53 and *hDM2* by drugs should release transcriptionally active p53, which could recover its 'guardian of genome' activity.

### 1.3.2. The Bcl-2 family interactions

The Bcl-2 (B cell lymphoma 2) proteins play a critical role in the regulation of apoptosis. The Bcl-2 proteins are divided in two groups: the pro-apoptosis (Bax, Bak, Bad and Bid) the anti-apoptosis (Bcl-2 and Bcl-x<sub>L</sub>) subfamilies. Structural studies on several Bcl-2 family proteins showed a common overall fold, in which the anti-apoptotic proteins have a hydrophobic groove acting as a binding site for  $\alpha$ -helical regions on pro-apoptotic proteins.

Mcl-1 (induced myeloid leukemia cell differentiation protein) binds to the BH3-only pro-apoptotic protein NOXA B. A crystal structure between the long  $\alpha$ -helical peptide of NOXA B and Mcl-1 has been solved (see Figure 6). This interaction is mediated through four key amino acids: Glu 74 (*i*), Leu 78 (*i*+4), Ile 81 (*i*+7) and Val 85 (*i*+11) that are presented on one face of the helix.

Unlike other BH3-only members such as BIM (Bcl-2 interacting mediator of cell death) and BID (BH3 interacting domain death agonist) which recognise different anti-apoptotic Bcl-2 family proteins, NOXA B only binds to Mcl-1.

The selectivity of the helical peptides for Mcl-1 over Bcl-x<sub>L</sub> is the presence of a Glu 74 residue displayed by NOXA B.

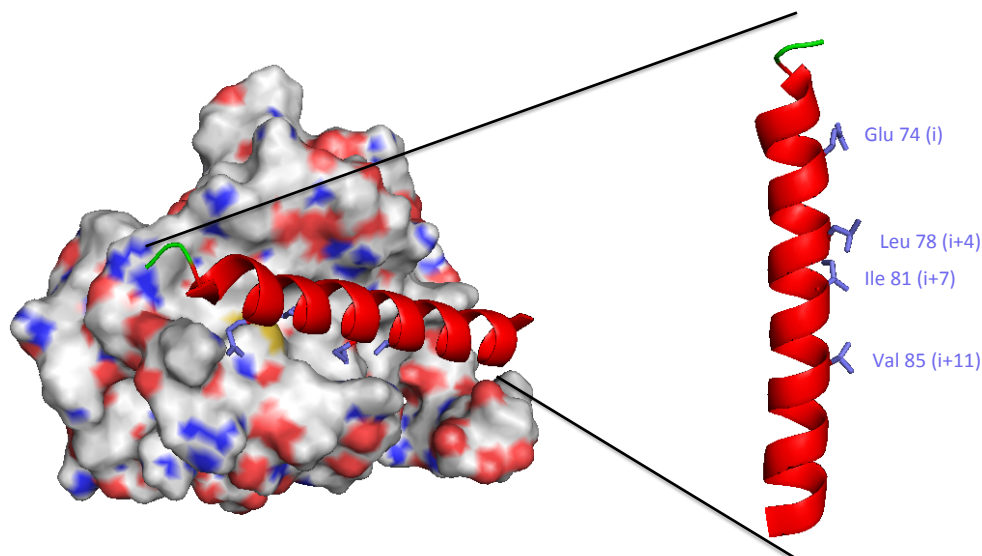


Figure 6. NOXA B/Mcl-1 interaction (PDB ID: 2JM6) showing the key residues of NOXA B.

A small helical fragment of the protein Bak is a promoter of apoptosis that interacts with the apoptosis inhibitor Bcl-x<sub>L</sub>. The interaction between Bak and Bcl-x<sub>L</sub> has been studied by NMR spectroscopy. One conformational state of the interaction is shown in Figure 7. The helical region of Bak (72-87 aa) binds to a hydrophobic cleft on the surface of Bcl-x<sub>L</sub>. The interaction is mediated through four critical hydrophobic amino acids: Val 574 (*i*), Leu 578 (*i*+4), Ile 581 (*i*+7) and Ile 585 (*i*+11).

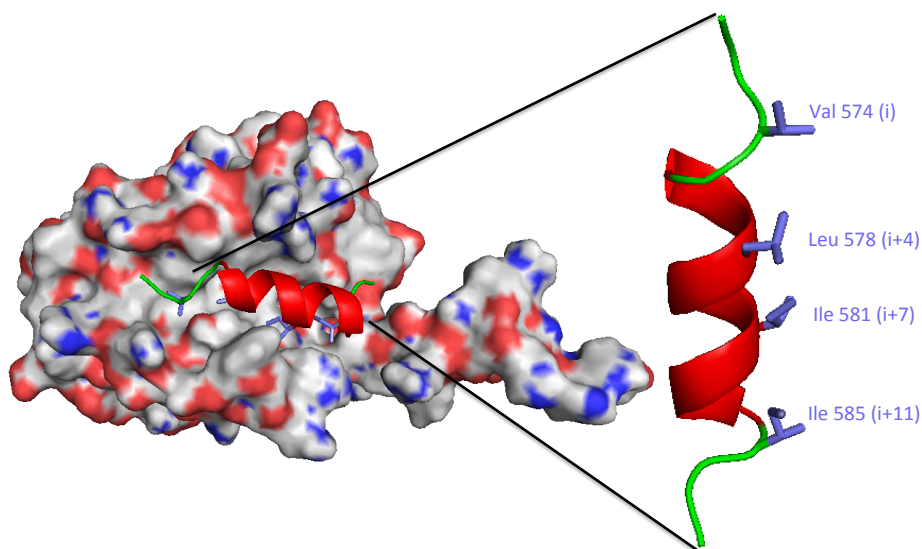


Figure 7. Bak/Bcl-x<sub>L</sub> interaction (PDB ID: 1BXL) showing the key residues of Bak.

The Bcl-2 family interactions are challenging to inhibit since they are based on four hot-spot residues spaced along a longer helical sequence.

### 1.3.1. The co-activator/estrogen receptor interaction

Estrogen receptor (ER) is a member of the steroid hormone nuclear receptor (NR) superfamily. ER regulates the expression of specific genes involved in reproduction, in central nervous system function, in maintenance of bone density and in immunity.

ERs share the characteristic domain organisation of NRs, a variable N-terminal transactivation domain (AF1) and the well-conserved DNA binding domain and a C-terminal ligand-binding domain (LBD). Estrogens bind to the LBD and induce a conformational change in the receptor that promotes homodimerization and subsequent binding to specific promoter DNA sequences modulating gene expression. This ligand-dependent signalling requires the direct binding of co-activator proteins effected by a conserved  **$\alpha$ -helical pentapeptide motif, LXXLL**, X corresponds to any residue. The interaction is mediated through the three hot-spot residues: Leu (*i*), Leu (*i*+4) and Leu (*i*+5).

Several crystal structures with bound co-activator peptides mimicking the  $\alpha$ -helix of co-activator proteins have been solved (see Figure 8). The small peptide forms an amphiphilic  $\alpha$ -helix in which the three conserved Leu are presented in two hydrophobic faces. This type of PPI is challenging to inhibit since it presents the hot-spot residues at unusual positions displaying them in two faces of the  $\alpha$ -helix.

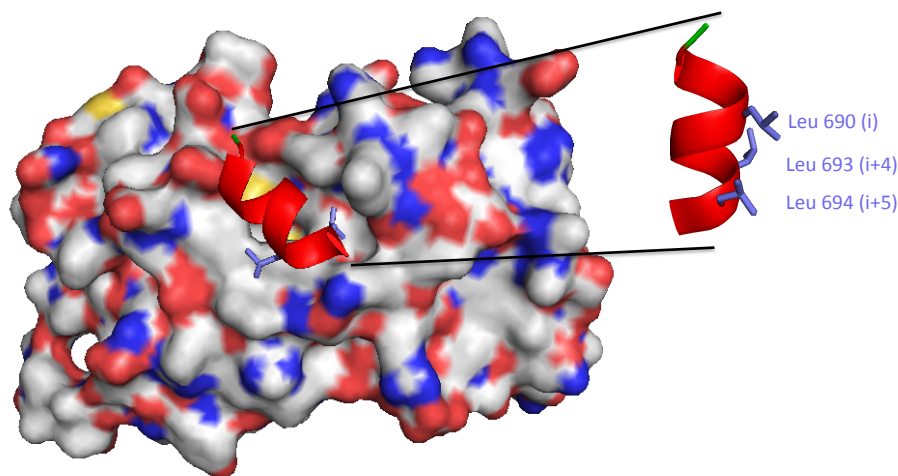


Figure 8. Estrogen receptor/co-activator interaction (PDB ID: 2QZO) showing the key residues of a co-activator peptide.

These four examples of protein interactions constitute attractive targets for the design of molecular mimetics, which could be very useful in the development of potential drugs.

## 2. Mimetics of the $\alpha$ -helix - State of the art

Although several engineered protein therapeutics have been marketed, the panel of protein structure and function is too vast to be generally targeted by designed proteins. Moreover it is still a challenge to produce 'tailor-made' proteins. Researchers need to deal with crucial factors as stability, solubility, pharmacokinetics and immunogenicity while preserving the functions of the produced protein. Therefore there is a real need for chemical entities which mimic the  $\alpha$ -helix with smaller scaffolds than an entire protein.

The first scaffolds that were historically developed to mimic the  $\alpha$ -helix were other native  $\alpha$ -helices. Although  $\alpha$ -helices are a common structural feature in proteins, they are essentially metastable. Helical peptides, which represent fragments from native protein, are compromised by two main factors for mimicking bioactivities of proteins:

- the **loss of structural integrity** upon removal from the stabilising environment of a protein. Small peptides (less than 20 amino acids) lose their helical conformation in protic solution. There is indeed a significant entropic penalty associated with the conformational restraints of the helix formation, which is only partially compensated by local stabilising interactions.
- the high **sensitivity to proteolytic degradation**.<sup>18</sup> The half-life of a small  $\alpha$ -peptide exposed to proteolytic enzymes is about 15 min.

In the past three decades, major advances have been made to stabilise or increase the helicity of small peptides by using:<sup>i</sup>

- **enhanced stabilisation of native  $\alpha$ -helices** by modifying the concatenation of the primary sequence,
- small molecule surrogates that mimic the surface of  $\alpha$ -helices, known as **type II mimetics**,
- non-peptide molecules that have no discernable helical structure that nonetheless project side-chains in an analogous fashion. They constitute **type III mimetics**,
- peptide molecules that adopt a robust helical conformation in solution that display side-chains on one or several helical faces constitute **type I mimetics**.

---

<sup>i</sup> Apart from the composition of helical peptide sequences, the effect of solvents has been largely studied to increase the helicity, notably through the use of **structure-inducing cosolvents** in aqueous environment. For example, TFE (trifluoroethanol) and HFE (hexafluoroethanol) are known as a helix-inducing solvent.<sup>19</sup>

## 2.1 Enhanced stabilisation of native $\alpha$ -helices

### 2.1.1. Helix-breaking and helix-promoting natural amino acids

The composition of the peptides (in terms of constituent amino acids) and the sequence order (i.e. the primary structure) can influence the helix stability.<sup>20</sup> The rules regarding helix-breaker and helix-promoter residues are not universal. Certain amino acids are considered to be helix-breakers at some positions, but could also serve as helix-promoters at others:

- Gly lacks side chains and is too flexible. At any position in a primary structure, Gly can be considered as an  $\alpha$ -helix breaker.
- Pro does not have the requisite dihedral angles for helix propagation and mostly destabilises  $\alpha$ -helices. However, when present at the N-terminal residue of a sequence, Pro behaves as a helix-promotor. For example, when comparing by simulation the helicity of a 14-mer peptide composed of Ala residues, Ac-AAAAAAAAAAAAAAAA-Mam, and the same peptide whose sequence started with a Pro residue, Ac-PAAAAAAAAAAAAAAAA-Mam, this latter sequence presented a decrease in the free energy of folding by 4 kJ/mol.<sup>21</sup>
- Hydrophobic aliphatic (Ala, Val, Ile, Leu) and aromatic (Phe, Trp, Tyr) residues stabilise helicity because their side-chains reduce the conformational freedom compared to Gly but do not disrupt the hydrogen-bonding network, being neither a hydrogen bond donor nor acceptor. This stabilisation is limited by the steric hindrance of the aliphatic side-chains according to the degree of substitution. For example, Val and Ile are weaker stabilisers than Ala and Leu.<sup>22</sup>
- The twelve other natural amino acids possess side-chains that can interfere with the hydrogen-bonding network of the  $\alpha$ -helix. According to their position in a specific sequence, they can disrupt or stabilise helicity, as detailed below.

### 2.1.1. N-terminal and C-terminal capping residues

The residue immediately preceding the N-terminal side of the helix is the N-cap, whereas the residue immediately following the C-terminal side of the helix is the C-cap. The capping residues have non-helical dihedral angles, since they define the end of the helix.

For example, Doig and Baldwin had carried out an extensive study on the C-capping and N-capping residues and tested the influence of the 20 natural amino acids at these positions on the  $\alpha$ -helical propensity of 17-mer peptides (see Figure 9).<sup>23</sup> The authors found that amino acids that can

accept hydrogen bonds have the highest N-cap preference because the N-terminus of an  $\alpha$ -helix has four amide hydrogens that lack the  $i$ -( $i+4$ ) backbone hydrogen bonds. However very little variation is observed when changing the identity of the C-cap residue.

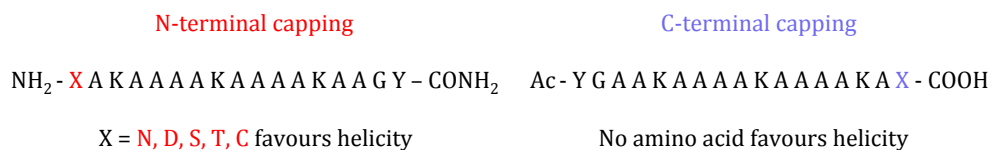


Figure 9. N-terminal and C-terminal capping with natural amino acids favouring helicity in short peptides.

## 2.1.2. Stabilisation by weak interactions between the side chains of natural amino acids

### 2.1.2.1. Hydrogen bonds

Sequences of native  $\alpha$ -helices are frequently composed of hydrogen donor amino acids (Ser, Thr, Lys, Arg, His) at  $i$  position and hydrogen acceptor amino acids (Glu, Gln, Asp, Asn) at  $i+4$  position, allowing a hydrogen bond between their side-chains thus stabilising an  $\alpha$ -helical turn.

For example, the sequence SPED, displaying Ser ( $i$ ) and Asp ( $i+4$ ), was used to promote  $\alpha$ -helical coiled-coil peptides.<sup>24</sup>

### 2.1.2.2. Salt bridges

Sequences composed of Glu-X-X-Lys, Asp-X-X-Lys, Arg-X-X-Asp are frequently found in peptides. Introducing acidic and basic side chains in position  $i$ ,  $i+4$ ,  $i+7$ ,  $i+11$ ... along the chain results in ionic interactions at physiologic pH forming salt-bridges that stabilise helicity or helical turns<sup>25,26</sup> (see Figure 10) by around  $-3$  kJ/mol.<sup>27,28</sup>

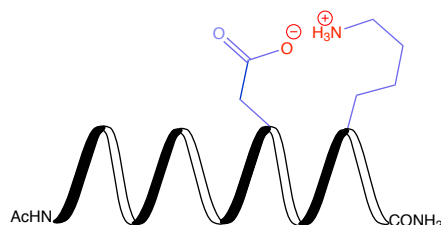


Figure 10. Salt-bridge stabilisation of  $\alpha$ -helical peptides through ionic interactions (in red) between the side chains of Asp and Lys at physiologic pH.

This strategy was employed for native short peptides showing  $\alpha$ -helical structure in aqueous solution with 30% of hexafluoro-2-propanol. For instance, motilin is a 22-residue gastrointestinal peptide hormone which folds into an  $\alpha$ -helix stabilised by charge-dipole interactions and a salt bridge.<sup>29</sup>

### 2.1.2.3. Cation- $\pi$ and $\pi$ - $\pi$ interactions

Other weak side-chain interactions between involving aromatic residues have been developed to stabilise  $\alpha$ -helical conformation of short peptides.

A cation- $\pi$  interactions has been designed for the side chains of Trp ( $i$ ) and Arg ( $i+4$ ),<sup>30</sup> and for Phe ( $i$ ) and Orn ( $i+4$ ) (see Figure 11 A.).<sup>31</sup> In each case, the cation- $\pi$  interaction contributes to the stabilisation of the  $\alpha$ -helical conformation in aqueous buffer by  $-1.67$  kJ/mol.

Hydrophobic interactions are known to be important in the stabilisation of protein structure. This is so for interactions between the side chains of aromatic residues at positions ( $i$ )-( $i+4$ ), which are able to form  **$\pi$ - $\pi$  interactions** that stabilise helical structure (see Figure 11 B.).<sup>32</sup> These interactions are at least as significant as hydrogen bonding or electrostatic interactions. For example, the interaction between the side chains of two Phe residues can contribute to a stabilisation of 4 kJ/mol<sup>-1</sup> in proteins.<sup>33</sup>

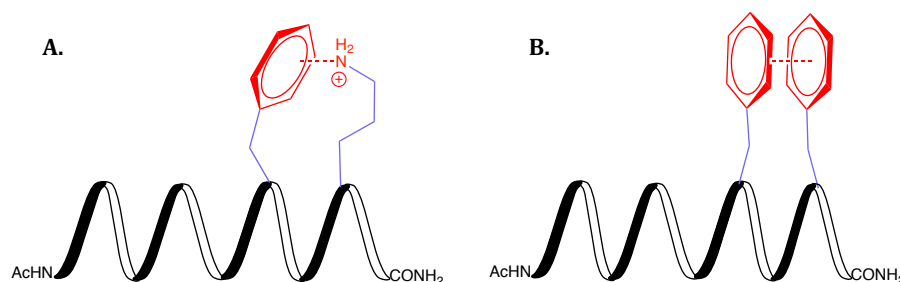


Figure 11. A: Cation- $\pi$ . (in red) between the side chains of Phe( $i$ )-Orn( $i+4$ ). B:  $\pi$ - $\pi$  interactions (in red) between Phe( $i$ )-Phe( $i+4$ )  $\alpha$ -helical peptides.

### 2.1.2.4. Metal ion chelation

The principles of stabilisation by weak interactions have been extended to the introduction of residues with side chains that can chelate metals such as  $\text{Cd}^{2+}$ ,  $\text{Cu}^{2+}$  or  $\text{Ru}^{\text{III}}$ .<sup>34</sup> For example, Ghadiri and Fernholtz have described the formation of a macrocyclic *cis*- $[\text{Ru}(\text{NH}_3)_4\text{L}_2]^{3+}$  complex, in which L represents the side chain of two His in positions  $i$  and  $i+4$ , (see Figure 12).<sup>35</sup> The authors were able to induce a helicity of 50% of a Ru(III)-complexed peptide while the uncomplexed peptide exhibited a random coil structure.

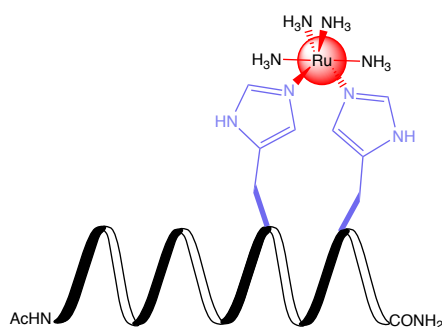


Figure 12. Helix ribbon illustrating Ru(III) complexation (in red) to the side chain of His residues (in blue) in positions  $i$  and  $i+4$ .

Although some of these helical stabilisations by weak interaction methods have had successful applications, the use of such peptide systems for exerting biological effects is often compromised. These three techniques are **weak stabilisers of helical secondary structures**. They are sensitive to the environment, the solvent polarity or changes in pH or electrolyte, meaning that the  $\alpha$ -helical conformation is vulnerable in native systems. The example of motilin nicely illustrates the helix fragility, since its helical propensity falls to 25% in aqueous medium in the absence of hexafluoro-2-propanol.

Moreover these techniques **do not improve the resistance to proteolytic degradation** since the primary sequence remains composed of natural  $\alpha$ -amino acids.

Instead of tailoring native  $\alpha$ -peptides, the search for smaller, easier to synthesise, proteolytically resistant and cell-penetrating molecules has gained much interest and the libraries of synthetic compounds meeting these requirements have expanded since the 1990's.

## 2.2 Type II mimetics

Type II mimetics are small non-peptide molecules that inhibit specific  $\alpha$ -helix-mediated PPI, but do not in any way resemble peptides and have helical architecture. For this reason, this family of mimetics will not be discussed in great detail.

These molecules are mainly identified by high-throughput screening (HTS) or fragment-based screening (FBS). These methods are not based on the rational design of the mimetics; there is no real link between the structures and the functions of the molecules discovered in this way.

HTS attempts to evaluate as many compounds as technologically possible (typically a million or more) in the hope of finding potent drug leads.<sup>36</sup> By contrast, FBS is a new drug discovery strategy that is based on screening a smaller number of compounds (typically several thousand) in the hope of finding low-affinity fragments; these fragments being further optimized to increase their potency.<sup>37</sup>



A library of diverse synthetic chemicals was screened using HTS by Hoffmann-La Roche to identify compounds that could inhibit p53/*mDM2* interaction.<sup>38</sup> A family of tetra-substituted *cis*-imidazole analogues, named Nutlins (for Nutley inhibitor), was optimized to bind to *mDM2*. These compounds displace p53 protein from its complex with *mDM2* and bind in the same hydrophobic cleft as the native helix (see Figure 13). The IC<sub>50</sub> values for the most potent one, Nutlin-3a, is 90 nM (see Figure 14 A).

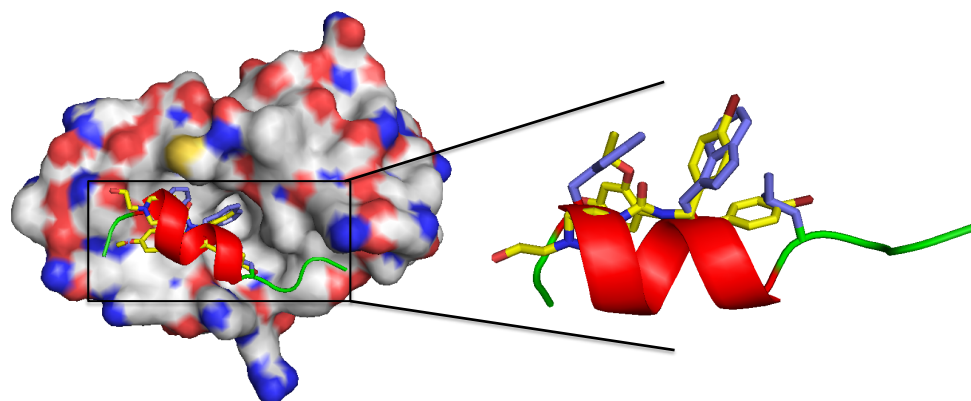


Figure 13. Crystal structure of Nutlin-2 (in red, green and blue) in complex with mDM2 (PDB ID: 1RV1) overlaid with p53 peptide (16-29) (in yellow).

Johnson & Johnson pharmaceuticals identified by HTS a benzodiazepinedione family able to disrupt the p53/hDM2 interaction (see Figure 14 B) with an IC<sub>50</sub> of 420 nM. Interestingly these compounds were tested *in vivo* and decreased the proliferation of tumour cells.<sup>39</sup>

Wang and co-workers employed a *de novo* structure-based approach to identify potent inhibitors of p53/mDM2 interaction. They designed a new class of inhibitors based on a spiro-oxindole template.<sup>40</sup> MI-219 was identified as the most potent compound with an excellent  $K_i$  value of 5 nM and a 10,000-fold selectivity in targeting the *mDM2* protein over *mDMX* (murine double minute X) (see Figure 14 C).

Recently, Sun and co-workers reported a potent and selective piperidinone *m*DM2 inhibitor ( $IC_{50} \approx 1$  nM) with a good oral bioavailability (see Figure 14 D).<sup>41</sup>

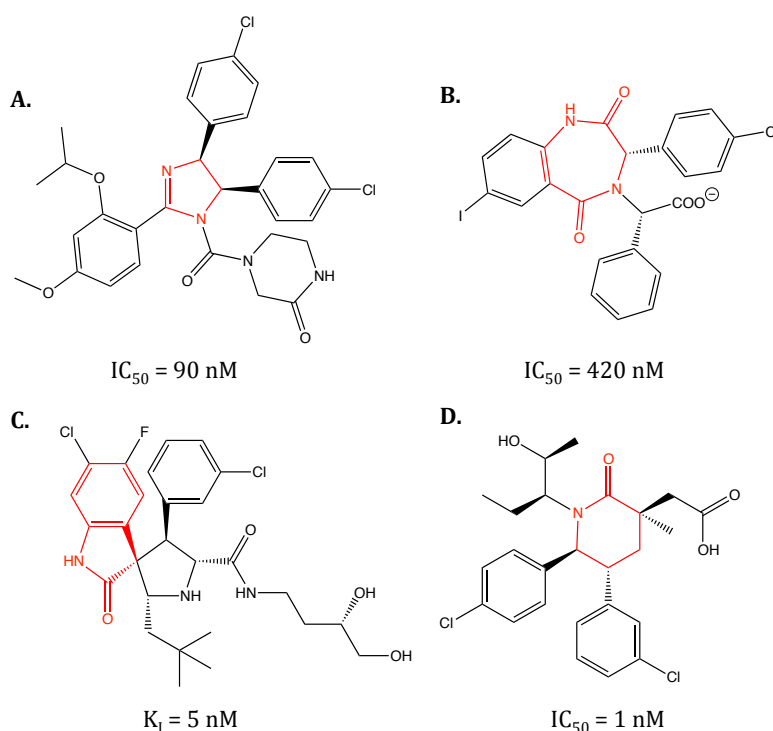


Figure 14. Type II mimetics of p53 peptide (16-29) with their potency against p53/mDM2 or hDM2 interaction - A: Nutlin-3a. B: Benzodiazepinedione-1. C: MI-219 Spiro-oxindole. D: Piperidinone.

Although HTS and FBS have produced good results, it should be noted that while 78% of good hits are found by HTS, FBS or combining both techniques, only 42% lead to a satisfying potency, with an  $IC_{50}$  less than 100 nM (see Figure 15).<sup>37</sup>

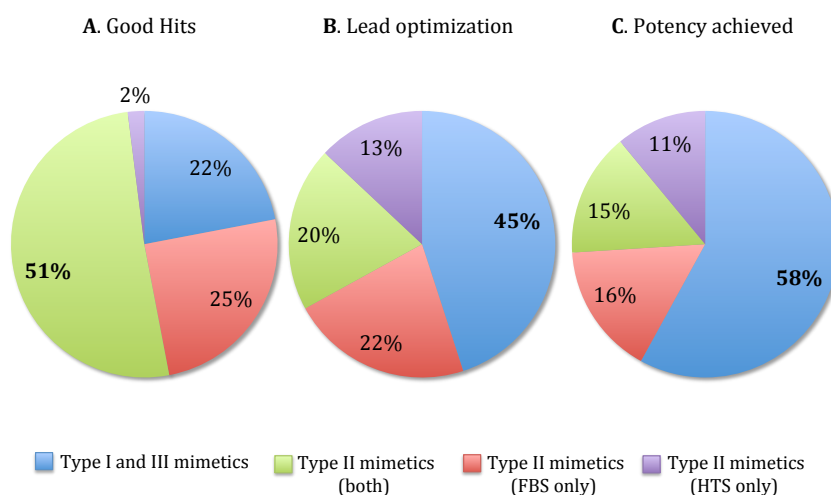


Figure 15. Comparing type I and III mimetics with type II mimetics efficiency: A. Chemically tractable hits. B. Lead optimisation initiated hits from the specified lead source. C. Potency (defined as  $IC_{50} < 100 \text{ nM}$ ) achieved from the specified lead source.

Even if certain small molecules can act as potent inhibitors of  $\alpha$ -helix-mediated PPI, their discovery and subsequent clinical uses are limited by:

- the **number of molecules available** in screening libraries. Even though these are on the increase, the methods employed are randomized, not rational and would need an infinite number of molecules to target all the protein interactome.

- their **weak specificity** for the targeted protein over other proteins due to their small size and the lack of functional groups mimicking the side chains of hot-spot residues. The recognition surface of an  $\alpha$ -helix is flat and large ( $>800 \text{ \AA}^2$  equivalent to 170 atoms).<sup>8</sup>

In the pharmaceutical industry it is accepted that chasing after potency at the expense of bioavailability, toxicity and target validity carries serious risks of failure owing to inadequate pharmacokinetic properties of the resulting hit compounds.

In parallel to the development of type II mimetics, the **rational design** of other types of  $\alpha$ -helix mimetics has attracted much interest. As shown in Figure 15, the search for type I and III mimetics to find good potent inhibitors is statistically more rewarding than the search for type II mimetics.

## 2.3 Type III mimetics

Type III mimetics, or proteomimetics, ‘match the topography of the original  $\alpha$ -helix by mimicking the spatial orientation of its key recognition residues’.<sup>42</sup> They are non-peptide molecules, rod-shaped objects and do not have helical architectures. They differ from the type II mimetics by presenting functional groups that mimic the hot-spot residues of a specific interaction. The goal of type III mimetics is to reduce the complexity of the helical backbone while keeping the critical functionality in a similar spatial arrangement (see Figure 17).

### 2.3.1. Pioneering work

#### 2.3.1.1. Indane scaffold

The Horwell group showed that trisubstituted indanes could mimic the presentation of the  $i$ ,  $i+1$  residues of an  $\alpha$ -helix (see Figure 16). These molecules constitute the first dipeptide proteomimetics. 1,1,6-Trisubstituted indanes bearing hydrophobic side chains were designed and were found to bind to the tachykinin receptors, NK1, NK2, and NK3, with a micromolar affinity.<sup>43</sup>

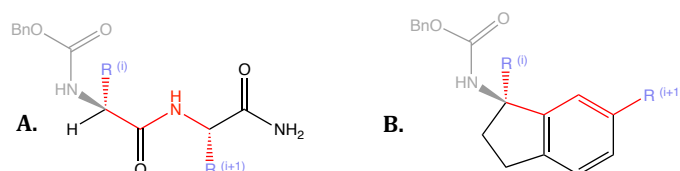


Figure 16. Indane template mimicking the side chains of  $i$ ,  $i+1$  residues (R( $i$ ) and R( $i+1$ )) of an  $\alpha$ -helix.

## 2.3.1.2. Terphenyl derivatives

Inspired by Horwell's pioneering work, the Hamilton group developed the first  $\alpha$ -helical proteomimetics.<sup>44</sup> The first generation of mimetics was based on a 3,2',2''-trisubstituted terphenyl scaffold (see Figure 17 A) synthesised by sequential Negishi coupling reactions. This scaffold was chosen for the modularity of its synthesis and most importantly for its conformational characteristics: due to the low rotational energy barrier of the phenyl-phenyl bonds, the trisubstituted terphenyl template can take up a staggered conformation in solution. The aryl core projects the ortho substituents in the appropriate position to mimic the *i*, *i*+3(4) and *i*+7 residues of an  $\alpha$ -helix (see Figure 17 B and C). Overlay of the substituents and the side-chains gives an excellent root mean square deviation (RMSD) value of 0.9 Å.<sup>45</sup>

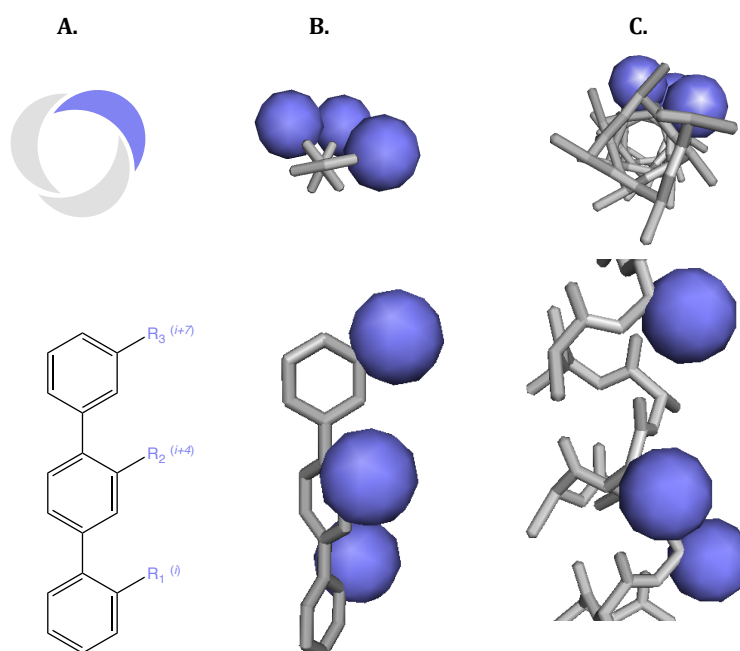


Figure 17. A: Side and top views of a 3,2',2''-trisubstituted-terphenyl backbone. B: Side and top views of an x-ray crystal structure of 3,2',2''-trisubstituted-terphenyl with three substituents displayed as blue spheres. C: Side and top views of an  $\alpha$ -helix with the *i*, *i*+3(4) and *i*+7 side chains displayed as blue spheres.

Derivatives of this family have been used to inhibit many PPI. For example, a 3-isobutyl, 2'-1-naphthalenemethylene, 2''-isobutyl sequence antagonist inhibits Bcl-x<sub>L</sub>/Bak interaction with an excellent IC<sub>50</sub> value of 114 nM.<sup>46</sup> The terphenyl derivatives have even been tested *in vivo* and they are effective in disrupting the interaction in intact cells.<sup>47</sup>

In contrast with most of type II mimetics, the primordial advantage of type III mimetics is the ability to **selectively inhibit PPI**. For example, a subtle change of a methyl-1-naphthyl for methyl-2-naphthyl in the side chain of a terphenyl sequence allows a selective inhibition of the Bak/Bcl-x<sub>L</sub> interaction over the p53/hDM2 interaction.

Extensive research has been carried out, with considerable contributions of the Hamilton group, on the diversification of scaffolds with **simplified synthesis** and **drug-like properties**.

### 2.3.2. *Hydrophilic backbones*

The main limitation of such polyphenyl backbone proteomimetics is their high hydrophobicity, which favours membrane penetration but seriously decreases solubility in aqueous solutions. Much efforts have been made to remedy this situation.

The Hamilton group first designed a terephthalimide scaffold (see Figure 18 A). The spatial arrangement of the substituents is similar to the terphenyl scaffold (RMSD = 0.34 Å), maintaining the *i*, *i*+4, *i*+7 side-chain mimics of an  $\alpha$ -helix (RMSD = 1.03 Å), while the synthesis is easier and the solubility is increased.<sup>48</sup> The flanking phenyl rings of the terphenyl scaffold were replaced by two functionalized carboxamide groups (in red). They retain a planar geometry due to the restricted rotation of the amide bonds. One introduces a hydrogen bond (in grey) between the amide-NH and the alkoxy oxygen atom that orientates the side chain R<sub>2</sub>. The introduction of the two carboxamide groups also increases the solubility of the scaffold. However, the most potent inhibitor of Bak/Bcl-x<sub>L</sub> interaction has a weaker inhibitory activity than the terphenyl inhibitors ( $K_i$  = 0.78  $\mu$ M).

The Hamilton group developed a scaffold to display more than three residues, in order to achieve a higher degree of specificity for the targeted PPI. It combines the hydrophobic core of the terphenyl series and the synthetically accessible carboxamide groups of the terephthalamide series (see Figure 18 B).<sup>49</sup> This biphenyl 4,4'-dicarboxamide scaffold mimics the *i*, *i*+4, *i*+7, *i*+11 side chains of an  $\alpha$ -helix (RMSD of 1.368 Å). A library of around fifty derivatives has been designed against Bak/Bcl-x<sub>L</sub> interaction. However, the most potent one has a lower inhibitory activity ( $K_i$  = 1.8  $\mu$ M) than the terephthalimide or terphenyl inhibitors that only possess three side chains. Mimicking an additional hot-spot residue of an  $\alpha$ -helix does not always improve the potency.

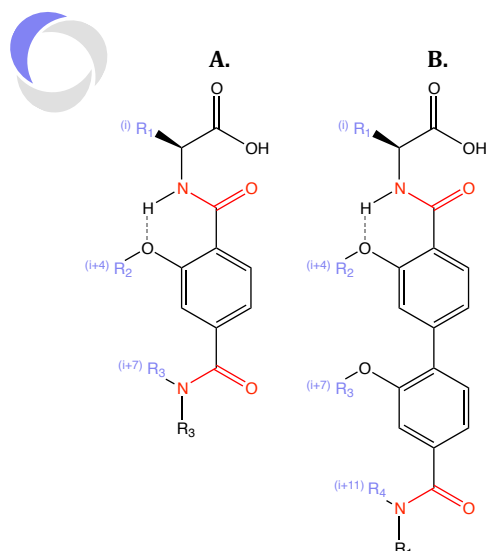


Figure 18. A: Terephthalamide scaffold. B: Biphenyl 4,4'-dicarboxamide scaffold.

Oligobenzylureas were synthesised from substituted para-aminobenzoic acids (see Figure 19 A). The urea moiety was introduced to increase the hydrophilicity of the scaffold. It also stabilises the structure through six-membered hydrogen-bonded rings. The molecules alternate benzene ring with hydrogen-bonded acylureas (in grey) with a similar overall shape to oligophenylene and a much simpler synthesis. The Hamilton group was thus able to elongate the oligobenzylurea scaffold to mimic a 37 Å  $\alpha$ -helix, equivalent to 30 residues.<sup>50</sup>

An enaminone scaffold that contains a similar hydrogen-bond network and thus presents a similar overall shape to oligophenylene has also been developed (see Figure 19 B).<sup>51</sup>

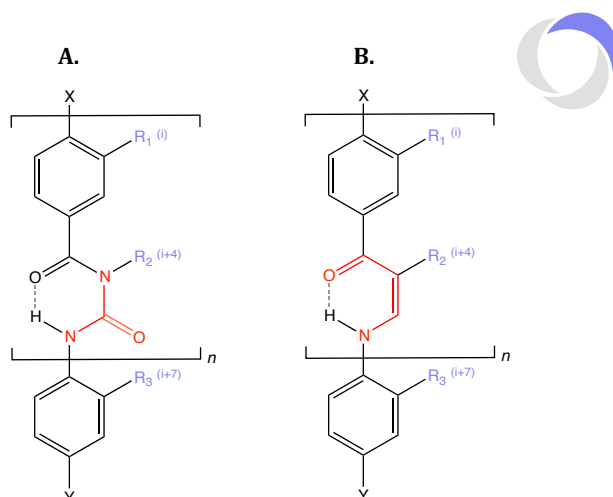


Figure 19: A: Oligobenzylurea scaffold. B: Enaminone scaffold ( $n = 1 - 4$ ).

Oligobenzylurea peptidomimetics present more functional groups which mimic side chains but possess lower inhibitory activities against Bak/Bcl- $x_L$  interaction (the best inhibitor gave  $K_i = 2.4 \mu\text{M}$ ) than the terephthalamide, biphenyl 4,4'-dicarboxamide and terphenyl derivatives.<sup>52</sup>

The Rebek group developed type III mimetics with increased hydrophilicity by introducing heterocyclic rings (see Figure 20 A). These rings form a hydrophobic surface for the recognition and a wet-edge (in red) that enhances the solubility. An original oxazole-pyridazine-piperazine scaffold reproduces  $i$ ,  $i+4$ ,  $i+7$  side-chains of a helix.<sup>53</sup> A library of these derivatives has been tested against Bak/Bcl- $x_L$  interaction but again the compounds are less potent than the terphenyl derivatives.

Similarly the Hamilton group designed a 5-6-5-imidazole-phenyl-thiazole scaffold in which the terminal positions are replaced with more hydrophilic five-membered heterocycles (see Figure 20 B). Based on the same scaffold, analogues with different side chains have been designed to mimic Gln ( $i$ ), Lys ( $i+4$ ) and Leu ( $i+7$ ) side-chains and tested to disrupt Cdc42/Dbp interaction.<sup>54</sup> However, these mimetics showed no detectable inhibitory activity, with the one exception (see Figure 20 B) which had  $IC_{50} = 67 \mu M$ .

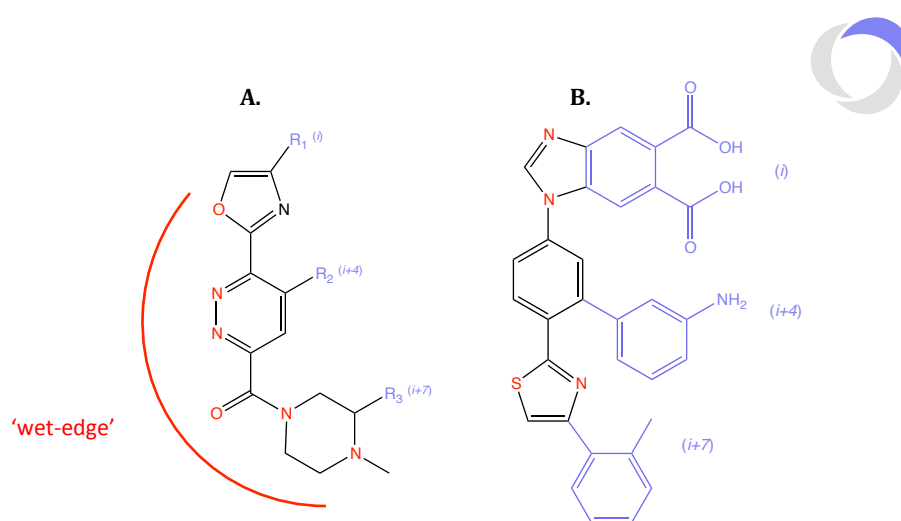


Figure 20. A: Oxazole-pyridazine-piperazine scaffold. B: 5-6-5-Imidazole-phenyl-thiazole scaffold.

### 2.3.3. Oligoarylamine derivatives

A new class of type III mimetics, the oligoarylaminides, recently emerged and rapidly became an attractive proteomimetics scaffold due to the facile synthetic access and the predictability of preferred conformations.<sup>55</sup>

The Huc group first reported the synthesis of a family of alternating 2,6-diaminopyridine (in grey) and substituted 2,6-pyridinedicarbonyl (in blue) unit derivatives (see Figure 21 A).<sup>56</sup> Such oligopyridine derivatives form large-diameter helices that are stabilised by intramolecular hydrogen bonds between the amide protons and the pyridine nitrogens (see Figure 21 B). The hydrogen-bonding network induces a curvature and leads to helical folding pattern (see Figure 21 C). The helical folding behaviour is robust even in water, thus revealing a strong improvement in stability compared to short  $\alpha$ -peptides.

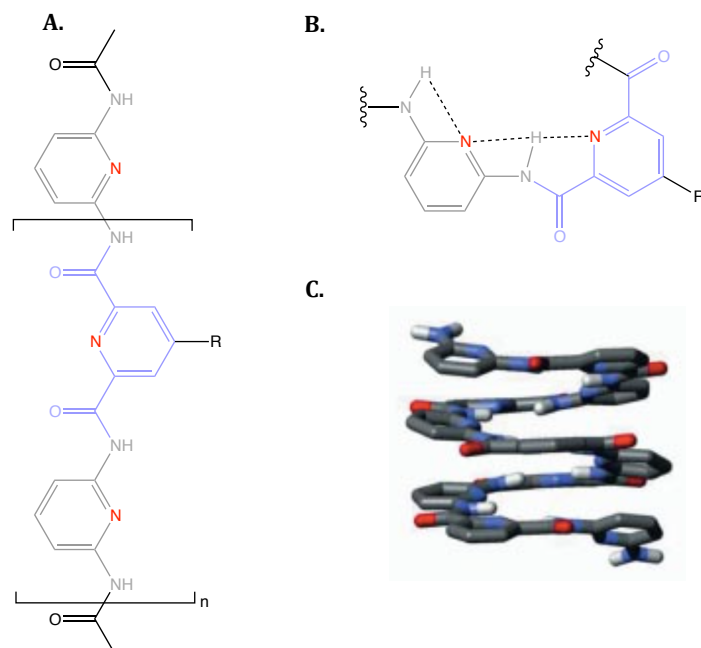


Figure 21. A: Backbone of alternating substituted 2,6-diamino and 2,6-dicarboxamide pyridine. B: Hydrogen-bonding pattern. C: Side view of a helical model.

Encouraged by these facets, the Hamilton group described a trispyridylamide scaffold (see Figure 22 A).<sup>57</sup> The hydrogen bonds between the amide protons and the pyridine nitrogens and the alkoxy oxygens stabilise a completely planar conformation. The alkoxy groups project the three side-chains on the same face of the molecule and mimic the  $i$ ,  $i+4$  and  $i+7$  residues of an  $\alpha$ -helix (RMSD = 0.94 Å). The functionalised 3-*O*-alkylated oligopyridylamide analogues were tested as proteomimetic scaffolds against Bcl-x<sub>L</sub>/Bak interaction. The best inhibitor gave a  $K_i$  value of 1.6  $\mu$ M.

Several groups developed scaffolds derived from Hamilton's work by replacing the pyridyl ring by a benzene ring (see Figure 22 B). This substitution deletes a hydrogen bond and increases the flexibility of the 3-*O*-alkylated oligobenzylamide scaffold; this in some cases leads to improve binding affinity. For example, the Wilson group synthesised inhibitors of the p53/*h*DM2 interaction and found an inhibitor ( $IC_{50}$  = 1.0  $\mu$ M) comparable in potency to the native peptide.<sup>58</sup>

The Wilson group later reported the synthesis of 2-*O*-alkylated regioisomers (see Figure 22 C).<sup>59</sup> The backbone possesses a reduced curvature due to more stable six-membered hydrogen-bonded ring compared to the 3-*O*-alkylated analogues. However, preliminary evaluation of the derivatives mimicking p53 revealed minimal differences in potency for p53/*h*DM2 interaction suggesting that strict geometrical matching of side chains is not essential for effective inhibition of the PPI.

In order to generate compound libraries, the Wilson group described the first solid-phase synthesis of type III mimetics. The group further optimized the synthesis by microwave coupling reaction.<sup>60</sup> Using this effective method, N-alkylated oligobenzamides (see Figure 22 D) were synthesised. These scaffolds are reminiscent of peptoids. They were tested against the p53/*h*DM2 interaction with the best inhibitor having an  $IC_{50}$  of 2.8  $\mu$ M.<sup>61</sup>



Other 3-alkylated oligobenzamides with side chains attached directly to the aromatic rings were described by the Guy group (Figure 22 E).<sup>62</sup> A library of 173 compounds targeting the p53/hDM2 interaction was developed through structure-based computational design and synthesised using solution-phase techniques. Interestingly the most potent inhibitor in this series ( $K_i = 12 \mu\text{M}$ ) had only two side-chain mimics whereas three hot-spot residues are involved in this PPI.

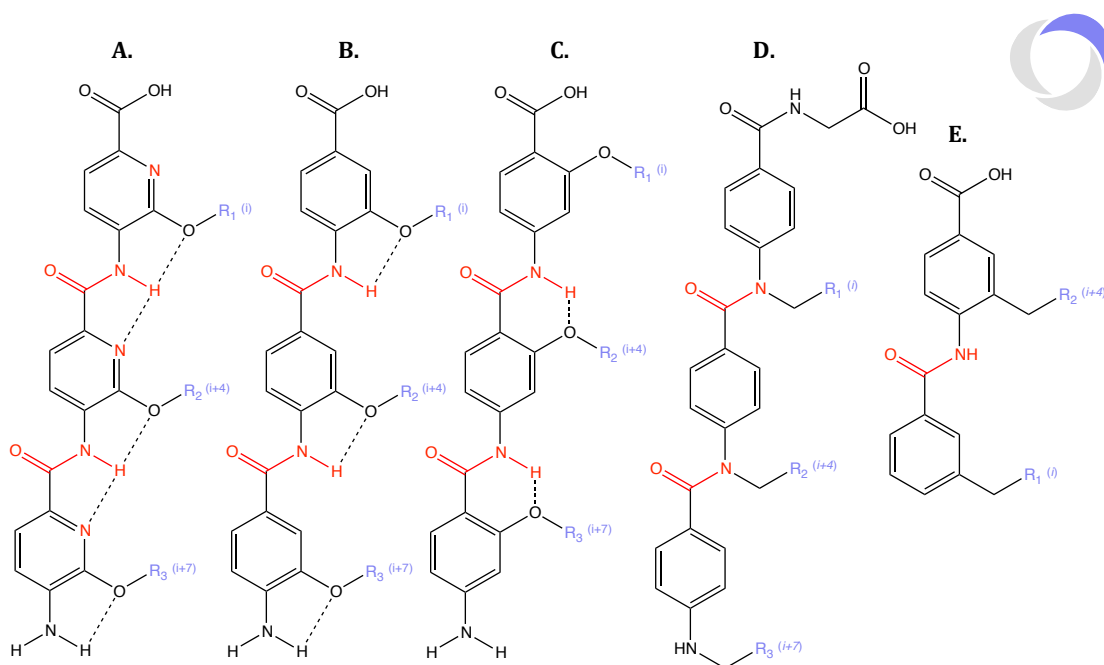


Figure 22. A: 3-O-alkylated oligopyridylamide scaffold. B: 3-O-alkylated Oligobenzamide scaffold. C: 2-O-alkylated oligobenzamide scaffold. D: N-alkylated oligobenzamide scaffold. E: 3-alkylated oligobenzamide scaffold.

The Lim group designed a pyrrolopyrimidine-based scaffold (see Figure 23 in red) that displays side-chain mimics at positions  $i$ ,  $i+4$ ,  $i+7$ .<sup>63</sup> The synthesis is based on a solid-phase strategy that is amenable to divergent synthesis of a large library of pyrrolopyrimidine derivatives. Among the 900-member library, 90 were randomly chosen and tested against p53/mDMX interaction. One analogue was identified as a cell-permeable dual inhibitor of p53/mDM2-mDMX ( $K_i = 0.62 \mu\text{M}$  against both) demonstrating that the designed molecules can act as  $\alpha$ -helix mimetics but without the same selectivity.

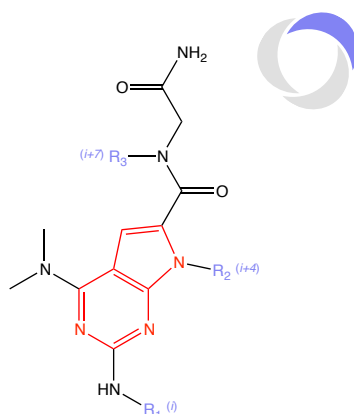


Figure 23. Pyrrolopyrimidine scaffold.

### 2.3.4. Multifacial mimics

The main limitation of type III mimetics is that they display functional groups which mimic the side-chains of only one face of the  $\alpha$ -helix (see the top view cartoon representations in the figures presented previously). The oligobenzamide and benzylurea scaffolds allow facile incorporation of a variety of different side-chain mimics. A few groups have recently tried to address this issue by introducing a substituent on the opposite side of the aromatic ring:

- The Ahn group introduced a second alkoxy group on the *O*-alkylated oligobenzamide scaffold allowing the proteomimetics to display side-chain mimics at position *i*, *i*+2, *i*+5, *i*+7, (see Figure 24 A),<sup>64</sup>
- The Hamilton group introduced a second alkoxy group on the *O*-alkylated oligobenzylurea scaffold allowing the proteomimetics to display side-chain mimics at positions *i*, *i*+1, *i*+4, *i*+6, *i*+8.<sup>65</sup>

While presenting ‘two-faced’ mimetics of  $\alpha$ -helices, no PPI inhibitory activity has been reported for these scaffolds.

Previously, the Hamilton group developed a template based on the original terphenyl scaffold with an indane ring in place of the central phenyl ring (see Figure 24 B).<sup>66</sup> This diphenylindane template mimics the *i*, *i*+3, *i*+4, *i*+7 side-chains of an  $\alpha$ -helix, *i*+3 and *i*+4 substituents being borne by the indane ring, as described by Horwell in a dipeptide mimetic (see 2.3.1.1).<sup>43</sup> The importance of *i*+3 and *i*+4 side chains of Bak and Bad peptides binding to Bcl-x<sub>L</sub> had been demonstrated<sup>67</sup> and warranted the synthesis of this scaffold.

Following the same idea, but with a more accessible template, the Hamilton group synthesised a bis-aryl pyridyl-pyridone scaffold designed to target the co-activator/ER interaction (see Figure 24 C). A small library of compounds was tested and some of them showed inhibition in the low micromolar range.<sup>68</sup>

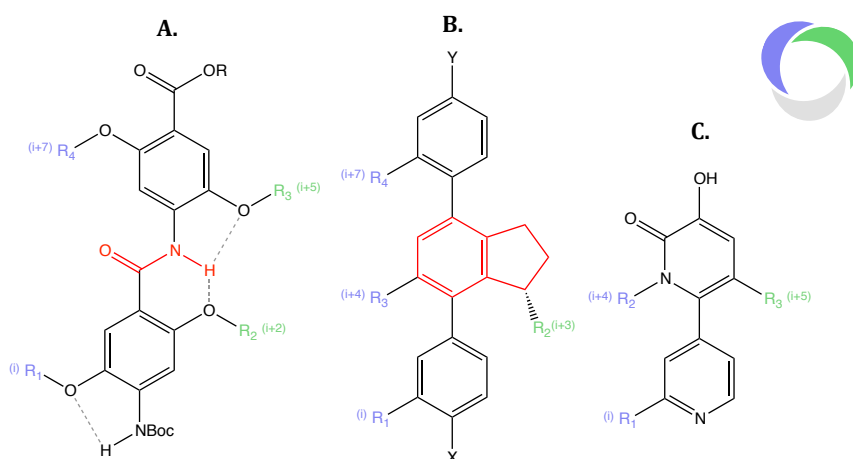


Figure 24. A: 2,5-O-alkylated oligobenzamide scaffold. B: Diphenylindane scaffold. C: Bis-aryl pyridyl-pyridone scaffold.

As illustrated by the cartoon representation, these double-sided scaffold mimics more than one face of the  $\alpha$ -helix.

### 2.3.5. Polysaccharides as $\alpha$ -helix mimetics

Polysaccharide templates have been used to mimic  $\alpha$ -helices. It is difficult to class them into one of the three types of mimetics, but the closest type is type III since they are a non-peptide (although not rod-shaped) molecules that mimic the spatial orientation of the key recognition residues.

The first example of polysaccharide  $\alpha$ -helix mimetics was presented by Xuereb et al. in 2000.<sup>69</sup> A pentasaccharide scaffold was used to mimic the basic helical region of the transcription factor GCN4. A bZIP domain of the GCN4 protein binds to the DNA major groove, through the  $\alpha$ -helical region displaying positively charged side-chains allowing ionic interaction with the phosphate moiety and the nucleotide bases. The saccharide building block used was the 2-deoxyfucose, which is more hydrophobic than fully oxygenated sugars, decorated with positively charged guanidinium groups (see Figure 25).

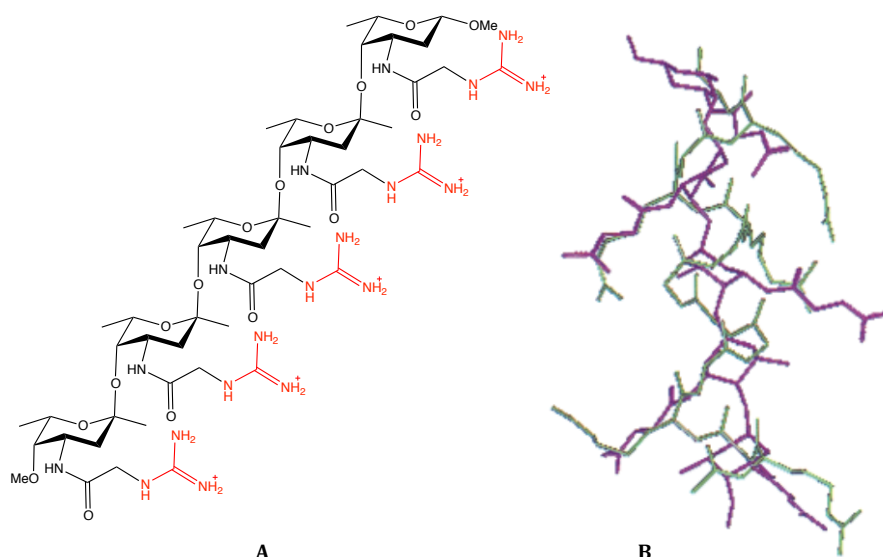


Figure 25. A: Structure of pentasaccharide based on a 2-deoxyfucose building block. B: Pentasaccharide (in purple) superimposed on GCN4 (231-244) from a crystal structure of the DNA complex (in green).

The conformational preferences of the pentasaccharide were studied in water by NMR. As seen in Figure 25 the side-chains of the lowest energy conformer (in purple) overlaid well with the side-chains of the crystal structure of GCN4 (231-244) complexed with DNA. However, even at high concentrations, the polysaccharide failed to bind to the DNA major groove, as had been the initial design objective. Instead, it was able to bind, albeit weakly compared to natural peptides, to the DNA minor groove. This point illustrates the challenge of using polysaccharides as  $\alpha$ -helix mimicry, since naturally occurring proteins rarely use the  $\alpha$ -helix motif in the minor groove recognition.

## 2.4 Type I mimetics

Type I mimetics are peptide molecules that adopt a **robust helical** conformation in solution and display functional side chains. The crucial feature of type I mimetics is that they mimic the global helical conformation of the native  $\alpha$ -helix, meaning that such mimetics can **be used in many diverse applications other than PPI**.

In the type I mimetics are found peptides constructed from unnatural amino acids “with a strong tendency to adopt a specific, compact conformation” stabilised by non-covalent interactions; they are also considered as **foldamers**.<sup>70,71</sup> Peptide foldamers collectively display a wide range of helical conformations which do not necessarily mimic the native  $\alpha$ -helix. The conformational preferences of helical peptide foldamers are detailed in a separate section (see 2.5).

### 2.4.1. Stabilisation of $\alpha$ -helical structure with unnatural amino acids

#### 2.4.1.1. Related unnatural $\alpha$ -amino acids bearing alkyl side-chains

Natural and related unnatural amino acids bearing alkyl side chains have been evaluated as modulators of the helicity of small peptides (see Figure 26).<sup>72</sup> The sequences succinyl-Tyr-Ser-Glu-Lys-Xaa-Glu-Lys-NH<sub>2</sub> were examined, in which Xaa was the guest amino acid with alkyl side-chain.

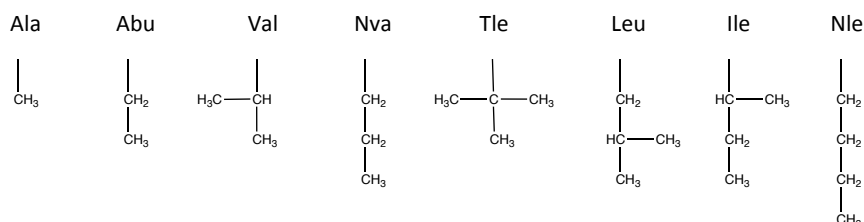


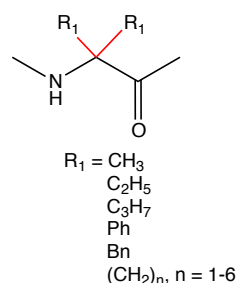
Figure 26. Natural and related unnatural amino acids testing the influence of alkyl side chains on the helicity.

From CD measurements, it appeared clearly that the more sterically hindered was the Xaa side-chain, the less helicity was displayed by the peptide. In the absence of branching, the chain length does not affect the helicity (Ala, Abu, Nva, Nle). However,  $\gamma$ -branching (Leu) decreases the helicity and  $\beta$ -branching decreases it dramatically (Val, Ile and Tle).

#### 2.4.1.2. $\alpha,\alpha$ -Disubstituted $\alpha$ -amino acids

$\alpha,\alpha$ -Disubstituted amino acids are  $\alpha$ -amino acids in which the hydrogen atom at the  $\alpha$  position is replaced by a substituent. The introduction of an extra  $\alpha$ -group severely restricts the possible rotations around  $\phi$  and  $\psi$  and, in consequence, limits the accessible secondary structures of peptides. Many  $\alpha,\alpha$ -di-substituted amino acids have been synthesised (see Figure 27).<sup>73</sup>

##### Achiral $\alpha,\alpha$ -disubstituted amino acids



##### Chiral $\alpha,\alpha$ -disubstituted amino acids

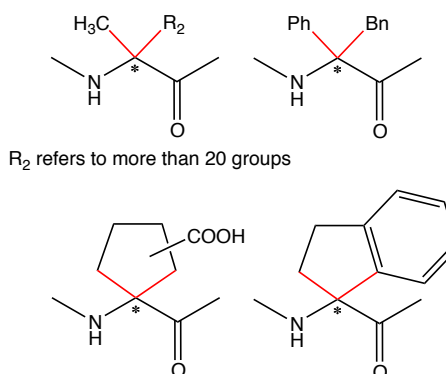


Figure 27. A selection of  $\alpha,\alpha$ -di-substituted amino acids.

For example, the incorporation of  $\alpha$ -methylalanine, also known as  $\alpha$ -amino isobutyric acid (Aib), into peptides and peptaibols has been much studied, notably by the Toniolo and by the Clayden groups.<sup>73,74</sup> It is actually a natural amino acid that occurs in peptides produced by microbial sources. The preferred dihedral angles of Aib are  $\pm 57^\circ$  for  $\phi$  and  $\pm 47^\circ$  for  $\psi$  (the  $\pm$  is due to the achirality of Aib). These are the ideal angles for incorporation of Aib in an  $\alpha$ -helix. However, depending on peptide length, environment, size and distribution of amino acid side-chains, peptides containing Aib can adopt either an  $\alpha$ -helix or a 3(10)-helix conformation:<sup>75</sup>

- peptides containing only Aib fold into a 3(10)-helix.<sup>73,74</sup>
- with peptides alternating Aib and  $\alpha$ -mono-substituting amino acids, a critical length of seven to eight residues is needed to favour the  $\alpha$ -helical conformation.<sup>76</sup>
- when only one Aib is incorporated as the N-terminal residue of a peptide sequence, it can behave as an  **$\alpha$ -helix initiator** (see following section).<sup>77</sup>

#### 2.4.1.3. $\alpha$ -Helix initiators

Another technique to induce helicity in small peptides is to covalently link them to helix-initiating templates without modifying the peptide sequence. Helical initiators are usually incorporated at the N- or C-terminus of a peptide. They strengthen an  $i-i+4$  hydrogen bond at the extremity of a helix, mimicking one full turn of an  $\alpha$ -helix.

The simplest example is the  $\alpha,\alpha$ -disubstituted Aib, but other more complex systems have been shown to induce helicity (see Figure 28). The challenge is to align hydrogen bond donor or acceptor functions in the correct geometry for helix initiation.

The Kahn group developed 7-member cyclic systems linked to an Aib residue where a peptide is attached to its C-terminus (see Figure 28 A).<sup>78</sup> They were incorporated into mimetics of neuropeptide Y as N-terminal caps. These mimetics showed higher helicity and NPY antagonist activity.

The Kemp group proposed a 12-membered macrocyclic triproline scaffold (Figure 28 B).<sup>79</sup> It possesses a 4,5'-methylenethio bridge between the first two prolines keeping the crucial *trans* configuration of the Pro2-Pro3 amide bond. The triproline template is a helix initiator though the cap again lacks the required number of aligned carbonyl groups.

Inspired by the proline-containing cap idea, the Lewis group endeavored to develop  $\alpha$ -helix initiators that provide three correctly oriented carbonyl groups, that have structural and electronic properties akin to a natural  $\alpha$ -helix and that are reasonably easy to synthesise.<sup>80</sup> With these three criteria in mind, they succeeded in synthesising the 12-membered macrocycle diproline scaffold (Figure 28 C) after several attempts.<sup>80,81</sup> The  $\alpha$ -helical character of the template is unfortunately weak since only the first attached amino acid residue is part of the helical structure.<sup>82</sup>

The Müller group constructed a conformationally rigid cage, which places three carbonyl groups in an ideal position for hydrogen bonding to the N-terminus of a small peptide (see Figure 28 D).<sup>83</sup> The peptide conjugates displayed significant helicity compared to untemplated peptides.

Arrhenius and Satterthwaith proposed a different approach implicating a 13-membered macrocycle to mimic the first turn of an  $\alpha$ -helix (see Figure 28 E). However the template initiated helicity only in the presence of TFE.<sup>84</sup>

The Bartlett group used a much simpler though synthetically challenging template based on hydroindol scaffold for  $\alpha$ -helix initiation (see Figure 28 F).<sup>85</sup> Again, three hydrogen bond acceptors carbonyl groups were present, one of which was a free carboxylate. The negative charge of carboxylate was expected to complement the helix dipole. Methyl substituents were placed at C-6 and C-3 to favor the pseudoaxial disposition of the carbonyl groups, thus orientating them to accept hydrogen bonds. The template exhibited excellent  $\alpha$ -helical inducing properties in aqueous buffer, without the need of other solvents in contrast with the above-mentioned cases. Up to 75% of helicity was induced in the linked sequence, H-EALAKA-NH<sub>2</sub>. This sequence was carefully selected for the study since it is stabilised by a salt bridge between the side chains of Glu and Lys, while the helix-promoting residues (Ala and Leu) were included.

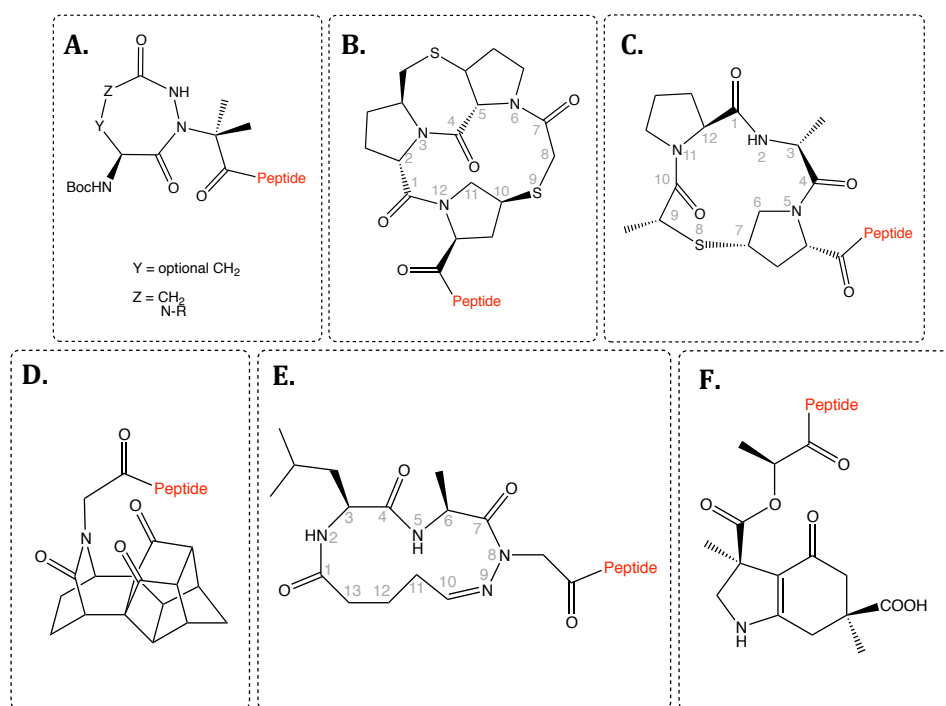


Figure 28. Different types of Helix initiators.

It can be argued that these helix initiators **act more as synthetic N- or C-caps** to avoid the  $\alpha$ -helix fraying rather than genuine inducers of helicity. Moreover their structural complexity necessitates lengthy and laborious syntheses. As an example, the synthesis of Kemp's triproline template required 26 steps. Furthermore the sequence of the peptide under study has always been carefully selected on the basis that it is highly amenable to  $\alpha$ -helix folding.

Nonetheless, the idea of grafting macrocyclic systems onto the  $\alpha$ -helix core to induce the helicity is still relevant and has been extended by the recent and promising development of **covalently-constrained peptides** or stapled peptides.

### 2.4.2. Stabilisation of $\alpha$ -helical structure through covalent interaction: stapled peptides

There has been a growing interest in the introduction of covalent linkages between residues close in space that strongly encourage helical secondary structure. Various types of covalent connections have been developed.

#### 2.4.2.1. Disulfide bridges

One way to stabilise an  $\alpha$ -helical conformation is to constrain a folded peptide with a disulfide bridge. The bridge is formed by the side-chains of two Cys residues at positions  $i$  and  $i+3$  of a peptide sequence (see Figure 29), in the presence of oxidative agents.<sup>86,87</sup> The distance between the two sulfur atoms prior ring closure determines the success of this operation, and is dependent on the configuration of each of the two Cys residues. The ideal sequence is D-Cys-X-X-L-Cys, which generates a distance of 3.9 Å between the two sulfurs prior-ring closing which almost corresponds to one turn of an  $\alpha$ -helix.<sup>88</sup>

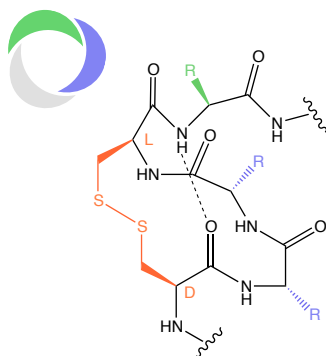


Figure 29. Generic structure of a peptide stapled with a Cys-Cys disulfide bridge (in orange).

The Spatola group synthesised a disulfide-bridged nonapeptide, which showed a disappointingly weak helical propensity (10%) in aqueous solution. Surprisingly, it was found to be a potent inhibitor of the co-activator/ER interaction, with a good  $K_i$  value of 25 nM. An X-ray crystal structure (see Figure 30) confirmed that the disulfide-linked peptide adopted a helical conformation when bound to the receptor.<sup>89,90</sup>



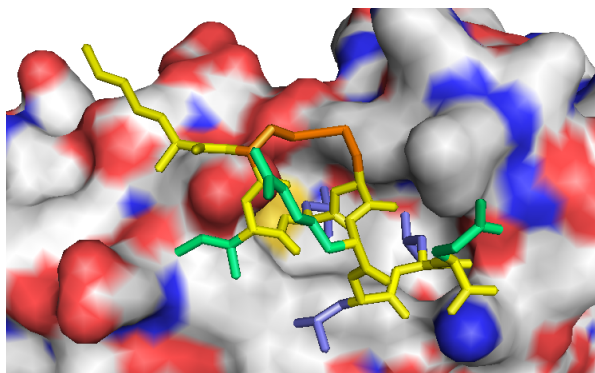


Figure 30. Crystal structure of ER $\alpha$  receptor in complex with a disulfide-bridged peptide (PDB ID: 1PCG).

#### 2.4.2.2. Lactam bridges

The lactam link is one of the most widely investigated methods for constraining a peptide, possibly because it involves the formation of an amide bond for which many coupling techniques are known to peptide chemistry. Usually natural amino acids are used, typically the  $\epsilon$ -amino group of Lys and the  $\beta$ - or  $\gamma$ -carboxyl group of Asp or Glu residues (see Figure 31).

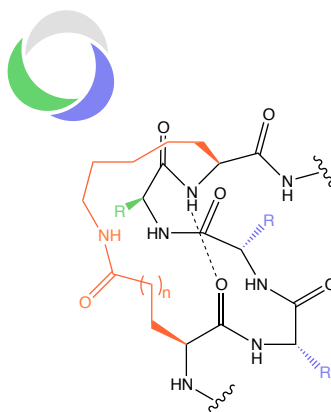


Figure 31. Generic structure of a peptide stapled with Glu ( $n=1$ )-Lys or Asp ( $n=0$ )-Lys lactam bridge (in orange).

The Rosenblatt group first reported the stabilisation of a parathyroid hormone analogue with a lactam bridge between Lys at position  $i$  and Asp at position  $i+4$ .<sup>91</sup> Although no detailed conformational studies were performed on the constrained analogue, it was 5-10 times more potent than the non-stapled parent peptide.

Other groups have successfully applied the lactam bridge strategy to develop libraries of stabilised estrogen-binding co-activator peptides, providing several potent inhibitors with IC<sub>50</sub> values of 100 nM or more.<sup>92</sup>

The Kim group reported on the stabilisation of a 14-residue peptide fragment of gp41 with a double lactam link.<sup>93</sup> The link is made between two Glu residues at position  $i$  and  $i+7$  with an  $\alpha,\omega$ -diaminobutane bridge. The constrained analogue does not display any helical propensity in aqueous solution, even with 50% of TFE as cosolvent. Nonetheless it is a potent inhibitor of the HIV-1 entry into

cells. The inhibition is more than 14-fold better with the covalently constrained peptide than with the wild type peptide.

Disulfide and lactam bridges are not always successful at stabilising  $\alpha$ -helices in aqueous solution, although in some cases they do seem to be able to provide inhibitors of  $\alpha$ -helix mediated PPI. However, they are naturally occurring functional groups and are prone to cellular degradation. Another type of tether, the hydrocarbon staple, has been developed to avoid this issue.

### 2.4.2.3. Hydrocarbon stapling

The hydrocarbon staple is an unsaturated aliphatic tether formed by a ring-closing metathesis reaction between two alkenyl side-chains (see Figure 32).

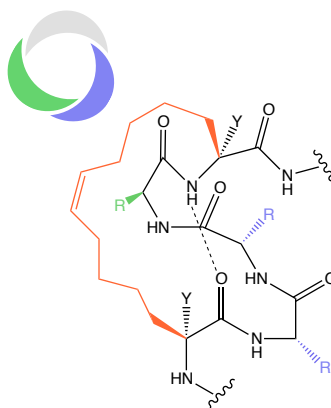


Figure 32. Generic structure of an all-hydrocarbon-stapled (in orange) peptide where  $Y = \text{Me}$  or  $\text{H}$ .

Originally, Grubbs and Blackwell introduced a hydrocarbon staple between two O-allyl L-serine residues (represented by X) at  $i$  and  $i+4$  positions in the peptide sequence Boc-VXLAibVXL-OMe. No particular evidence of enhancing helical stability was observed.<sup>94</sup>

The Verdine group introduced  $\alpha, \alpha'$ -disubstituted amino acids that bears  $\alpha'$ -alkenyl side-chains, which underwent a ruthenium catalysed RCM to afford peptides stapled at  $i - i+4$  or  $i+7$  (see in orange).<sup>95</sup>

Interestingly, the Wilson group later reported on a peptide containing an  $\alpha$ -alkenyl mono-substituted staple.<sup>96</sup> The use of  $\alpha$ -alkenyl glycine instead of  $\alpha$ -alkenyl alanine did not affect the helicity of the constrained peptide, which retained inhibitory activity against the Bcl-x<sub>L</sub>/Bak interaction comparable to its di-substituted analogue.

This all-hydrocarbon-stapled backbone approach has provided a springboard for a large number of significant studies over the last decade. Several potent inhibitors of Bcl-x<sub>L</sub>/Bak, NOXA B/Mcl-1, co-activator/ER and p53/*mDM2* interactions were discovered using this approach. Recently, a stapled peptide, ATSP-7041, has entered phase I clinical trials.<sup>97</sup> ATSP-7041 binds both *mDM2* and

*mDMX* with nanomolar affinities and shows sub-micromolar cellular activity in cancer cell lines in the presence of serum.

Crystal structures of some of these interactions revealed that the hydrocarbon staple itself participates in the binding process. For example, a stapled-p53 peptide was crystallised in a complex with *mDM2*. Figure 33 shows the hydrophobic interaction between the staple (in orange) and the hydrophobic pocket of *mDM2* and in this case augments the binding surface.<sup>98</sup>

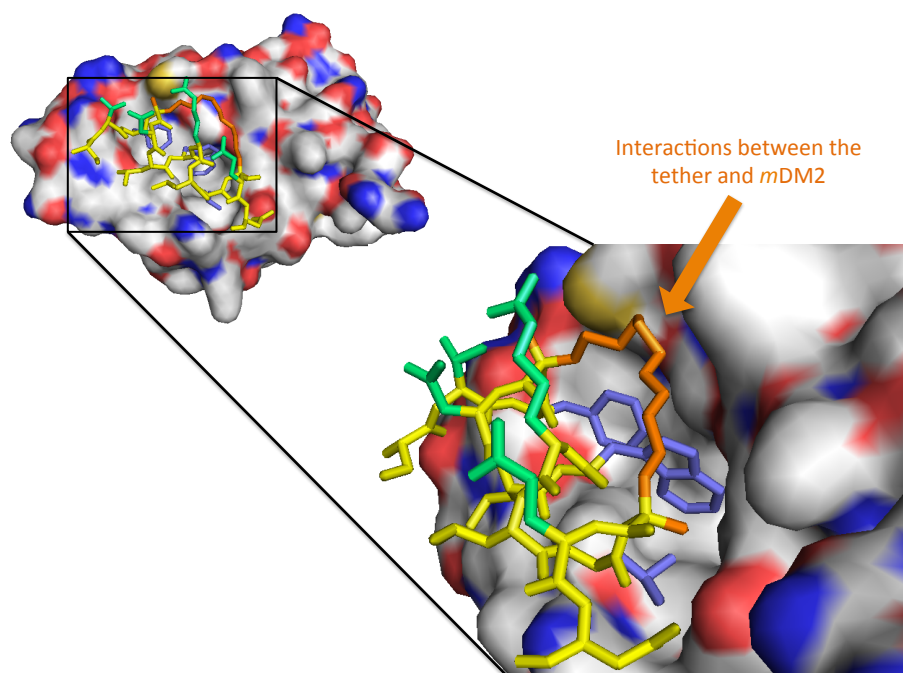


Figure 33. Crystal structure of a hydrocarbon-stapled peptide in complex with *mDM2* (PDB ID: 3V3B).

The relationship between structure and function for the covalently stapled peptide mimetics needs to be carefully considered. They can have negative impact on the binding affinity by hindering one face of the helix mimetic and decreasing the specificity to the targeted protein. To avoid this phenomenon, the hydrocarbon stapling has been adapted to provide Hydrogen Bond Surrogate.

#### 2.4.2.4. Hydrogen Bond Surrogate

Helical stabilisation through Hydrogen Bond Surrogate (HBS) implicates the replacement of one of the hydrogen bonds of an  $\alpha$ -helix with a covalent linkage (see Figure 34). The tether is thus located on the inside core of the helix. This promising approach was inspired by the work of the Satterthwaith group who explored the use of a hydrazone link to stabilise  $\alpha$ -helices.<sup>99</sup>

The installation of an HBS reaction between the  $\omega$ -alkenyl chain borne by the N atom of *i* residue and the pent-4-enoic acid residue *i*+4 employed a ring-closing metathesis. This resulted in a covalent linkage in place of a native hydrogen bond.<sup>100</sup>

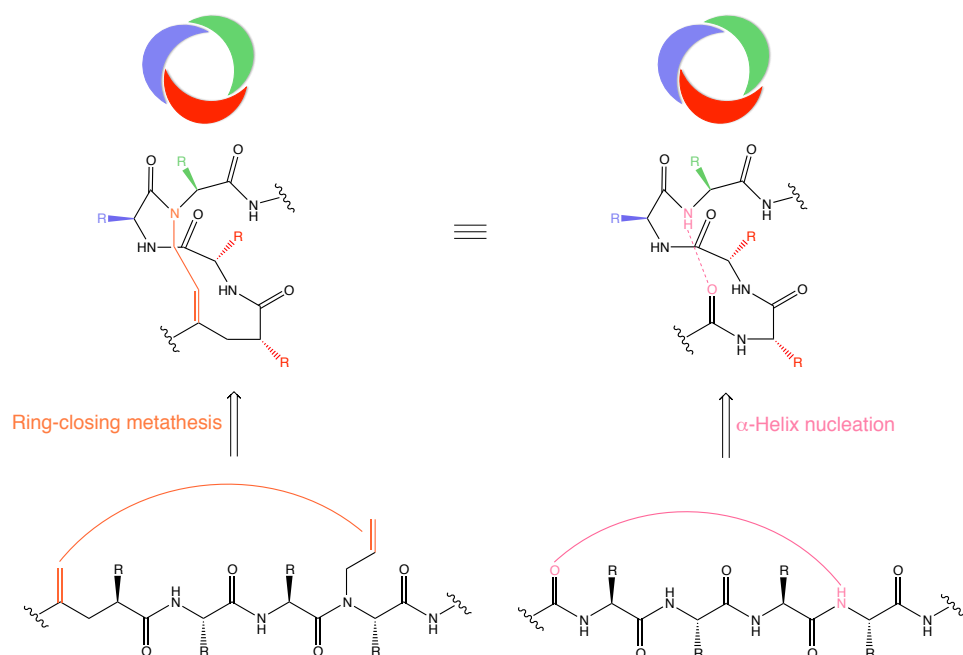


Figure 34. Hydrogen Bond Surrogate strategy.

The key advantage of HBS strategy is the placement of the crosslink on the **inside of the helix**. As a consequence, it overcomes certain limits of side-chain tethers:

- no side chains are sacrificed to nucleate stable helical conformation. All side chains are available for molecular recognition or orientation.
- it does not block one face of the putative  $\alpha$ -helix and does not impose steric hindrance. The three faces of the  $\alpha$ -helix are thus maintained (see cartoons in Figure 34).
- as a consequence of the above, it allows all the surfaces to be exposed to solvent and facilitates the orientation of the  $\alpha$ -helix for recognition process.

The HBS strategy is therefore very attractive; it allows strict preservation of the helix surfaces.

To show the advantages of HBS strategy compared to other stapled-peptide methods, the Arora group designed Bak BH3 peptide mimetics constrained by HBS against Bcl-x<sub>L</sub>.<sup>101</sup> The HBS-derived Bak peptide was able to bind Bcl-x<sub>L</sub> with a  $K_d$  of 69 nM, three fold better than the native peptide, whereas lactam-bridged Bak BH3 peptides were unable to bind Bcl-x<sub>L</sub>.<sup>102</sup>

The Arora group also designed a HBS-peptide mimetic of p53 that bound strongly and selectively to mDM2 with a  $K_d$  value of 160 nM.<sup>103</sup>

#### 2.4.2.5. Photocontrolled helicity

The Alleman group developed a system in which the helical conformation of a small peptide could be controlled by irradiation in a reversible manner.<sup>104</sup> An azobenzene crosslinker was introduced via the side chains of two Cys residues at positions  $i, i+7$  or  $i, i+11$ . Introduced at positions  $i,$

$i+7$ , the azobenzene crosslinker underwent a *trans/cis*-isomerisation upon irradiation forming a stable  $\alpha$ -helix (see Figure 35 A.), whereas when introduced at positions  $i$ ,  $i+11$ , it underwent a *trans/cis*-isomerisation destabilising the  $\alpha$ -helix (see Figure 35 B.).

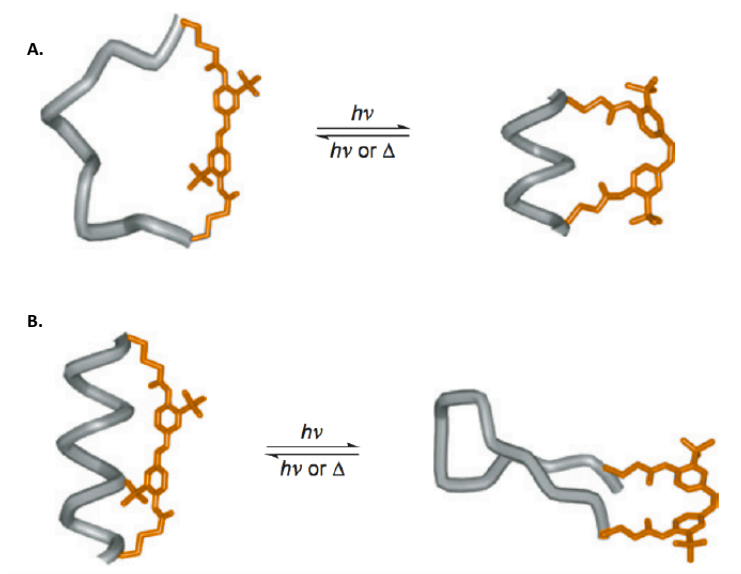


Figure 35. Photocontrol of peptide conformational preference.

Applying this principle, the Alleman group synthesised photocontrollable helices based on the BH3 domain peptides of Bak to target the anti-apoptotic Bcl-x<sub>L</sub>. Azobenzene crosslinks were located at the  $i$ ,  $i+7$  and  $i$ ,  $i+11$  positions in a Bak peptide. The Bak peptide in its helix-stabilized configuration displayed much higher affinities for Bcl-x<sub>L</sub> than its extended counterpart. The helix-stabilised configuration even showed a 200-fold selectivity for binding to Bcl-x<sub>L</sub> over helix-binding hDM2.

#### 2.4.2.6. Porphyrin-peptide conjugate

Geier and Sasaki developed an original conjugation system based on a porphyrin ring.<sup>105</sup> The porphyrin link was predicted to stabilise the  $\alpha$ -helical conformation of the 14-residue peptide Ac-ACEQLLKELLQKCA-NH<sub>2</sub> (see Figure 36 B). The  $\alpha$ -helicity reached 70% in phosphate buffer with 10% of TFE. The helical propensity was largely due to a connection between the side chains of two Cys residues  $i$  and  $i+11$  to a porphyrin ring (in orange), two salt bridges between Lys and Glu side chains (in blue) and the introduction of hydrophobic and helix-promoter residues, Ala and Leu (in red) (see Figure 36 A).

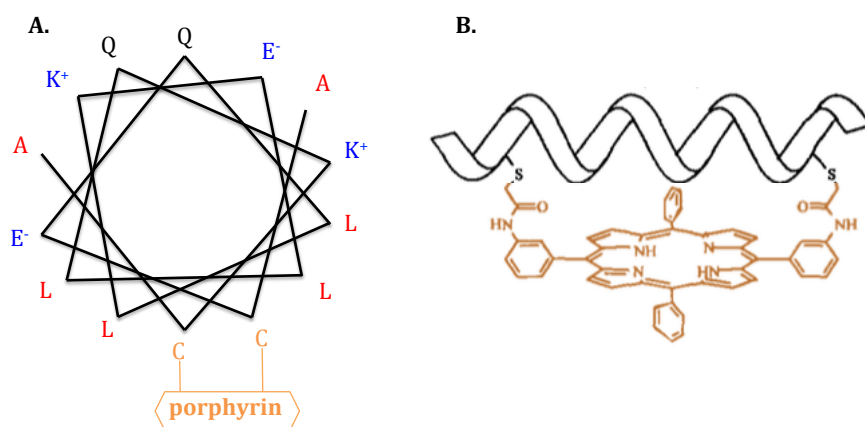


Figure 36. A: Helical wheel view. B:  $\alpha$ -Helix ribbon strapped porphyrin between two Cys residues.

The porphyrin ring also functions as a **potential catalytic site** for oxidation of organic substrates mimicking the oxidative activity of the cytochrome P450 monooxygenase family. In this way, the  $\alpha$ -helical peptide provides a chiral, hydrophobic substrate-binding. This study is one of the first examples of **mini-protein mimetics** and shows another promising application of  $\alpha$ -helix mimetics.

### 2.4.3. Use of non-helical peptides

Other platform-based peptides can be used to mimic the  $\alpha$ -helix interacting surface, as long as they provide a robust presentation platform upon which the side-chains required for protein surface recognition can be displayed in a structurally defined manner.

The Fasan group designed a macrocyclic  $\beta$ -hairpin, stabilised by a D-Pro–L-Pro dipeptide motif to mimic the  $\alpha$ -helix of p53(15-29) peptide.<sup>106</sup> On one face, the  $\beta$ -hairpin displayed the key side-chains by providing a geometry similar to that seen in p53 (see Figure 37 A).

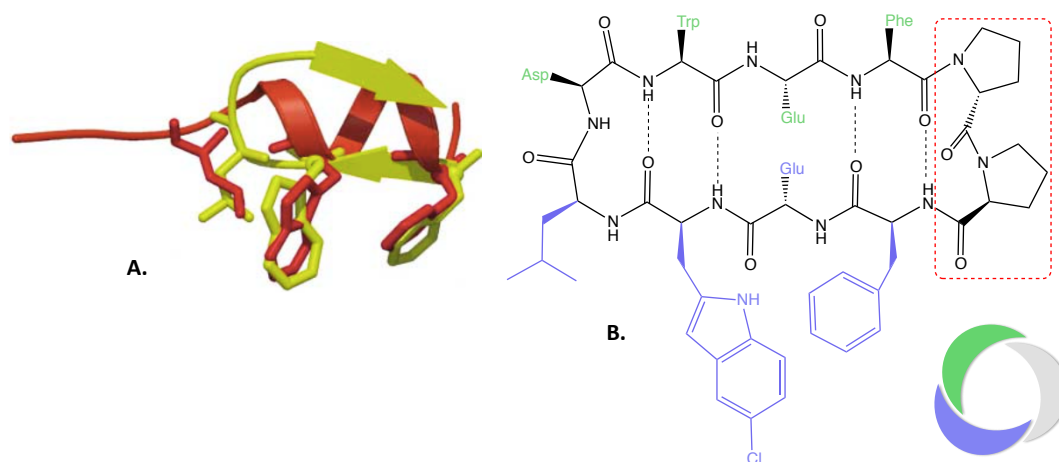


Figure 37. A: Macrocyclic  $\beta$ -hairpin (in yellow) superimposed on p53 (15-29) peptide (in orange). B:  $\beta$ -hairpin with the smallest  $IC_{50}$  against p53/hDM2, showing the hot-spot residues (in purple) and the D-Pro-L-Pro (in red).

The distance between the C $\alpha$  atoms of two residues  $i$  and  $i+2$  along one strand of a  $\beta$ -hairpin was similar to the C $\alpha$  atoms of two residues  $i$  and  $i+4$  along an  $\alpha$ -helix. This feature was well illustrated by the perfect superimposition of the Trp and Phe side-chains of the  $\beta$ -hairpin mimetic and the  $\alpha$ -helical p53 in Figure 37 A. The Fasan group carried out a competitive assay with a library of  $\beta$ -hairpin mimetics against the p53/hDM2 interaction and found the best inhibiting candidate (see Figure 37 B) to have an excellent IC<sub>50</sub> of 140 nM.<sup>106</sup>

Despite these encouraging results, several drawbacks impose limits on the general use of these scaffolds as  $\alpha$ -helix mimetics:

- only two faces of the helix can be mimicked, as it is illustrated in Figure 37.
- the rigidity of this hairpin. Molecular modelling of a  $\beta$ -hairpin mimetics under nOe restraints is shown in Figure 38 A. The structures before and after optimisation are completely overlaid, with a RMSD of 0.53 Å, showing again the extreme rigidity of the system (see Figure 38 B).

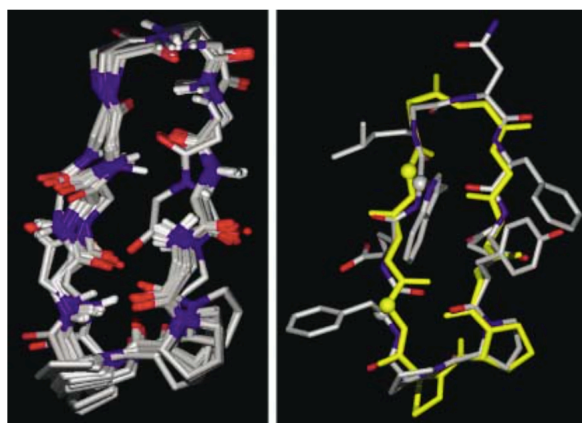


Figure 38. A: Superimposition of 20  $\beta$ -hairpin backbone atoms optimised by molecular modelling. B: Superposition of one typical optimised structure and the starting  $\beta$ -hairpin model peptide (in yellow).

## 2.5 Use of helical peptide foldamers as $\alpha$ -helix mimetics

The major challenges of  $\alpha$ -helix mimetics have not been entirely overcome even using constrained  $\alpha$ -peptide mimetics:

- their  **$\alpha$ -helical structure is not stable in aqueous solution**. Mostly one helical turn is promoted and the rest of the helix frays rapidly, decreasing the overlay of the side-chain mimics.
- even when the mimetics are successful,  $\alpha$ -peptides are **very sensitive to proteolytic degradation**, limiting *in vivo* application.

To face these major issues, the use of synthetic oligomers containing unnatural amino acids has emerged significantly these past two decades. These peptidomimetics are a large subgroup, and the first studied, in the emerging science of foldamers. A foldamer is ‘any oligomer that folds into a

conformationally ordered state in solution, the structures of which are stabilised by a collection of noncovalent interactions between nonadjacent monomer units'.<sup>71</sup>

### 2.5.1. $\beta$ -Peptides

#### 2.5.1.1. Helical diversity adopted by $\beta$ -peptides

The most thoroughly studied  $\alpha$ -helix peptide mimetics containing unnatural amino acids are  $\beta$ -peptides. Related to  $\alpha$ -amino acids,  $\beta$ -amino acids are homologated analogues having an additional backbone carbon atom inserted between the carboxylic acid and the amino groups. According to the position of the additional carbon,  $\beta$ -amino acids are called  $\beta^3$ -amino acid when it is adjacent to the carboxylic acid group and  $\beta^2$ -amino acid when the insertion is adjacent to the amino group (see Figure 39).<sup>ii</sup> By extension, the di-, tri- and tetra-substituted amino acids including cyclic  $\beta$ -amino acids are defined in Figure 39.

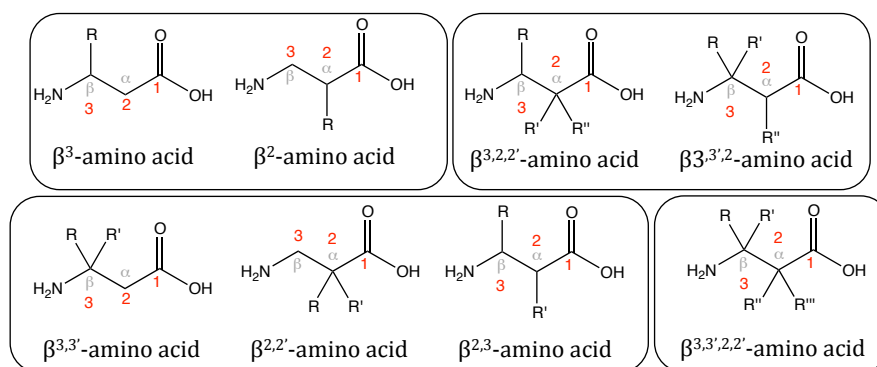
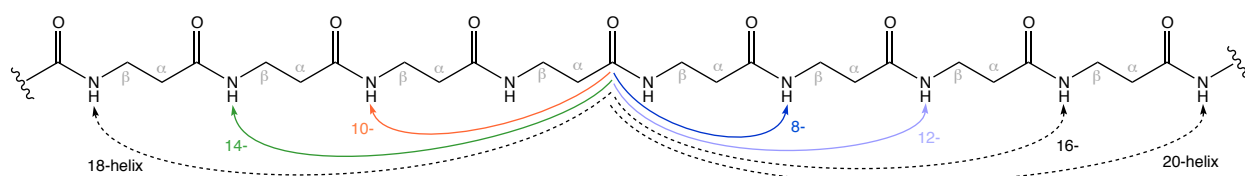


Figure 39. Definition of different classes  $\beta$ -amino acids

There is a wide diversity of acyclic and cyclic  $\beta$ -amino acids, whose different dihedral angle values theoretically allow seven types of helix predicted by the Hofmann group by *ab initio* calculations (see Figure 40).<sup>107</sup> Their hydrogen-bonded rings are illustrated by the full arrows in Figure 40.



Figure

40. Poly  $\beta$ -amino acid backbone. The arrows indicate hydrogen bonds associated with the seven tightest helices available to  $\beta$ -peptides.

<sup>ii</sup>  $\beta^3$ -amino acids that feature unchanged side chains of their analogous  $\alpha$ -amino acid (X), are called  $\beta^3$ -hX. For example, 3-amino-3-methyl-propanoic acid is called  $\beta^3$ -hAla.



Six distinct helices have been described so far: the 8-, 10-, 10/12-, 12-, 14- and 18/20-helices.

The **8-helix** is rarely encountered in peptides. The Seebach group found the first example of a  $\beta$ -peptide stabilised by 8-membered hydrogen-bonded rings. The hexapeptide was a homooligomer of a particular achiral  $\beta^{2,2}$ -amino acid, 1-aminomethylcyclopropanecarboxylic acid, and had a stair-like arrangement rather than a proper helical conformation (see Figure 41 A).<sup>108</sup> The Cosstick group reported an 8-helical conformation adopted by a four-residue  $\beta$ -peptide.<sup>109</sup> The tetramer was composed of thymidine  $\beta$ -amino acids based on deoxyribose rings (see Figure 41 B). The Ortuño group suggested that a small tetramer of *trans*-ACBC (2-aminocyclobutanecarboxylic acid) was able to adopt an 8-helical conformation in organic solvents (see Figure 41 C).<sup>110</sup> Recently, a longer stable 8-helix was obtained in the Aitken group, using a homooligomer of *trans*-ACBC with a AAzC (*N*-aminoazetidine-2-carboxylic acid) promoter at the N-terminal position (see Figure 41 D).<sup>111</sup> The 8-helical conformation was induced by a strong hydrazine turn (in pink) adopted by the AAzC residue and was stable in protic solution for a peptide length up to 6 residues.

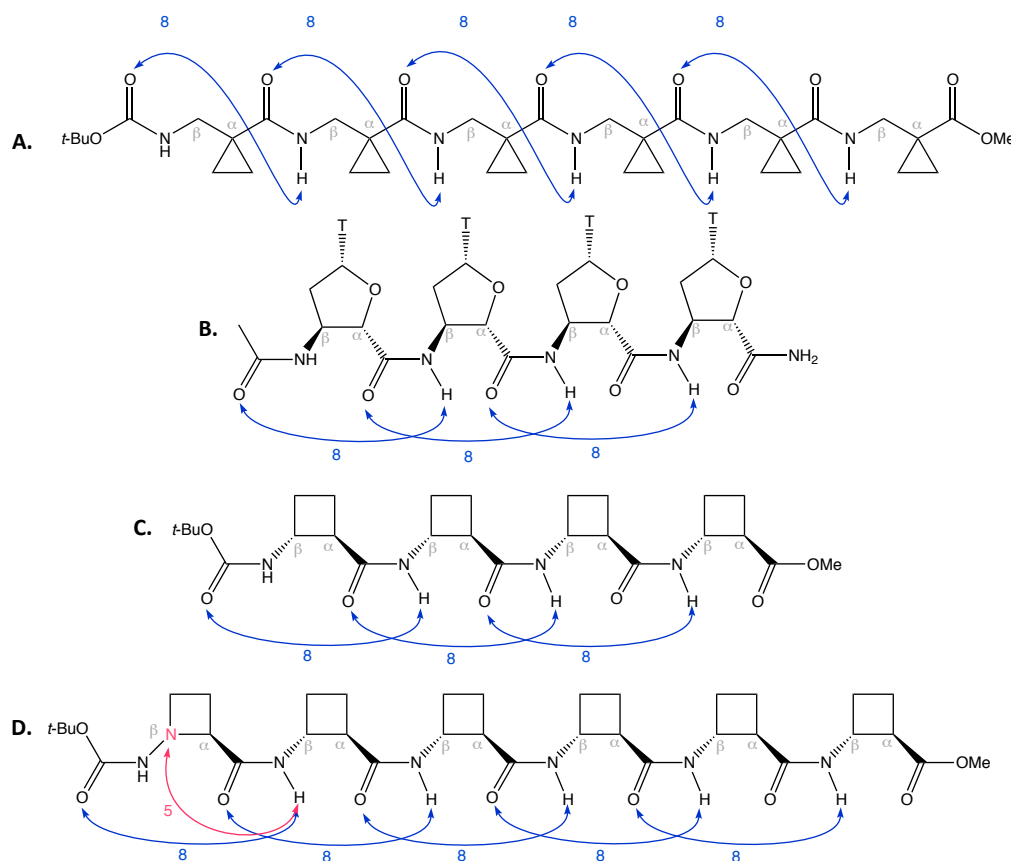


Figure 41. 8-Helices adopted by  $\beta$ -peptides.

Like the 8-helix, the **10-helix** is a rarity for  $\beta$ -peptides. The Fülöp group reported that a tetramer of *trans*-ACHC (2-aminocyclohexanecarboxylic acid) was able to fold into a 10-helix in protic solution (see Figure 42 A).<sup>112</sup> The Fleet group showed that a hexamer of a substituted *cis*-oxetane  $\beta$ -

amino acid was able to form a 10-helix in organic solvent (see Figure 42 B).<sup>113</sup> It is of note that in contrast, homooligomers of *cis*-ACBC adopt a strand conformation stabilised by 6-membered hydrogen-bonded rings.<sup>114</sup>

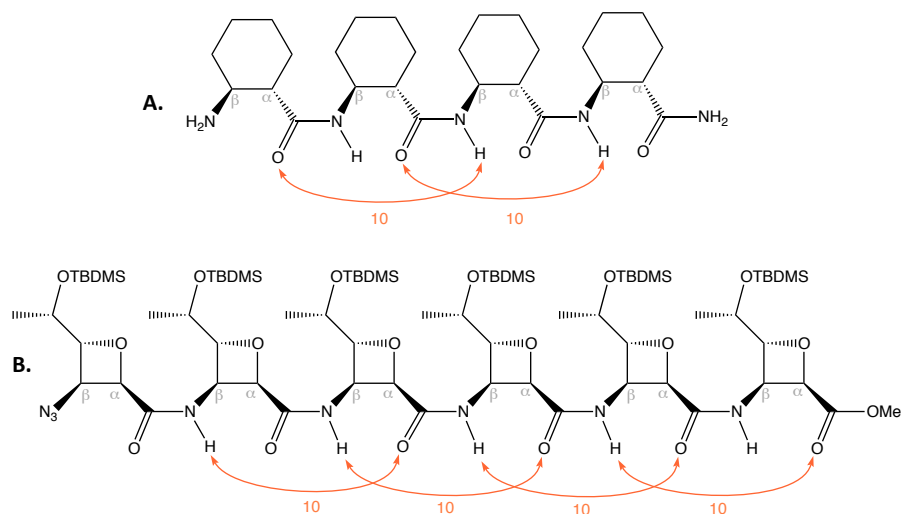


Figure 42. 10-Helices adopted by  $\beta$ -peptides.

The Fülöp group found that oligomers of *trans*-ACPC (*trans*-2-aminocyclopentanecarboxylic acid) adopt various conformations depending on the configuration of the building block.<sup>115</sup> The heterochiral hexamer of N-terminal unprotected *cis*-ACPC adopts the **10/12-helix** consisting of 10- and 12-membered hydrogen-bonded rings (see Figure 43 A), whereas heterochiral hexamer of *trans*-ACPC forms parallel and anti-parallel strands stabilised by intermolecular hydrogen bonds. More recently, the Fülöp and Martinek group observed that the type of helix adopted by a heterochiral heptamer of *cis*-ACPC in solution changed with its concentration. This heptamer folded into the 10/12-helix at very low concentration (10  $\mu$ M) but was able to fold into the largest-diameter foldameric helix currently known, the **18/20-helix**, at higher concentration (100  $\mu$ M).<sup>116</sup> The Seebach group found another 10/12-helix with less steric constraints: a hexapeptide alternating  $\beta^3$ - and  $\beta^2$ -amino acids (see Figure 43 B).<sup>117</sup>

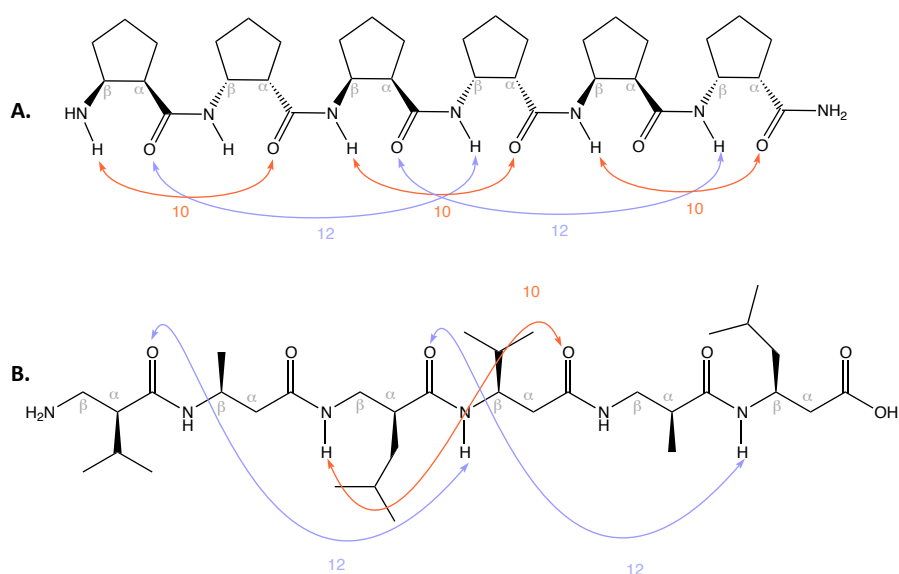


Figure 43. 10/12-Helices adopted by *cis*-ACPC oligomer.

The **12-helix** has only been experimentally observed for oligomers of cyclic  $\beta^{2,3}$ -amino acids. It is characterised by a 12-membered hydrogen-bonded ring network between the CO of residue  $i$  and NH of residue  $i+3$ .

According to the theoretical studies by Hofmann, the 12-helix is favoured by  $\beta$ -amino acids with a  $\theta$  dihedral angle of  $87^\circ$ .<sup>107</sup> A value of around  $90^\circ$  is found in *trans*-ACPC and *trans*-ACBC. Indeed, homooligomers of these cyclic  $\beta$ -peptides behave as a 12-helices in protic solvents (see Figure 44 A B).<sup>118,119</sup> It is important to note that the folding behaviour of *trans*-ACBC oligomers changes according to the oligomer length. From a sequence of six amino acids, a global folding into a 12-helix is favoured over the local folding imposed by the spontaneous 8-membered hydrogen-bonded rings of *trans*-ACBC.<sup>120</sup>

Besides monocyclic  $\beta$ -amino acid building blocks, the effect of strained bridged bicyclic amino acids have also been investigated. For example, homooligomers of *trans*-ABHC (2-amino-6,6-dimethyl-bicyclo[3.1.1]-heptane-3-carboxylic acid) were synthesised and studied by the Fülöp group. The apopinane moiety is a dimethyl-substituted and methylene-bridged analogue of *trans*-ACHC. Molecular modelling of a *trans*-ABHC  $\beta$ -hexapeptide gave two low-energy conformers: a 12-helix, which dominated the conformational landscape (see Figure 44 C) and a less abundant **16-helix**, which has not yet been detected experimentally.<sup>112</sup>

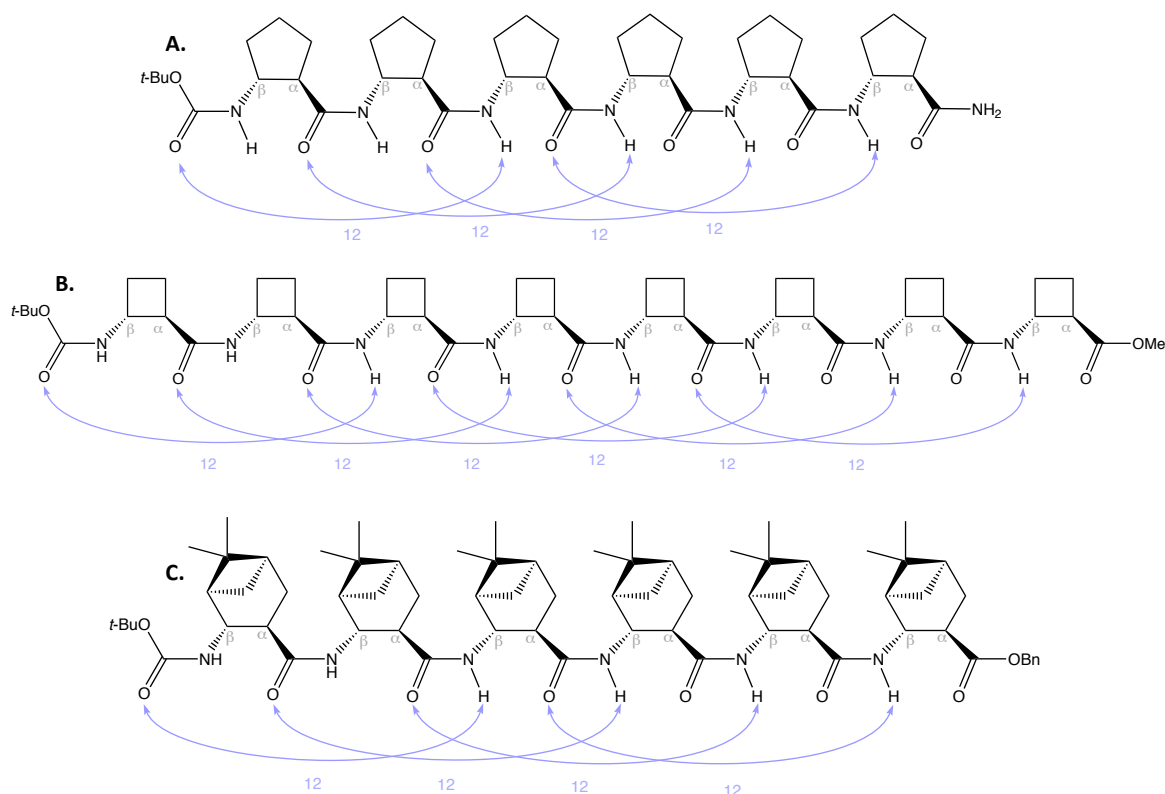


Figure 44. 12-Helices adopted by  $\beta$ -peptides.

The **14-helix** has been the most documented of the helical folding structures of  $\beta$ -peptides. It is characterised by a 14-membered hydrogen-bonded ring network between the NH of residue  $i$  and CO of residue  $i+2$ , implicating three-residue in each hydrogen-bonded ring.

One of the simplest  $\beta$ -sequences is composed of homologated  $\beta^3$ -amino acids. The Seebach group showed that a hexapeptide constructed from  $\beta^3$ -amino acids bearing hydrophobic side chains was able to fold spontaneously into a 14-helix in protic solvents (see Figure 45 A). The study was extended to consider peptides constructed from  $\beta^2$ -amino acids featuring similar side chains. These  $\beta^2$ -peptides also folded into a 14-helix but this structure was less stable than its  $\beta^3$ -peptide congener due to weaker hydrogen bonds (see Figure 45 B).<sup>121</sup> In contrast, hexapeptides constructed alternatively from  $\beta^2$ - and  $\beta^3$ -amino acids fold into a 10/12-helix (see Figure 43 B).<sup>117</sup> Furthermore, tripeptides of di-substituted  $\beta^{2,3}$ -amino acids adopt a  $\beta$ -strand-like structure rather than a helical structure.<sup>122</sup>

Constrained cyclic amino acids, with the appropriate  $\theta$  dihedral angles of  $60^\circ$ , are also able to give a 14-helix. Homooligomers of *trans*-ACHC were predicted to fold into helical structures with the 14-helix as the most stable conformer.<sup>123</sup> As seen previously, tetrapeptides of unprotected *trans*-ACHC fold into a 10-helix while tetrapeptides of correctly N-protected *trans*-ACHC and longer oligomers fold into a stable 14-helix (see Figure 45 C).<sup>124</sup>

Mixed peptides composed alternately of cyclic  $\beta$ -amino acids and unsubstituted amino acids were investigated by the Ortuño group.<sup>125</sup> A tetrapeptide alternating *cis*-ACBC and  $\beta$ -alanine was reported to fold into a short **14-helix** through two hydrogen bonds. In contrast with other foldamers,

the conformational freedom brought by  $\beta$ -alanine was the key feature for the peptide to be able to adopt its global folding behaviour; as we mentioned before, homooligomers of *cis*-ACBC adopted a local folding through 6-membered hydrogen-bonded rings.<sup>114</sup>

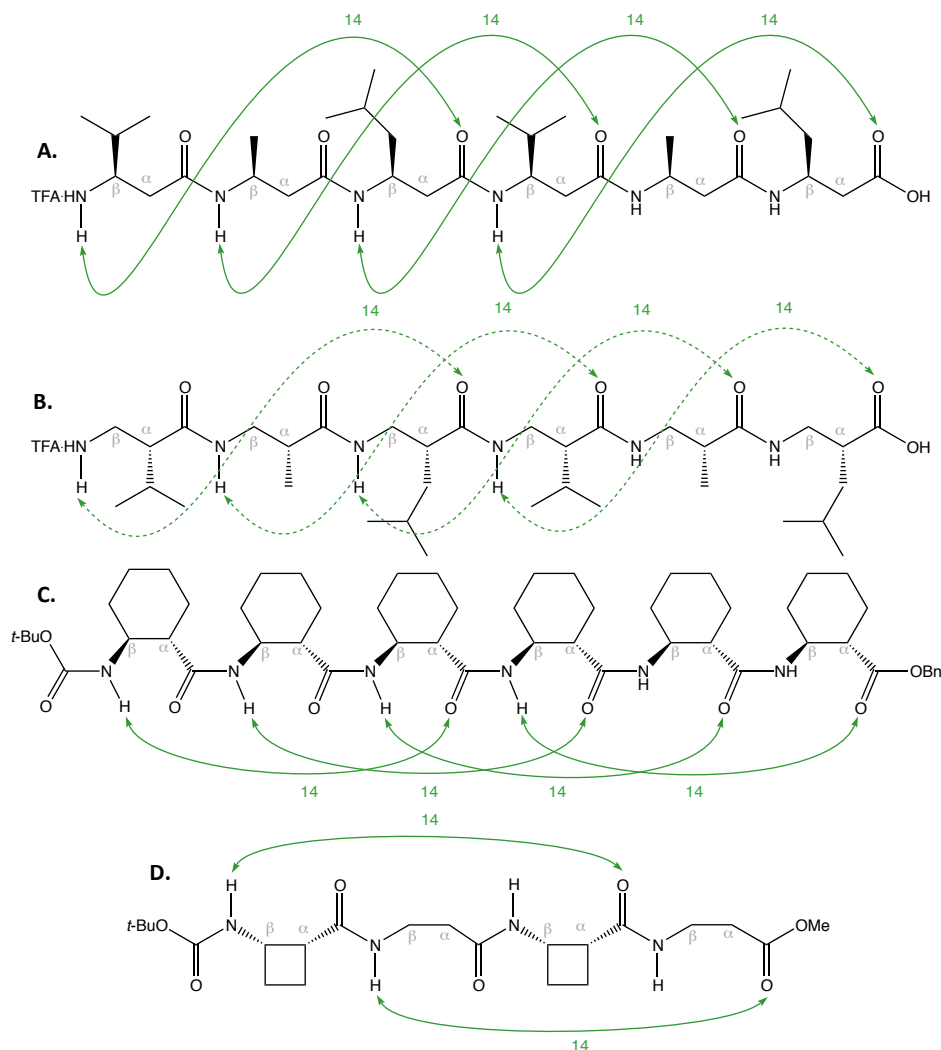


Figure 45: The 14-helices adopted by  $\beta$ -peptides

As it was indicated on several occasions in this section, the types of helix adopted by short  $\beta$ -peptides conformation may change with the length of their sequence (see Table 2). For example, the oligomer of *trans*-ACBC adopts a stable 8-helix up to 4 residues and a 12-helix in peptides longer than 6 residues. And the homooligomer of unprotected *trans*-ACHC adopts a 10-helix up to 4 residues and a 14-helix beyond.

Retrospectively it would have been interesting to study the folding behaviour of longer oligomers than tetramer of thymidine  $\beta$ -amino acids or tetramer of 1-aminomethylcyclopropanecarboxylic acid.

Table 2: Folding behaviour of  $\beta$ -peptides in solution according to their length

Building blocks of homooligomer	Folding behaviour in solution		
	Up to 4 residues	Up to 6 residues	Longer than 6 residues
Thymidine $\beta$ -amino acid	8-helix	ND	ND
1-aminomethyl-cyclopropanecarboxylic acid	8-ribbon	ND	ND
<i>trans</i> -ACBC	8-helix	12-helix	12-helix
<i>trans</i> -ACBC with <i>trans</i> -AAzC promoter	8-helix	8-helix	12-helix
Unprotected <i>trans</i> -ACHC	10-helix	14-helix	14-helix

### 2.5.1.2. Helical $\beta$ -peptides mimicking the $\alpha$ -helix

The 12-helix and 14-helix are the closest structures adopted by  $\beta$ -peptides that match the backbone of the native  $\alpha$ -helix (which is also a 13-helix). Considering the 12-helix constructed from (*S,S*)- $\beta^{2,3}$ -amino acids and the 14-helix constructed from (*S*)- $\beta^3$ -amino acids, it is possible to compare the three helices (see Figure 46).

The 12-helix or 2.5(12)-helix of  $\beta$ -peptides was thought to be well suited to mimic the native  $\alpha$ -helix. The macrodipoles are oriented in the same direction with respect to the orientation N-terminus to C-terminus and the chirality of the helix is the same (P). The two helices also have a similar pitch of 5.4 despite a difference of almost one residue per turn, 3.6 for the  $\alpha$ -helix and 2.5 for the 12-helical  $\beta$ -peptide.

The 14-helix or 3(14)-helix of  $\beta^3$ -peptides possesses 3 residues per turn which is close to the  $\alpha$ -helix. The chirality of the 14-helix is the same (P), but the pitch is larger for the 14-helix and the macrodipole is oriented in the reverse direction of the  $\alpha$ -helix with respect to the orientation N-terminus to C-terminus.

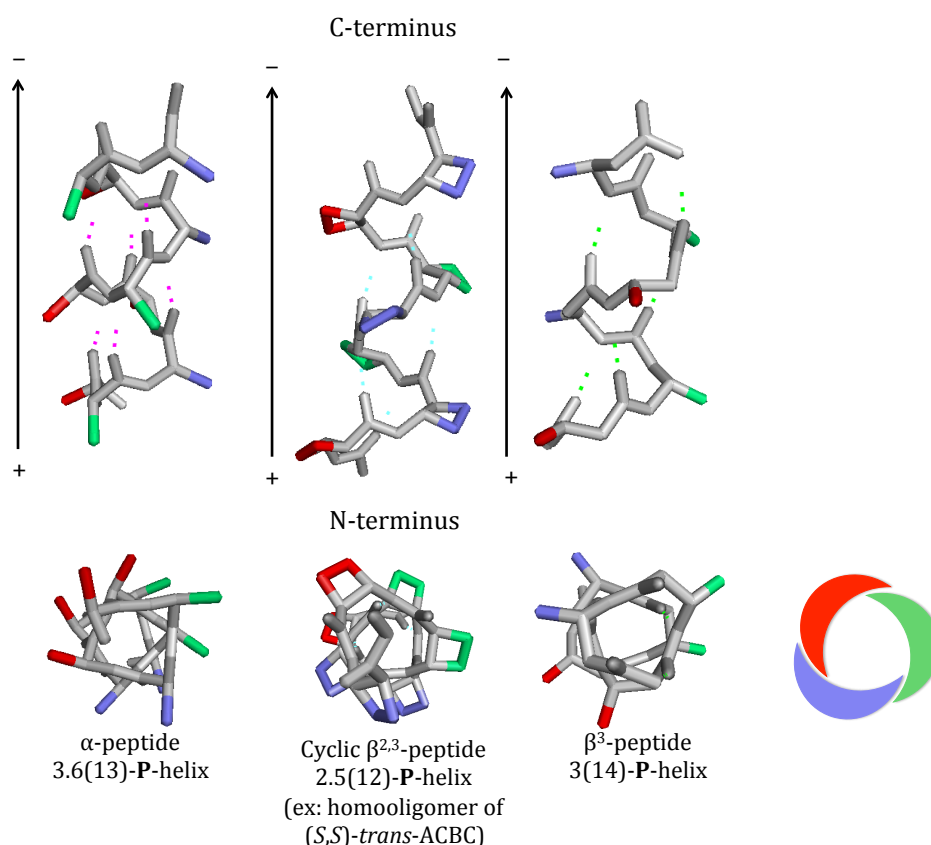


Figure 46. Comparison between the  $\alpha$ -helix and the 12- and 14-helices of  $\beta$ -peptides.

The structure similarities between 12- and 14-helical  $\beta$ -peptides and the native  $\alpha$ -helix have led researchers to develop them as scaffolds for  $\alpha$ -helix mimetics and evaluate them in several biological applications.

Type I mimetics are composed of various helical peptides including  $\alpha$ -peptides. However, even with a helical conformation, these peptides are still prone to proteolytic degradation limiting their utility as pharmaceutical drugs. Foldamers composed of unnatural amino acids present the crucial advantage of being **resistant to the proteolytic enzymes**. Many tests were carried out on  $\beta$ -peptides with all types of enzymes, from mammals, yeasts and bacteria, and *in vivo* examination, in mice, rats, insects and plants; these showed that they were completely stable towards proteolysis. Two  $\beta$ -peptides were even shown to be stable towards catabolism. In addition to being stable, such  $\beta$ -peptides display **weak cytotoxic**, antiproliferative, hemolytic, immunogenic, or inflammatory properties either in cell cultures or *in vivo*.<sup>126</sup>

Most multicellular organisms produce antimicrobial  $\alpha$ -helical peptides as part of their natural defence system.<sup>10</sup> Because of their more stable helical propensity,  $\beta$ -peptides have been developed as **antibacterials**. They were designed to be helical and amphiphilic by displaying cationic side chains or charged atoms in the ring of cyclic residues.

The Gellman group synthesised a 17-residue  $\beta$ -peptide with an antibiotic activity similar to the family of natural  $\alpha$ -peptides, the magainins.<sup>127</sup> The  $\beta$ -peptide was made up of *trans*-ACP (*trans*-4-aminopyrrolidine-3-carboxylic acid) and *trans*-ACPC residues that form a cationic (in blue) and a hydrophobic faces (in red) respectively. It was able to fold into a 12-helix in methanol and aqueous buffer (see Figure 47) whereas the magainins do not adopt a helical structure in the absence of membranes. The introduction of *trans*-ACP residues is crucial for the aqueous solubility and for displaying cationic side chains to selectively target the negatively charged microbial membranes.

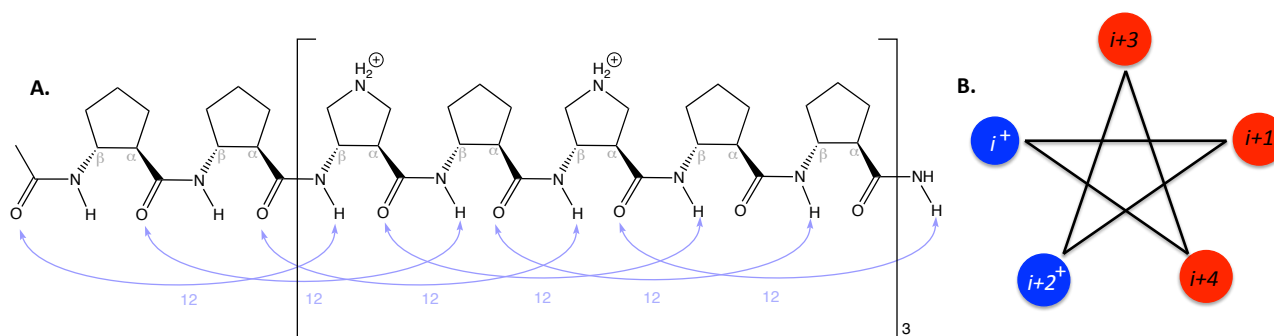


Figure 47. A: A 12-helical antimicrobial  $\beta$ -peptide. B: Top view of the  $\beta$ -peptide displaying the cationic residues (in blue) and the hydrophobic residues (in red).

Several 12- and 14-helical  $\beta$ -peptides have been designed as  $\alpha$ -helix mimetics to serve as inhibitors of PPIs.

The Gellman group designed many 12-helical  $\beta$ -peptides to mimic the p53(15-29) segment<sup>iii</sup> by incorporating the 12-helix-promoting residue *trans*-ACPC. However, the introduction of this residue makes the external diameter of the 12-helix considerably wider leading to a very low inhibition of p53/*mDM2* interaction with the most active derivative presenting an  $IC_{50}$  of 250  $\mu$ M in a p53/*mDM2* ELISA.<sup>128</sup> Although in principle the 12-helix was thought to be an ideal  $\alpha$ -helix mimetic, 12-helical  $\beta$ -peptides are actually not well suited for mimicry of  $\alpha$ -helical domains due to steric hindrance imparted by the constrained 12-helix-promoting residues.

The Schepartz group developed a  $\beta^3$ -peptide, called  $\beta^3$ 53, that is able to fold into a 14-helix, as expected for  $\beta^3$ -peptides (see Figure 48 A).<sup>129</sup> As noted previously with  $\alpha$ -peptides (see 2.1.2), the helicity was enhanced by salt bridges between the  $\beta^3$ -*hOrn* (*i*) and  $\beta^3$ -*hGlu* (*i*+4) residues on one face of the helix (green face).  $\beta^3$ 53 was designed to mimic the p53(15-29) segment by displaying the three hot-spot residues involved in the p53/*hDM2* interaction. Because a 14-helical  $\beta^3$ -peptide adopted an inverse chirality turn compared to the  $\alpha$ -helix, the hot-spot residues (in blue) were positioned in the reverse order:  $\beta^3$ -*hLeu* at position *i*,  $\beta^3$ -*hTrp* at *i*+4 and  $\beta^3$ -*hPhe* at *i*+7. The key residues were arrayed along one helical face (blue face) in the folded conformation and overlay well with the key residues of p53(15-29) co-crystallised with *hDM2* (Figure 48 B).  $\beta^3$ -53 and other derivatives were tested in a

<sup>iii</sup> p53(15-29) corresponds to the segment of amino acids from position 15 to 29 of p53 protein.



competitive assay against p53/hDM2.  $\beta$ 53 had a weak inhibition ( $IC_{50} = 94 \mu M$ ) and a derivative that displayed  $\beta^3$ -hIle instead of  $\beta^3$ -hVal residues was the most potent ( $IC_{50} = 13 \mu M$ )  $\beta$ -peptides.<sup>130</sup>

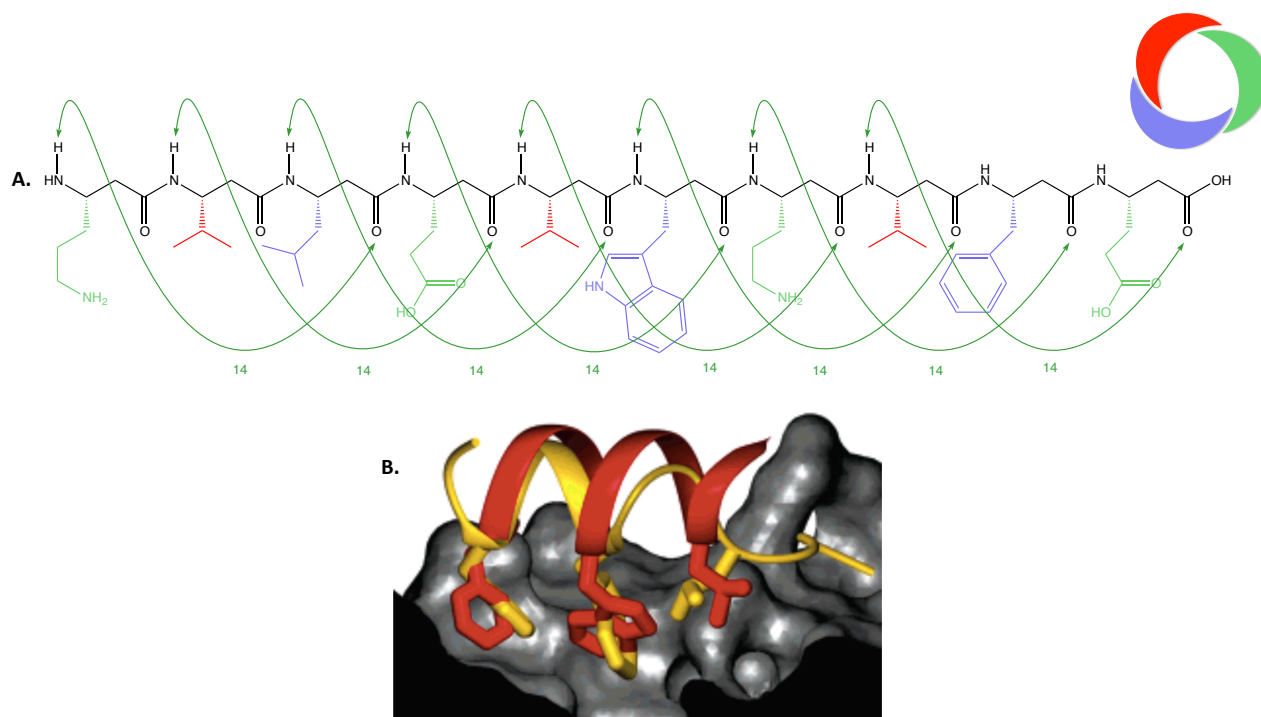


Figure 48. A: A 14-helical  $\beta$ -peptide designed as p53 mimetics. B: Superimposition of the 14-helical  $\beta$ -peptide and co-crystal of p53(15-29) in the binding pocket of hDM2 (PDB ID: 1YCR).

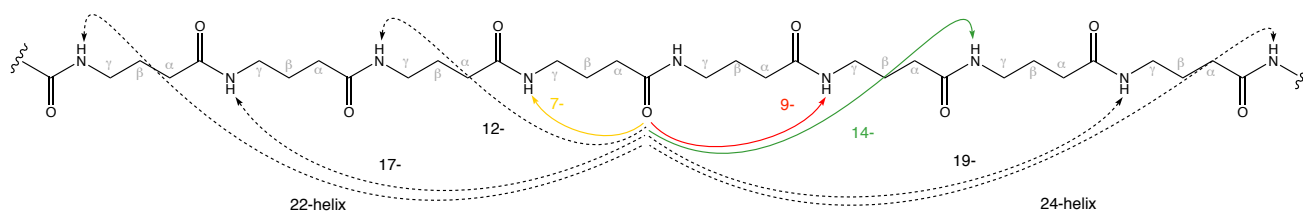
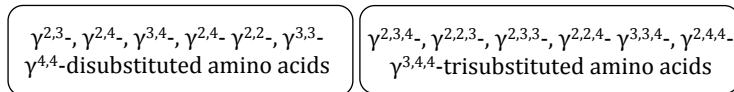
These studies on the application of  $\beta$ -peptides proved that **12-helical** and **14-helical  $\beta$ -peptides can be used as type I mimetics of the  $\alpha$ -helix** in different biological contexts.

## 2.5.2. $\gamma$ -Peptides

### 2.5.2.1. Helical diversity adopted by $\gamma$ -peptides

Related to  $\alpha$ -amino acids,  $\gamma$ -amino acids are doubly-homologated analogues having two additional carbons inserted between the carboxylic acid and the amino groups. According to the position of the side-chain,  $\gamma$ -amino acids are called  $\gamma^2$ -amino acid when the substituent is adjacent to the carboxylic acid group (or at the  $\alpha$  position),  $\gamma^3$ -amino acid when it is at the  $\beta$  position and  $\gamma^4$ -amino acid when it is adjacent to the amino group (or at the  $\gamma$  position) (see Figure 49).<sup>iv</sup> By extension, the di-, tri-, tetra-, penta- and hexa-substituted amino acids including cyclic  $\gamma$ -amino acids give 24 possibilities of substitution.

<sup>iv</sup>  $\gamma^4$ -amino acids that feature unchanged side chains of their analogous  $\alpha$ -amino acid (X), are called  $\gamma^4$ -hX. For example, 4-amino-4-methyl-butanoic acid is called  $\gamma^4$ -hAla.



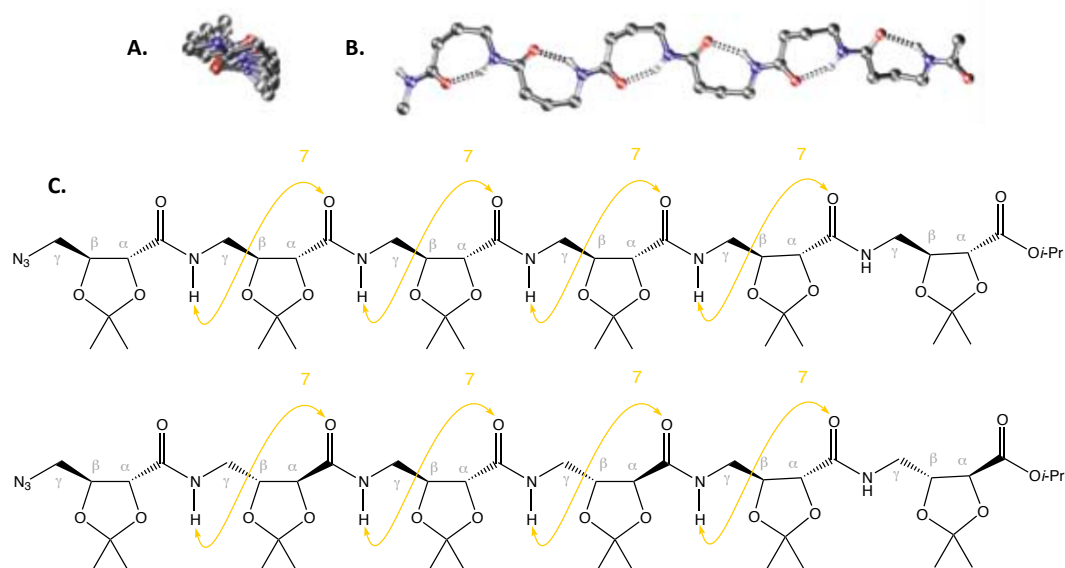


Figure 51. A: Top and B: Side view of the theoretical 7-helix composed of GABA also considered as a 7-ribbon. C: The 7-ribbon adopted by trans-dioxolane homooligomers.

According to the theoretical work of Hofmann, the 9-helix is one of the two most stable helical conformers for  $\gamma$ -peptides. The Kunwar group synthesised  $\gamma$ -peptides comprised alternately of a  $\gamma^4$ -amino acid derived from D-xylose and the unsubstituted  $\gamma$ -amino acid, GABA. A regular **9-helix** was observed for these  $\gamma$ -peptides in solution (see Figure 52).<sup>133</sup> Such an observation contrasts with the work of Ortuño on  $\beta/\gamma$ -peptides, developed later (see 2.5.5). Significantly, it transpires that only one substituent borne by one in every two residues in a  $\gamma$ -peptide was sufficient to induce 9-membered hydrogen-bonded rings. Here the GABA residue did not act as a spacer, but participated in the propagation of the H-bond network leading to the global folding behaviour of the  $\gamma$ -peptide.

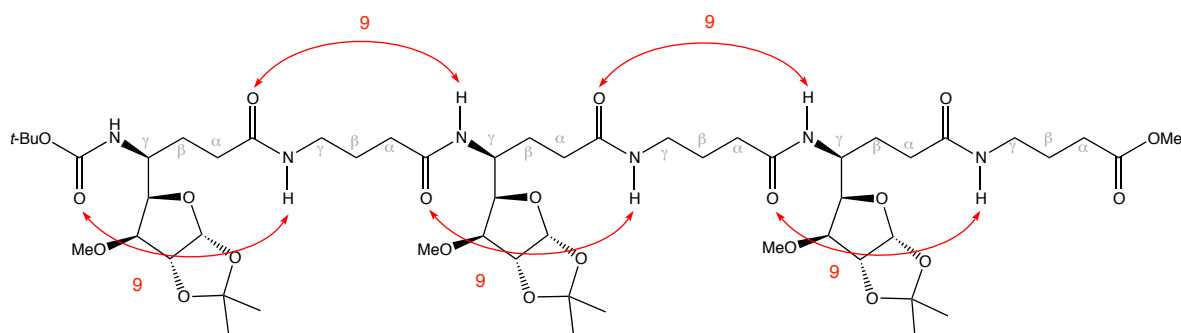


Figure 52. The 9-helix adopted by alternating carbo- $\gamma^4$ -amino acid and GABA hexamer.

The other most stable helical conformer of a  $\gamma$ -peptide is the **14-helix**. The Hannessian and Seebach groups independently discovered this structure by studying the folding behaviour of  $\gamma$ -peptides substituted on positions  $\gamma^4$ -,  $\gamma^3$ -,  $\gamma^2$ -,  $\gamma^{2,4}$ - and  $\gamma^{2,3,4}$ -. Surprisingly,  $\gamma^4$ -,  $\gamma^{2,4}$ - and  $\gamma^{2,3,4}$ -peptides all fold into the same 14-helix (see Figure 53)<sup>134–137</sup> while  $\gamma^3$ - and  $\gamma^2$ -peptides appear to adopt a flexible structure which is therefore hard to determine. From these results, it clearly appears that a single substituent at the  $\gamma^4$  position is sufficient to promote a robust 14-helix in  $\gamma$ -peptides.

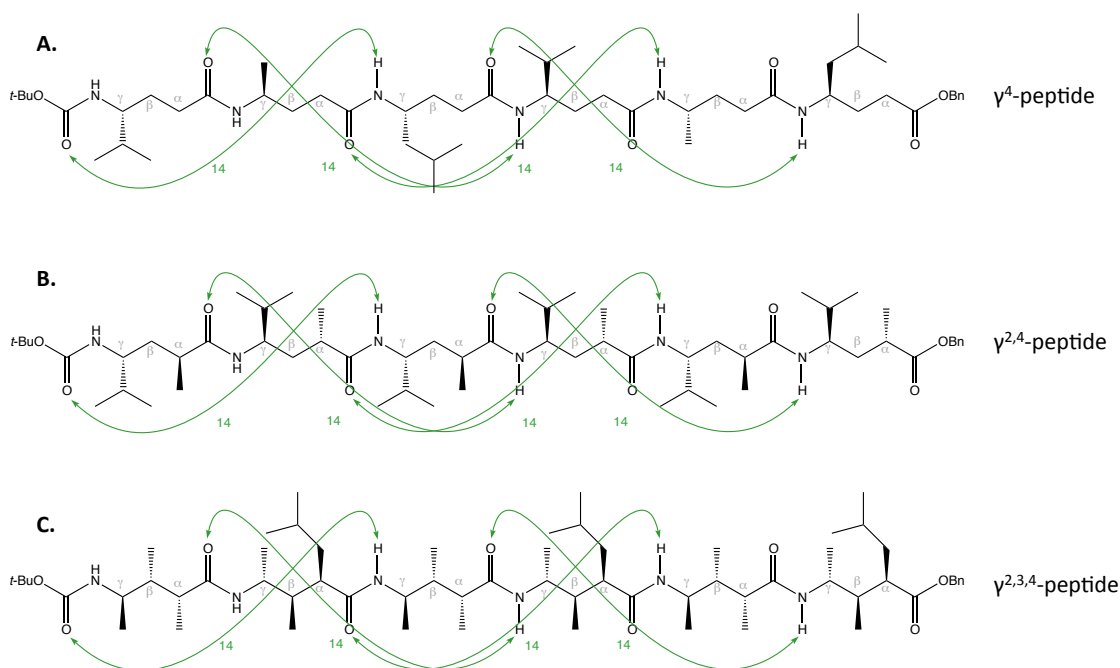


Figure 53. The 14-helix adopted by  $\gamma$ -peptides.

It is remarkable that a hexapeptide composed only of mono-substituted  $\gamma^4$ -amino acids should have a strong tendency to adopt a specific helical conformation in solution. The molecule appears, at first glance, to be much more flexible than an analogous  $\alpha$ -peptide which would not fold spontaneously into a helical structure in the same conditions.<sup>135</sup>

Other more highly constrained  $\gamma$ -amino acids have been incorporated into  $\gamma$ -peptides, such as cyclic  $\gamma^{2,4}$ -amino-L-Pro,  $\gamma^{2,3}$ cyclopropane and  $\gamma^{2,3}$ -cyclobutane, but the resulting  $\gamma$ -peptides display non-helical folding behaviour.

#### 2.5.2.2. Applications of helical $\gamma$ -peptides

The 14-helix is the closest structure adopted by  $\gamma$ -peptides that resembles the backbone of the native  $\alpha$ -helix. Considering the 14-helix constructed from (*R*)- $\gamma^4$ -amino acids, it is possible to compare the two helices (see Figure 54). The 14-helix of  $\gamma$ -peptides, or 2.6(14)-helix, presents the same chirality as the  $\alpha$ -helix (P) and a macrodipole oriented in the same direction as that of the  $\alpha$ -helix.<sup>138</sup> But the number of residues per turn is one residue less compared to the  $\alpha$ -helix, which leads to a shift in the side chains superimposition. The pitch of the 14-helix is also wider than the  $\alpha$ -helix.

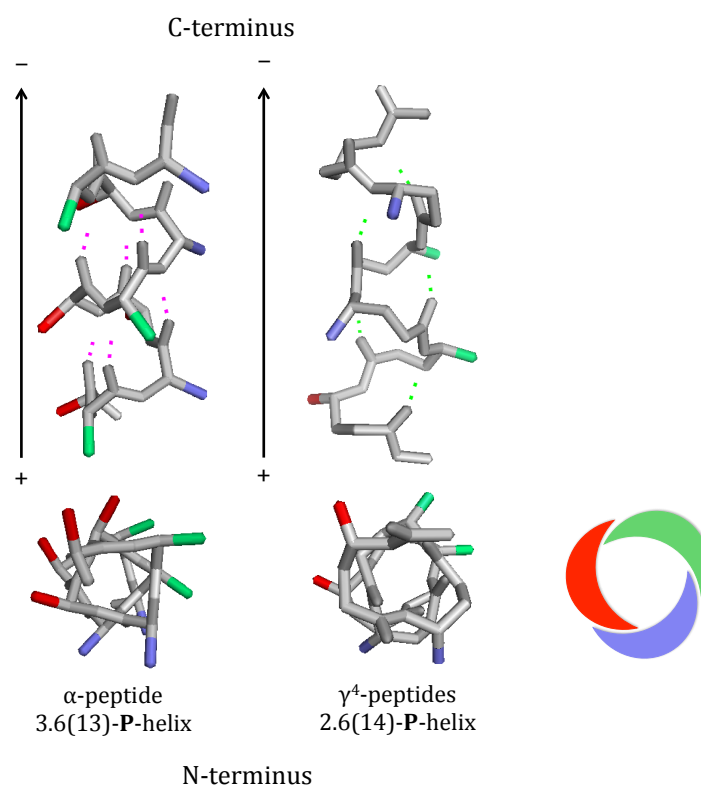


Figure 54. Comparison between the  $\alpha$ -helix and the 14-helix of  $\gamma$ -peptides.

The stability to proteolytic degradation was evaluated for a few 14-helical  $\gamma$ -peptides. The compounds shown in Figure 53 were subjected to 15 proteolytic enzymes and as expected no degradation was observed after 48 h, whereas similar  $\alpha$ -peptides were degraded after 15 min.<sup>139</sup> This resistance to proteolytic enzymes illustrates the potential of using  $\gamma$ -peptides for biological application.

Despite the potential of the 14-helical  $\gamma$ -peptides to serve as  $\alpha$ -helix mimetics, no biological applications have been developed so far. For now, these oligomers have been prepared essentially in order to study their folding behaviour.

### 2.5.3. Hybrid $\alpha/\beta$ -peptides<sup>v</sup>

More recently, mixed heterogeneous peptides have gained much attention especially hybrid  $\alpha/\beta$ - and  $\alpha/\gamma$ -peptides because of the incorporation of highly accessible  $\alpha$ -amino acids in the sequence.

#### 2.5.3.1. Helical diversity adopted by $\alpha/\beta$ -peptides

The Hofmann group explored by *ab initio* calculations the possibility of the formation of different helices in  $\alpha/\beta$ -peptides, using an octapeptide free of constraints alternating glycine and  $\beta$ -alanine.<sup>140</sup> The authors found that  $\alpha/\beta$ -peptides should fold into 8 different stable helical forms: 9-, 9/11-, 11/9-, 11-, 12/13-, 15/14-, 16/18- and 18/16-helices. Four of these helical structures have been experimentally observed in solution: the 11/9-, 11-, 12/13- and 15/14-helices, as we detail below.

A very simple  $\alpha/\beta$ -peptide sequence was envisaged by the Kunwar group, employing alternately a monosubstituted  $\alpha$ -amino acid and a  $\beta^3$ -amino acid. This  $\alpha/\beta^3$ -peptide displayed two distinct hydrogen-bonding patterns, having opposite orientations relative to the backbone direction, defining a robust **11/9-helix** (see Figure 55).<sup>141</sup>

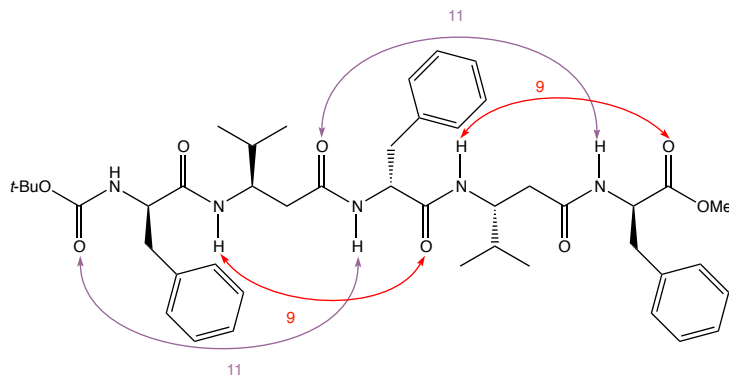


Figure 55. The 11/9-helix adopted by an  $\alpha/\beta$ -peptide.

<sup>v</sup> Hereafter we will discuss helical hybrid peptides and a clarification regarding nomenclature is warranted.

A mixed peptide is designated as a  $\mu/\nu$ -peptide wherein the constituent  $\nu$ -amino acid is a higher homologue of the constituent  $\mu$ -amino acid. In a  $m/n$ -helix, the  $\mu$ -amino acid residues are included in each  $m$ -membered hydrogen-bonded ring, while the  $\nu$ -amino acid residues are included in each  $n$ -membered hydrogen-bonded ring.

For example, in a 9/11-helical  $\alpha/\beta$ -peptide, the  $\alpha$ -amino acid NHs are implicated in a 9-membered hydrogen-bonded ring while the  $\beta$ -amino acid NHs are implicated in a 11-membered hydrogen-bonded ring.

The Reiser group prepared a heptamer composed of alternating L-Ala and *cis*-ACC (*cis*-2-aminocyclopropanecarboxylic acid) (see Figure 56). The mixed  $\alpha/\beta$ -peptide adopted a stable helical conformation in solution. The authors describe the structure as a 3(13)-helix stabilised by *i-i+2* hydrogen bonds.<sup>142</sup> However, this hydrogen-bond network corresponds to a **12/13-helix**, predicted by Hofmann.

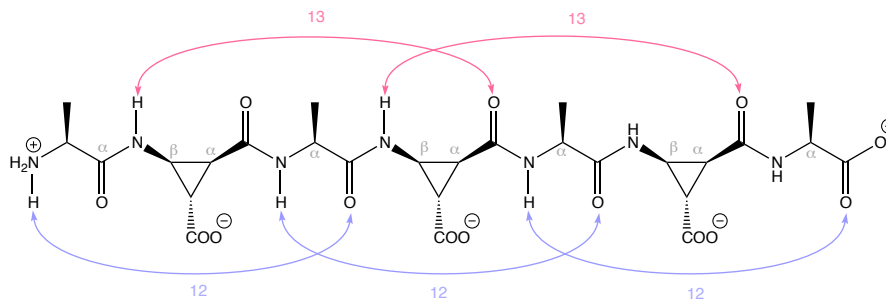


Figure 56. The 12/13-helix adopted by an  $\alpha/\beta$ -peptide.

The Jagadeesh group reported the synthesis of  $\alpha/\beta$ -peptides consisting of alternating L-Ala and a *cis*-FSAA (*cis*- $\beta$ -furanoid sugar amino acid) as building blocks (see Figure 57 A). These oligomers were similar to the one developed by the Reiser group in terms of constraints and stereochemistry but behaved differently in solution because of the different dihedral angles imposed by the cyclic part of the building block. The folding behaviour of the tetra- and octapeptides is very interesting and illustrates nicely the dynamics of peptides in solution, which are sometimes neglected. The peptides are in a **dynamic equilibrium** between two solution-state conformers: the **11-helix** and the **15/14-helix**.<sup>143</sup> According to Hofmann's studies, these two helices are indeed the two most stable helical conformers for  $\alpha/\beta$ -peptides, after the 11/9-helix; this latter cannot be adopted by Jagadeesh's peptides.

The Gellman group was able to observe separately the two helices described by the Jagadeesh group, with two different peptides (see Figure 57 B and C). The peptide folding into a 11-helix consisted of alternating Aib and *trans*-ACPC.<sup>144</sup> The peptide folding into a 15/14-helix only differed by the identity of the first N-terminal  $\alpha$ -amino acid, L-Ala, which therefore appeared to be a 15/14-helix promoter by favouring the first 14-membered hydrogen-bonded ring.<sup>145</sup> The very small difference between the two sequences led to a different helical folding propensity, illustrating the fine borderline between these two helices of similar energies.

In contrast with related studies on  $\beta$ -peptides alternating  $\beta$ -Ala and *cis*-ACBC, the Ortuño group suggested that  $\alpha/\beta$ -peptides employing alternately Gly and *cis*-ACBC showed no preference for a single conformation in solution, and among the diversity of conformers, none presented a helical conformation.<sup>125</sup> The conformational constraints brought by *cis*-ACBC were not sufficient to compensate for the conformational freedom brought by Gly.

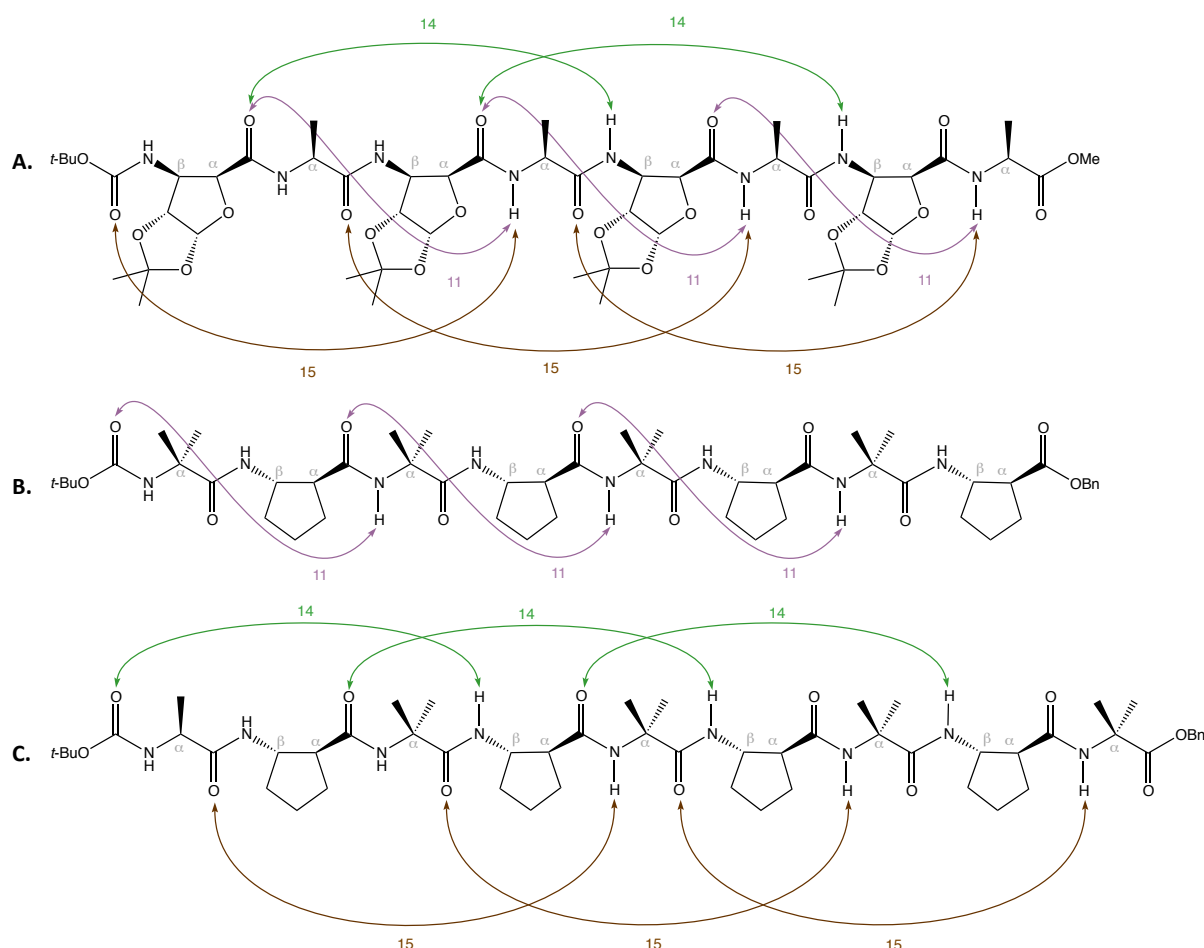


Figure 57. The 11-helices and 15/14-helices adopted by  $\alpha/\beta$ -peptides.

### 2.5.3.2. Applications of $\alpha/\beta$ -peptides mimicking the $\alpha$ -helix

The Gellman group sought to use  $\alpha/\beta$ -helices for the inhibition of  $\alpha$ -helix mediated PPI. They screened over 200 peptides adopting different helical conformations against the Bak/Bcl-x<sub>L</sub> interaction but failed to identify a potent inhibitor. The most active compound presented a 15/14-helical conformation in solution and exhibited a moderate inhibition activity of 4.2  $\mu$ M.<sup>146</sup> The authors moved on to the rational design of chimeric foldamers, mixing a N-terminal  $\alpha/\beta$ -fragment and a C-terminal  $\alpha$ -fragment. The N-terminal  $\alpha/\beta$ -fragment was designed to adopt a 15/14-helical structure by employing *trans*-ACP and *trans*-ACPC building blocks and to mimic the N-terminal fragment of Bak, while the C-terminal  $\alpha$ -fragment would adopt the native  $\alpha$ -helical folding behaviour of Bak (see Figure 58 A). This chimeric  $\alpha/\beta+\alpha$ -peptide bound to Bcl-x<sub>L</sub> (see Figure 58 B) with a satisfying nanomolar inhibition interaction ( $K_i = 2$  nM), displaying on one face the hot-spot residues of the interaction (in blue).<sup>147</sup> This study proved that a **15/14-helix may be used to mimic the  $\alpha$ -helix**, and in doing so it displays the three faces: the direct recognition face (in blue), the proximal  $\beta$ -residues (in red) and the solvent exposed face (in green) (see Figure 58 C).



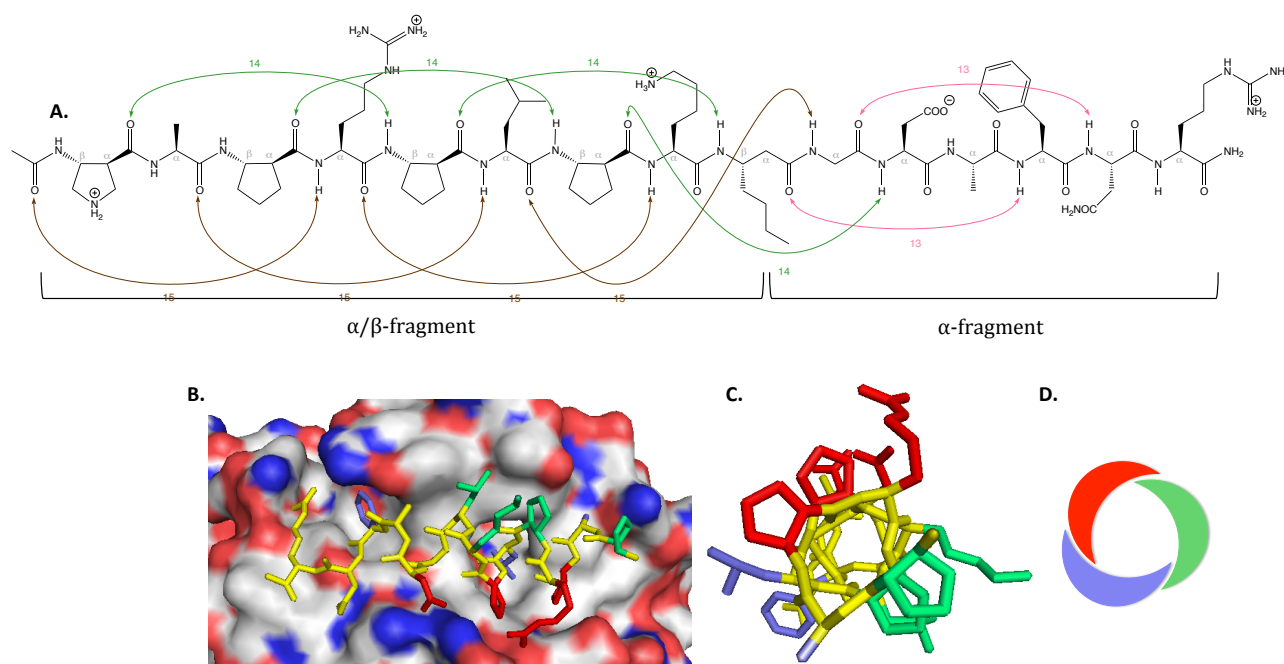


Figure 58. A: Structure and folding pattern of the chimeric  $\alpha/\beta+\alpha$ -peptide. B: Crystal structure of the chimera bound to Bcl-x<sub>L</sub> (PDB ID: 3FDL). C: Top view of the chimeric  $\alpha/\beta+\alpha$ -peptide. D: Cartoon representing the three faces of the helix.

The work on  $\alpha/\beta$ -peptide foldamers was adapted for the development of peptide sequences closer to the native  $\alpha$ -helix. The strategy relies on the placement of constrained and/or structuring  $\beta$ -amino acids at selected positions within an  $\alpha$ -helix to give a hybrid foldamer with enhanced stability. The Gellman group investigated new hybrid peptides based on the **repetitive  $\alpha\alpha\beta\alpha\alpha\beta$  heptad**. The  $\beta$ -amino acid can be acyclic allowing the presence of key side chains or cyclic to decrease flexibility of the mimetics. The Gellman group demonstrated that the position of the  $\beta$ -amino acids influenced the affinity and selectivity for the targeted proteins.<sup>148</sup> For example, a chimeric peptide was found to bind both to Bcl-x<sub>L</sub> ( $K_i = 2$  nM) and Mcl-1 ( $K_i = 150$  nM).<sup>149</sup> Although this peptide is a potent inhibitor of PPI, the lack of selectivity is a limiting factor for the development of therapeutics based on this scaffold.

#### 2.5.4. Hybrid $\alpha/\gamma$ -peptides

Inspired by the folding patterns displayed by many hybrid  $\alpha/\beta$ -peptides, research groups have investigated the folding propensity of hybrid  $\alpha/\gamma$ -peptides.

The Hofmann group explored by *ab initio* calculations the possibility of the formation of different helices in  $\alpha/\gamma$ -peptides, using an octapeptide free of constraint alternating Gly and GABA.<sup>150</sup> The authors found that  $\alpha/\gamma$ -peptides should fold into 11 different stable helical forms: 10-, 10/12-, 12/10-, 12-, 15/17-, 18-, 18/20-, 20/18-, 20-, 21/23- and 26-helices. Only two of these helical

structures have been experimentally observed in solution: the 12- and 12/10-helices, as we detail below.

The Balaram group synthesised a wide range of  $\alpha/\gamma$ -peptides composed of various  $\alpha$ -amino acids and Gpn (gabapentin) as the  $\gamma$ -amino acid residue.<sup>151</sup> One nonapeptide alternating Aib and Gpn residues was able to fold into a regular **12-helix** (see Figure 59 A).<sup>152</sup> This helical preference arose from the preferred torsion angles of the constituted amino acids:  $\psi$  dihedral angles were *gauche* for the  $\alpha$ -amino acids and,  $\theta$  and  $\zeta$  dihedral angles were *gauche* for the  $\gamma$ -amino acids. These values were entirely consistent with the prediction of Hofmann for the promotion of the 12-helical  $\alpha/\gamma$ -peptide.

The Gellman group studied a highly constrained  $\alpha/\gamma$ -peptide alternating L-Ala and *trans*-(*R,R,R*)-EtACHA (ethyl-*cis*-2-(aminocyclohexane)acetic acid). As anticipated, the hexapeptide folded into a 12-helix in solution (see Figure 59 B).

Following these studies, the Gopi group examined  $\alpha/\gamma^4$ -peptides. Although presenting less constraints than Balaram's and Gellman's  $\alpha/\gamma$ -peptides, the tetra- and hexapeptides were able to fold in solution and in the solid state into a **12-helix** (see Figure 59 C).<sup>153</sup> The 'intriguing' (according to the authors) stable 12-helix was stabilised by favourable  $\theta$  and  $\zeta$  torsion angle values of *gauche*<sup>+</sup> and *gauche*<sup>+</sup> adopted by the  $\gamma$ -residue. The authors overlaid backbone and side-chain projections of their  $\alpha/\gamma^4$ -peptide helices with a native  $\alpha$ -helix and suggested that these former could indeed be exploited mimetics of the latter. It is noticeable that the Gopi group used Aib for two of the three  $\alpha$ -amino acids in the nonapeptide, presumably in order to promote the helicity. It would be interesting to test the folding propensity of  $\alpha/\gamma^4$ -peptides containing only  $\alpha$ -proteogenic amino acids which would provide the opportunity for the inclusion of functional side chains.

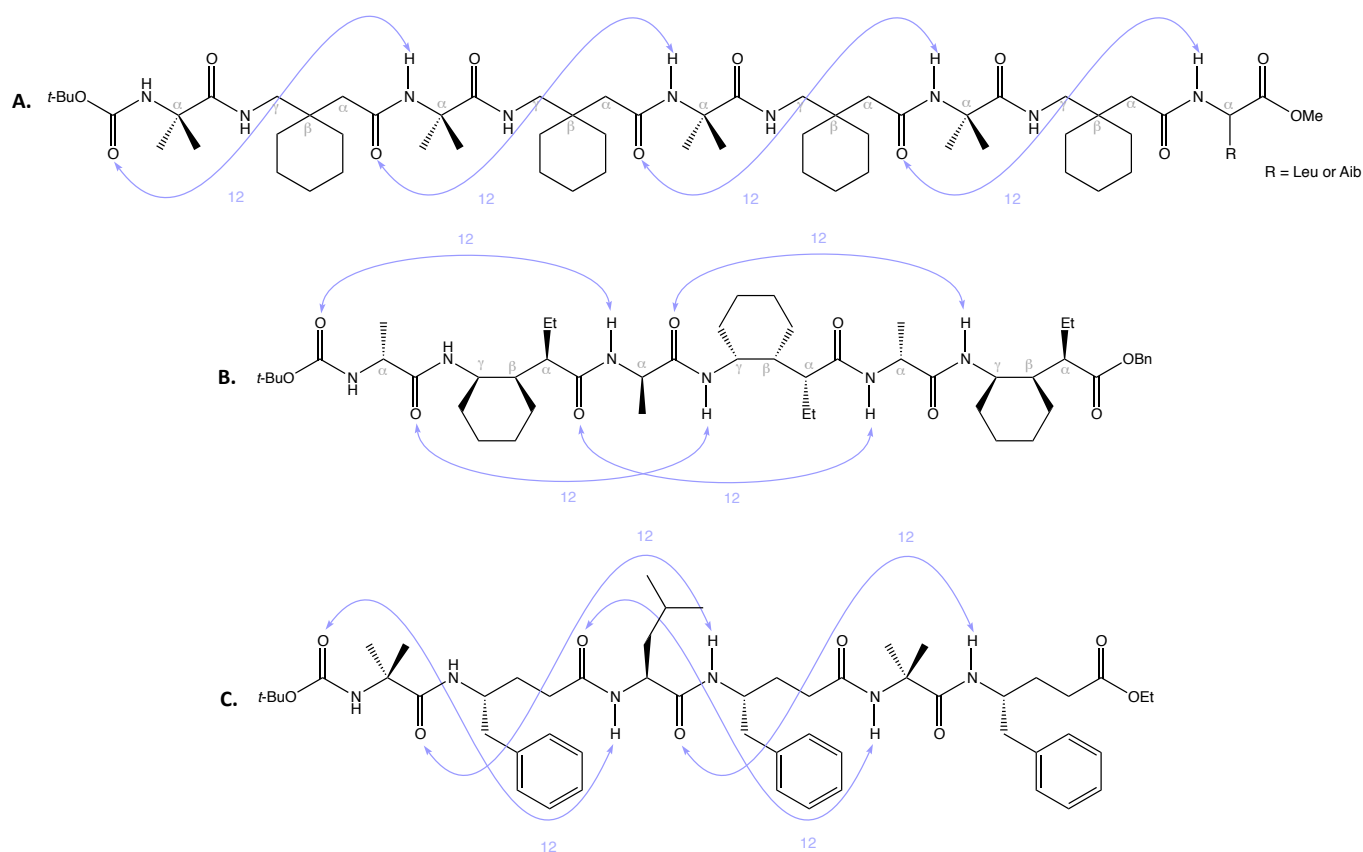


Figure 59. The 12-helix adopted by  $\alpha/\gamma$ -peptides.

The Kunwar group prepared  $\alpha/\gamma^4$ -peptides derived from the dipeptide repetitive unit alternating Ala and C-linked carbo- $\gamma$ -amino acid derived from D-mannose.<sup>154</sup> Tetra- and hexapeptides adopted a **12/10-helix** (see Figure 60 A).

Recently, the Gellman group studied  $\alpha/\gamma$ -peptides which incorporate L-Ala and (*R,R,S*)-APCH (2-(1-aminopropyl)cyclohexanecarboxylic acid), which can be seen as a structural isomer of (*R,R,R*)-EtACHA.<sup>155</sup> The two hexapeptides have a different behaviour in solution; the hexapeptide alternating L-Ala and (*R,R,S*)-APCH adopted a **12/10-helix** in solution (see Figure 60 B).

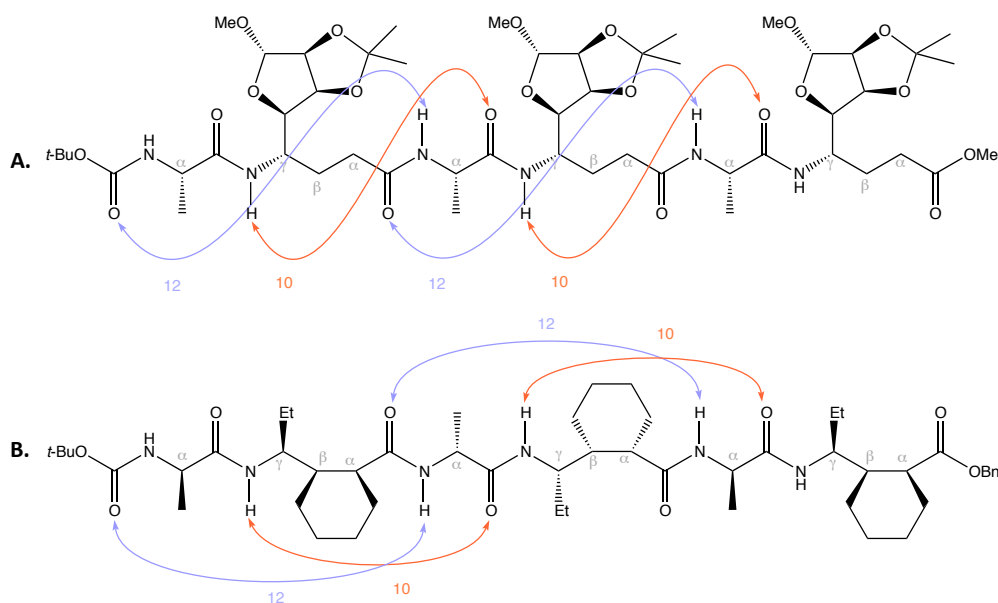


Figure 60. The 12/10-helix adopted by  $\alpha/\gamma$ -peptides.

Studies on  $\alpha/\gamma$ -peptide manifolds are incomplete and further investigations will be needed to explore the helical diversity of this family suggested by the Hofmann group in 2006.<sup>150</sup> At present no direct biological application of  $\alpha/\gamma$ -peptides has been reported although the 12-helix recently obtained by Gopi would be promising to diversify for future  $\alpha$ -helix mimetics.

### 2.5.5. Hybrid $\beta/\gamma$ -peptides

Heterogeneous peptides that do not include  $\alpha$ -amino acid residues have received limited attention, perhaps because  $\alpha$ -amino acids are far more readily available and in diverse forms than their homologated derivatives. However, very interesting results have emerged from theoretical studies and from the three  $\beta/\gamma$ -peptide systems studied experimentally to date.

The Hofmann group explored by *ab initio* calculations the possibility of the formation of different helices in  $\beta/\gamma$ -peptides, using an octapeptide free of constraint alternating  $\beta$ -Gly and GABA.<sup>150</sup> The authors found that  $\beta/\gamma$ -peptides should fold into ten different stable helical forms: 11-, 11/13-, 13/11-, 13-, 15/16-, 18/17-, 20-, 20/22-, 22/20- and 22-helices. Among the most stable helices is included **the 13-helix, which is a  $\beta/\gamma$ -peptide mimetic of the  $\alpha$ -helix**. A  $\beta/\gamma$ -dipeptide has indeed the same number of atoms (13 atoms) between the N- and C-termini as an  $\alpha$ -tripeptide (see Figure 61 A). The superimposition of a theoretical 13-helical  $\beta/\gamma$ -peptide and an  $\alpha$ -helix showed very good correspondence between the two helix patterns (RMSD = 0.7 Å) (see Figure 61 B).

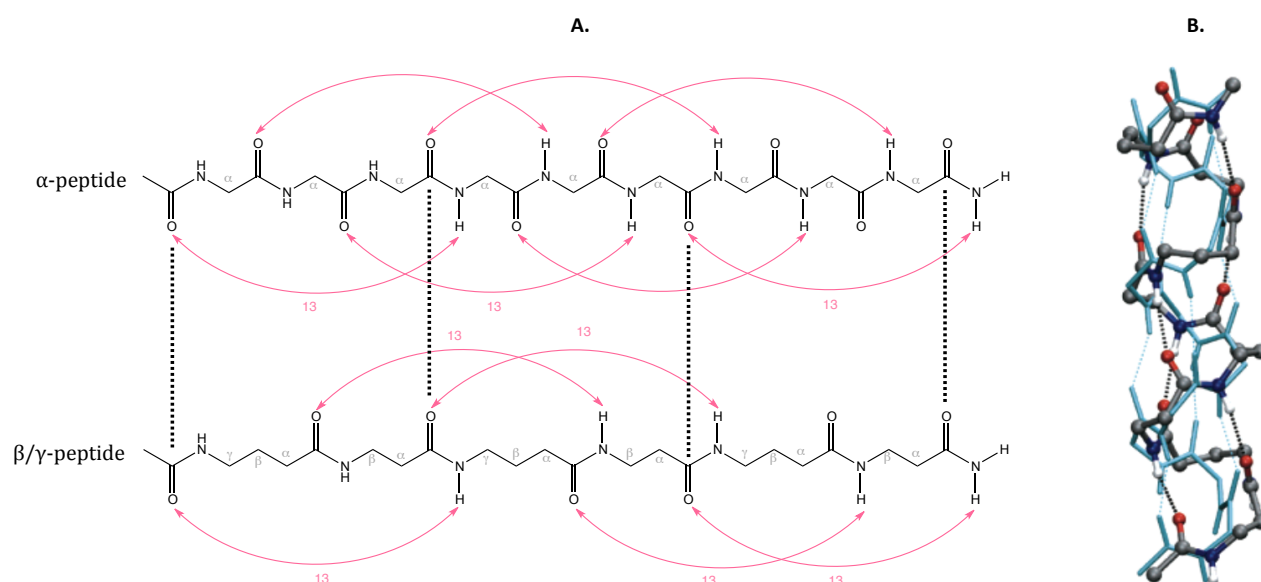


Figure 61. A: Similarity of backbones between an  $\alpha$ -peptide and a  $\beta/\gamma$ -peptide. B: Stereoview of the superimposition of a 13-helical  $\beta/\gamma$ -peptide and an  $\alpha$ -helix.

Only two of the theoretical helical structures have been experimentally observed in solution: the 11/13- and 13-helices, as we detail below.

The Sharma group prepared the first hybrid  $\beta/\gamma$ -peptides using D-xylose-derived  $\beta^3$ - and  $\gamma^4$ -amino acids (see Figure 62).<sup>154</sup> The conformational analyses of tetra- and hexapeptides in organic solvent revealed the **11/13-helix** predicted by Hofmann. This helix is stabilised by hydrogen bonds in alternating directions.

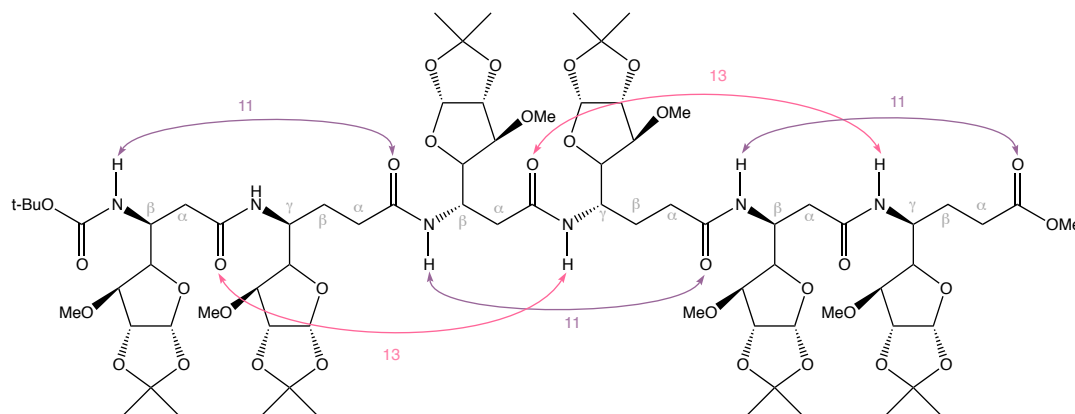


Figure 62. The 11/13-helix adopted by a  $\beta/\gamma$ -peptide.

The Gellman group endeavoured to design  $\beta/\gamma$ -peptides which would fold into a **13-helix**. Using as a guide the backbone dihedral angles suggested by Hofmann to privilege the adoption of a 13-helical conformation, the Gellman group combined the appropriately restricted (*R,R*)-*trans*-ACPC and (*R,R,R*)-EtACHA as the  $\beta$ - and  $\gamma$ -amino acid components (respectively) in the hybrid  $\beta/\gamma$ -peptides. The tetrapeptide was too short to fold regularly; two hydrogen-bonded rings, one 13-membered and the other 8-membered, were observed in solution and in the solid state (see Figure 63 A). The

hexapeptide presented a regularly folded 13-helix in solution and in the solid state (see Figure 63 B).<sup>156</sup>

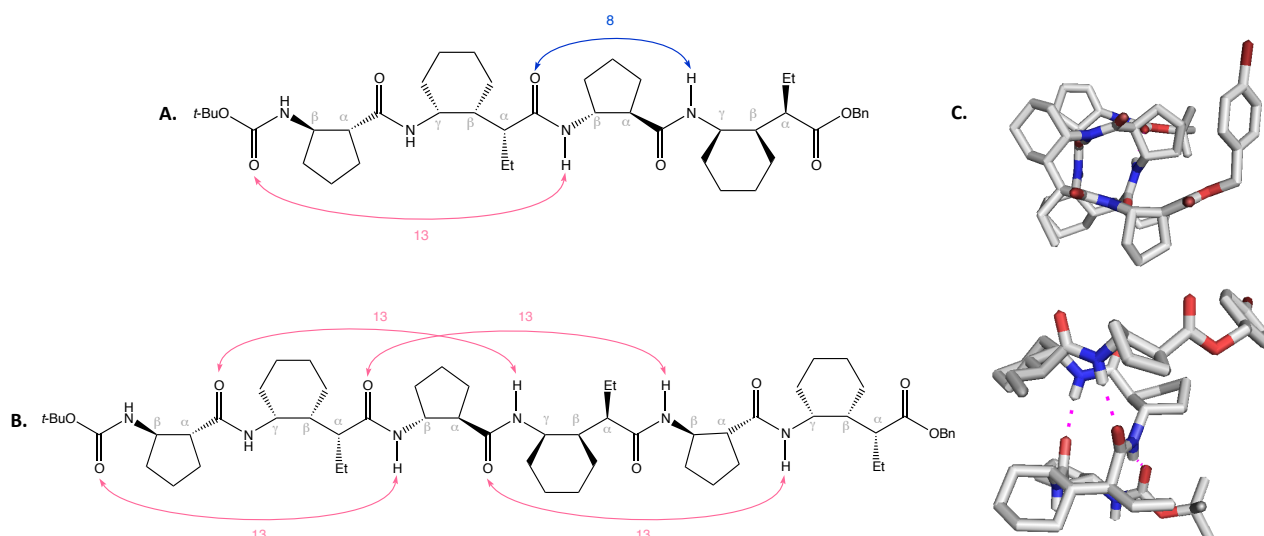


Figure 63. A: Backbones of the H-bonding features of Gellman's  $\beta/\gamma$ -tetrapeptide. B: Backbones of the H-bonding features of Gellman's  $\beta/\gamma$ -hexapeptide, which is a 13-helix. C: Top and side views of the 13-helical hexapeptide.

Similarly to related studies on  $\alpha/\beta$ -peptides alternating *cis*-ACBC and Gly, the Ortuño group suggested that  $\beta/\gamma$ -peptides alternating *cis*-ACBC and GABA showed no preference for a single conformation in solution, and among the diversity of conformers none presented a helical conformation.<sup>125</sup> The lowest-energy conformer presented various hydrogen-bonded rings (see Figure 64). The presence of the GABA spacer did not have an impact on the hydrogen-bonding behaviour of the *cis*-ACBC residues, which invariably displayed an intra-residue 6-membered hydrogen-bonded ring feature.

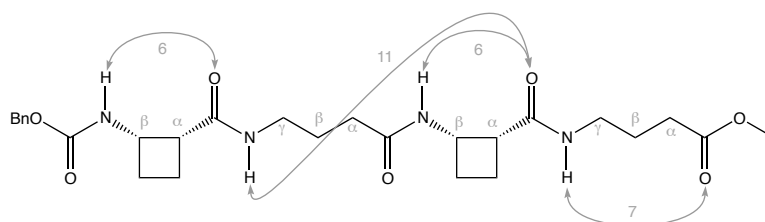


Figure 64. The most stable conformer of  $\beta$ -*cis*-ACBC/GABA peptide.

More recently constrained  $\beta$ - and  $\gamma$ -amino acids have been introduced in the sequence of helical  $\alpha$ -peptides to enhance their helicity and increase the resistance to proteolytic degradation. For example, the Gellman group synthesised a **new hybrid  $\alpha/\beta/\gamma$ -peptide**: a repeating  $\alpha\gamma\alpha\alpha\beta\alpha$  hexad pattern that has the same number of atoms as a heptad of  $\alpha$ -residues.<sup>157</sup> The  $\beta$ - and  $\gamma$ -residues were respectively the constraint (*S,S*)-ACPC and (*S,S,S*)-EtACHA amino acids. The 12-mer system supported a helical conformation in aqueous solution which was very similar to an  $\alpha$ -helix. A direct comparison

with a conventional  $\alpha$ -peptide revealed that the  $\alpha/\beta/\gamma$ -peptide had a much stronger folding propensity due to the constrained  $\beta$ - and  $\gamma$ -amino acids. Although the enhanced folding propensity of the hybrid  $\alpha/\beta/\gamma$ -peptides are promising, no biological application has been reported yet.

### 3. Aim of this project – *trans*-ACBC-based $\beta/\gamma$ -peptide manifolds as $\alpha$ -helix mimetics

$\alpha$ -,  $\beta$ -,  $\gamma$ -,  $\alpha/\beta$ -,  $\alpha/\gamma$ - and  $\beta/\gamma$ -Peptide foldamers proved to be a rich source of helical secondary structures. They possess attractive features to serve as mimics of the  $\alpha$ -helix due to their **intrinsic helical structure** stabilised by **unnatural amino acids** that confer a considerable **resistance against proteolytic degradation**. They can be used to mimic the  $\alpha$ -helix in **different biological contexts** unlike the other types of  $\alpha$ -helix mimetics that only serve to mediate PPI.

However, only a few of these peptides have been tested as  $\alpha$ -helix mimetics because foldamers are often too constrained and have a limited ability to present key side-chains, reducing their functionality.

The Aitken group is specialised in the synthesis of unnatural amino acids incorporating small rings and the development of oligomers based on these building blocks. Such cyclic amino acids present specific  $\theta$  dihedral angles that confer to them the ability to promote stable conformations in oligomers. The  $\beta$ -amino acid ***trans*-ACBC** (*trans*-2-aminocyclobutanecarboxylic acid) possesses a  **$\theta$  dihedral angle of  $95^\circ$** , that is known to promote a 12-helix conformer in its homo-oligomer.<sup>119</sup> However, this 12-helical  $\beta$ -peptide (like every 12-helix reported so far) is too constrained and no positions are available for facile introduction of side-chains, though the synthesis of **substituted ACBC** is currently being explored in the Aitken group.<sup>158</sup>

The  $\theta$  dihedral angle of around  $90^\circ$  was suggested by Hofmann to be optimal for the  $\beta$ -amino acid component in a 13-helical  $\beta/\gamma$ -peptide.<sup>150</sup> This prediction was effectively validated by the Gellman group using *trans*-ACPC as the  $\beta$ -amino acid, in the first and so far only 13-helical  $\beta/\gamma$ -peptide (see Figure 63).<sup>156</sup> However, the 13-helical peptide proposed by the Gellman group is too sterically hindered and lacks functional side-chains, thus limiting its potential for biological applications.

The present work aims at preparing **13-helical hybrid  $\beta/\gamma$ -peptides** that match to the backbone of the native  $\alpha$ -helix with a minimum input of steric constraints. In this way, the options for the introduction of functional side-chains in a modular manner remain large: the 13-helix core manifolds may therefore be used to prepare functional mimetics of selected  $\alpha$ -helix motifs in natural proteins.

We propose the investigation of novel  $\beta/\gamma$ -peptides, in which the  **$\beta$ -amino acid is the strongly constrained *trans*-ACBC** and the  **$\gamma$ -amino acid bears as little constraints as possible** (see Figure 65).



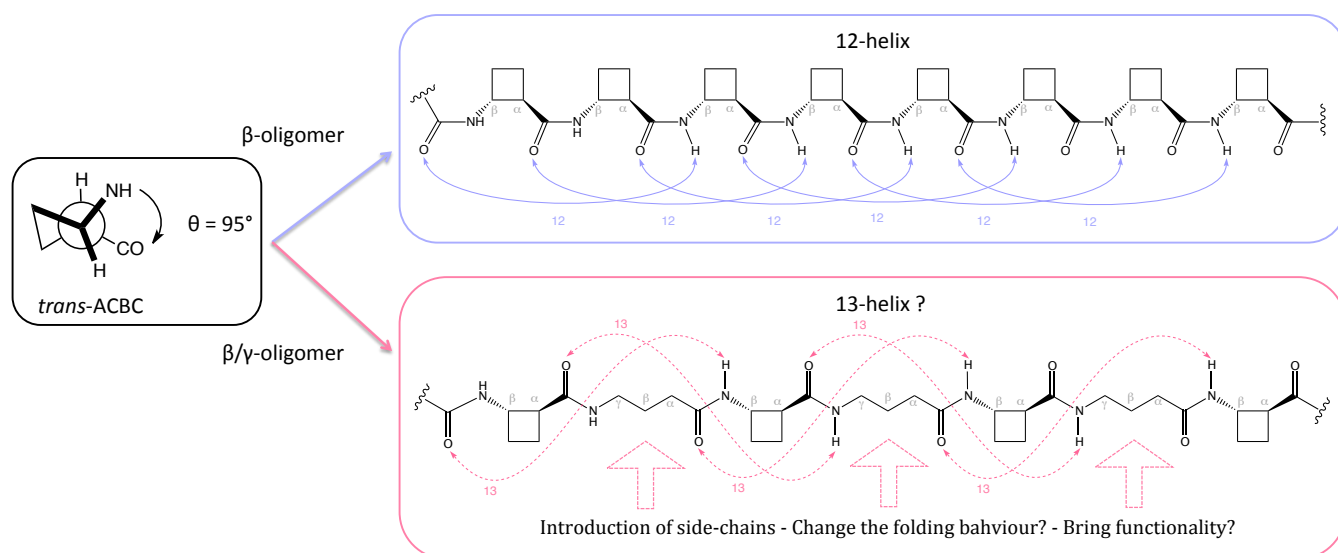


Figure 65: Novel  $\beta/\gamma$ -peptide manifold showing the 13-helical folding pattern promoted by the presence of *trans*-ACBC

In part II of this thesis, the synthesis and conformational study of new  **$\beta/\gamma$ -peptides alternating *trans*-ACBC and GABA** will be presented and discussed in the first chapter. The folding behaviour promoted by *trans*-ACBC will be evaluated through structural analyses completed by theoretical calculations. In the following chapter, the synthesis of  **$\beta/\gamma$ -peptides, alternating *trans*-ACBC and  $\gamma^4$ -amino acids**, will be presented and the folding behaviour of these compounds evaluated. In the final chapter, an investigation of these new foldamers as  $\alpha$ -helix mimetics will be presented through the design of  **$\alpha/\beta/\gamma$ -peptides as inhibitors protein-protein interactions** as a proof of concept.

## **PART II. RESULTS AND DISCUSSION**



## 1. Synthesis and structural studies of $\beta/\gamma$ -peptides alternating *trans*-ACBC and GABA: a robust 9/8-ribbon

It is proposed in this chapter to explore the conformational behaviour of  $\beta/\gamma$ -peptides composed alternately of *trans*-2-aminocyclobutanecarboxylic acid (*trans*-ACBC) as the highly constrained  $\beta$ -amino acid component, and GABA as the completely unrestricted  $\gamma$ -amino acid component (see Figure 66).

In the search for a  $\beta/\gamma$ -peptide manifold which mimics the native  $\alpha$ -helix, *trans*-ACBC provides a favourable torsion angle ( $\theta$ ); what remains to be established is the set of preferred torsion angles (if any) displayed by GABA.

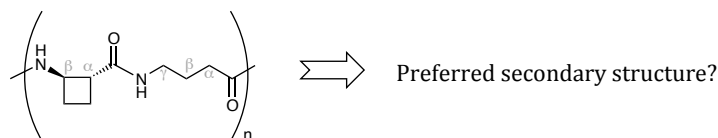


Figure 66.  $\beta/\gamma$ -Dipeptide unit based on *trans*-ACBC and GABA.

While GABA and its derivatives are commercially available, *trans*-ACBC is not. The first task was therefore to synthesise *trans*-ACBC in enantiomerically pure form.

### 1.1 The constrained $\beta$ -amino acid *trans*-ACBC

#### 1.1.1. Presentation of ACBC

ACBC is a  $\beta$ -amino acid that incorporates  $C_\alpha$  and  $C_\beta$  as part of a cyclobutane ring. It possesses two asymmetric centres giving four diastereoisomers (1*R*,2*S*)- and (1*S*,2*R*)-*cis*-ACBC [1] and (1*R*,2*R*)- and (1*S*,2*S*)-*trans*-ACBC [2].

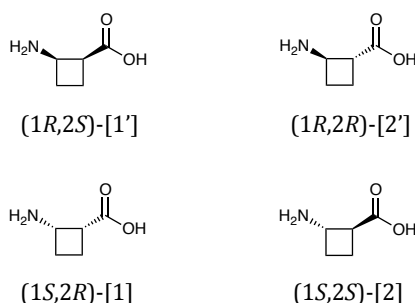
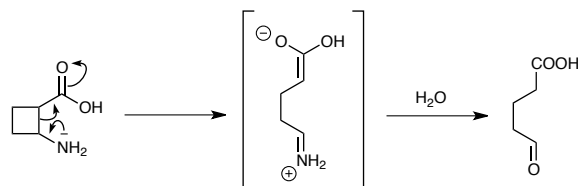


Figure 67. The four isomers of ACBC.

It is not a trivial amino acid to work with because it is intrinsically unstable due to the push-pull effect operating between the electron-donating amino group and the electron-withdrawing

carboxylic acid group. The push-pull effect may lead to the irreversible opening of the cyclobutane ring followed by a retro-Mannich reaction (see Scheme 1).<sup>159</sup>

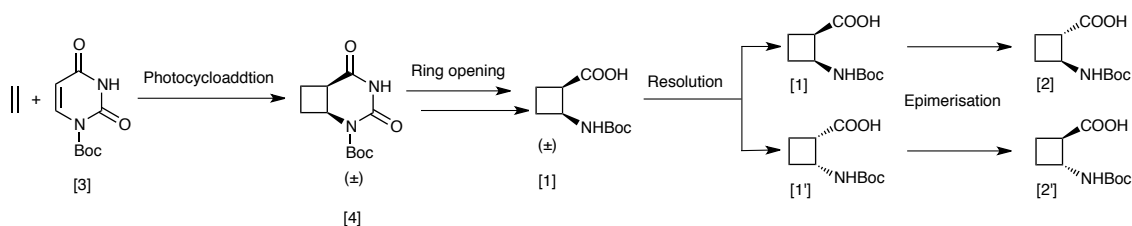


Scheme 1. Push-pull effect leading to the opening of the ACBC ring.

This degradation can be avoided by deactivating the donor aptitude of the lone pair of the nitrogen; ACBC is stable when *N*-protected by an electron-attracting group. A carbamate is a logical choice and a Boc (*t*-butyloxycarbonyl) protecting group is particularly convenient, because it is cleaved in acidic conditions under which the free nitrogen of ACBC remains temporarily deactivated as an ammonium ion.

Diverse synthetic methods were developed but were not ideal to obtain adequately *N*-protected ACBC. *N*-protected ACBC has been prepared according to two distinct strategies: transformations of cyclobutane-1,2-dicarboxylic acid,<sup>114,160–162</sup> in which the 4-membered ring is already present; and photochemical<sup>163–165</sup> or rearrangement<sup>166</sup> reactions which construct the cyclobutane.

Over a number of years, the Aitken group has refined the **photochemical approach** and today it arguably represents the most efficient synthesis of both enantiomers of *cis*- and *trans*-ACBC (see Scheme 2).<sup>165</sup> The key step of the strategy relied on a [2+2] photocycloaddition reaction between two readily available starting materials, ethylene and *N*<sup>1</sup>-Boc-uracil [3]. The main limiting factor of this strategy was the scale upon which the photochemical step could be conducted. The cycloadduct [4] obtained from the photocycloaddition was then selectively ring-opened to give racemic Boc-*cis*-ACBC. Racemic Boc-*cis*-ACBC [1] and [1'] were separated and underwent a simple epimerisation in basic conditions to give **Boc-*trans*-ACBC** [2] and [2'] in enantiomerically pure form (on subgram scale).



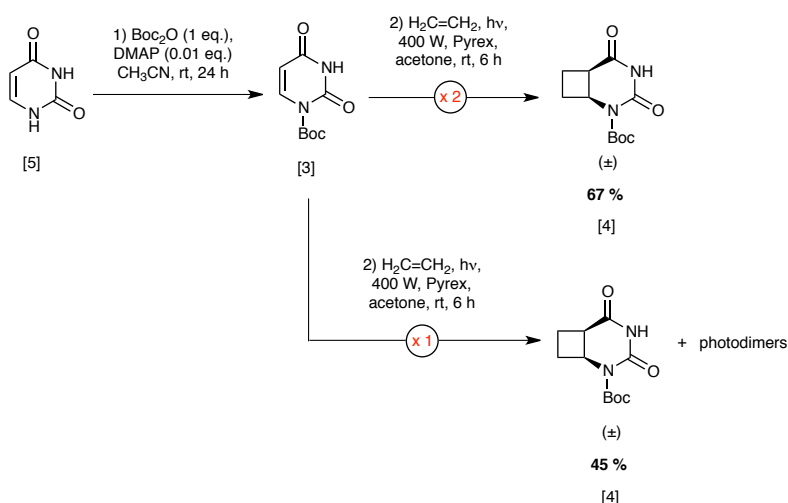
Scheme 2. Strategy for the synthesis of *trans*-ACBC.

### 1.1.2. Synthesis of *trans*-ACBC in enantiomerically pure form

Following the above described synthetic strategy from the Aitken group, enantiomerically pure Boc-*trans*-ACBC was prepared on a large scale.

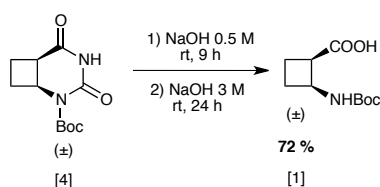
The selective protection of uracil [5] was carried out on 10 g scale with Boc<sub>2</sub>O in the presence of 10% of DMAP according to the procedure of the Jaime-Figueroa group.<sup>167</sup> The *N*<sup>1</sup>-Boc-uracil [3] was not purified but was split into two equal batches.

Each batch was engaged directly in a [2+2] photocycloaddition with ethylene in acetone in a 1 L reactor equipped with a 400 W mercury and a Pyrex filter to provide a 280 nm wavelength cutoff. The acetone is both the solvent of the reaction and a photosensitizer. This transformation gave the cycloadduct [4] with a good yield of 67%. A concentration of 45 mmol/L of *N*<sup>1</sup>-Boc-uracil [3] was found to be optimal in a photochemical reactor of 1 L. With a higher concentration, yields of cycloadduct [4] decrease significantly in favour of photodimers of undetermined structures (see Scheme 3).



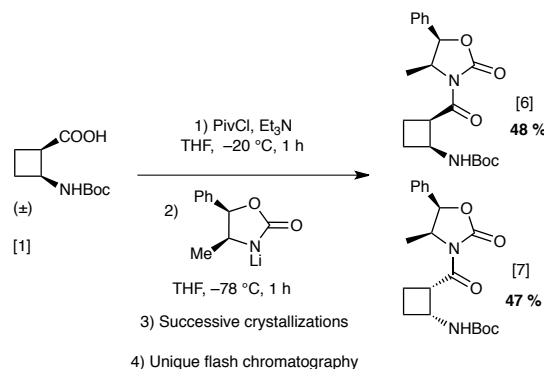
Scheme 3. Synthesis of the photoadduct [4] underlining the importance of concentration in the photochemical step.

The combined batches of photoadduct [4] were purified by automatic flash chromatography (20 g scale) then subjected to a mild basic treatment with 0.5 M NaOH for 9 hours followed by a stronger basic treatment with 3 M NaOH for 24 hours, to secure the sequential cleavage of N3-C4 and N1-C2 bonds in a single operation. The sequential cleavage protocol notably avoided the epimerization of C $\alpha$  centre. Racemic Boc-*cis*-ACBC [1] was obtained with a satisfying yield of 56% in only three steps from uracil (see Scheme 4).



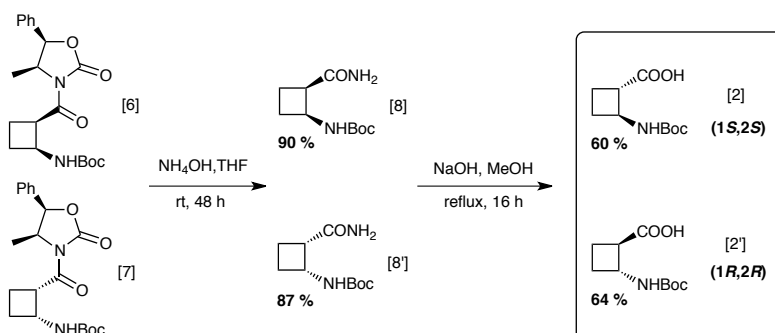
Scheme 4. Cleavage of cycloadduct [4] to provide ( $\pm$ ) Boc-*cis*-ACBC [1].

Resolution of racemic Boc-*cis*-ACBC was achieved using (*S*)-4-methyl-(*R*)-5-phenyl-oxazolidin-2-one.<sup>165</sup> The carboxylic acid function was activated as a mixed anhydride using pivaloyl chloride, and was coupled with the oxazolidin-2-one, which was activated as its lithium salt. The reaction gave a clean mixture of the two diastereoisomers [6] and [7] with an excellent combined yield of 95% (see Scheme 4).

Scheme 5. Derivatisation of Boc-*cis*-ACBC ( $\pm$ )-[1] to give two diastereoisomers [6] and [7].

The literature reports separation of these compounds by flash chromatography.<sup>165</sup> In our hands, this was impractical on a 5 g scale and necessitated five successive chromatographic columns to provide satisfactory separation. An alternative method of separation based on selective crystallization was therefore investigated. After dissolution of the mixture of diastereoisomers in a minimum of cyclohexane at reflux, only the (1*S*,2*R*)-diastereoisomer [7] crystallized when the mixture was cooled to room temperature. The separation of the mixture of diastereoisomers (for 15 g scale) was complete with a succession of **5 crystallizations** to give pure [7] followed by **a unique purification by flash chromatography** of the combined mother liquors, to give pure [6].

For each derivative [6] and [7], the chiral auxiliary was cleaved advantageously with a biphasic mixture of ammonium hydroxide and THF over 2 days to give the two enantiopure Boc-*cis*-ACBC amide derivatives [8] and [8']. The oxazolidinone was recovered and purified by simple flash chromatography, and was recycled for further use. Final treatment of these amides [8] and [8'] with 6 M NaOH in refluxing methanol overnight induced complete epimerization followed by hydrolysis and provided the two enantiomers Boc-*trans*-ACBC [2] and [2'] in good yields, on gram scale.

Scheme 6. Final steps of the synthesis the two Boc-*trans*-ACBC enantiomers [2] and [2'].

Each enantiomer of Boc-*trans*-ACBC was thus obtained with an overall yield of **25 % in six steps** from uracil giving enough material for the peptide synthesis described hereafter.

## 1.2 Synthesis of peptides alternating *trans*-ACBC and GABA [9]-[14]<sup>vi</sup>

The syntheses of  $\beta/\gamma$ -peptides (see Figure 68) alternating *trans*-ACBC, as the rigid  $\beta$ -amino acid and GABA, as the  $\gamma$ -amino acid devoid of constraint, were undertaken. Two series of peptides were prepared: one with *trans*-ACBC at the N-terminal position [9], [10], [11] and the other with GABA at the N-terminal position [12], [13], [14], in order to investigate the influence of the position of the structuring residue *trans*-ACBC.

The synthesis of Boc-*trans*-ACBC described above gave access to its both enantiomers; the enantiomer (1*R*,2*R*) [2'] was used in this Chapter for the synthesis of  $\beta/\gamma$ -peptides based on GABA and *trans*-ACBC, while the other enantiomer (1*S*,2*S*) [2] will be used in Chapters 2 and 3.

The protecting groups for peptide synthesis were easily chosen. Since the synthesis of *trans*-ACBC gave access to the stable Boc-*trans*-ACBC, a benzyl ester was selected as the orthogonal C-terminal protecting group.

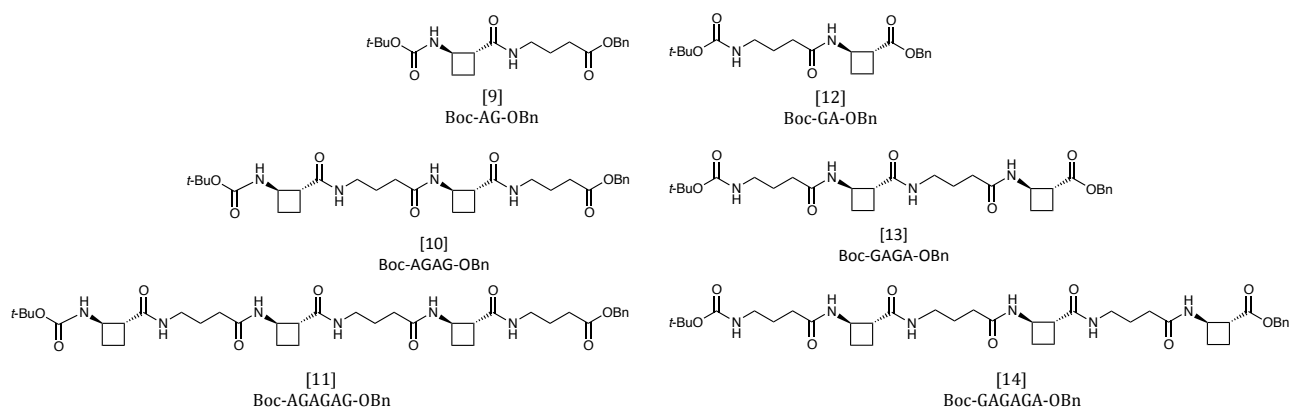


Figure 68. Synthesised  $\beta/\gamma$ -peptides alternating *trans*-ACBC and GABA

<sup>vi</sup> The peptides synthesised in this chapter are called in this manuscript following a code in which *trans*-ACBC is represented by the letter A and GABA by the letter G. For example, the dipeptide alternating *trans*-ACBC and GABA is called Boc-AG-OBn.



### 1.2.1. Linear synthesis of peptides with *trans*-ACBC as the *N*-terminal residue [9]-[11]

#### 1.2.1.1. Activation of *trans*-ACBC and synthesis of Boc-AG-OBn [9]

The reactivity of the carboxylic acid function of Boc-*trans*-ACBC was studied in order to identify the best coupling condition for the reaction with GABA-OBn to give the dipeptide Boc-AG-OBn [9]. The activation of Boc-*trans*-ACBC [2'] on gram scale was tested with the following classes of coupling reagents: chloroformate, uronium, carbodiimide and phosphoryl reagents (see Table 3).

Table 3. Coupling reagents tested for the coupling reaction between Boc-*trans*-ACBC and GABA.

Entry	Coupling conditions	Temperature of activation	Yield
1	IBCF, Et <sub>3</sub> N, THF	- 20 °C	65%
2	HATU, DIPEA, (CH <sub>2</sub> Cl <sub>2</sub> /DMF:4/1)	25 °C	62 %
3	EDCI, HOBT, DIPEA, DMF	25 °C	56%
4	FDPP, DIPEA, (CH <sub>2</sub> Cl <sub>2</sub> /DMF):(4/1)	25 °C	40 %

Isobutyl chloroformate (entry 1) and HATU (entry 2) provided the desired dipeptide [9] with the highest yields. The yields were slightly lower than those previously reported for coupling reactions of Boc-*trans*-ACBC (carried out on mg scale).<sup>168</sup>

It was decided to retain HATU for all subsequent coupling reactions involving Boc-*trans*-ACBC due to its simplicity. The activation was performed at room temperature, was not sensitive to traces of water and allowed the use of non-distilled solvents and could be performed open-to-air. Moreover the use of this coupling reagent was compatible with microwave coupling conditions, which were much more rapid and gave equally good yields.

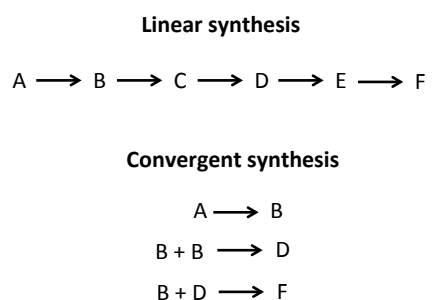
Some general comments are warranted here regarding the coupling reactions described in this manuscript. Coupling reactions conducted with HATU were performed via a preliminary activation of the carboxylic acid residue by HATU with two equivalents of DIPEA to generate the activated carboxylate *in situ* in a mixture of CH<sub>2</sub>Cl<sub>2</sub> and DMF. The addition of DMF during the activation stage allowed a better dissolution of HATU. The activation of the carboxylic acid residue was confirmed by the colouration (orange to brown) of the reactive mixture due to HOAt released by HATU. Once the

activation was complete, usually within 10 min, the amine partner, in solution in  $\text{CH}_2\text{Cl}_2$  with a sufficient amount of DIPEA to neutralize the excess of TFA that served to cleave the Boc protecting group, was added to the reactive mixture. After several hours of reaction, the reactive mixture was purified to give the desired peptide.

#### 1.2.1.2. When $2+2 = 3$

To build upon the dipeptide Boc-AG-OBn [9] and reach the required tetrapeptide Boc-AGAG-OBn [10] and hexapeptide Boc-AGAGAG-OBn [11], two strategies could be envisaged: **linear** and **convergent** (see Figure 69).

The linear synthesis is a strategy in which several steps are performed one after each other until the targeted molecule is complete. In this type of strategy, the overall yield drops quickly with each reaction step. In contrast a convergent synthesis is a strategy that aims to improve the efficiency of a multistep synthesis through fragment couplings. In this type of synthesis several individual fragments of a complex molecule are synthesised apart in stage one and in stage two they are combined together.



A: monomer  
B: di-, C: tri-, D: tetra-, E: penta-, F: hexapeptides

Figure 69. Linear and convergent synthesis.

As illustrated in Figure 69, the synthesis of a hexapeptide requires 5 coupling reactions via a linear strategy and 3 coupling reactions via a convergent strategy. Therefore, in the first instance, a convergent synthesis strategy was envisaged to access the tetrapeptide [10] and the hexapeptide [11].

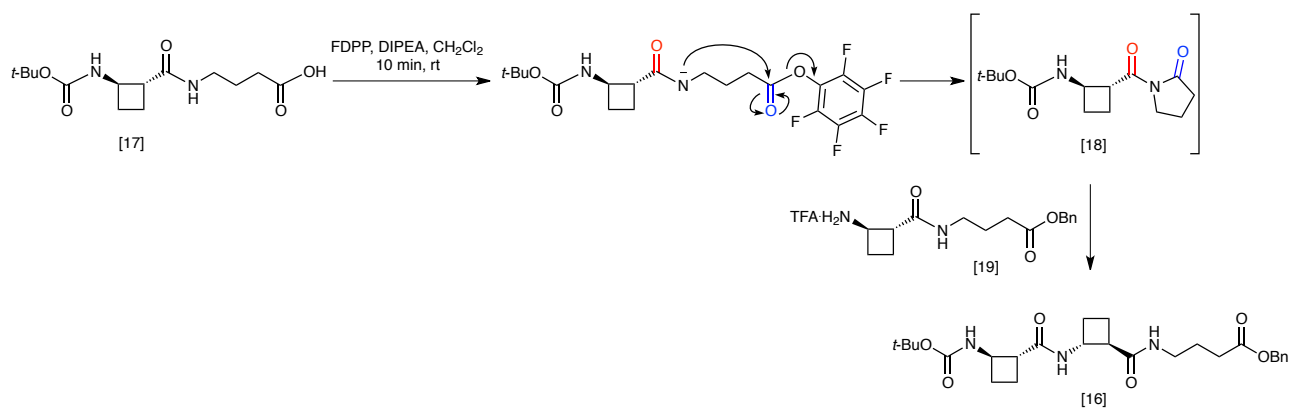
Starting from dipeptide [9], the convergent synthesis was initiated by coupling together two selectively-deprotected dipeptide derivatives. The *N*-Boc protecting group of [9] was cleaved by treatment with 30 eq. of TFA in  $\text{CH}_2\text{Cl}_2$  to give the corresponding TFA salt in quantitative yield. The benzyl ester protecting group of [9] was cleaved in  $\text{CH}_2\text{Cl}_2$  by hydrogenolysis under an atmosphere of dihydrogen in the presence of Pd/C-10% to give the corresponding carboxylic acid in quantitative yield.

These two monoprotected intermediates were coupled using HATU to give tetrapeptide [10] with a disappointing yield of 27% (see Table 4 entry 1). The two monoprotected intermediates were also coupled using IBCF since it was the best coupling reagent for the formation of dipeptide [9]. No desired tetrapeptide [10] was observed but a side product [15] was obtained instead (see entry 2). Finally, FDPP was also tested as coupling reagent; previously the Ortuño group had found FDPP to be the best coupling reagent for a comparable coupling reaction.<sup>125</sup> However coupling the two monoprotected dipeptides did not lead to the expected tetrapeptide [10]. Surprisingly, it gave the tripeptide Boc-AAG-OBn [16] which contains two *trans*-ACBC residues but only one GABA (see entry 3).

Table 4. Failed convergent synthesis of tetrapeptide [10].

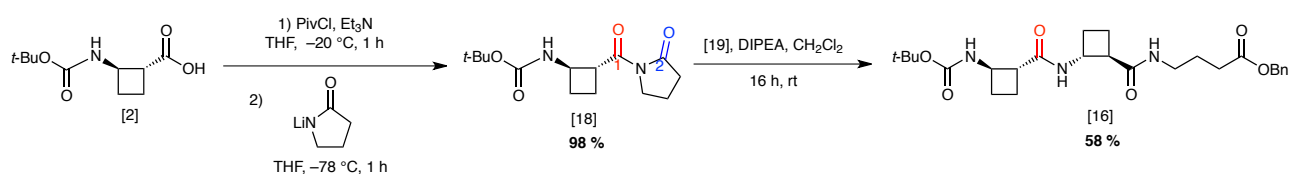
Entry	Coupling conditions	Peptide	Yield
1	HATU, DIPEA, (CH <sub>2</sub> Cl <sub>2</sub> /DMF:4/1), 25 °C	 [10]	27%
2	IBCF, Et <sub>3</sub> N, THF, -20 °C	 [15]	77 %
3	FDPP, DIPEA, (CH <sub>2</sub> Cl <sub>2</sub> /DMF:4/1), 25 °C	 [16]	56 %

To explain the formation of [16], it is proposed that the carbonyl of the amide (in red) undergoes the nucleophile attack of the amine partner instead of the activated carbonyl (in blue), which is unexpected (see Scheme 7). It is assumed that the carbonyl of *trans*-ACBC (in red) is activated or/and the carbonyl of GABA (in blue) is somehow deactivated. It is hypothesised that an intermediate  $\gamma$ -lactam [18] may be generated during the activation. It might be formed by the intramolecular nucleophile attack of NH amide onto the activated carbonyl of GABA.



Scheme 7. Formation of the proposed  $\gamma$ -lactam intermediate [15].

The intermediate  $\gamma$ -lactam [18] is a key feature of this proposed mechanism. Unfortunately, it could not be isolated nor observed during the synthesis. It was prepared unambiguously by coupling Boc-*trans*-ACBC activated by pivaloyl chloride with the lithium salt of 2-pyrrolidinone and was characterised spectroscopically. It was then treated with one equivalent of [19] and DIPEA in  $\text{CH}_2\text{Cl}_2$  overnight (see Scheme 8).



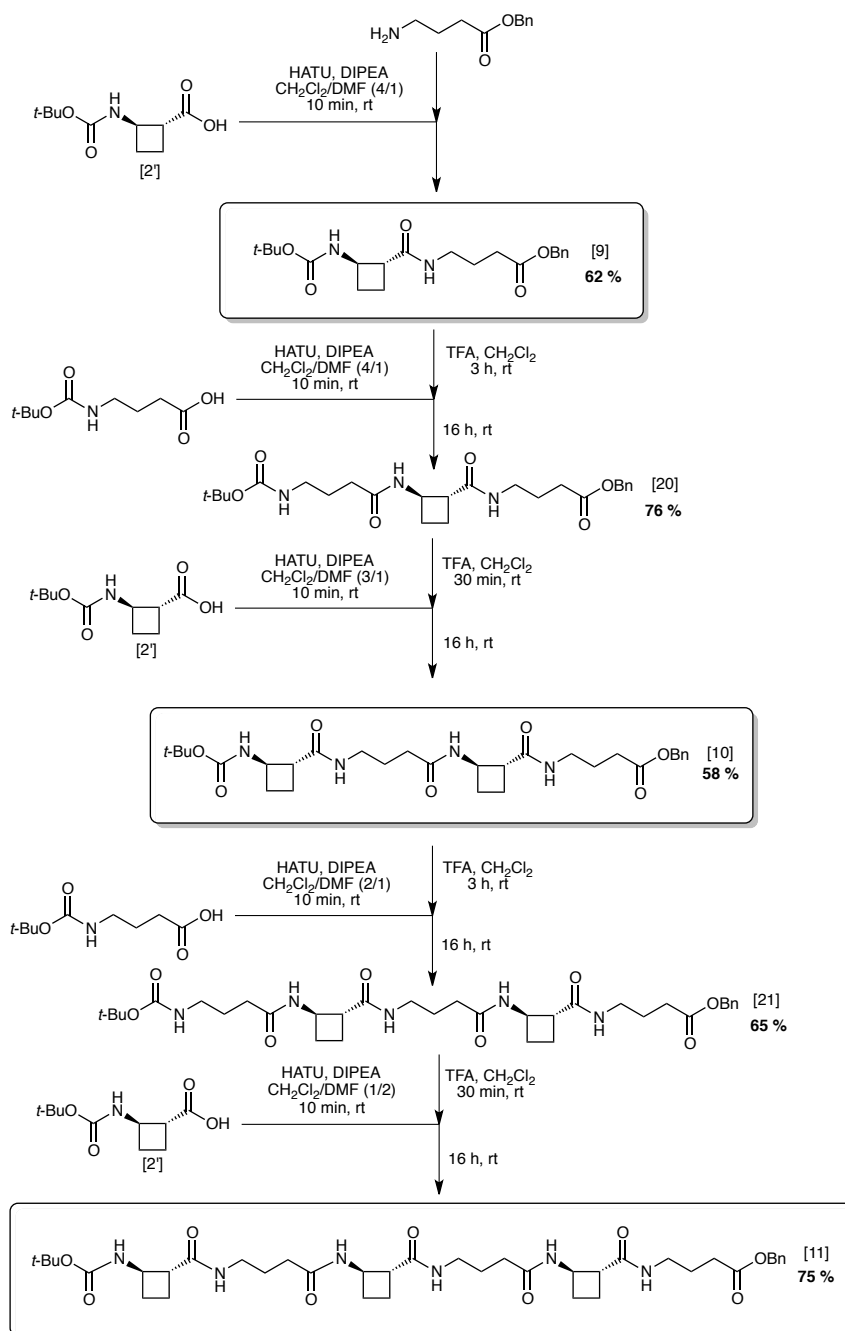
Scheme 8. Synthesis of the  $\gamma$ -lactam intermediate [18] via coupling of Boc-*trans*-ACBC with 2-pyrrolidinone.

The tripeptide [16] was obtained with 58% yield accompanied of a small quantity of the desired tetrapeptide [10]. This observation supported the mechanistic hypotheses presented in Scheme 7. It was concluded that a convergent strategy was not appropriate for the synthesis of tetrapeptide [10] and hexapeptide [11]. The alternative linear strategy was therefore examined.

#### 1.2.1.3. Synthesis of peptides [10] and [11]

Boc-GABA was activated by HATU and was treated with C-terminal protected dipeptide [9] to form the tripeptide Boc-GAG-OBn [20] in a good yield of 76 %. The *N*-Boc protecting group of the tripeptide [20] was cleaved by treatment with a large excess of TFA and coupled to Boc-*trans*-ACBC [2] activated by HATU to give the tetrapeptide Boc-AGAG-OBn [10] with a satisfactory yield of 58 %. The peptide chain was elongated twice more using the same procedure, via the pentapeptide Boc-AGAGA-OBn [21], obtained with a yield of 65 %, and finally the hexapeptide Boc-AGAGAG-OBn [11], with a yield of 75 % (see Scheme 9).

Tetrapeptide [10] was obtained with a yield of **27 % over three steps** and hexapeptide [11] was obtained with a yield of **13 % over five steps** from the Boc-*trans*-ACBC [2].



Scheme 9. Linear synthesis of dipeptide [9], tetrapeptide [10] and hexapeptide [11].

### 1.2.2. Convergent synthesis of peptides with GABA as the N-terminal residue [12]-[14]

For the synthesis of the dipeptide Boc-GA-OBn [12], tetrapeptide Boc-GAGA-OBn [13] and hexapeptide Boc-GAGAGA-OBn [14] with GABA as the N-terminal residue, a preliminary C-terminal protection of Boc-*trans*-ACBC [2'] was needed. The carboxylic acid [2'] was deprotonated using dry cesium carbonate in DMF and the resulting carboxylate was alkylated using benzyl bromide to give the Boc-*trans*-ACBC-OBn [22] with a yield of 75 % on gram scale (see Scheme 10).

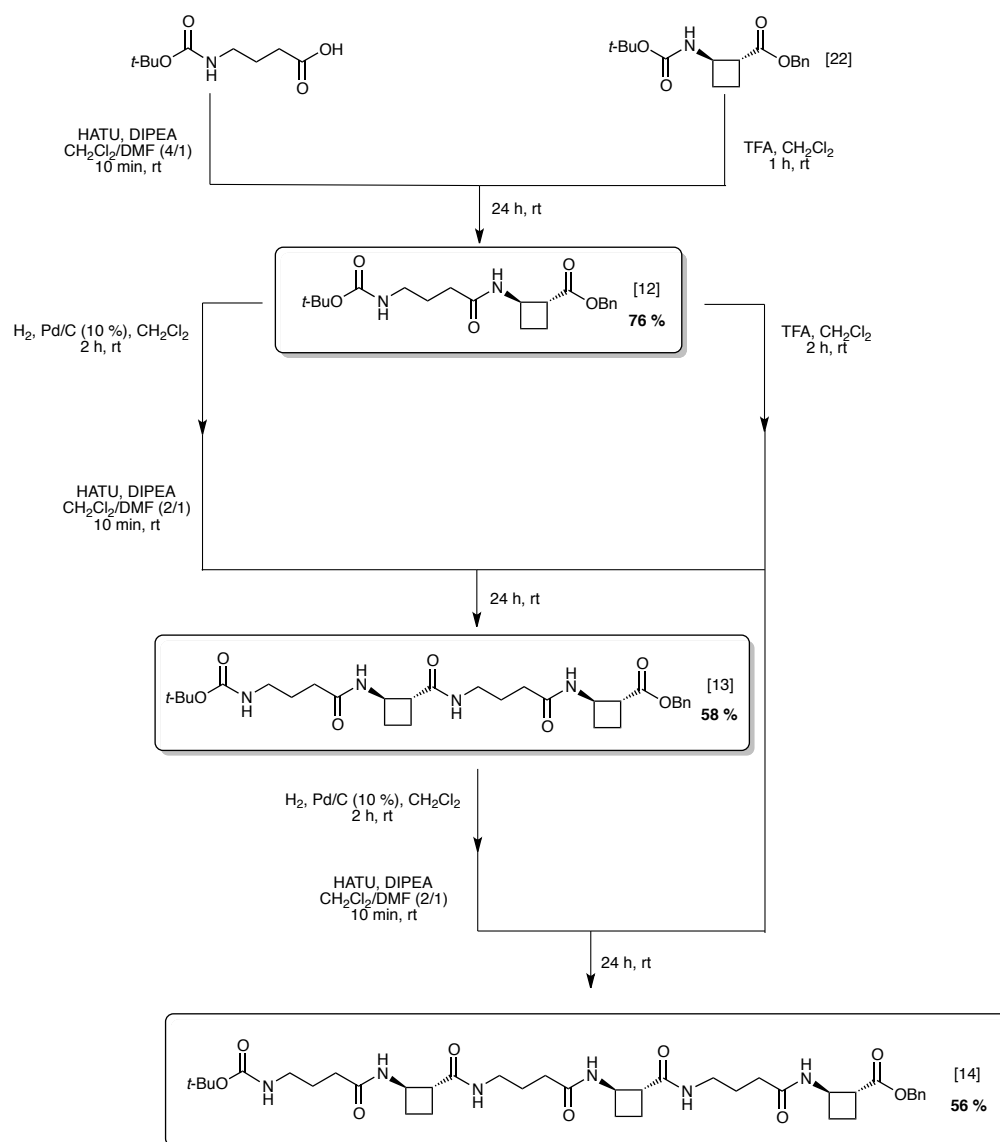


Scheme 10. Synthesis of Boc-*trans*-ACBC-OBn [22].

The synthesis of peptides [12]-[14] was carried out following a convergent strategy using the dipeptide GA fragment as the repeating unit (see Scheme 11).

The *N*-boc protecting group of [22] was cleaved by treatment with a large excess of TFA for 1 h to give the corresponding TFA salt. Coupling with Boc-GABA was performed using HATU in an overnight reaction and gave the dipeptide [12] with a good yield of 76 %. A sample of this dipeptide [12] was selectively N-terminal deprotected with a large excess of TFA for 2 h. Another sample of [12] was selectively C-terminal deprotected by hydrogenolysis under a dihydrogen atmosphere in the presence of Pd/C (10%) for 2 h. The two monoprotected dipeptide fragments were coupled using HATU in an overnight reaction to give the tetrapeptide [13] with a yield of 58 %. The benzyl ester protecting group of tetrapeptide [13] was cleaved by hydrogenolysis for 2 h and the resulting acid was coupled with another sample of the *C*-monoprotected dipeptide [12] using HATU in an overnight reaction to afford the hexapeptide [14] with a yield of 56 %.

Dipeptide [12] was obtained with a yield of 76%, tetrapeptide [13] was obtained with a yield of 44% over two steps and hexapeptide [14] was obtained with a yield of 25 % over only three steps from Boc-*trans*-ACBC-OBn [22]. Although lower yields were observed for each coupling reaction, this convergent strategy gave an overall yield twice as good as the linear strategy described in the previous section.



Scheme 11. Convergent synthesis of dipeptide [12], tetrapeptide [13] and hexapeptide [14].

### 1.3 Structural analyses of the peptides in solution-state

#### 1.3.1. General procedures for solution-state structural analyses

The structural analyses described in this thesis were carried out using a combination of several experimental and theoretical techniques.

We decided to conduct the analyses of the peptide series in a solution-state that minimises interactions between solvent and peptide and that favours peptide folding. These phenomena are best seen in aprotic and weak polar solvents as chloroform.

The  $^1\text{H}$  and  $^{13}\text{C}$  NMR spectral assignments for individual residues within each peptide were established by a combination of 2D NMR experiments:  $^1\text{H}$ - $^1\text{H}$  COSY,  $^1\text{H}$ - $^1\text{H}$  ROESY,  $^1\text{H}$ - $^{13}\text{C}$  HSQC,  $^1\text{H}$ - $^{13}\text{C}$  HMBC.

**DMSO- $d_6$  NMR titration** was used to assign the **free and H-bonded N-H**. Increasing aliquots of DMSO- $d_6$  (20  $\mu\text{L}$ , 40  $\mu\text{L}$ , 60  $\mu\text{L}$ , 80  $\mu\text{L}$  and 100  $\mu\text{L}$ ) were successively added to an NMR tube containing the peptides in  $\text{CDCl}_3$  (10 mM) and the  $^1\text{H}$  spectra were recorded after each addition. The addition of DMSO into the tube changes the polarity of the environment of the peptides. N-H engaged in hydrogen bonds are less sensitive to the DMSO- $d_6$  addition than the free N-H. A small difference of chemical shifts was observed for bonded N-H while a significant difference was observed for free N-H.

$^1\text{H}$ - $^1\text{H}$  **ROESY NMR experiments** provided direct information about the 3D molecular geometry of the peptides in solution by studying through-space magnetic interactions, or dipolar couplings, that give rise to the nOe (nuclear Overhauser effect).

ROESY experiments were chosen in preference to NOESY experiments because of the molecular weights of the larger peptides under study. The nOe can become weak and vanishing for molecules with molecular weights of around 1000 daltons and rotating-frame nOe (ROE) measurements become more sensitive in such cases.

For ROESY experiments, the peptide concentration was selected so as not to be too high, to avoid false correlations due to intermolecular contacts, and not too low, to avoid lengthy acquisition times. A convenient compromise was found for a concentration of 10 mM in  $\text{CDCl}_3$ .

Solution-state **Infrared (IR)** spectra were used to confirm the observations made by NMR. IR spectra were recorded in order to determine the presence and the type of hydrogen bonds between N-H and C=O functions of the peptides.<sup>169</sup> Distinct amide environments can be identified for free and bound N-H, when the amide stretching region (3200-3500  $\text{cm}^{-1}$ ) was examined. The stretching vibration for a free N-H bond is generally between 3400 and 3500  $\text{cm}^{-1}$ . When the hydrogen of a N-H is engaged in a hydrogen bond, the bond strength is weaker leading to a vibration frequency below 3400  $\text{cm}^{-1}$ . The concentration must be low to avoid intermolecular interactions usually between 5 and 10 mM. In this way, hydrogen-bonded N-H vibrations should only arise from intramolecular interactions.

**Molecular modelling** studies were carried out in parallel with the above spectroscopic assays. Calculations were performed in two steps; first a hybrid Monte Carlo Multiple Minima (MCMM) conformational search was carried out in a chloroform medium using MacroModel 04 from Schrödinger software and the Merck Molecular Force Field (MMFF). 10 000 conformers were generated by MCMM. Low energy conformers (up to 10 or 20  $\text{kJ}\cdot\text{mol}^{-1}$  of relative energy) were retained



and were sorted according to their conformer families. Then the geometries of the lowest energy conformer of each family were subjected to *ab initio* geometrical optimization by Density Functional Theory (DFT) using GAUSSIAN 09 and the B3LYP/6-311G(d,p) basis set in a chloroform medium. When the optimization converged, the Gibbs free energy was calculated, which allowed determination of Boltzmann distributions at 300 K.

The calculations were performed without constraints from experimental data. Thus they were **used as a theoretical tool** and are **completely independent from experimental data**.

**Circular dichroism** (CD) spectra were sometimes used to characterize peptide structure. The choice of solvents for CD spectral measurement is very restrictive because of the far-UV region implicated. Many common organic solvents, such as chloroform, dichloromethane, ethyl acetate, tetrahydrofuran, are incompatible with far-UV CD. Only aqueous media, alcohols, alkanes and acetonitrile are available to measure spectra of peptide derivatives. In addition to the question of solvent effects, it should be pointed out that CD data are not sufficient for drawing firm conclusions on the conformational preferences of peptides.

The spectra of peptides in this manuscript were recorded at a concentration of 0.2 mM in methanol or in acetonitrile when soluble.

### ***1.3.2. Complete characterisation in chloroform***

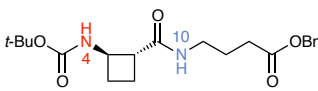
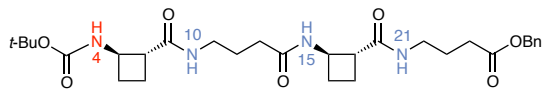
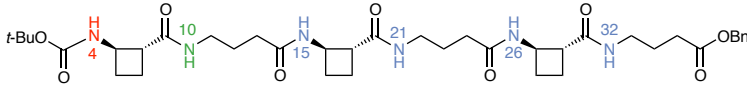
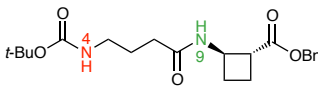
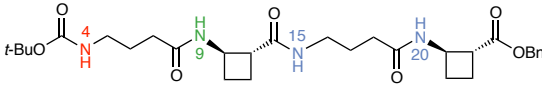
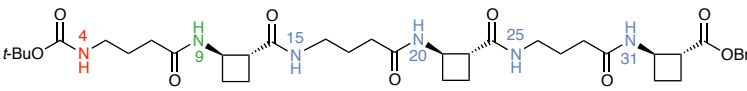
#### ***1.3.2.1. Titration of DMSO- $d_6$ by $1D^1H$ NMR***

All  $^1H$  and  $^{13}C$  signals pertinent for conformational analyses of Boc-AG-OBn [9], Boc-AGAG-OBn [10], Boc-AGAGAG-OBn [11], Boc-GA-OBn [12], Boc-GAGA-OBn [13] and Boc-GAGAGA-OBn [14] were unambiguously assigned, except for certain  $H\beta$  and  $H\gamma$  of GABA residues that could not be clearly assigned (see in PART III).

It was first helpful that chemical shift of carbamate N-H was considerably more shielded (a 2 ppm difference) than amide N-H.

The titration of  $CDCl_3$  solutions by DMSO- $d_6$  was carried out for all six [9]-[14]. The differences of chemical shifts of the N-H between 0% and 50% of added DMSO- $d_6$  were determined and were classified by a colour code as: high (in red), medium (in green) and low (in blue) (see Table 5).

Table 5. DMSO-*d*<sub>6</sub> titration of β/γ-peptides [9]-[14].

Δδ(NH(4))	1.93	 [9]
Δδ(NH(10))	0.18	
Δδ(NH(4))	1.5	 [10]
Δδ(NH(10))	0.14	
Δδ(NH(15))	0.15	
Δδ(NH(21))	-0.21	
Δδ(NH(4))	2.04	 [11]
Δδ(NH(10))	0.96	
Δδ(NH(15))	0.16	
Δδ(NH(21))	0	
Δδ(NH(26))	0.08	
Δδ(NH(32))	-0.18	
Δδ(NH(4))	1.49	 [12]
Δδ(NH(9))	1.17	
Δδ(NH(4))	1.39	 [13]
Δδ(NH(9))	0.69	
Δδ(NH(15))	-0.1	
Δδ(NH(20))	0.38	
Δδ(NH(4))	1.72	 [14]
Δδ(NH(9))	0.97	
Δδ(NH(15))	-0.01	
Δδ(NH(20))	0.16	
Δδ(NH(25))	-0.16	
Δδ(NH(31))	0.31	

Each β/γ-peptide showed only one N-H with a high DMSO-*d*<sub>6</sub> titration coefficient indicating only one free N-H. This was the N-terminal carbamate N-H (in red) (easy to distinguish by its chemical shift from the other amides).

### 1.3.2.2. ROESY experiments by 2D <sup>1</sup>H-<sup>1</sup>H NMR

ROESY experiments were carried out for all six peptides [9]-[14] using in CDCl<sub>3</sub> solutions at a concentration of 10 mM. Several ROEs were detected and the significant ones are presented in Figure 70.

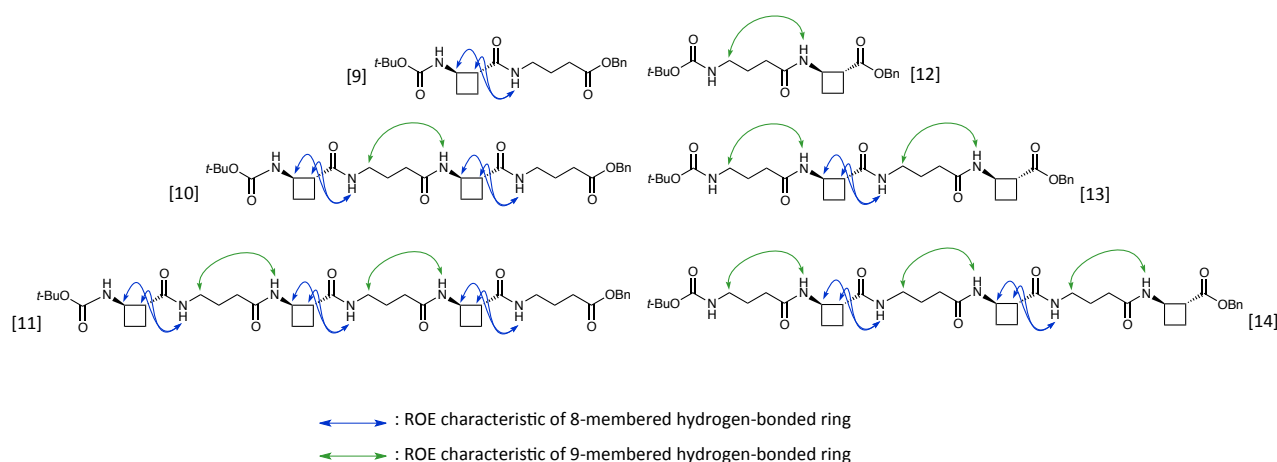


Figure 70. ROEs of [9]-[14] observed in  $\text{CDCl}_3$ .

The ROEs shown in blue,  $\text{H}\alpha(i)\text{-NH}(i+1)$  and  $\text{H}\beta(i)\text{-NH}(i+1)$  in Figure 70, have already been observed in the literature for derivatives of *trans*-ACBC (see Figure 71 A).<sup>120</sup> They are diagnostic of an 8-membered hydrogen-bonded ring (or C8) adopted around the *trans*-ACBC residue. Boc-AG-OBn [9] clearly adopted a C8 pattern (see Figure 72).

Similarly the ROEs shown in green,  $\text{H}\gamma(i)\text{-NH}(i+1)$  in Figure 70 have already been observed in the literature around a GABA residue (see Figure 71 B).<sup>133</sup> They are diagnostic of a 9-membered hydrogen-bonded ring (or C9) that is adopted by the GABA residue. Boc-GA-OBn [20] clearly adopted a C9 pattern (see Figure 72).

Tetrapeptides Boc-AGAG-OBn [10], Boc-GAGA-OBn [13] and hexapeptides Boc-AGAGAG-OBn [11], Boc-GAGAGA-OBn [14] presented repetitive ROEs diagnostic of 9- and 8-membered hydrogen-bonded rings indicating a regular folding pattern, featuring alternating C9 and C8 patterns (see Figure 72).

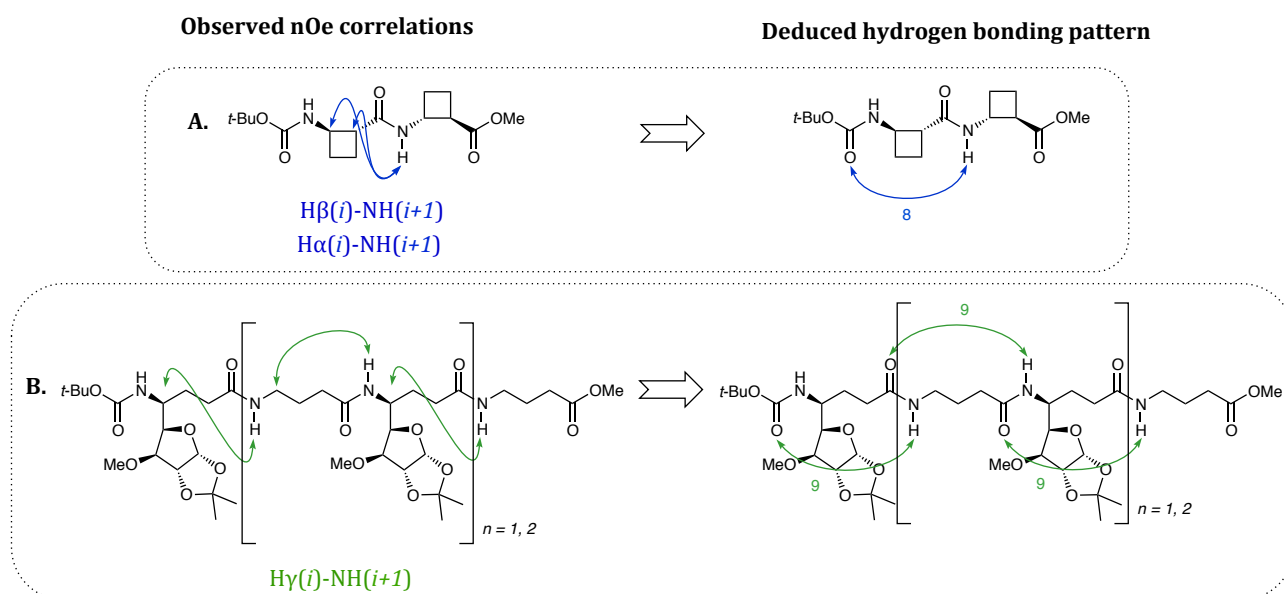


Figure 71. A: Observed nOes linked with the hydrogen bonding patterns of published structures adopting 8-membered hydrogen-bonded rings. B: Observed nOes linked with the hydrogen bonding patterns of published structures adopting 9-membered hydrogen-bonded rings.

Furthermore the results from DMSO- $d_6$  titrations, which presented only a free N-H corresponding to the carbamate, were perfectly consistent with the conformational preferences of the six  $\beta/\gamma$ -peptides presented in Figure 72.

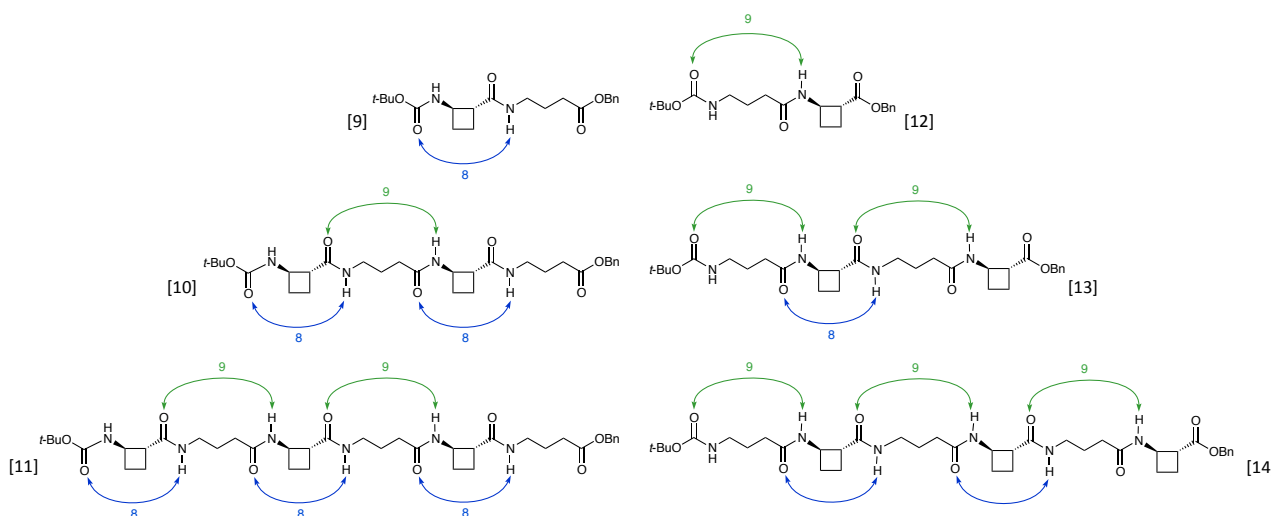


Figure 72. Alternative C9/C8 adopted by the  $\beta/\gamma$ -peptides [9]-[14].

### 1.3.2.3. Infrared studies

IR spectra of the six peptides, [9]-[14], were recorded in  $CDCl_3$  solutions at a concentration of 5 mM (see Figure 73). At a first glance, the six peptides all displayed the same general features in the N-H stretch regions: a fairly sharp band at  $3450\text{ cm}^{-1}$  corresponding to a free N-H and a large band from  $3230$  to  $3370\text{ cm}^{-1}$  corresponding to hydrogen-bonded N-H.

The band at  $3300\text{ cm}^{-1}$  of Boc-AG-OBn [9] was diagnostic of its amide N-H engaged in the 8-membered hydrogen-bonded ring, clearly determined by NMR experiments. The band at  $3350\text{ cm}^{-1}$  of Boc-GA-OBn [12] was indicative of its amide N-H engaged in the 9-membered hydrogen-bonded ring, showed by NMR experiments.

Tetrapeptides [10], [13] and hexapeptides [11], [14] presented two bands in the hydrogen-bonded N-H stretch region: one at  $3275\text{ cm}^{-1}$  corresponding to amide N-H engaged in the 8-membered hydrogen-bonded rings and  $3350\text{ cm}^{-1}$  corresponding to amide N-H engaged in the 9-membered hydrogen-bonded rings.

The IR spectra were clearly consistent with the conformational preferences suggested by NMR experiments: a C8 adopted by Boc-AG-OBn [9], a C9 adopted by Boc-GA-OBn [12] and alternating C9/C8 adopted by Boc-AGAG-OBn [10], Boc-GAGA-OBn [13] and hexapeptides Boc-AGAGAG-OBn [11], Boc-GAGAGA-OBn [14].

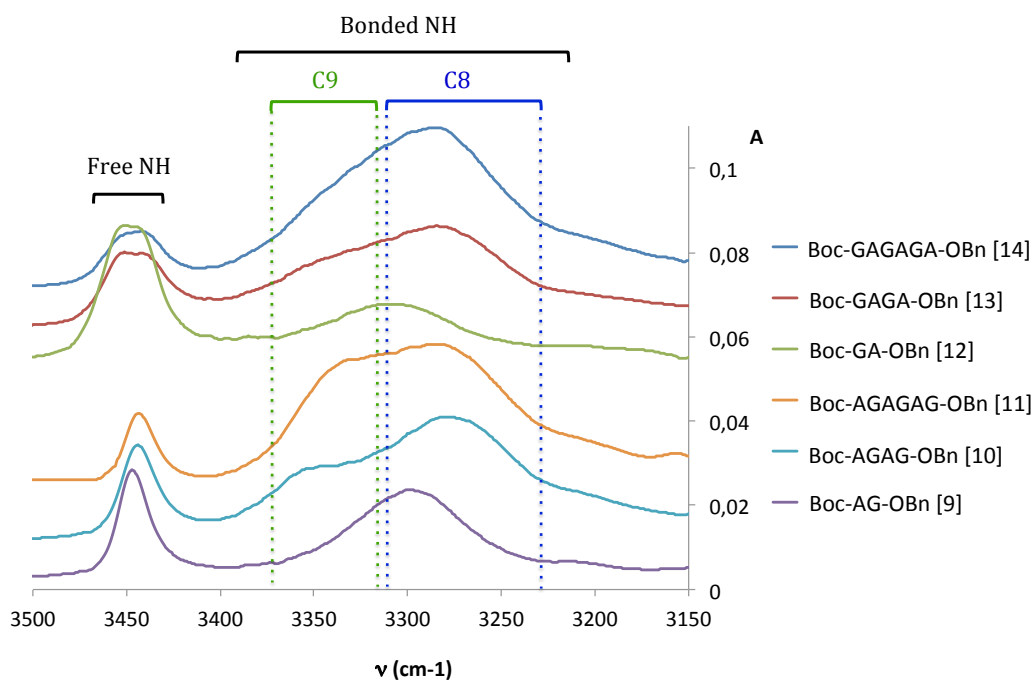


Figure 73. Superimposition of the IR spectra of  $\beta/\gamma$ -peptides [9]-[14] (5 mM in  $\text{CDCl}_3$ ) in the N-H stretching bands.

#### 1.3.2.4. Molecular modelling

Molecular modelling was carried out to provide further details of the folding behaviour evidenced experimentally.

##### 1.3.2.4.1. Hybrid Monte Carlo Multiple Minima calculations

A MCOMM (Monte Carlo Multiple Minima) calculation was first performed on the tetrapeptides [10], [13] and hexapeptides [11], [14] to investigate the conformational landscape of these  $\beta/\gamma$ -peptides in chloroform. The different conformations, up to 10 kJ/mol, were sorted according to the hydrogen-bonded ring systems they possessed (see Figure 74) and their abundance is given in Table 6:

- a C9/C8-conformer was composed only of alternating and distinctive 9- and 8-membered H-bonded rings (C9 and C8).
- the other conformers were composed diversely of 8-, 9-, 13- and 17-membered hydrogen-bonded rings. The discreet, successive rings are separated by the symbol '-'. The 13- and 17-membered H-bonded rings implicate a carbonyl oxygen that is bifurcated between two amide hydrogens, thus forming two rings wherein the larger ring includes the smaller; the combined system is noted with the symbol ','.

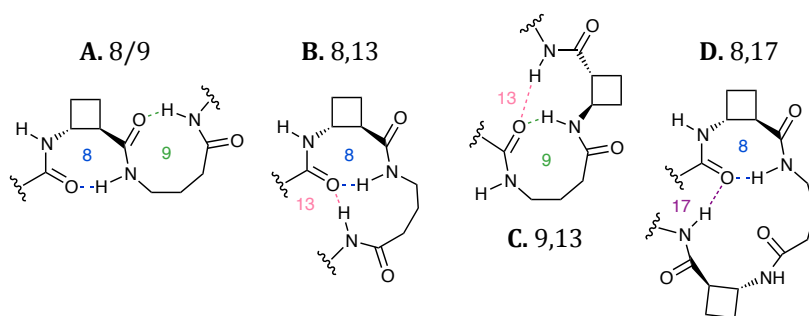


Figure 74. Hydrogen-bonding patterns found by MCMM.

Table 6. Abundance of conformer families found after Monte Carlo calculations in chloroform - \*: corresponded to 9/8-ribbon conformers

Conformations	Abundance of each conformer family (number of conformers of that family/total number of conformers; expressed as %)	Conformations	Abundance of each conformer family (number of conformers of that family/total number of conformers < 10 kJ.mol <sup>-1</sup> ; expressed as %)
Boc-AGAG-OBn [10] (261 conformers < 10 kJ.mol <sup>-1</sup> )		Boc-AGAGAG-OBn [13] (616 conformers < 10 kJ.mol <sup>-1</sup> )	
8-9-8*	98	9-8-9*	94
8-9,13	2	9-8,13	6
Boc-AGAGAG-OBn [11] (827 conformers < 10 kJ.mol <sup>-1</sup> )		Boc-GAGAGA-OBn [14] (961 conformers < 10 kJ.mol <sup>-1</sup> )	
8-9-8-9-8*	92	9-8-9-8-9*	75
8-9-8-9,13	5	9-8-9-8,13	16
8-9-8,13-9	3	9-8-9,13-9	2
		9-13-13-13	3
		9-8,13-8,17	2
		17,8-8,17	2

In all cases the conformational landscape was **dominated by C9/C8-conformer families**. The structure of these C9/C8-conformer families did not have a helical topology, being flattened and resembling a **9/8-ribbon** (see Figure 75)

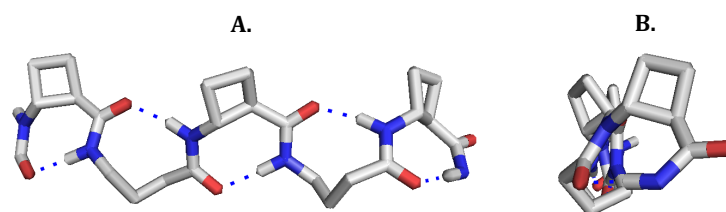


Figure 75: Backbone of the 9/8-ribbon adopted by Boc-AGAGAG-OBn [11]

It is notable that contributions from helical conformers are non-existent. Occasionally C13 features are detected, meaning that 13-membered hydrogen-bonded rings are accessible for  $\beta/\gamma$ -peptides containing *trans*-ACBC residues. In one case, three successive C13 are observed. This is an important point, with respect to the declared objective of establishing  $\beta/\gamma$ -peptide mimetics of an  $\alpha$ -helix.

## 1.3.2.4.2. DFT optimization: Gibbs energy and Boltzmann distribution

The lowest-energy conformer of each conformer family of each peptide was subjected to *ab initio* geometrical optimization by DFT in a chloroform medium to determine its Gibbs free energy (see Table 7). Relative Gibbs energies were then deduced between conformer families. A Boltzmann distribution was then calculated to evaluate the relative populations (in %) of the conformer families in solution at room temperature.

Table 7. Relative Gibbs energy and Boltzmann distribution for the different conformer families determined by DFT.

Conformations		Relative Gibbs energy (kJ.mol <sup>-1</sup> )	Boltzmann distribution (%)	
Boc-AGAG-OBn [10]				
9/8-ribbon		0	100	
8-9,13		13.6	0	
Boc-GAGA-OBn [13]				
9/8-ribbon (4 conformers)	A	0.20	25	99
	B	0	27	
	C	0.44	22	
	D	0.21	25	
9-8,13		7.30	1	
Boc-AGAGAG-OBn [11]				
9/8-ribbon		0	88.9	
8-9-8-9,13		5.30	10.6	
8-9-8,13-9		13.1	0.5	
Boc-GAGAGA-OBn [14]				
9/8-ribbon (8 conformers)	A	0.07	11	93
	B	0.38	12	
	C	0.46	12	
	D	0.58	12	
	E	0.19	11	
	F	0.15	12	
	G	0.15	13	
	H	0	10	
9-8-9-8,13		1.48	7	
9-8-9,13-9		8.71	0	
9-13-13-13		10.5	0	
9-8,13-8,17		17.1	0	
17,8-8,17		did not converge	0	

After DFT optimization, the landscape is still largely dominated by **9/8-ribbon** conformers, which presented alternating C9 and C8 features.

The hydrogen bonds were all strong and in the same range of O...H-N distances, between 1.7 and 1.9 Å. The rigid *trans*-ACBC residues display highly uniform ( $\varphi$ ,  $\theta$ ,  $\psi$ ) torsion angle values (90°, -100°, 30°) very close to those which characterize this residue in an optimized 8-helix foldamer.<sup>111</sup> Each

GABA residue adopted favourable *gauche* local conformations for the  $(\theta, \zeta)$  torsion angles, facilitating formation of the 9-membered hydrogen-bonded ring and concomitant orientation of its N–H towards an (*i*–2) carbonyl and of its C=O towards an (*i*+1) amide N–H.

Boc–AGAG–OBn [10] and Boc–AGAGAG–OBn [11] showed a very limited number of low-energy **9/8-ribbon conformers**. Boc–AGAG–OBn [10] gave a single 9/8-ribbon conformer (see Figure 76) while Boc–AGAGAG–OBn [11] showed three conformers of which the most populated (88.9 %) was also a unique 9/8-ribbon (see Figure 77). The second conformer (11.1 %) showed a 9/8-ribbon frayed at the C-terminal by displaying a bifurcated C13 feature. The third conformer was negligible (0.5 %).

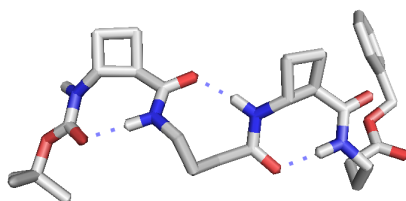


Figure 76. Side view of the 9/8-ribbon adopted by [10].

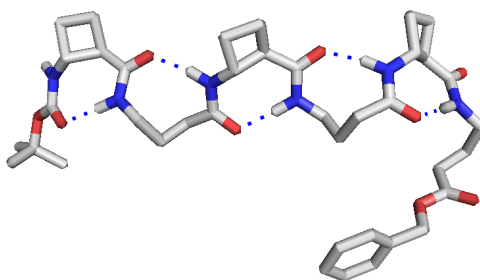


Figure 77. Side view of the 9/8-ribbon adopted by [11].

The conformational analysis of Boc–GAGA–OBn [13] and Boc–GAGAGA–OBn [14] was more complex but was still dominated by **9/8-ribbon conformers**. Boc–GAGA–OBn [13] showed four distinct 9/8-ribbon conformers (see Figure 78), almost equally populated, and differing by no more than 0.44 kJ.mol<sup>–1</sup> in energy. Boc–GAGAGA–OBn [14] showed eight distinct 9/8-ribbon conformers (see Figure 79), again almost equally populated, differing by less than 0.58 kJ.mol<sup>–1</sup> in energy. The other conformers were much less abundant the only significant one (7 %) being a 9/8-ribbon frayed at the C-terminal by a bifurcated C13 feature instead of a C9 feature.



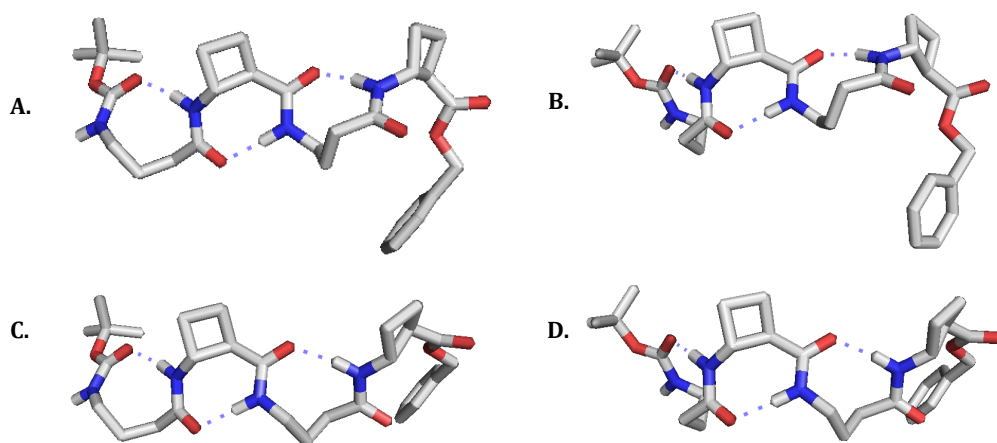


Figure 78. Side views of the four 9/8-ribbon conformers adopted by [13].

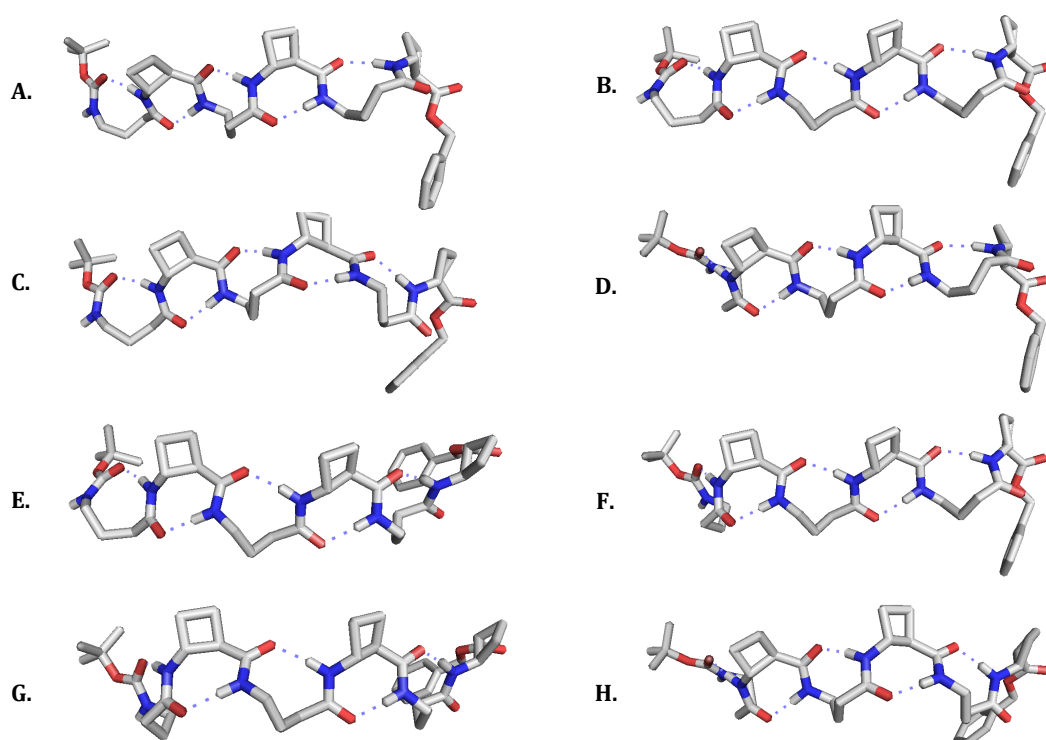


Figure 79. Side views of the eight 9/8-ribbon conformers adopted by [14].

The presence of several 9/8-ribbon conformer families can be explained by the flexibility of the GABA residue. The GABA residues facilitated 9-hydrogen membered-rings by displaying *gauche*  $\theta$  and *gauche*  $\zeta$  torsion angles. Each GABA residue presented  $g^+, g^+$  (hereafter  $G^+$ ) or  $g^-, g^-$  ( $G^-$ ) local conformations. A peptide with  $n$  9-membered hydrogen-bonded rings accommodated by  $n$  GABA residues can present  $2^n$  combinations of conformations.

Boc-AGAG-OBn [10] possessed one 9-membered hydrogen-bonded ring in which the first GABA presented a  $G^+$  local conformation. Boc-GAGA-OBn [13] possessed two 9-membered hydrogen-bonded rings accommodated by two GABA residues leading to all four possible combinations ( $G^+G^+$ ,  $G^+G^-$ ,  $G^-G^+$ ,  $G^-G^-$ ). The four combinations of torsion angles were found in the four 9/8-ribbon conformers.

Boc-AGAGAG-OBn [11] possessed two 9-membered hydrogen-bonded rings but showed a single 9/8-ribbon conformer family within ( $G^+G^-$ ) for the two GABA residues. Boc-GAGAGA-OBn [14] possessed three 9-membered hydrogen-bonded and showed eight 9/8-ribbon conformer families within all eight possible  $G^+$  and  $G^-$  combinations ( $G^+G^+G^+$ ,  $G^+G^-G^+$ ,  $G^-G^+G^+$ ,  $G^-G^-G^+$ ,  $G^+G^+G^-$ ,  $G^+G^-G^-$ ,  $G^-G^+G^-$ ,  $G^-G^-G^-$ ).

#### 1.3.2.4.3. Relationship between GABA local conformations and global molecular shape

Inspection and comparison of the 9/8-ribbon conformer families of Boc-GAGA-OBn [13] and Boc-GAGAGA-OBn [14] revealed a fascinating feature: the ribbons showed a certain **degree of curvature** in the plane perpendicular to that of the propagation of the 9/8-ribbon axis (see Figure 81 for Boc-GAGA-OBn [13] and Figure 82 for Boc-GAGAGA-OBn [14]).

The extent of curvature for any given conformer was characterized in terms of the relative orientations of consecutive H-bonded rings, qualified as “straight” (–) or “bent” (∩). For a given conformer, the dihedral angles defined by the four atoms engaged in two successive H-bonded rings which constituted a C9/C8/C9 system centered around a residue *trans*-ACBC<sub>(i)</sub> were measured according to Figure 80:

- the four-atom sets CO<sub>(i-2)</sub>-HN<sub>(i)</sub>-CO<sub>(i-1)</sub>-HN<sub>(i+1)</sub> for the C9→C8 relationship
- the four-atom sets CO<sub>(i-1)</sub>-HN<sub>(i+1)</sub>-CO<sub>(i)</sub>-HN<sub>(i+2)</sub> for the C8→C9 relationship

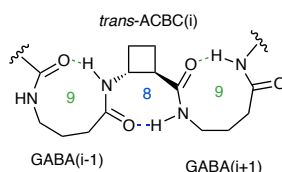


Figure 80. Measurement of dihedral angles between two successive H-bonds.

Only two value ranges were observed:

- For the C9→C8 relationship, these were in the range of 164° to 178°, which constituted a “straight” (–) segment of the molecular architecture, or from 122° to 136° which constituted a “bent” (∩) segment.
- For the C8→C9 relationship, the observed value ranges were from 160° to 168° for a “straight” (–) segment, or from –136° to –144° for a “bent” (∩) segment.

This phenomenon did not correlate with any single GABA conformation ( $G^+$  or  $G^-$ ) as such, but instead with the combined local conformation types of the GABA pair on either side of the intervening *trans*-ACBC residue in a given C9/C8/C9 segment.

An unambiguous code existed between GABA-(*i*)/GABA-(*i*+2) conformation pairs and the relative orientations of the pairs of H-bonded rings around which they were folded.

For example, in conformer C of Boc-GAGA-OBn [13] (see Figure 81), the ( $G^+G^+$ ) GABA conformer set translated to a “straight” GABA-1-*trans*-ACBC-2 fragment followed by a “bent” *trans*-ACBC-2-GABA-3 fragment. The ( $G^+G^-$ ) GABA conformer A set translated to a “straight” GABA-1-*trans*-ACBC-2, “straight” *t*ACBC-2-GABA-3 fragment. The ( $G^-G^-$ ) GABA conformer B set translated to a “bent” GABA-1-*trans*-ACBC-2, “straight” *trans*-ACBC-2-GABA-3 fragment. The ( $G^-G^+$ ) GABA conformer D set translated to a “bent” GABA-1-*trans*-ACBC-2, “bent” *trans*-ACBC-2-GABA-3 fragment.

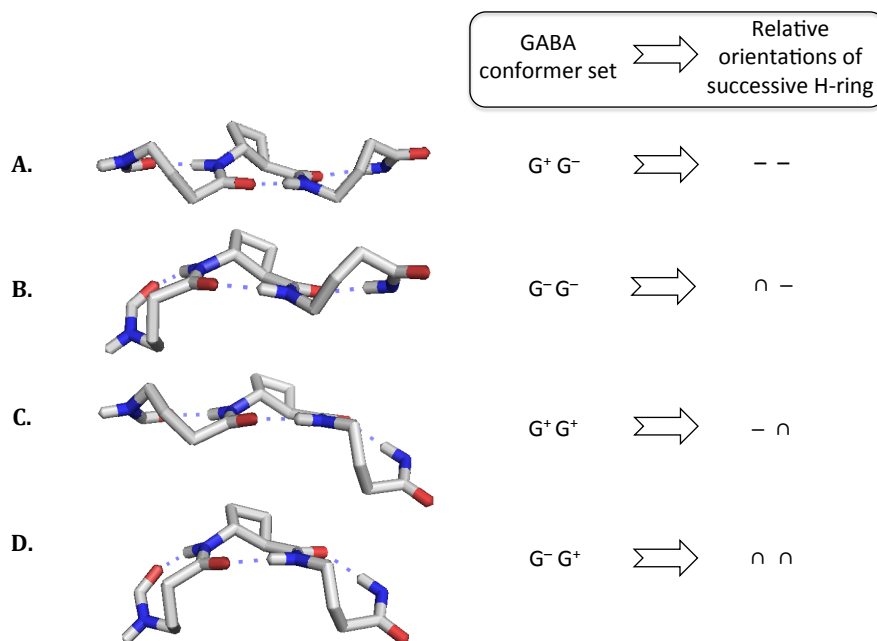


Figure 81. GABA conformer sets linked to the molecular shape of [13].

To determine the topology of Boc-GAGAGA-OBn [14], the code observed in Boc-GAGA-OBn [13] was applied for three GABA conformer sets. For example, in conformer [14 B] (see Figure 82), with a ( $G^+G^+G^-$ ) GABA conformer set, the first pair ( $G^+G^+$ ) correlated to a “straight-bent” GABA-1-*trans*-ACBC-2-GABA-3 segment while the second pair ( $G^+G^-$ ) translated to a “straight-straight” GABA-3-*trans*-ACBC-4-GABA-5 segment. Following this code, we identified the remaining seven topology sets corresponding to the seven GABA conformer sets.

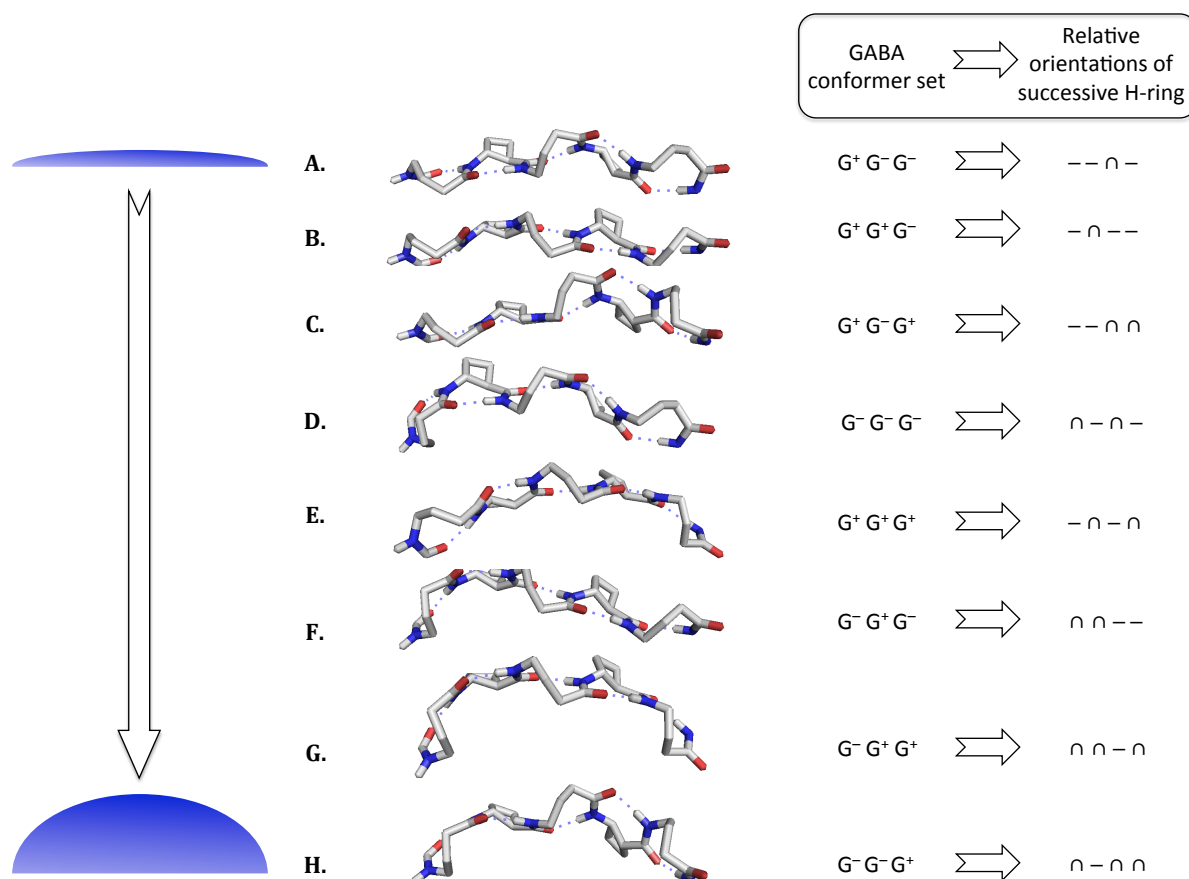


Figure 82. GABA conformer sets linked to the molecular shape of [14].

Intriguingly, the mathematical nature of this code made it impossible to generate a 9/8-ribbon conformer having three or more consecutive “straight” or “bent” fragments. This suggested that 9/8-ribbons could not lie flat in a plane nor adopt highly-rounded structures; they were intrinsically destined to adopt slightly curved architectures.

Retrospectively, the code allowed the assignment of the central C9/C8/C9 fragment of the low energy conformer of peptide Boc-AGAGAG-OBn [11] with a ( $G^+G^-$ ) pair; a “straight-straight” topology was adopted.

#### 1.3.2.5. Partial characterisation in protic solvent

The conformational preference of peptides is often solvent-dependent and this is especially important when biological applications are envisaged objectives. The  $\beta/\gamma$ -peptides described above are soluble in few solvents: chloroform, mixtures of chloroform and DMSO, and methanol to a small extent. The limited solubility in methanol is nonetheless interesting, because it allows characterisation of the peptides by CD.

## 1.3.2.5.1. Circular Dichroism

CD spectra were recorded as 0.2 mM solution in methanol for each of the six peptides [9]-[14] (see Figure 83). The per-residue normalised Cotton effect, although quite low, increased with the length of the peptides. Both hexapeptides [11] and [14] presented a similar  $\theta$  maximum at 203-204 nm and a small  $\theta$  minimum at 224 nm Cotton effect.

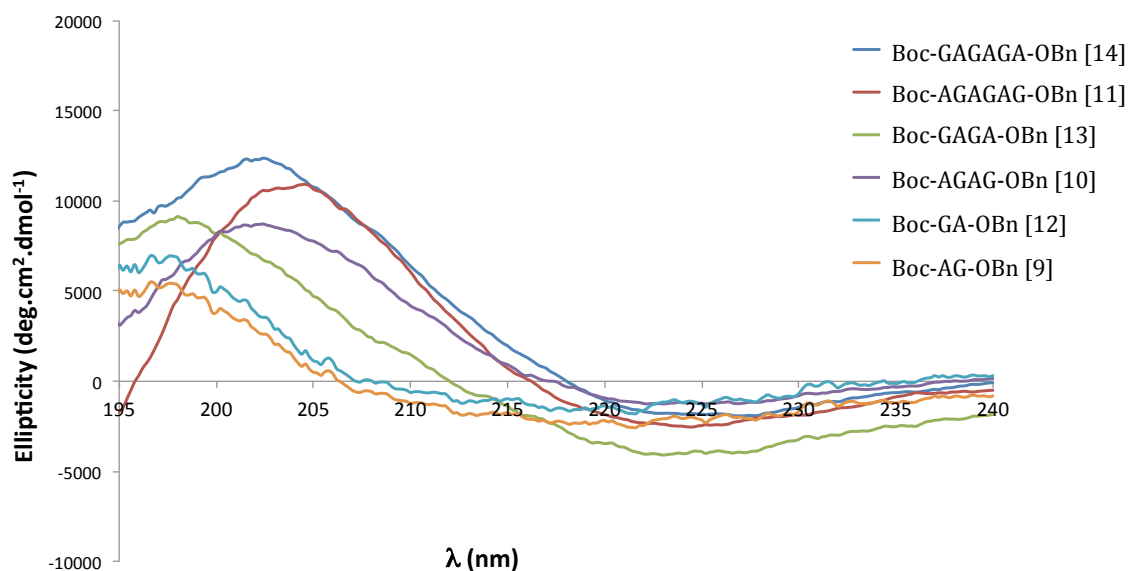


Figure 83. CD spectra of the  $\beta/\gamma$ -peptides [9]-[14].

Since all other data (previous sections) were obtained in chloroform solution, it was not possible to conclude that the CD spectra in methanol were the signatures of 9/8-ribbons. The structural studies of the peptides would need to be completed by a further characterisation in methanol.

However, a full characterisation in methanol solution was not feasible. Indeed IR spectra in methanol bring no information on the N-H region because of persistent O-H band even with a solvent background subtraction.

## 1.3.2.5.1. Molecular Modelling

MCMM calculations were performed on the tetrapeptides [10], [13] and hexapeptides [11], [14] to determine the conformational landscape of these  $\beta/\gamma$ -peptides in octanol (methanol is not available in the MacroModel 04 software). The different types of conformation were sorted according to the hydrogen-bonded ring systems they possessed and their abundance is given in Table 8.

Table 8. Abundance of conformer families found after Monte Carlo calculations in octanol. \*: corresponds to a 13-helix.

Conformations	Abundance of each conformer family (number of conformers of that family/total number of conformers; expressed as %)	Conformations	Abundance of each conformer family (number of conformers of that family/total number of conformers < 10 kJ.mol <sup>-1</sup> ; expressed as %)
Boc-AGAG-OBn [10] (179 conformers < 10 kJ.mol <sup>-1</sup> )		Boc-GAGA-OBn [13] (190 conformers < 10 kJ.mol <sup>-1</sup> )	
13-13-13*	95	13-13-13*	58
13-8	5	13-9	25
		13-/-	16
		9-8-/-	1
Boc-AGAGAG-OBn [11] (80 conformers < 10 kJ.mol <sup>-1</sup> )		Boc-GAGAGA-OBn [14] (51 conformers < 10 kJ.mol <sup>-1</sup> )	
13-13-13-8	49	13-13-13-13*	2
8-13-13-13	23	9-13-13-13	2
8-9-13-13	17	13-13-/-13	49
13-13-9-8	11	17-13-13	17
		13-8-/-13	10
		13-17-13	8
		13-9-13	8
		9-8-9-13	4

Unexpectedly, the 9/8-ribbon structures were not found for any of the peptides. The landscape was **dominated by conformer families bearing C13 features**. C8 or C9 features were less frequently detected. These results are more encouraging from the point of view of the objective to mimic the  $\alpha$ -helix with  $\beta/\gamma$ -peptides.

The change of folding preferences of foldamer peptides with the solvents has been described by the Aitken group.<sup>111</sup> For  $\beta$ -peptides composed of *trans*-ACBC and an AAzC residue at the N-terminal position, two regular secondary structures were available for these compounds: an 8-helix and a 12-helix. Regardless of the peptide length, there was a greater preference for the 12-helix when the solvent was methanol than was the case with chloroform.

### 1.3.2.6. Conclusion

In conclusion to this chapter, the objective of mimicking the  $\alpha$ -helix with a 13-helical  $\beta/\gamma$ -peptide constructed from *trans*-ACBC and GABA has not been reached. However, we have discovered an **unprecedented** regular folded structure that can be adopted by these peptides in chloroform, a **9/8-ribbon**. This study enhances the contribution of ribbons in the foldamer field with a structure that shows distinctive features, notably the facile coexistence of several low energy 9/8-ribbon conformers due to the local flexibility of the GABA components and governed by a combination of the stereochemical factors imparted by both the rigid *trans*-ACBC components (configuration) and the GABA components (conformation).

Moreover this study underlines the importance of the solvent for structural studies (see Figure 84). The 9/8-ribbon conformers are dominant in a chloroform medium but are not found in a alcohol medium in which a majority of C13 features are detected instead. This also illustrates the dynamics of peptides in solution that must not be neglected if biological applications are anticipated.

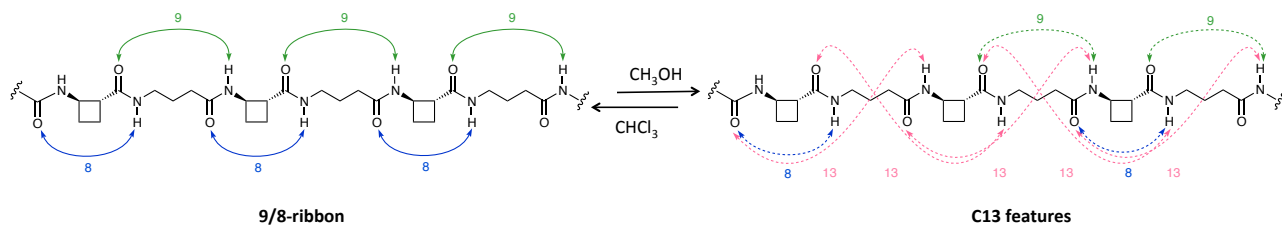


Figure 84. A robust 9/8-ribbon conformer in chloroform adopted by  $\beta/\gamma$ -peptides alternating *trans*-ACBC and GABA

## 2. Synthesis and structural studies of $\beta/\gamma$ -peptides alternating *trans*-ACBC and $\gamma^4$ -amino acids: a robust 13-helix<sup>vii</sup>

It is proposed in this chapter to investigate whether the presence of a substituent on  $\gamma$ -amino acid on  $\gamma^4$ -position induces preferential folding into a 13-helix.

### 2.1 Peptide selection

The objective of this research was to mimic the native  $\alpha$ -helix with a  $\beta/\gamma$ -peptide manifold. In Chapter I, we discovered that  $\beta/\gamma$ -peptides constructed alternately from *trans*-ACBC and GABA did not adopt a 13-helical conformation in solution, but a 9/8-ribbon. We found that the torsion angles in the 9/8-ribbon of GABA components were  $(\theta, \zeta) = (68^\circ, 75^\circ)$ , but based on the work of the Hofmann group, the  $\gamma$ -component of a 13-helical  $\beta/\gamma$ -peptide would possess torsion angles of  $(\theta, \zeta) = (61^\circ, 62^\circ)$ .<sup>150</sup> We propose that the introduction of a side-chain at the  $\gamma^4$ -position of the  $\gamma$ -amino acid component should favour  $(\theta, \zeta)$  torsion angles close to  $60^\circ$ . The **steric constraints of a  $\gamma^4$ -amino acid** should therefore **destabilise the 9/8-ribbon and favour the 13-helix**.

Furthermore, the introduction of side-chains would give functionality to the  $\beta/\gamma$ -peptides, which anticipates the design of functional  $\alpha$ -helix mimetics (see Chapter 3).

In contrast with a GABA residue, the  $\gamma$ -amino acids studied in this chapter are chiral. Configurations of all backbone stereogenic centres – (*R*)- $\gamma^4$ -amino acid and (1*S*,2*S*)-*trans*-ACBC – were chosen in order to privilege the P-helix folding sense, in analogy with the native  $\alpha$ -helix. The  $\gamma^4$ -amino acids were chosen in order to favour helical propensity and to avoid interference from side chain interactions (see PART I). Hydrophobic aromatic and aliphatic residues,  $\gamma^4$ -*h*Phe and  $\gamma^4$ -*h*Leu, were thus used. These  $\gamma$ -amino acids were also chosen in order to facilitate the NMR assignments.

In the previous Chapter, the influence of the position of the structuring *trans*-ACBC was investigated via the study of the two series of  $\beta/\gamma$ -peptides.

Two C-terminal protecting groups, benzyl ester and benzyl amide, were also compared to evaluate the influence of an additional C-terminal H-bond.

These considerations led to the study of twelve peptides presented in Figure 85.

<sup>vii</sup> The peptides described in this chapter are called in this manuscript following a code in which *trans*-ACBC is represented by the letter A and  $\gamma^4$ -*h*X by the letter Gx. For example, the dipeptide alternating *trans*-ACBC and  $\gamma^4$ -*h*Phe (or  $\gamma^4$ -*h*F) is called Boc-AGf-OBn.



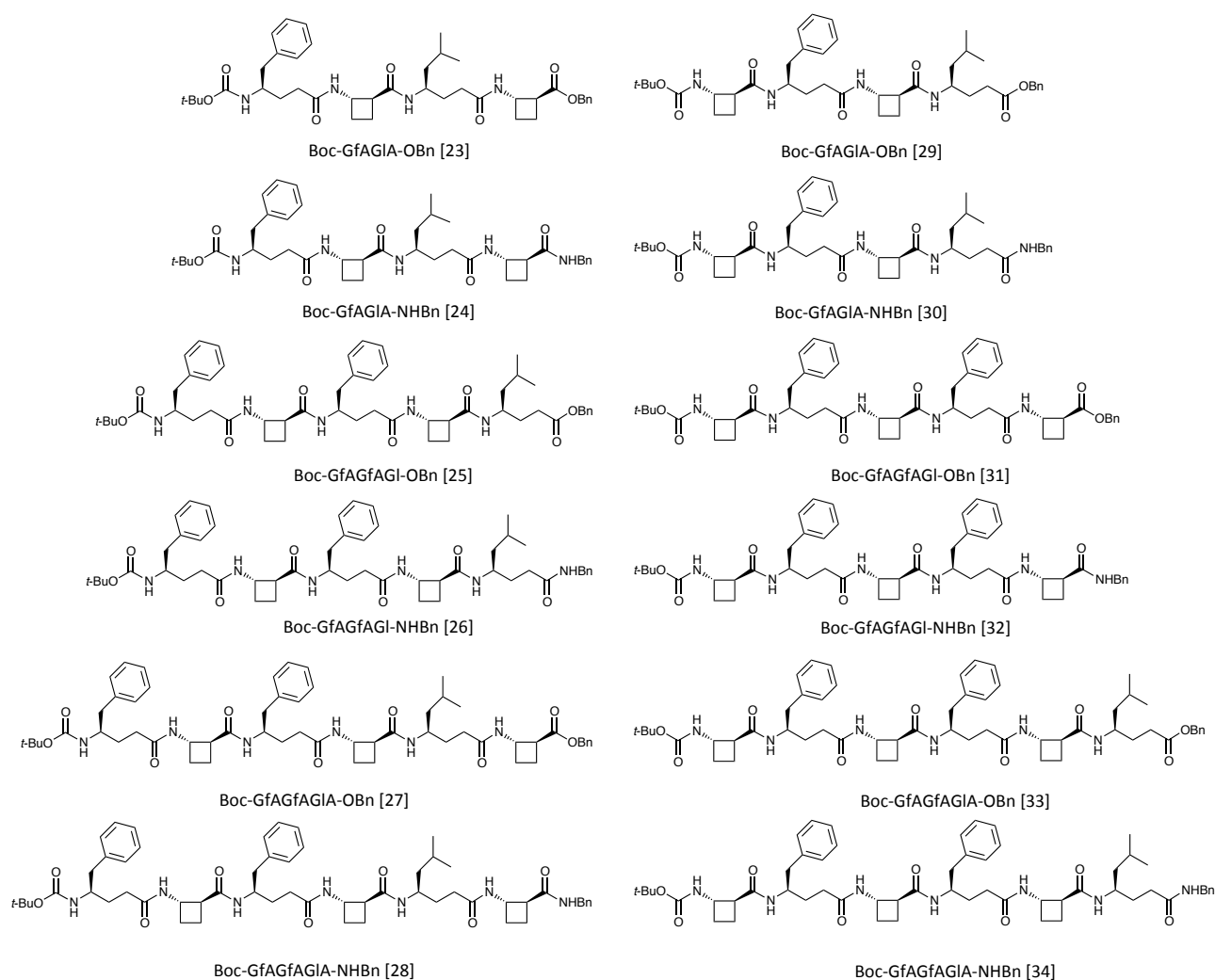


Figure 85.  $\beta/\gamma$ -Peptides alternating *trans*-ACBC and  $\gamma^4$ -amino acids [23]-[34].

## 2.2 Synthesis of $\beta/\gamma$ -peptides alternating *trans*-ACBC and $\gamma^4$ -amino acids [23]-[34]

### 2.2.1. Synthesis of peptides with $\gamma^4$ -amino acids at the N-terminal [23]-[28]

The syntheses of tetrapeptides Boc-GfAGIA-OBn [23], Boc-GfAGIA-NHBn [24] and hexapeptides Boc-GfAGfAGIA-OBn [27], Boc-GfAGfAGIA-NHBn [28] were carried out using a convergent strategy based on dipeptides Boc-GfA-OBn [35] and Boc-GIA-OBn [36] (see Scheme 12).

The *N*-Boc protecting group of [22] was cleaved by treatment with a large excess of TFA for 2 h to give the corresponding TFA salt.  $\gamma^4$ -*h*Phe was coupled to the TFA salt of [22] using HATU in an overnight reaction to give the dipeptide [35] with a good yield of 76 %.  $\gamma^4$ -*h*Leu was coupled to the TFA salt of [22] using HATU in an overnight reaction to give the dipeptide [36] with a good yield of 86 %.

The *N*-Boc protecting group of dipeptide [36] was cleaved by treatment with a large excess of TFA during 2 h, while the benzyl ester protecting group of dipeptide [35] was removed by

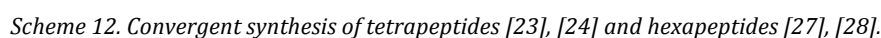
hydrogenolysis for 3 h. The two monoprotected dipeptides were coupled using HATU in an overnight reaction to give the tetrapeptide [23] with a yield of 62 %.

Benzyl ester of tetrapeptide [23] was removed by hydrogenolysis for 3 h. The acid form of [23] and benzylamine were coupled using HATU in an overnight reaction to give the tetrapeptide [24] with a yield of 64 %.

The *N*-Boc protecting group of tetrapeptide [23] was then cleaved by treatment with a large excess of TFA during 1 h to give the corresponding TFA salt. The TFA salt and the acid form of deprotected dipeptide [35] were coupled using HATU in an overnight reaction to finally afford hexapeptide [27] with a yield of 30 %. Purification of this hexapeptide was laborious and resulted in some loss of material.

Benzyl ester of hexapeptide [27] was removed by hydrogenolysis in CH<sub>2</sub>Cl<sub>2</sub> for 24 h. The acid form of [27] and benzylamine were coupled using HATU in an overnight reaction to give the hexapeptide [28] with a yield of 40 %.

Tetrapeptides [23] and [24] were synthesised with yields of 47 % and 30 % over two and three steps respectively from Boc-*trans*-ACBC-OBn [22]. Hexapeptides [27] and [28] were synthesised with yields of 15 % and 6 % over three and four steps from Boc-*trans*-ACBC-OBn [22].



The synthesis of pentapeptide Boc-GfAGfAGl-OBn [25] might have been envisaged from tetrapeptide Boc-AGfAGl-OBn [29] by a single coupling reaction with a residue of Boc- $\gamma^4$ -hPhe.

However, for practical reasons the synthesis of pentapeptide [25] and [26] was carried out according to Scheme 13. The available quantities of tetrapeptide [29] were devoted to structural analyses and the synthesis of hexapeptides [33] and [34].

Starting from the dipeptide [35], *N*-Boc deprotection was achieved by treatment with a large excess of TFA over 2 h to give the corresponding TFA salt. The benzyl ester of the same dipeptide [35] was removed by hydrogenolysis for 2 h. The two monoprotected dipeptides were coupled using HATU in an overnight reaction to give tetrapeptide [37] with a yield of 79 %.

The benzyl ester of tetrapeptide [37] was removed by hydrogenolysis for 2 h while the *N*-Boc protecting group of Boc- $\gamma^4$ -*h*Leu-OBn was cleaved with a large excess of TFA for 1 h. The generated carboxylate and the TFA salt were coupled using HATU in an overnight reaction to finally afford pentapeptide [25] with a yield of 57 %.

The benzyl ester of pentapeptide [25] was removed by hydrogenolysis in CH<sub>2</sub>Cl<sub>2</sub> for 6 h. The acid form of [25] and benzylamine were coupled using HATU in an overnight reaction to give the pentapeptide [26] with a yield of 45 %.

Pentapeptides [25] and [26] were synthesised with a yield of 19 % and 8 % over three and four steps respectively from Boc-*trans*-ACBC-OBn [22].

### 2.2.2. Synthesis of peptides with trans-ACBC at the N-terminal [29]-[34]

Starting from the protected dipeptide [35], the two tripeptides were synthesised. The *N*-Boc protecting group of [35] was cleaved by treatment with a large excess of TFA during 4 h to give the corresponding TFA salt, which was coupled with Boc-*trans*-ACBC [2] using HATU in an overnight reaction to give tripeptide [38] with a yield of 43 %. Benzyl ester cleavage from dipeptide [35] was achieved by hydrogenolysis while the *N*-Boc protecting group of Boc- $\gamma^4$ -*h*Leu-OBn was cleaved by treatment with a large excess of TFA during 1 h. The corresponding carboxylate and TFA salt were coupled using HATU in an overnight reaction to give tripeptide [39] with a yield of 66 %.

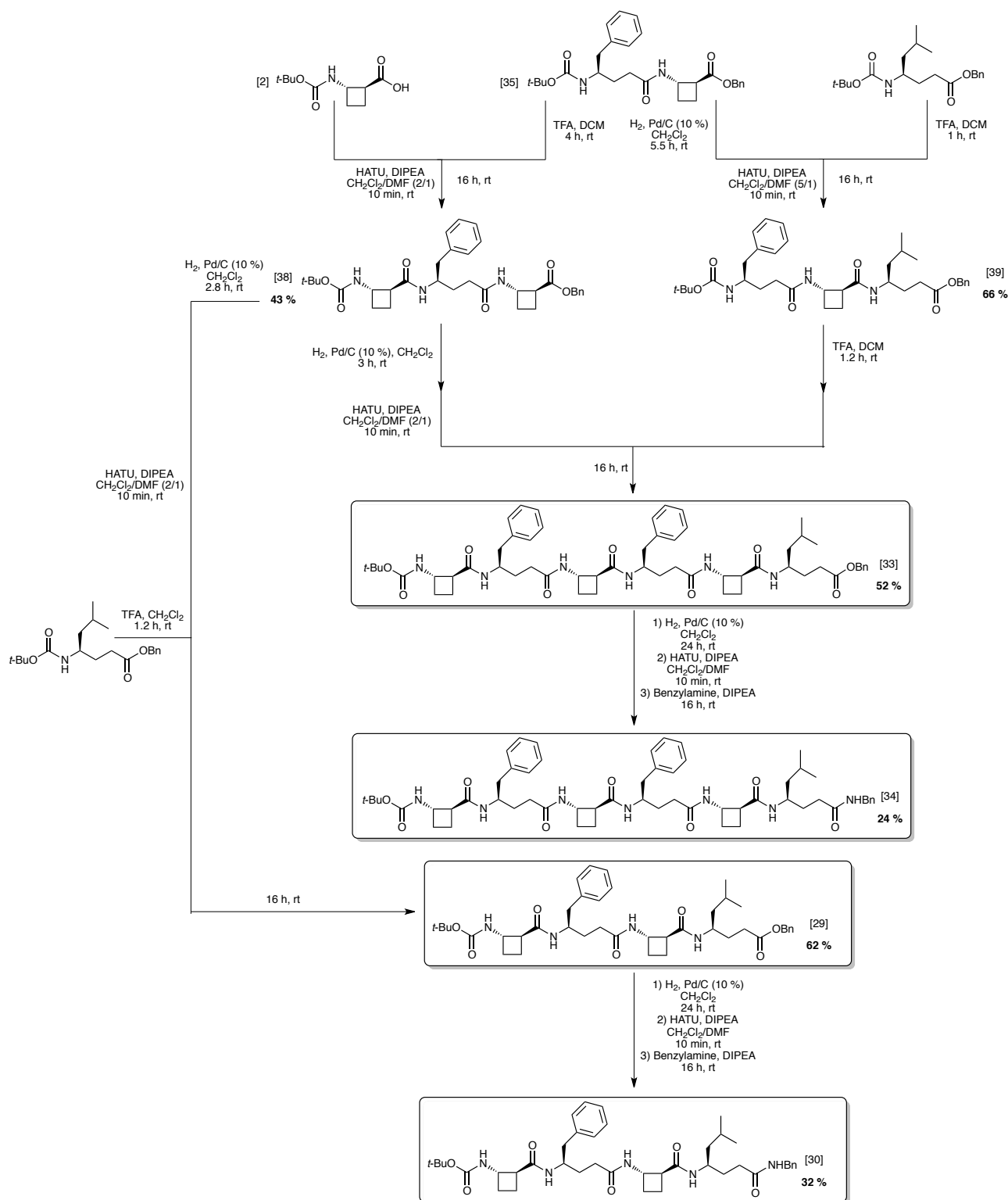
Benzyl ester removal from tripeptide [38] was achieved by hydrogenolysis while the *N*-Boc protecting group of Boc- $\gamma^4$ -*h*Leu-Bn was cleaved by treatment with a large excess of TFA for 1 h. The corresponding carboxylate and TFA salt were coupled using HATU in an overnight reaction to give tetrapeptide [29] with a yield of 62 %.

Benzyl ester of tetrapeptide [29] was removed by hydrogenolysis for 8 h. The acid form of [29] and benzylamine were coupled using HATU in an overnight reaction to give the tetrapeptide [30] with a yield of 32 %.

The benzyl ester removal from tripeptide [38] was achieved by hydrogenolysis while the *N*-Boc protecting group of tripeptide [39] was cleaved by treatment with a large excess of TFA for 1 h. The corresponding tripeptides carboxylate and TFA salt were coupled using HATU in an overnight reaction to give hexapeptide [33] with a yield of 52 %.

The benzyl ester of hexapeptide [33] was removed by hydrogenolysis for 24 h. The acid form of [33] and benzylamine were coupled using HATU in an overnight reaction to give the hexapeptide [34] with a yield of 32 %.

Tetrapeptides [29] and [30] were synthesised with yields of 11 % and 4 % over three and four steps respectively from Boc-*trans*-ACBC [2]. Hexapeptides [33] and [34] were synthesised with yields of 15 % and 4 % over three and four steps respectively from Boc-*trans*-ACBC [2].



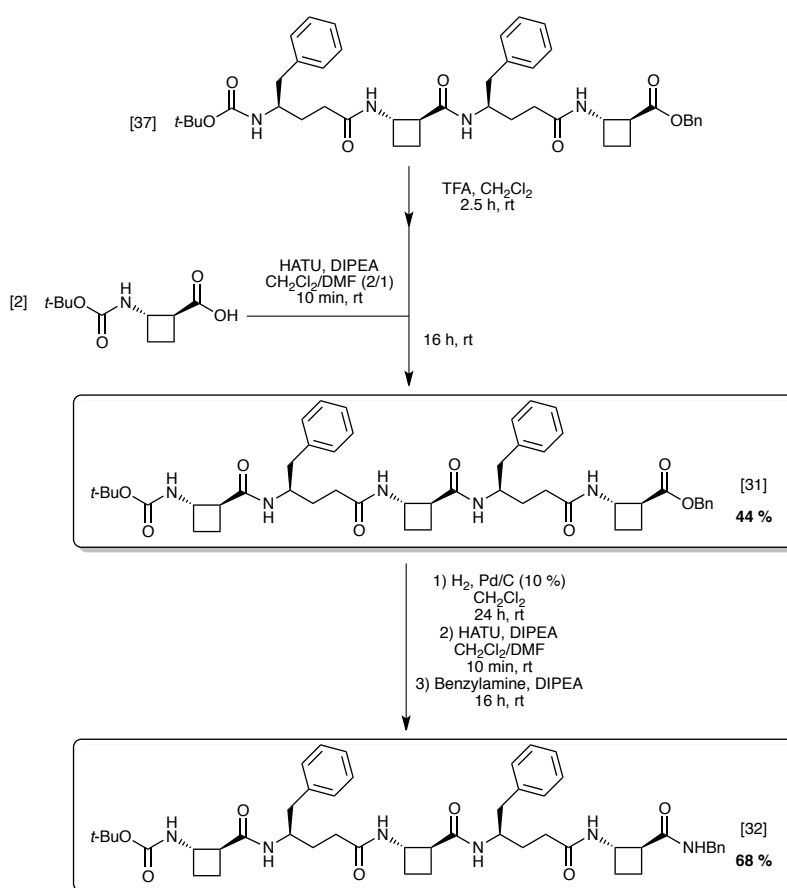
Scheme 14. Convergent synthesis of tetrapeptides [29], [30] and hexapeptides [33], [34].

Tetrapeptide [37] which was prepared as indicated on Scheme 13, was also used for the synthesis of pentapeptides Boc-AGfAGfA-OBn [31] and Boc-AGfAGfA-NHBn [32] (see Scheme 15).

The *N*-Boc protecting group of tetrapeptide [37] was cleaved by treatment with an excess of TFA for 2.5 h to give the corresponding TFA salt. Boc-*trans*-ACBC [2] and the TFA salt of [29] were coupled using HATU in an overnight reaction to give pentapeptide [31] with a yield of 44 %.

The benzyl ester of pentapeptide [31] was removed by hydrogenolysis for 24 h. The acid form of [31] and benzylamine were coupled using HATU in an overnight reaction to give the pentapeptide [32] with a yield of 68 %.

Pentapeptides [31] and [32] were synthesised with yields of 15 % and 10 % over three steps and four steps respectively from Boc-*trans*-ACBC-OBn.



Scheme 15. Synthesis of pentapeptides [31] and [32].

In each case, the change of benzyl ester for *N*-benzyl amide gave rather low yields for a simple change of protecting group. This might be explained by the filtration, removing Pd/C (10 %) catalyst after the hydrogenolysis step, due to the low solubility of the acid C-deprotected peptides in organic solvent.

The twelve peptides were synthesised in only three steps as benzyl esters or four steps for *N*-benzyl amides from *trans*-ACBC derivatives with satisfactory yields, affording **sufficient material for structural analyses**: greater than 50 mg in every case.



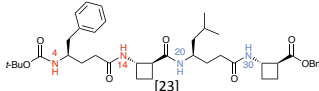
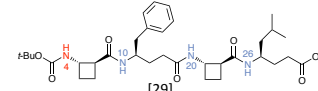
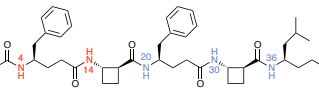
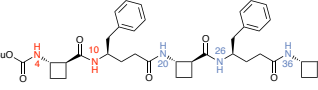
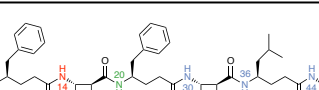
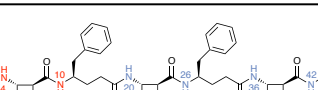
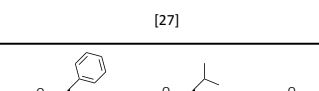
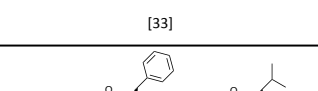
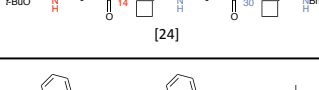
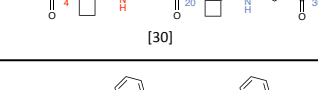
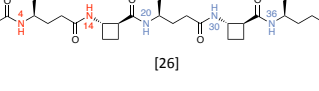
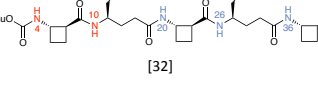
## 2.3 Structural studies and molecular modelling of the peptides

### 2.3.1. Titration of DMSO- $d_6$ by 1D $^1\text{H}$ NMR

All  $^1\text{H}$  and  $^{13}\text{C}$  signals pertinent for conformational analyses of Boc-GfAGIA-OBn [23], Boc-GfAGIA-NHBn [24], Boc-GfAGfAGI-OBn [25], Boc-GfAGfAGI-NHBn [26], Boc-GfAGfAGIA-OBn [27] and Boc-GfAGfAGIA-NHBn [28], Boc-AGfAGI-OBn [29], Boc-AGfAGI-NHBn [30], Boc-AGfAGfA-OBn [31], Boc-AGfAGfA-NHBn [32], Boc-AGfAGfAGI-OBn [33] and Boc-AGfAGfAGI-NHBn [34] were unambiguously assigned, except for certain H $\beta$ , C $\beta$ , H $\gamma$  and aromatic protons and carbons of  $\gamma^4$ -residues that could not be clearly assigned (see in PART III).

The titration of  $\text{CDCl}_3$  solutions by DMSO- $d_6$  was carried out for all twelve peptides [29]-[34]. The differences of chemical shifts of the N-H between 0% and 50% of added DMSO- $d_6$  were determined and were classified by a colour code as: high (in red), medium (in green) and low (in blue) (see Table 9).

Table 9. DMSO- $d_6$  titration of the  $\beta/\gamma$ -peptides [23]-[34].

$\Delta\delta(\text{NH}(4))$	1.92		$\Delta\delta(\text{NH}(4))$	1.67	
$\Delta\delta(\text{NH}(14))$	1.57		$\Delta\delta(\text{NH}(10))$	0.67	
$\Delta\delta(\text{NH}(20))$	-0.07		$\Delta\delta(\text{NH}(20))$	-0.05	
$\Delta\delta(\text{NH}(30))$	0.3		$\Delta\delta(\text{NH}(26))$	-0.45	
$\Delta\delta(\text{NH}(36))$	1.6		$\Delta\delta(\text{NH}(36))$	1.51	
$\Delta\delta(\text{NH}(4))$	1.38		$\Delta\delta(\text{NH}(4))$	1.46	
$\Delta\delta(\text{NH}(14))$	0.30		$\Delta\delta(\text{NH}(10))$	0.17	
$\Delta\delta(\text{NH}(20))$	0.07		$\Delta\delta(\text{NH}(20))$	0.11	
$\Delta\delta(\text{NH}(30))$	-0.24		$\Delta\delta(\text{NH}(26))$	0.06	
$\Delta\delta(\text{NH}(36))$	1.82		$\Delta\delta(\text{NH}(36))$	1.55	
$\Delta\delta(\text{NH}(4))$	1.84		$\Delta\delta(\text{NH}(4))$	1.4	
$\Delta\delta(\text{NH}(14))$	0.94		$\Delta\delta(\text{NH}(10))$	0.19	
$\Delta\delta(\text{NH}(20))$	0.09		$\Delta\delta(\text{NH}(20))$	0.11	
$\Delta\delta(\text{NH}(30))$	0.34		$\Delta\delta(\text{NH}(26))$	-0.1	
$\Delta\delta(\text{NH}(36))$	0.13		$\Delta\delta(\text{NH}(36))$	-0.09	
$\Delta\delta(\text{NH}(44))$	0.13		$\Delta\delta(\text{NH}(4))$	2.34	
$\Delta\delta(\text{NH}(14))$	1.57		$\Delta\delta(\text{NH}(10))$	2.21	
$\Delta\delta(\text{NH}(20))$	0.34		$\Delta\delta(\text{NH}(20))$	0.35	
$\Delta\delta(\text{NH}(30))$	0.19		$\Delta\delta(\text{NH}(26))$	0.36	
$\Delta\delta(\text{NH}(36))$	0.13		$\Delta\delta(\text{NH}(36))$	0.32	
$\Delta\delta(\text{NH}(4))$	1.78		$\Delta\delta(\text{NH}(4))$	1.43	
$\Delta\delta(\text{NH}(14))$	1.67		$\Delta\delta(\text{NH}(10))$	1.61	
$\Delta\delta(\text{NH}(20))$	0.72		$\Delta\delta(\text{NH}(20))$	0.37	
$\Delta\delta(\text{NH}(30))$	0.36		$\Delta\delta(\text{NH}(26))$	0.32	
$\Delta\delta(\text{NH}(36))$	0.16		$\Delta\delta(\text{NH}(36))$	0.09	
$\Delta\delta(\text{NH}(44))$	0.17		$\Delta\delta(\text{NH}(42))$	-0.05	
$\Delta\delta(\text{NH}(4))$	1.71		$\Delta\delta(\text{NH}(4))$	1.87	
$\Delta\delta(\text{NH}(14))$	1.65		$\Delta\delta(\text{NH}(10))$	1.87	
$\Delta\delta(\text{NH}(20))$	0.77		$\Delta\delta(\text{NH}(20))$	0.45	
$\Delta\delta(\text{NH}(30))$	0.18		$\Delta\delta(\text{NH}(26))$	0.07	
$\Delta\delta(\text{NH}(36))$	0.33		$\Delta\delta(\text{NH}(36))$	0.30	
$\Delta\delta(\text{NH}(44))$	0.05		$\Delta\delta(\text{NH}(42))$	0.19	
$\Delta\delta(\text{NH}(50))$	-0.08		$\Delta\delta(\text{NH}(50))$	0.23	

All of the  $\beta/\gamma$ -peptides clearly possessed two N-H signals with a high DMSO- $d_6$  titration coefficient that is to say two free N-H (in red), with the exception of tetrapeptide Boc-AGfAGI-OBn

[29] that possessed only one free N–H. The other N–H signals all showed a low titration coefficient suggesting that they are not exposed to solvents and engaged into a H-bond (in blue).

These observations suggest that the folding behaviour of the eleven peptides (except [29]) differ from a 9/8-ribbon structure in which only one N–H is free.

### 2.3.2. 2D $^1\text{H}$ - $^1\text{H}$ ROESY experiments and characteristic ROEs

ROESY experiments of the twelve peptides [23]-[34] were recorded in  $\text{CDCl}_3$  solutions at a concentration of 10 mM.

From the literature and the results of Chapter 1, three types of secondary structures adopted by  $\beta/\gamma$ -peptides have been characterised by NMR and the associated diagnostic NOEs and ROEs are known. In 9/8-ribbons, the ROEs,  $\text{H}\gamma(i)\text{-NH}(i+2)$  and  $\text{H}\beta(i)\text{-NH}(i+1)$  in blue and  $\text{NH}(i+1)\text{-H}\gamma(i)$  in green, were reported as diagnostic of C8 and C9 features (see Figure 86 A).<sup>170</sup> In 11/13-helices, the ROEs,  $\text{H}\gamma(i)\text{-NH}(i+2)$  in pink and  $\text{NH}(i)\text{-NH}(i+1)$  in purple were reported as diagnostic of C13 and C11 features (see Figure 86 B).<sup>154</sup> In 13-helices, the ROEs,  $\text{H}\beta(i)\text{-NH}(i+2)$ ,  $\text{H}\beta(i)\text{-H}\alpha(i+2)$  and  $\text{H}\gamma(i)\text{-NH}(i+2)$  in pink were reported as diagnostic of C13 features (see Figure 86 C).<sup>156</sup>

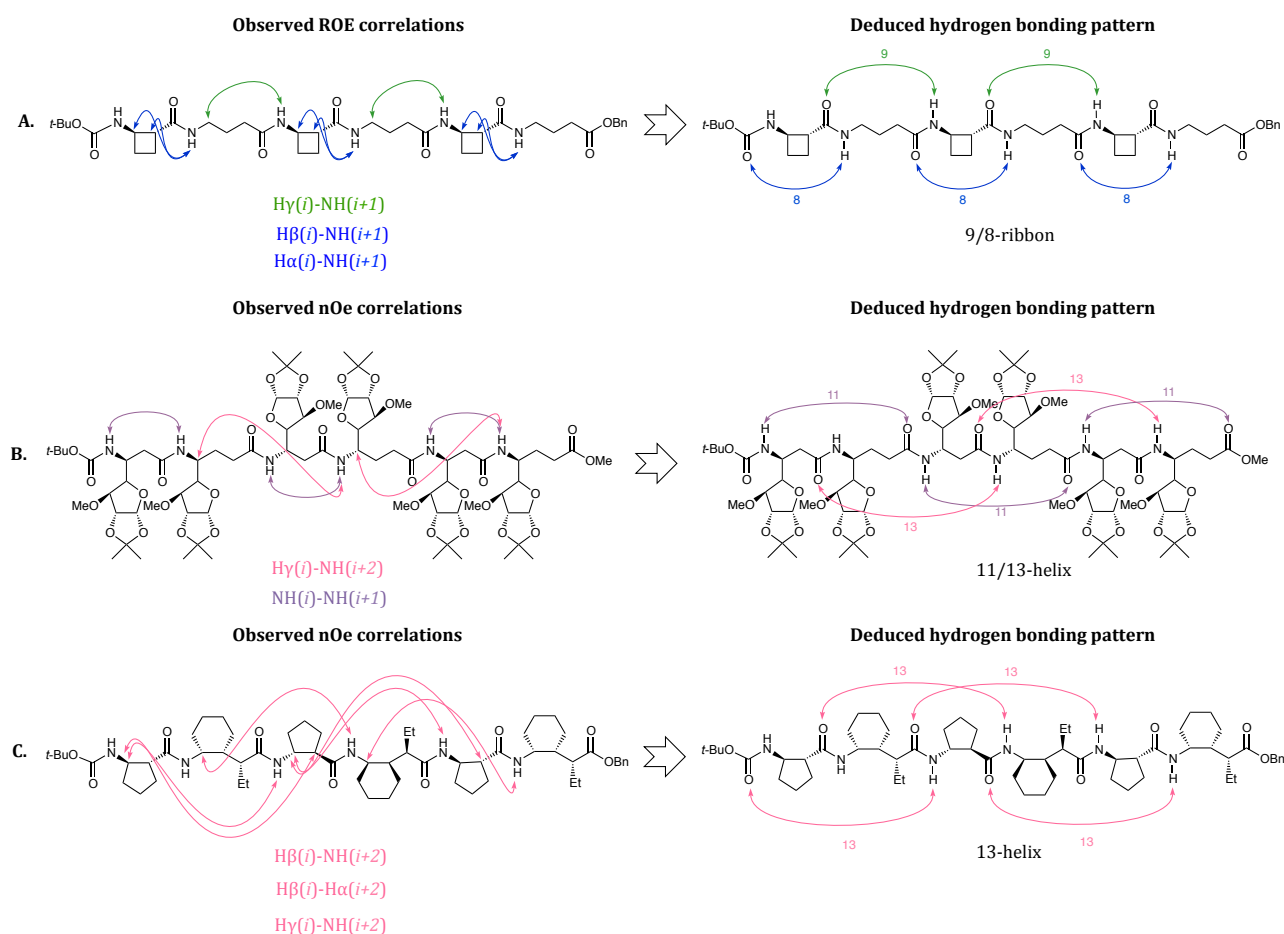


Figure 86. Observed ROEs and NOEs linked with the hydrogen bonding patterns of secondary structures- A: 9/8-ribbon. B: 11/13-helix. C: 13-helix.

These ROEs correlations from the literature were compared with the ROEs of the twelve  $\beta/\gamma$ -peptides in order to identify secondary structures. The results of the ROE studies of the twelve peptides are described below in three distinct parts for more clarity: four tetrapeptides (see Figure 87), four pentapeptides (see Figure 88) and four hexapeptides (see Figure 89).

Boc-AGfAGI-OBn [29] presented  $H\gamma(i)-NH(i+1)$  and  $H\beta(i)-NH(i+1)$  correlations around *trans*-ACBC 1 and *trans*-ACBC 3 (in blue) and  $NH(i+1)-H\gamma(i)$  correlation around  $\gamma^4$ -*h*Phe 2 (in green). These ROEs as we saw in Chapter 1, are two C8 features around *trans*-ACBC 1 and *trans*-ACBC 3 and a C9 feature around  $\gamma^4$ -*h*Phe 2. This was consistent with the DMSO- $d_6$  titration, which revealed the free carbamate N-H. Boc-AGfAGI-OBn [29] therefore adopted a 9/8-ribbon folding, as the only conformer.

Boc-GfAGIA-OBn [23] presented  $H\gamma(i)-NH(i+1)$  and  $H\beta(i)-NH(i+1)$  correlations around *trans*-ACBC 2 (in blue),  $NH(i+1)-H\gamma(i)$  correlations around  $\gamma^4$ -*h*Phe 1 and  $\gamma^4$ -*h*Leu 3 (in green). These ROEs are diagnostic of a C8 feature around *trans*-ACBC, two C9 features around  $\gamma^4$ -*h*Phe 1 and  $\gamma^4$ -*h*Leu 3. A longer-distance ROE  $H\gamma(i)-NH(i+2)$  around  $\gamma^4$ -*h*Phe 1 and *trans*-ACBC 2 was observed. It cannot be explained by the concatenation of C9 and C8 features, but was reported by the Gellman group as diagnostic of a C13 feature. It is therefore deduced that two conformers were present in solution, a

9/8-ribbon conformer and a 13-9 conformer. The contribution of the latter was fairly significant since the DMSO- $d_6$  titration revealed the two N-terminal N-H as being free.

Boc-AGfAGI-NHBn [30] presented  $H\beta(i)$ -NH( $i+2$ ),  $H\beta(i)$ -H $\alpha(i+2)$  and  $H\gamma(i)$ -NH( $i+2$ ) correlations at the N-terminal (in pink),  $H\gamma(i)$ -NH( $i+1$ ) and  $H\beta(i)$ -NH( $i+1$ ) correlations around *trans*-ACBC3 (in blue), NH( $i+1$ )- $H\gamma(i)$  around  $\gamma^4$ -*h*Leu4 (in green). The pink ROEs were the three correlations reported as diagnostic of a C13 feature around a  $\beta/\gamma$ -tripeptide unit. The pink ROEs were diagnostic of two C13 features around *trans*-ACBC1- $\gamma^4$ -*h*Phe 2-*trans*-ACBC 3. The blue ROEs were diagnostic of a C8 feature around *trans*-ACBC 3 and the green ROEs were diagnostic of a C9 feature around  $\gamma^4$ -*h*Leu 4. It is assumed that two conformers were present in solution, a 13-8-9 conformer and a 13-13-9 conformer. This was consistent with the DMSO- $d_6$  titration, which revealed the two N-terminal N-H as being free.

Boc-GfAGIA-NHBn [24] presented  $H\beta(i)$ -NH( $i+2$ ),  $H\beta(i)$ -H $\alpha(i+2)$  and  $H\gamma(i)$ -NH( $i+2$ ) correlations along the entire peptide (in pink),  $H\gamma(i)$ -NH( $i+1$ ) and  $H\beta(i)$ -NH( $i+1$ ) correlations around *trans*-ACBC 2 and *trans*-ACBC 4 (in blue), NH( $i+1$ )- $H\gamma(i)$  correlations around  $\gamma^4$ -*h*Phe 1 and  $\gamma^4$ -*h*Leu 3 (in green). The pink ROEs were diagnostic of four successive C13 features. The blue ROEs were diagnostic of two C8 feature around *trans*-ACBC 2 and *trans*-ACBC 4 and the green ROEs were diagnostic of two C9 feature around  $\gamma^4$ -*h*Phe 1 and  $\gamma^4$ -*h*Leu 4. These combinations of ROEs might be explained by the presence up to seven conformers: a 9/8-ribbon, 13-9-8, 13-13-8, 13-9-13, 8-13-13, 8-13-9 conformers and a 13-helix. The conformers bearing a C13 feature at N-terminal were probably the most abundant since the DMSO- $d_6$  titration revealed the two N-terminal N-H as being free.

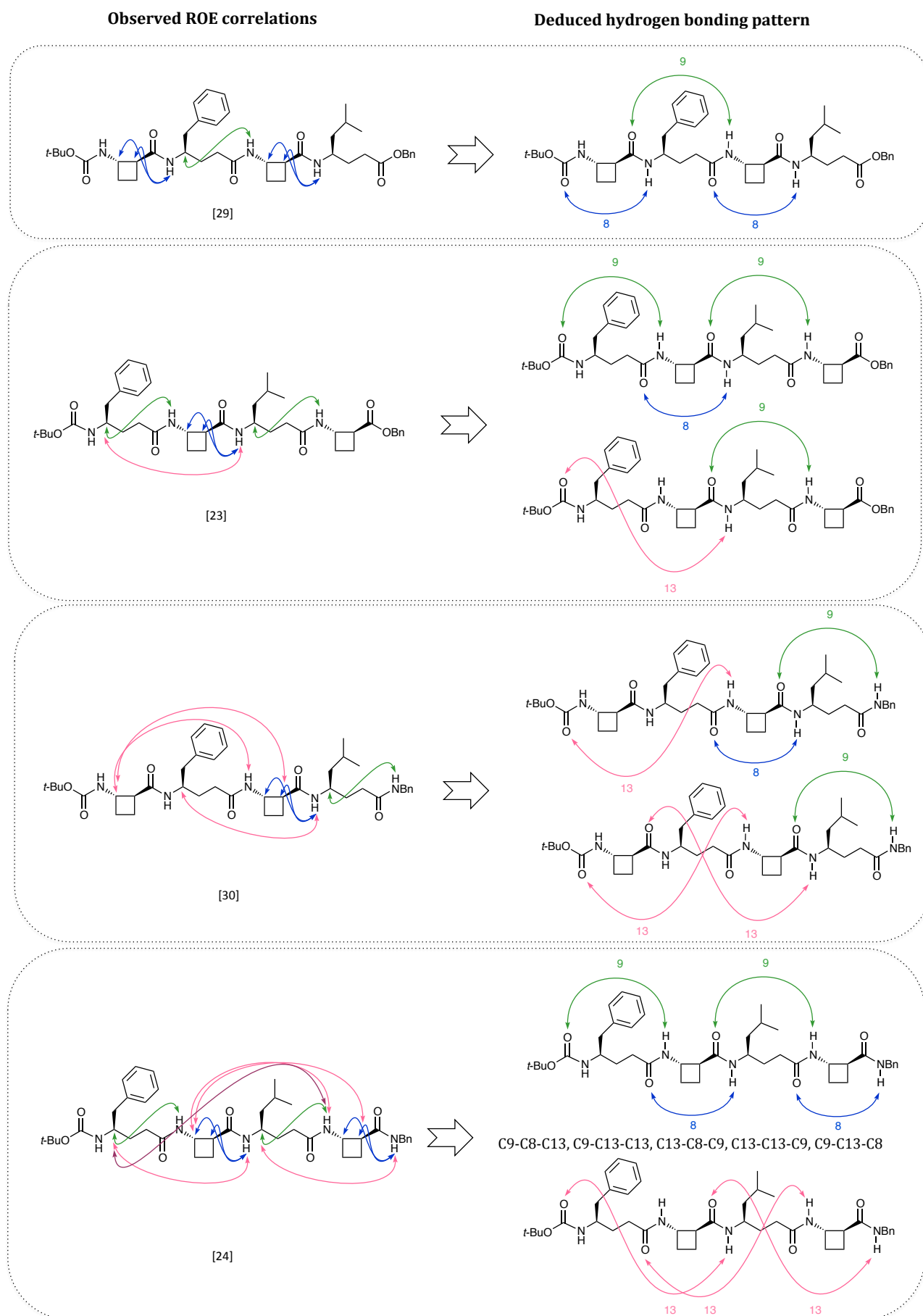


Figure 87. ROE correlations and deduced hydrogen-bonding pattern of tetrapeptides [23], [24], [29], [30].

Boc-AGfAGfA-OBn [31] presented  $H\beta(i)$ -NH( $i+2$ ),  $H\beta(i)$ -H $\alpha(i+2)$  and  $H\gamma(i)$ -NH( $i+2$ ) correlations along the entire peptide (in pink),  $H\gamma(i)$ -NH( $i+1$ ) and  $H\beta(i)$ -NH( $i+1$ ) correlations around *trans*-ACBC 3 (in blue), NH( $i+1$ )- $H\gamma(i)$  correlation around  $\gamma^4$ -hLeu 4 (in green). The pink ROEs were diagnostic of three successive C13 features. The blue ROEs were diagnostic of a C8 feature around *trans*-ACBC 3 and the green ROEs were diagnostic of a C9 feature around  $\gamma^4$ -hLeu 4. It is assumed that three conformers were present in solution, a 13-8-9, a 13-13-9 and a 13-13-13 conformers. The presence of 13-13-9 is compatible with the data but is not the only possible explanation of the ROEs. The three conformers were consistent with the DMSO- $d_6$  titration, which revealed the two N-terminal N-H as being free.

Boc-GfAGfAGl-OBn [25] presented similar ROEs to Boc-GfAGlA-NHBn [24];  $H\beta(i)$ -NH( $i+2$ ),  $H\beta(i)$ -H $\alpha(i+2)$  and  $H\gamma(i)$ -NH( $i+2$ ) correlations along the entire peptide (in pink),  $H\gamma(i)$ -NH( $i+1$ ) and  $H\beta(i)$ -NH( $i+1$ ) correlations around *trans*-ACBC 2 and *trans*-ACBC 4 (in blue), NH( $i+1$ )- $H\gamma(i)$  correlations around  $\gamma^4$ -hPhe 1 and  $\gamma^4$ -hPhe 3 (in green). The pink ROEs were diagnostic of four successive C13 features. The blue ROEs were diagnostic of two C8 features around *trans*-ACBC 2 and *trans*-ACBC 4 and the green ROEs were diagnostic of two C9 features around  $\gamma^4$ -hPhe1 and  $\gamma^4$ -hPhe4. These combinations of NOEs might be explained by the presence of up to seven conformers: a 9/8-ribbon, a 13-9-8, a 13-13-8, a 13-9-13, a 8-13-13, a 8-13-9 and a 13-13-13-13 conformers. The conformers bearing a C13 feature at N-terminal were probably the most abundant since the DMSO- $d_6$  titration revealed the two N-terminal N-H as being free.

Boc-AGfAGfA-NHBn [32] presented  $H\beta(i)$ -NH( $i+2$ ),  $H\beta(i)$ -H $\alpha(i+2)$  and  $H\gamma(i)$ -NH( $i+2$ ) correlations along the entire peptide (in pink) and  $H\gamma(i)$ -NH( $i+2$ ) and  $H\beta(i)$ -NH( $i+1$ ) correlations around *trans*-ACBC 3 (in blue). The blue ROEs (represented with dashed arrows) around *trans*-ACBC 3 were weak and were not considered as being unambiguously indicative of a C8 feature.<sup>viii</sup> The other blue ROE was diagnostic of one C8 feature around *trans*-ACBC 5. The pink ROEs were diagnostic of four successive C13 features suggesting a 13-helix folding, as the single conformer. This was consistent with the DMSO- $d_6$  titration, which revealed the two N-terminal N-H as being free.

Boc-GfAGfAGl-NHBn [26] presented  $H\beta(i)$ -NH( $i+2$ ),  $H\beta(i)$ -H $\alpha(i+2)$  and  $H\gamma(i)$ -NH( $i+2$ ) correlations along the entire peptide (in pink). These ROEs were diagnostic of four successive C13 features suggesting a 13-helix folding, as the single conformer. This was consistent with the DMSO- $d_6$  titration, which revealed the two N-terminal N-H as being free.

---

<sup>viii</sup> The existence of C9 and C8 features cannot be unambiguously deduced when a C13 feature is observed around the same residues. The ROEs observed for C9 and C8 features are indeed compatible with a C13 feature; however the opposite is not possible. Nonetheless the ROEs of C9 and C8 are qualitatively smaller than the C13 ROEs for any given C13 feature. In such cases, they are illustrated with dashed arrows and are considered as being part of the signature of C13 features. In other cases, the presence of both correlations, in full arrows, indicates a mixture of conformers.

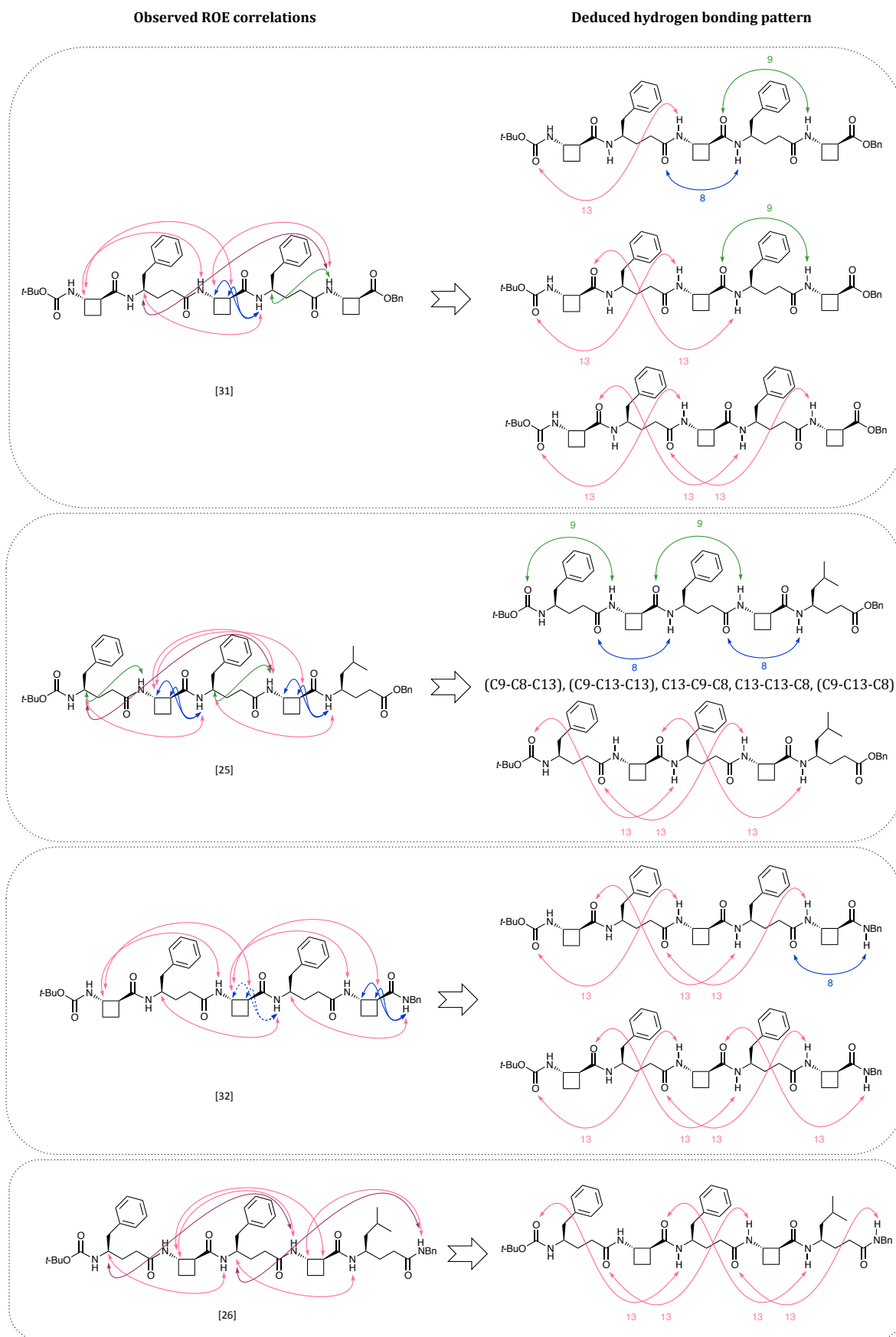


Figure 88. ROE correlations and deduced hydrogen-bonding pattern of pentapeptides [25], [26], [31], [32].

Boc-AGfAGfAGl-OBn [33] presented  $H\beta(i)$ -NH( $i+2$ ),  $H\beta(i)$ -H $\alpha(i+2)$  and  $H\gamma(i)$ -NH( $i+2$ ) correlations along the entire peptide (in pink),  $H\gamma(i)$ -NH( $i+1$ ) and  $H\beta(i)$ -NH( $i+1$ ) correlations around *trans*-ACBC 5 (in blue) and a weak NH( $i+1$ )- $H\gamma(i)$  correlation around  $\gamma^4$ -hPhe 4 (in green). The pink ROEs were diagnostic of four successive C13 features. The blue ROEs were diagnostic of a C8 feature around *trans*-ACBC 5 and the green ROEs were not considered due to its weakness of the signal. These combinations of ROEs indicated two conformers: a 13-helix and a 13-13-13-8 conformer. This was consistent with the DMSO- $d_6$  titration, which revealed the two N-terminal N-H as being free.

Boc-AGfAGfAGl-NHBn [34] presented  $H\beta(i)$ -NH( $i+2$ ),  $H\beta(i)$ -H $\alpha(i+2)$  and  $H\gamma(i)$ -NH( $i+2$ ) correlations along the entire peptide (in pink). The ROEs at C-terminal were drawn dashed because could not be entirely deduced from ROESY spectrum due to proton signal overlapping. The ROEs were diagnostic of five successive C13 features indicating a 13-helix folding, as the single conformer. This was consistent with the DMSO- $d_6$  titration, which revealed the two N-terminal N-H as being free.

Boc-GfAGfAGlA-OBn [27] presented  $H\beta(i)$ -NH( $i+2$ ),  $H\beta(i)$ -H $\alpha(i+2)$  and  $H\gamma(i)$ -NH( $i+2$ ) correlations along the entire peptide (in pink) and weak  $H\gamma(i)$ -NH( $i+1$ ) and  $H\beta(i)$ -NH( $i+1$ ) correlations around *trans*-ACBC 4 (in blue). These ROEs were diagnostic of four successive C13 features suggesting a 13-helix folding, as the single conformer. This was consistent with the DMSO- $d_6$  titration, which revealed the two N-terminal N-H as being free.

Boc-GfAGfAGlA-NHBn [28] presented only  $H\beta(i)$ -NH( $i+2$ ),  $H\beta(i)$ -H $\alpha(i+2)$  and  $H\gamma(i)$ -NH( $i+2$ ) along the entire peptide (in pink). These ROEs were diagnostic of five successive C13 features suggesting a 13-helix folding, as the single conformer. This was consistent with the DMSO- $d_6$  titration, which revealed the two N-terminal N-H as being free.

Another ROE in dark pink,  $H\gamma(i)$ -NH( $i+3$ ), was observed around each C13 feature in [24], [25], [26], [27], [28], [31], [32], [33], [34]. It is proposed that this could be diagnostic of C13 feature although this long-distance correlation has never been reported in the literature.



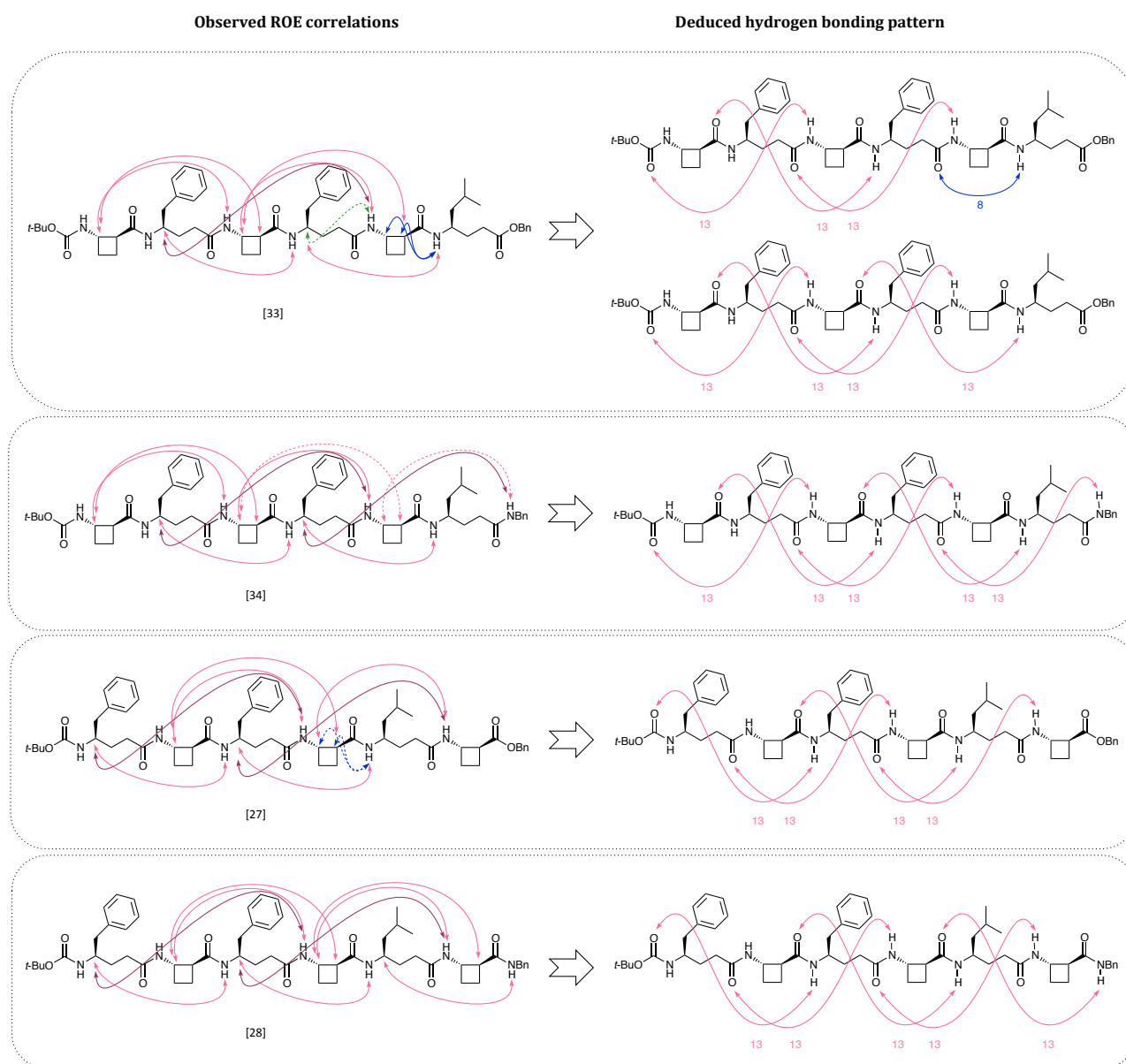


Figure 89. ROE correlations and deduced hydrogen-bonding pattern of hexapeptides [27], [28], [33], [34].

Interestingly no NH(i)-NH(i+1) ROE was observed, suggesting the absence of C11 features and likewise the absence of 11/13-helices, which were not anticipated in any case, considering the  $\theta$  torsion angle imposed by *trans*-ACBC.

From all the collected data, tetrapeptides favoured C9 and C8 features. Pentapeptides showed an intermediate folding propensity by presenting both C9 and C8 features and successive C13 features, suggesting 13-helix folding. Hexapeptides clearly favoured successive C13 features along the entire peptide, suggesting 13-helix folding.

### 2.3.3. Infrared studies

IR spectra of the twelve peptides [23]-[34] were recorded in  $\text{CDCl}_3$  solutions at a concentration of 10 mM (see Figure 90).

At a first glance, the twelve spectra presented two types of N-H stretch absorptions. In each case, sharp bands between 3440 and 3450  $\text{cm}^{-1}$  corresponded to the free N-Hs while a broad band in the range of 3250-3350  $\text{cm}^{-1}$  corresponded to amide N-Hs engaged in intramolecular hydrogen bonds.

Upon closer inspection, the lower frequency band presented different maxima, one or two, according to the length of the peptides.

Boc-AGfAGI-OBn [29] presented two maxima, one at 3350 and one at 3260  $\text{cm}^{-1}$ , which corresponded to amide N-H engaged in 9- and 8-membered hydrogen-bonded rings respectively, as shown in Chapter 1. This was consistent with the conclusions deduced from NMR experiments.

Boc-GfAGfAGI-NHBn [26], Boc-GfAGfAGIA-OBn [27], Boc-GfAGfAGIA-NHBn [28] and Boc-AGfAGfAGI-NHBn [34] each presented a unique maximum at 3325  $\text{cm}^{-1}$  that was diagnostic of one type of hydrogen-bonded ring. The IR spectra confirmed that these four peptides showed unambiguously (determined by ROESY experiments) a unique conformer displaying successive C13 features. The maximum at 3325  $\text{cm}^{-1}$  was thus diagnostic of amide N-Hs engaged in 13-membered hydrogen-bonded rings.

Boc-AGfAGI-NHBn [30] and Boc-AGfAGIA-OBn [31] each presented a unique maximum at 3330  $\text{cm}^{-1}$ , suggesting the presence of a unique conformer, which displayed C13 features (blue shifted from the maximum of the four peptides [26], [27], [28], [34]). The conformers displaying only C13 features were also deduced from NMR experiments. But the other conformers found in ROESY experiments might contribute very few.

Boc-GfAGIA-OBn [23], Boc-GfAGIA-NHBn [24] and Boc-GfAGfAGI-OBn [25] presented two maxima, one at 3350 and one at 3260  $\text{cm}^{-1}$ , which corresponded to amide N-H engaged in 9- and 8-membered hydrogen-bonded rings respectively. These observations were consistent with ROESY experiments which suggested the presence of C8 and C9 features. The presence of other conformers displaying C13 features was not excluded. It seemed that N-H engaged in 13-membered rings underwent a red shift with increasing peptide length. It was possible that isolated C13 features presented a maximum close to that of C9 features.

Boc-AGfAGfA-NHBn [32] and Boc-AGfAGfAGI-OBn [33] each presented a maximum at 3325  $\text{cm}^{-1}$  diagnostic of amide N-Hs engaged in 13-membered hydrogen-bonded rings and a small shoulder at 3250  $\text{cm}^{-1}$  diagnostic of N-Hs engaged in 8-membered hydrogen-bonded rings. These observations were consistent with the presence of conformers displaying successive C13 features and fraying at C-terminal by C8 features, also observed in NMR experiments.

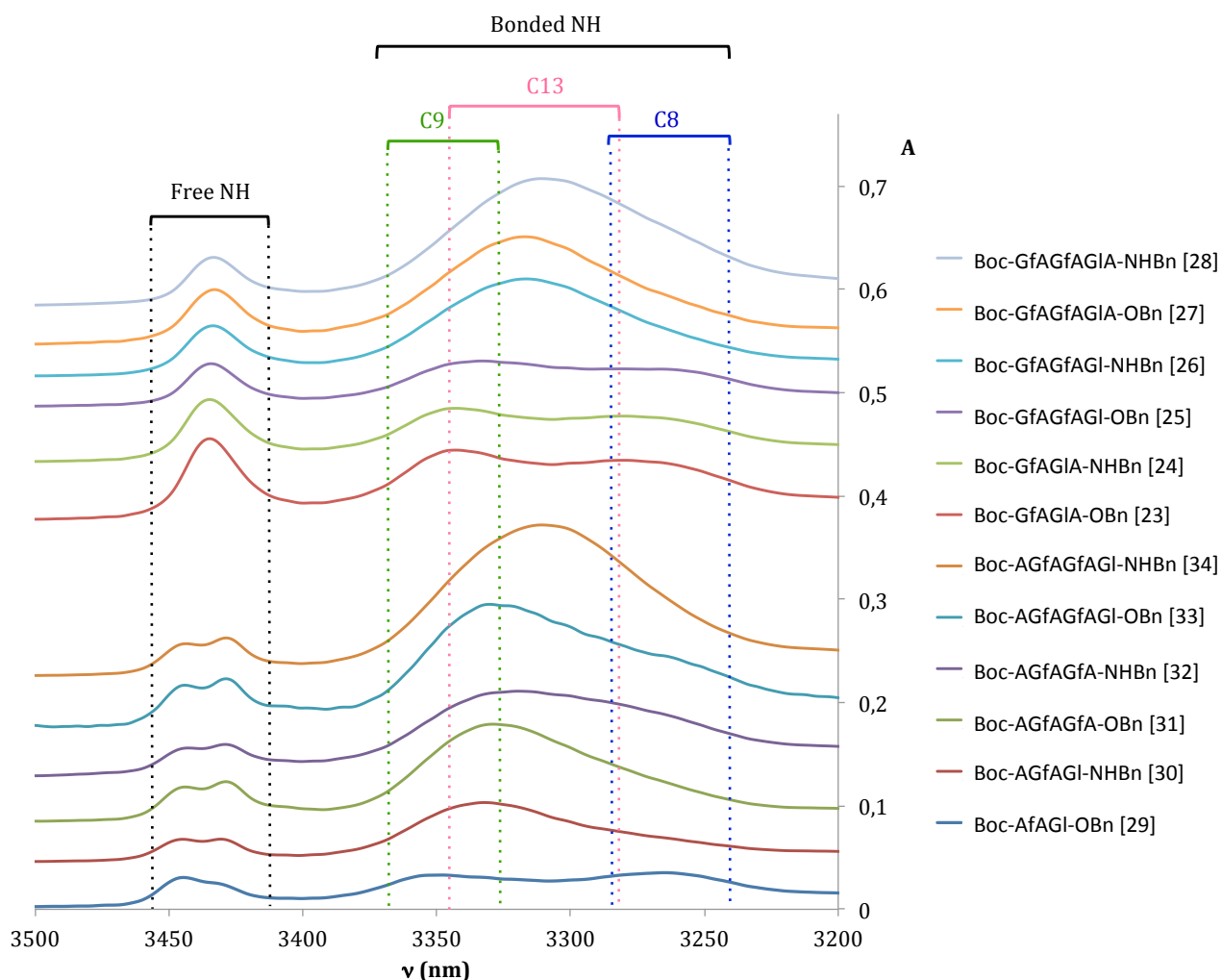


Figure 90. Infrared spectra of  $\beta/\gamma$ -peptides [23]-[34].

### 2.3.4. Molecular Modelling

#### 2.3.4.1. Hybrid Monte Carlo Multiple Minima calculations

MCMM calculations were performed to explore the conformational landscape of these twelve  $\beta/\gamma$ -peptides in chloroform. The different conformations were sorted into families according to their hydrogen-bonded ring systems. They are presented along with their abundances in Table 10:

- the 9/8-ribbon type conformer is composed of alternating 9- and 8-membered H-bonded rings (C9 and C8), essentially as we described in the previous chapter.
- the 13-helix conformer contains only 13-membered hydrogen-bonded rings (C13).
- the other conformers are composed of different combinations of 8-, 9-, 13- and 18-membered H-bonded rings. The system of notation is similar to the one described in Chapter 1. Discreet, successive rings are separated by the symbol '-'. The 13- and 18-membered H-bonded rings which implicate a carbonyl oxygen that is bifurcated between two amide hydrogens, form two

rings, wherein the larger ring includes the smaller; the combined system is noted with the symbol ‘.’.

Table 10. Abundance of conformer families found after Monte Carlo calculations in chloroform - \*: corresponds to the 13-helix.

Conformations	Abundance of each conformer family (number of conformers of that family/total number of conformers < 20 kJ.mol <sup>-1</sup> ; expressed as %)	Conformations	Abundance of each conformer family (number of conformers of that family/total number of conformers < 20 kJ.mol <sup>-1</sup> ; expressed as %)
Boc-GfAGIA-OBn [23] (276 conformers < 20 kJ.mol <sup>-1</sup> )		Boc-AGfAGI-OBn [29] (135 conformers < 20 kJ.mol <sup>-1</sup> )	
13-9	5	13-13*	42
9/8-ribbon	95	8-9,13	14
		9/8-ribbon	44
Boc-GfAGIA-NHBn [24] (389 conformers < 20 kJ.mol <sup>-1</sup> )		Boc-AGfAGI-NHBn [30] (88 conformers < 20 kJ.mol <sup>-1</sup> )	
13-13-13-13	2	13-13-13-13	10
13-9,13	3	8-9,13-8	19
13-13-8	15	8-9-8,13	7
13-9-8	6	9/8-ribbon	64
9-8-9,13	6		
9/8-ribbon	68		
Boc-GfAGfAGI-OBn [25] (66 conformers < 20 kJ.mol <sup>-1</sup> )		Boc-AGfAGfA-OBn [31] (100 conformers < 20 kJ.mol <sup>-1</sup> )	
13-13-13*	59	13-13-13*	84
9-13-13	34	13-13-9	16
13-13-8	6		
Boc-GfAGfAGI-NHBn [26] (134 conformers < 20 kJ.mol <sup>-1</sup> )		Boc-AGfAGfA-NHBn [32] (101 conformers < 20 kJ.mol <sup>-1</sup> )	
13-13-13-13*	100	13-13-13-13*	34
		13-13-9,13	5
		13-13-13-8	35
		13-13-9-8	12
		8-9-13-13	14
Boc-GfAGfAGIA-OBn [27] (98 conformers < 20 kJ.mol <sup>-1</sup> )		Boc-AGfAGfAGI-OBn [33] (75 conformers < 20 kJ.mol <sup>-1</sup> )	
13-13-13-13*	75	13-13-13-13*	65
13-13-13-9	25	13-13-13-8	19
		13-13-9-8	9
		8-13-13-13	7
Boc-GfAGfAGIA-NHBn [28] (127 conformers < 20 kJ.mol <sup>-1</sup> )		Boc-AGfAGfAGI-NHBn [34] (99 conformers < 20 kJ.mol <sup>-1</sup> )	
13-13-13-13-13*	86	13-13-13-13-13*	95
13-13-13-13-8	7	8-18-8-18	5
9-13-13-13-13	7		

At first glance, the MCM low-energy conformational landscapes of  $\beta/\gamma$ -peptides alternating *trans*-ACBC and  $\gamma^4$ -amino acids were gratifyingly dominated by C13 features and including, the **13-helix** family. Other conformer families incorporated combinations of **C9**, **C8** and **C13** features and the **9/8-ribbon** was also in evidence.

### 2.3.4.2. DFT optimization: Gibbs energy and Boltzmann distribution

All the conformer families for each peptide were subjected to *ab initio* geometrical optimization by DFT in a chloroform medium to determine their Gibbs free energy (see Table 11). Relative Gibbs energy was then deduced from the lowest energy family giving an idea of the stability of each conformer family. A Boltzmann distribution was then calculated to evaluate the population distribution (in %) of the conformer families in solution.

Table 11. Relative Gibbs energy and Boltzmann distribution for the different conformer families determined by DFT. ‡: these values seemed to be unrealistic. \*: calculations in progress.

Conformations	Relative Gibbs energy (kJ.mol <sup>-1</sup> )	Boltzmann distribution (%)	Conformations	Relative Gibbs energy (kJ.mol <sup>-1</sup> )	Boltzmann distribution (%)
Boc-GfAGIA-OBn [23]			Boc-AGfAGI-OBn [29]		
13-9	4.28	15	13-helix	0	100
9/8-ribbon	0	85	8-9,13	15.78‡	0
			9/8-ribbon	19.45‡	0
Boc-GfAGIA-NHBn [24]			Boc-AGfAGI-NHBn [30]		
13-helix	0	45	13-helix	0	100
13-9,13	15.41	0	8-9,13-8	35.11‡	0
13-13-8	4.16	9	8-9-8,13	26.15‡	0
13-9-8	4.78	7	9/8-ribbon	99.13‡	0
9-8-9,13	9.84	1			
9/8-ribbon	0.42	38			
Boc-GfAGfAGI-OBn [25]			Boc-AGfAGfA-OBn [31]		
13-helix	1.71	31	13-helix	4.84	15
9-13-13	0	62	13-13-9	0	85
13-13-8	5.29	7			
Boc-GfAGfAGI-NHBn [26]			Boc-AGfAGfA-NHBn [32]		
13-helix	0	100	13-helix	0	83
			13-13-9,13	15.27	0
			13-13-13-8	6.10	7
			13-13-9-8	6.07	7
			8-9-13-13	8.52	3
Boc-GfAGfAGIA-OBn [27]			Boc-AGfAGfAGI-OBn [33]		
13-helix	6,21	8	13-helix	0	91
13-13-13-9	0	92	13-13-13-8	7.06	5
			13-13-9-8	8.04	4
			8-13-13-13	18.10	0
Boc-GfAGfAGIA-NHBn [28]			Boc-AGfAGfAGI-NHBn [34]		
13-helix	0		13-helix	0	100
13-13-13-13-8	*		8-18-8-18	does not converge	0
9-13-13-13-13	*				

After DFT optimization, the conformational landscape changed with the length of the peptides and herein the number of hydrogen bonds involved in the folding.

For short peptides, the amide and ester tetrapeptides, different conformers displaying C9, C8 and C13 features were found, including 9/8-ribbon and 13-helices. The conformational landscapes were slightly different from those suggested by experimental data.

For longer peptides, i.e. the penta- and hexapeptides, the landscape was largely dominated by **13-helical** conformers, which presented successive C13 features (see Figure 91). This was gratifyingly consistent with the IR and NMR experimental data.

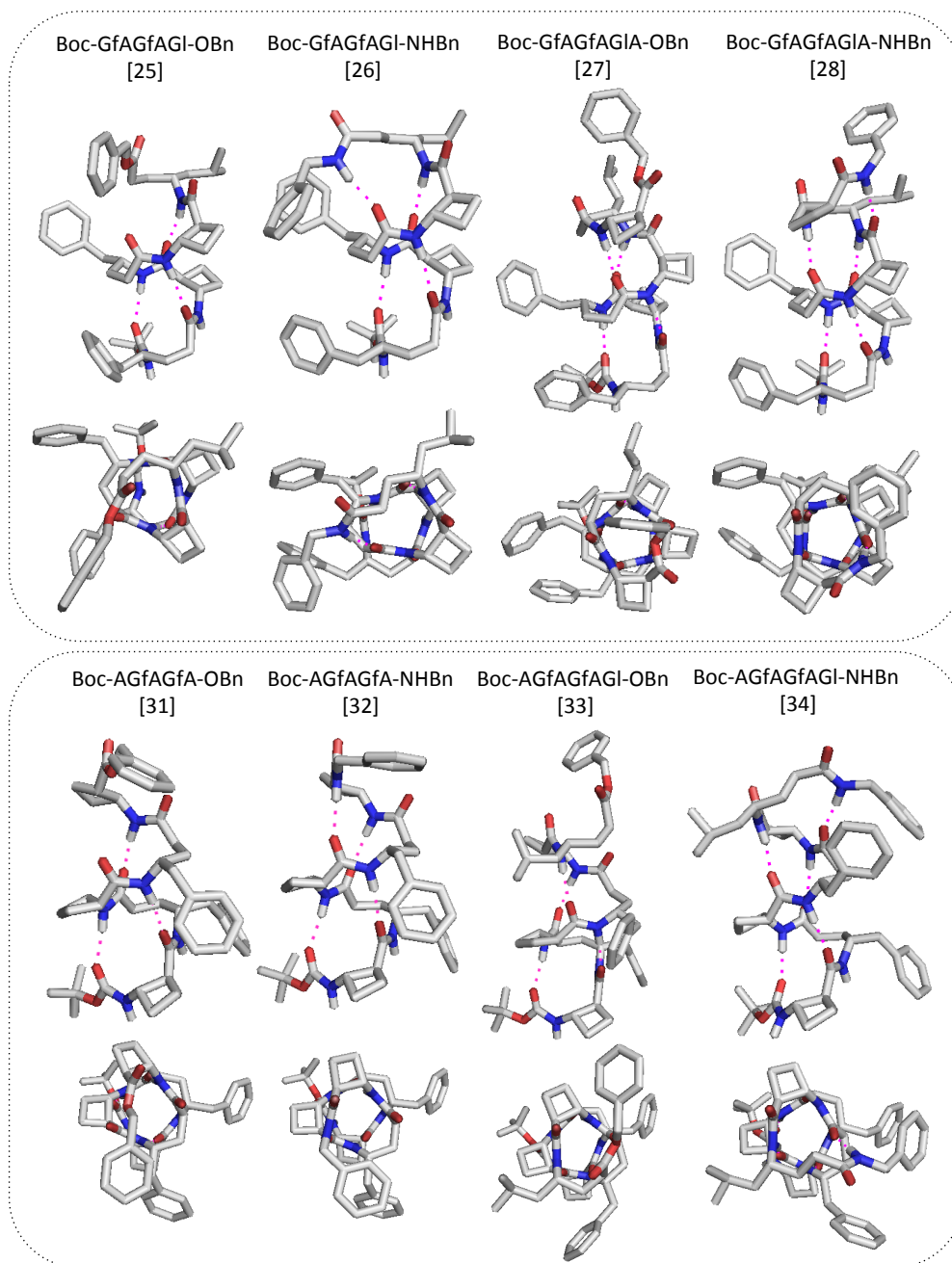


Figure 91. Side and top views of the 13-helical backbone adopted by  $\beta/\gamma$ -pentapeptides and  $\beta/\gamma$ -hexapeptides.

The 13-helical backbone of the  $\beta/\gamma$ -peptides was compared with the 13-helical backbone of a native  $\alpha$ -peptide (see Figure 92). The 13-helix of the  $\beta/\gamma$ -peptides pleasingly exhibited the same

orientations of the helix dipole and a pitch similar in diameter. As the configurations of *trans*-ACBC and  $\gamma^4$ -amino acids were anticipated, the chirality of the 13-helix of  $\beta/\gamma$ -peptides was the same (P).  $\beta/\gamma$ -Peptide units might well adopt the  $\alpha$ -helix conformation in native peptide sequences despite the different number and positions of the peptide bonds.

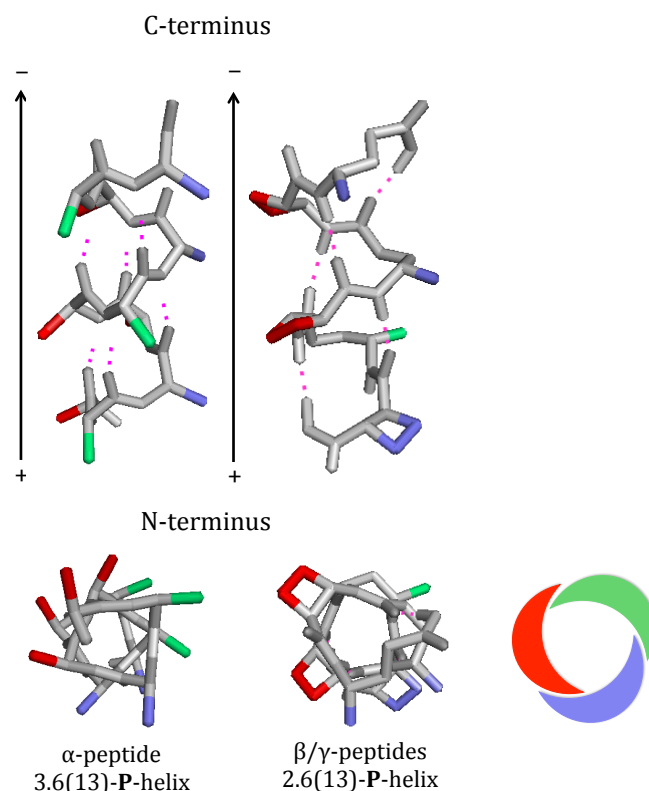


Figure 92. Comparison of the native  $\alpha$ -helix and the 13-helix adopted by  $\beta/\gamma$ -peptides.

### 2.3.5. Circular Dichroism

As was stated previously, chloroform is not suitable for far-UV CD spectra. The far-UV CD spectra of the twelve peptides were recorded in 0.2 mM methanol solutions (see Figure 93).

All the spectra displayed a minimum Cotton effect near 206 nm and a maximum Cotton effect near 224 nm. The spectra showed increase in Cotton effect with increasing peptide length. For the A series, but not for the B series, there was a slight red-shift in the minimum with increasing peptide length (204 nm to 208 nm).

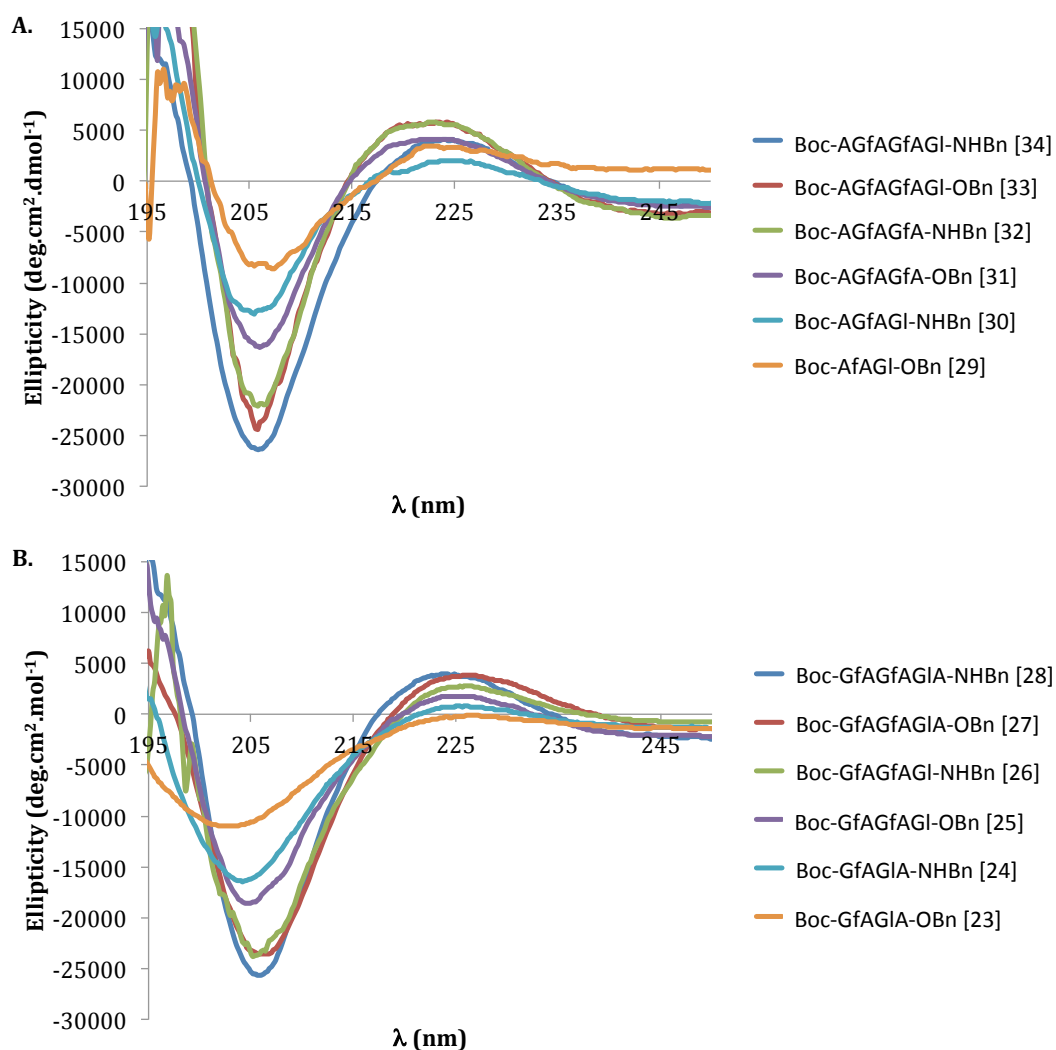


Figure 93. A: CD spectra of the  $\beta/\gamma$ -peptides [29]-[34]. B: CD spectra of the  $\beta/\gamma$ -peptides [23]-[28].

The CD curve of Boc-AGfAGfAGI-NHBn [34] was compared with that of the 12-helical octamer of *trans*-ACBC, Boc-AAAAAAAA-OMe, in the same solvent. The CD spectrum of [34] resembled a slightly blue-shifted version of the characteristic signature of the 12-helix octamer of *trans*-ACBC (see Figure 94 A).



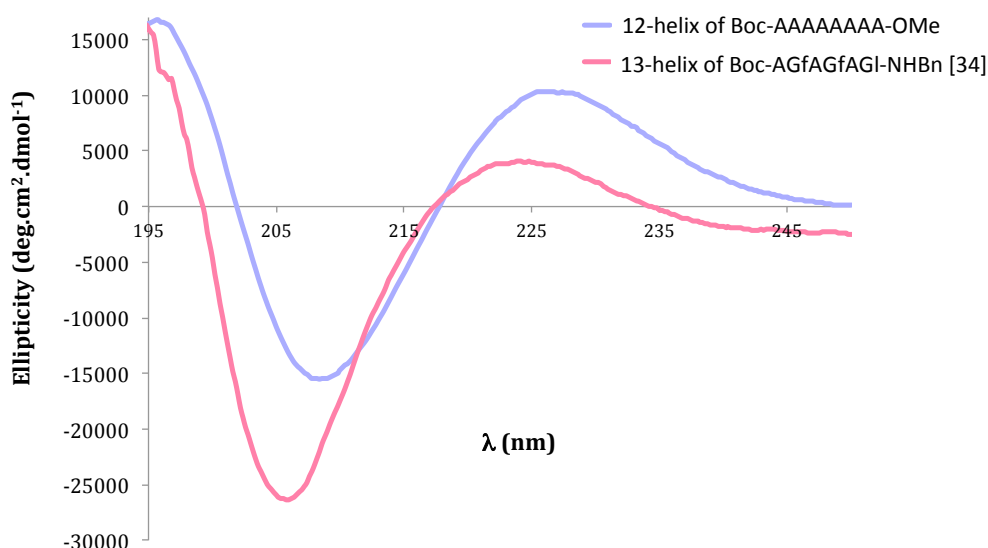


Figure 94. A. Comparison between the CD spectra of a 12-helix and a 13-helix.

The similarity between the CD spectra of the two helices brought additional evidence of the 13-helical folding behaviour of  $\beta/\gamma$ -peptides. This similarity can be explained by a good backbone matching between the 12-helix and the 13-helix (see Figure 95). It was clear that the peptides presented similar orientations of the carbonyl groups and of the hydrogen-bonded patterns imposed by the helical folding and thus forming a similar macrodipole.

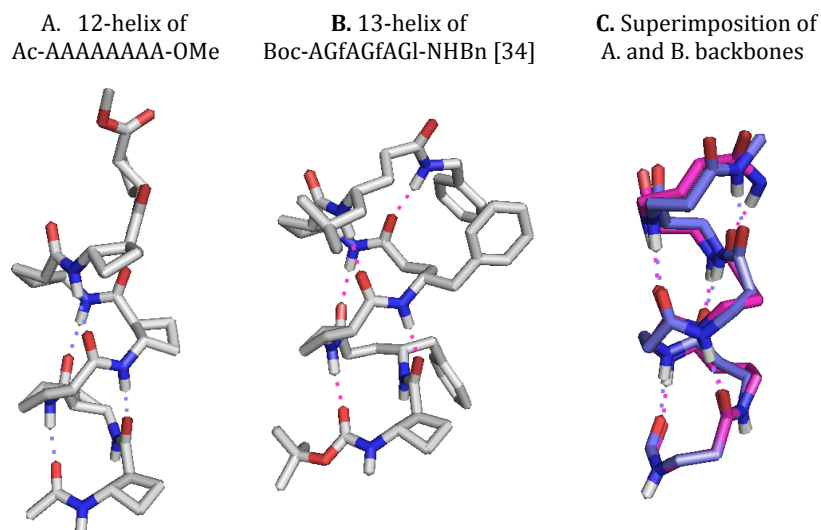


Figure 95. A: 12-helix adopted by octamer of *trans*-ACBC. B: 13-helix adopted by amide  $\beta/\gamma$ -hexapeptide [34]. C: Superimposition of the backbones of Ac-AAAAAAAA-OMe in blue and [34] in pink.

## 2.4 Conclusion

In conclusion to this Chapter, the objective of mimicking the  $\alpha$ -helix with a 13-helical  $\beta/\gamma$ -peptide constructed from *trans*-ACBC and  $\gamma^4$ -amino acids was achieved. The introduction of a single substituent on the  $\gamma$ -amino acids induced a change in the conformational preferences from 9/8-ribbon to 13-helix (see Figure 96).

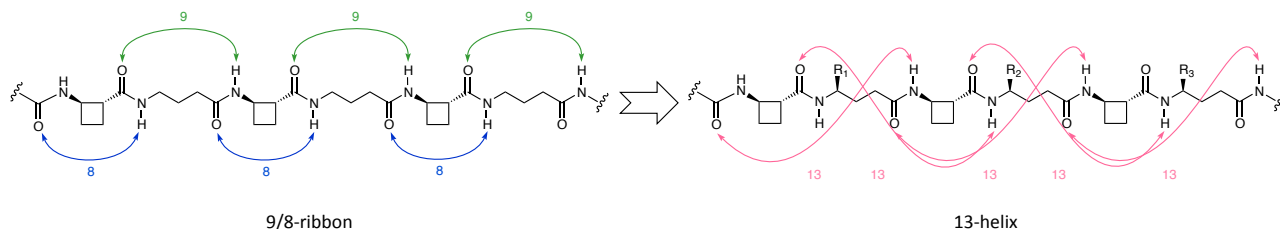


Figure 96. Conformational preferences of  $\beta/\gamma$ -peptides according to the degree of substitution of the  $\gamma$ -amino acid.

The stability of the 13-helix depended on the length of the  $\beta/\gamma$ -peptide and the number of hydrogen bonds engaged in the folding behaviour. When the maximum number of hydrogen bonds which could be formed was less than four hydrogen bonds, the conformational behaviour of short  $\beta/\gamma$ -peptides was not limited to one predominant conformer. Mixture of conformers displaying C9, C8 and C13 features, including 13-helices, were observed in different abundances. With the possibility of forming four (or more) hydrogen bonds, longer  $\beta/\gamma$ -peptides strongly favoured a global folding into 13-helices.

In conclusion,  **$\beta/\gamma$ -peptides alternating *trans*-ACBC and  $\gamma^4$ -amino acids** folded into a **robust 13-helix** stabilised with a minimum of **four H-bonds** in chloroform.

### 3. Design of inhibitors of $\alpha$ -helix-mediated PPIs containing *trans*-ACBC and $\gamma^4$ -amino acids

In this Chapter, we will examine the ability of the new 13-helical  $\beta/\gamma$ -peptide manifold described in the previous Chapter to behave as mimetics of the  $\alpha$ -helix of native proteins. It is proposed here to design hybrid peptides which can mimic the helical segment (19-26) of p53 protein. It is also proposed to test these hybrid peptides as inhibitors of the  $\alpha$ -helix-mediated p53/hDM2 interaction.<sup>ix</sup>

#### 3.1 $\alpha/\beta/\gamma$ -Peptides designed as the helical segment (19-26) of p53 mimetics

In a first objective, we endeavoured to design  $\beta/\gamma$ -peptides which mimic the  $\alpha$ -helical segment (19-26) of p53 protein.<sup>x</sup> It was proposed that the mimetic should possess the three known hot-spot residues at the correct positions: Phe(*i*), Trp(*i*+4) and Leu(*i*+7). To begin the design process, the primary sequence of p53(19-26) and a  $\beta/\gamma$ -peptide backbone alternating *trans*-ACBC and  $\gamma$ -amino acids were aligned, in order to map appropriately positioned side-chains.

The first mimetic structure [40] was proposed by making a direct positional mapping of the hot-spot side-chains (see Figure 97). In this way, the indole ring of Trp 23 and the isobutyl chain of Leu 26 were conveniently represented by  $\gamma^4$ -*h*Trp and  $\gamma^4$ -*h*Leu, respectively. The phenyl ring of Phe 19 was located at the C4 position of the first *trans*-ACBC residue, arbitrarily in a *cis*-arrangement with respect to the C1 carbonyl. In order to privilege 13-helix folding,  $\gamma^4$ -*h*Ala was preferred to GABA at the first  $\gamma$ -amino acid position; notionally, the methyl group represents the hydroxymethyl side chain of Ser 20. The configurations of all backbone stereogenic centres – (*S,S*) for *trans*-ACBC, (*R*) for the  $\gamma^4$ -amino acids – were chosen in order to favour the P-helix folding sense, in analogy with the native peptide segment. The  $\beta/\gamma$ -peptide thus designed was completed with N-terminal Boc and C-terminal methyl ester capping groups.

MCMM calculations of [40] were carried out in chloroform. The conformational landscape was dominated by **well-defined 13-helix**. The low-energy 13-helical conformer was superimposed to the crystal structure of p53(16-29) peptide with a good RMSD of 0.90 Å.

---

<sup>ix</sup> p53/hDM2 interaction was targeted as it represents a benchmark system for therapeutics discovery.

<sup>x</sup> The  $\alpha$ -helical segment of p53 protein corresponding to the amino acids 19 to 26 was named hereafter p53(19-26).

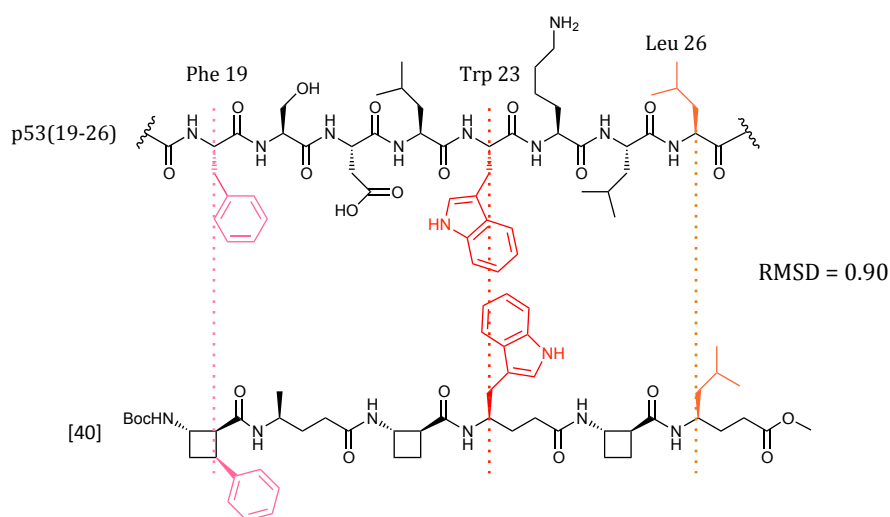


Figure 97.  $\beta/\gamma$ -Peptide [40] designed as a mimetic of p53(19-26).

The main problem perceived in this first mimetic structure was the matter of obtaining the 4-phenyl-ACBC residue. This compound has not been described previously and its synthesis appeared far from trivial. Furthermore, the rigidity of the four-membered ring severely restricted the spatial orientation of the phenyl ring which might have had a negative effect on the intended biological activity. A second mimetic structure [41] was therefore derived from the first, by replacing 4-phenyl-ACBC with a simpler, acyclic  $\beta$ -amino acid bearing the requisite aromatic side chain:  $\beta^2$ -hPhe. The (*S*) configuration for this residue was appropriate.

MCMM calculations of [41] were carried out in chloroform. The conformational landscape was also dominated by a **well-defined 13-helix** that is superimposed to the crystal structure of p53(16-29) with a good RMSD of 0.84 Å (see Figure 98).

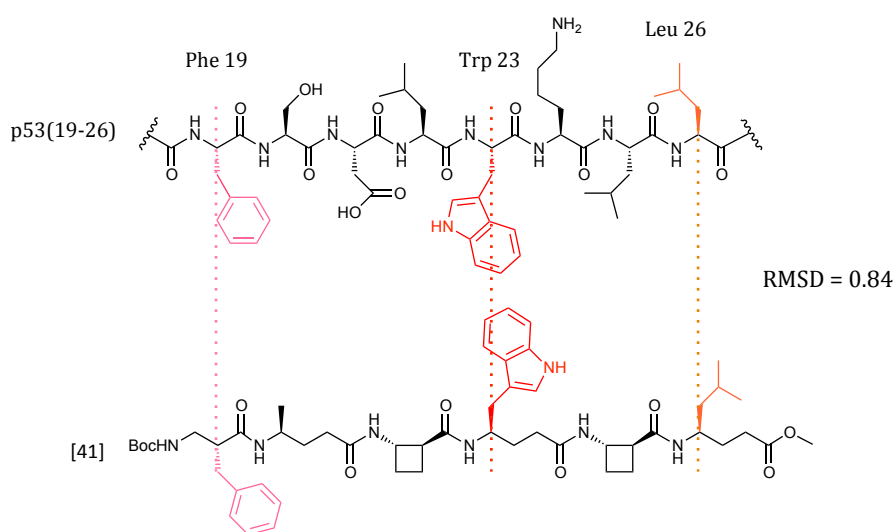


Figure 98.  $\beta/\gamma$ -Peptide [41] designed as a mimetic of p53(19-26).

While the synthesis of (*S*)- $\beta^2$ -*h*Phe has been described, it required 8 steps and the product was obtained with poor enantiomeric excess.<sup>171</sup> A third mimetic structure [42] was therefore designed with a view to further simplification (see Figure 99). In this way the implication of (*S*)- $\beta^2$ -*h*Phe was avoided and instead the Phe 19 of the native peptide was simply retained in the sequence.

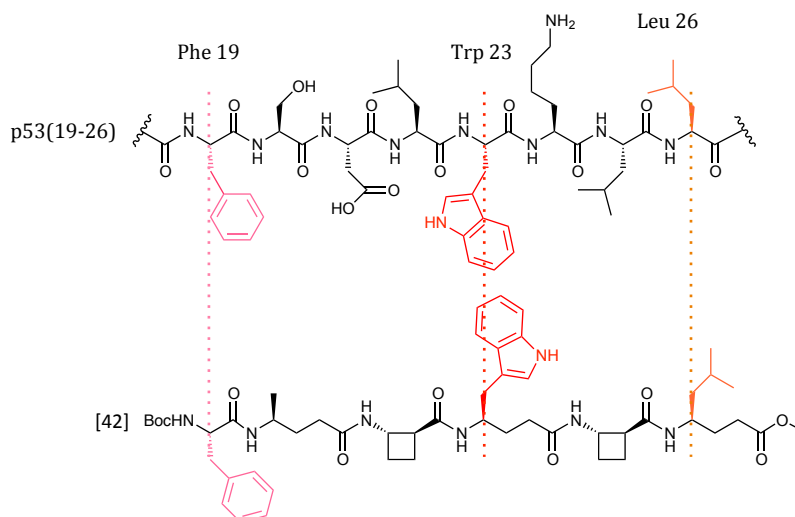


Figure 99.  $\beta/\gamma$ -Peptide [42] designed as a mimetic of p53(19-26).

MCMM calculations of [42] were carried out in chloroform. The conformational landscape was dominated by a **well-defined 12/13-helical structure** that was superimposed to the crystal structure of p53(16-29) with a good RMSD of 0.89 Å (see Figure 100).

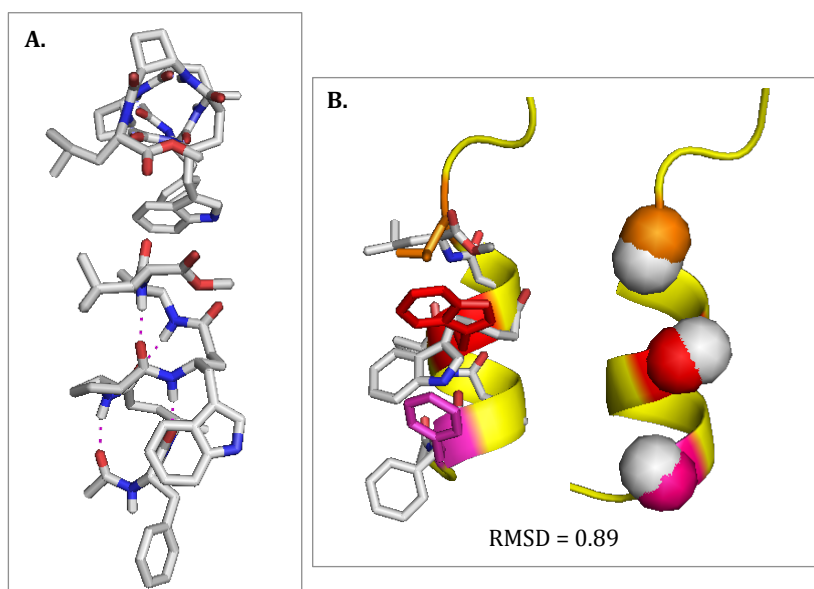


Figure 100. A: Top and side views of [42]. B: Superimposition of backbones.

Now using [42] as the lead, three other peptides were devised for study (see Figure 101). While the side-chain of the N-terminal  $\gamma^4$ -*h*Leu residue is a prerequisite, only the N-H of this residue is

involved in the secondary structure pattern. A simpler mimetic Boc-FGaAGwAL-OMe [43] in which  $\gamma^4$ -*h*Leu was replaced by Leu was therefore proposed.

Since the manipulation of  $\gamma^4$ -*h*Trp was perceived as having potential difficulties, two related mimetics Boc-FGaAGfAGl-OMe [44] and Boc-FGaAGfAL-OMe [45], in which  $\gamma^4$ -*h*Trp was replaced by  $\gamma^4$ -*h*Phe, were proposed as well. It is noteworthy that studies on p53  $\alpha$ -helix mimetics have shown that replacement of Trp 21 by Phe 21 does not necessarily alter the affinity of the mimetics to *h*DM2.<sup>128</sup>

The *N*-Boc protecting group is rarely featured in the design of PPI inhibitors, perhaps because of its considerable steric bulk. Four mimetics derived from [42]-[45], [46]-[59], in which the *N*-Boc protecting group was replaced by an *N*-acetamide were devised for study.

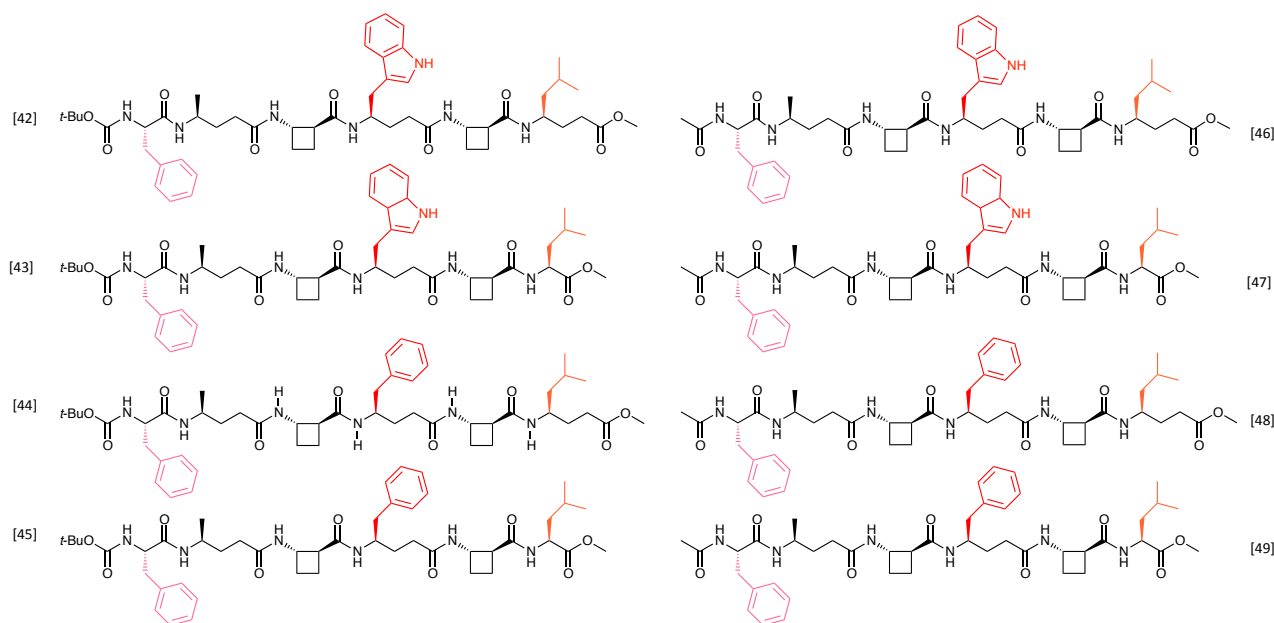


Figure 101.  $\alpha/\beta/\gamma$ -Peptides [42-49] designed as p53(19-26) mimetics.

Molecular modelling calculations were carried out to verify the capacity of the four *N*-Boc protected peptides [42]-[45] to adopt helical structures. It was assumed that the *N*-acetamide peptides [46]-[49] would show similar conformational preferences.

MCMM calculations were carried out in chloroform and octanol to investigate the behaviour of  $\alpha/\beta/\gamma$ -peptides in protic solvents, since the intended biophysical assays were to be performed in aqueous buffer. The different conformations were sorted into families according to their hydrogen-bonded ring systems. They are presented along with their abundances in Table 12.

Table 12. Abundance of conformer families found after Monte Carlo calculations in chloroform - \*: the pattern 12-13-13-13 corresponds to the 12/13-helix.

Conformations in CHCl <sub>3</sub>	Abundance of each conformer family (number of conformers of that family/total number of conformers; expressed as %)	Conformations in C <sub>8</sub> H <sub>17</sub> OH	Abundance of each conformer family (number of conformers of that family/total number of conformers < 10 kJ.mol <sup>-1</sup> ; expressed as %)
Boc-FG <sub>A</sub> AG <sub>W</sub> AL-OMe [43] (67 conformers < 10 kJ.mol <sup>-1</sup> )		Boc-FG <sub>A</sub> AG <sub>W</sub> AL-OMe [43] (48 conformers < 10 kJ.mol <sup>-1</sup> )	
12-13-13-13*	100	12-13-13-13*	100
Boc-FG <sub>A</sub> AG <sub>W</sub> AG <sub>L</sub> -OMe [42] (15 conformers < 10 kJ.mol <sup>-1</sup> )		Boc-FG <sub>A</sub> AG <sub>W</sub> AG <sub>L</sub> -OMe [42] (41 conformers < 10 kJ.mol <sup>-1</sup> )	
12-13-13-13*	100	12-13-13-13*	100
Boc-FG <sub>A</sub> AG <sub>F</sub> AL-OMe [45] (19 conformers < 10 kJ.mol <sup>-1</sup> )		Boc-FG <sub>A</sub> AG <sub>F</sub> AL-OMe [45] (21 conformers < 10 kJ.mol <sup>-1</sup> )	
12-13-13-13*	74	12-13-13-13*	100
12-13-13-8	26		
Boc-FG <sub>A</sub> AG <sub>F</sub> AG <sub>L</sub> -OMe [44] (32 conformers < 10 kJ.mol <sup>-1</sup> )		Boc-FG <sub>A</sub> AG <sub>F</sub> AG <sub>L</sub> -OMe [44] (13 conformers < 10 kJ.mol <sup>-1</sup> )	
12-13-13-13	67	12-13-13-13*	100
12-13-13-8	33		

The conformational landscapes were largely dominated by a single **12/13-helical conformer**. In chloroform, other conformers that populated for 12/13-helical conformers frayed at C-terminal were detected; whereas only one 12/13-helix conformer was found in methanol. The side and top views of these helical  $\alpha/\beta/\gamma$ -peptides are displayed in Figure 102.

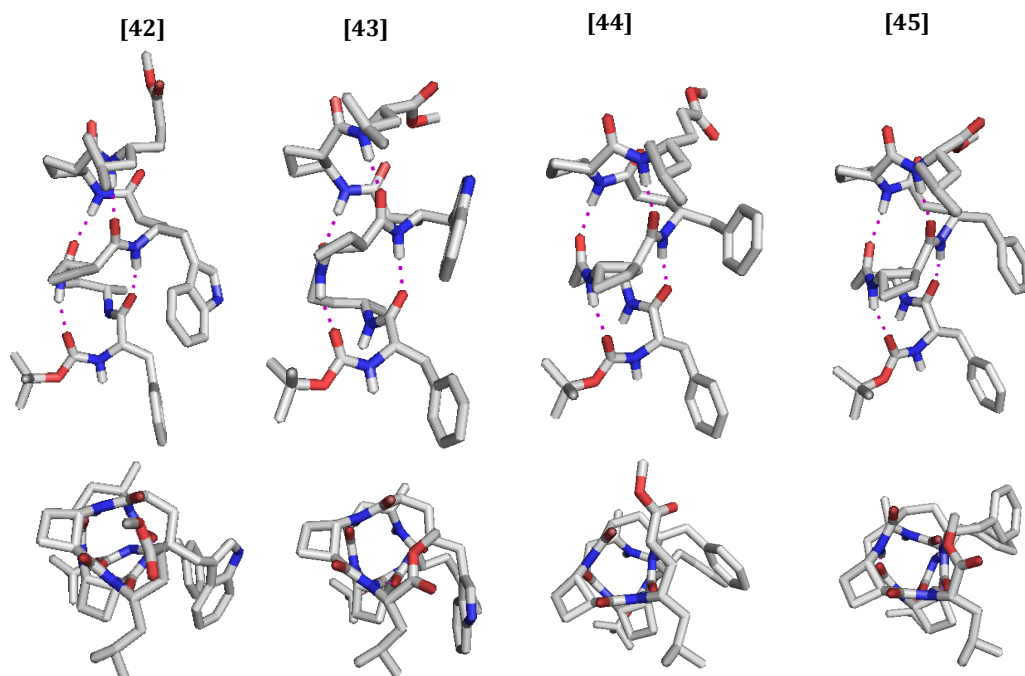


Figure 102. Side and top views of  $\alpha/\beta/\gamma$ -peptides [42]-[45].

From these design considerations, eight target  $\alpha/\beta/\gamma$ -peptides therefore emerged, [42]-[49]

## 3.2 Synthesis of the designed $\alpha/\beta/\gamma$ -peptides

### 3.2.1. Synthesis of $\alpha/\beta/\gamma$ -peptides bearing $\gamma^4$ -*h*Trp [42], [43], [46], [47]

The synthesis of hexapeptides Boc-FGaAGwAL-OMe [43], Boc-FGaAGwAGI-OMe [42], Ac-FGaAGwAL-OMe [45], Ac-FGaAGwAGI-OMe [44] were carried out as shown in Scheme 16.

The esterification of [2] was carried out using TMSCl in methanol allowing the cleavage of the *N*-Boc protecting group overnight to give the corresponding methyl ester hydrochloride salt. This was engaged directly with Boc- $\gamma^4$ -*h*Ala using HATU in an overnight reaction to give the dipeptide [50] with a yield of 72 %.

The methyl ester hydrochloride salt of [2] was engaged directly with Boc- $\gamma^4$ -*h*Trp using HATU in an overnight reaction to give the dipeptide [51] with a yield of 81 %.

The *N*-Boc protecting group of dipeptide [50] was cleaved by treatment with a large excess of TFA for 1 h to give the corresponding TFA salt. The subsequent coupling reaction with Boc-Phe required optimization in order to avoid epimerisation of the  $\alpha$ -amino acid during the activation step. Non-negligible epimerisation was observed when HATU or HATU and HOAt were used as coupling reagents. Boc-Phe was activated using EDCI·HCl and HOAt at 0 °C in the absence of base then coupled overnight with the TFA salt of [50] to give tripeptide [52] with a yield of 55 %. No evidence of epimerisation was observed in these conditions.

The methyl ester protecting group of [51] was hydrolysed with lithium hydroxide at room temperature for 3 h to give the corresponding carboxylic acid, which was then activated using HATU and coupled to the hydrochloride salt of Leu-OMe (commercial) in an overnight reaction to afford tripeptide [53] with a yield of 51 %.

The *N*-Boc protecting group of tripeptide [53] was cleaved by treatment with a large excess of TFA during 2.5 h while the methyl ester of tripeptide [51] was hydrolysed using lithium hydroxide at room temperature for 3 h. The two monoprotected tripeptides were coupled using HATU in an overnight reaction to afford the target hexapeptide [43] with a yield of 62 %.

The *N*-Boc protecting group of hexapeptide [43] was cleaved by treatment with a large excess of TFA during 3 h to give the corresponding TFA salt. The TFA salt was acetylated with acetic anhydride in an overnight reaction to give the hexapeptide [47] with a yield of 81 %.

A similar strategy was adopted for the synthesis of hexapeptide [42], using the same intermediate *N*-terminal tripeptides but using a C-terminal tripeptide bearing  $\gamma^4$ -*h*Leu instead of Leu. For the preparation of this fragment, the methyl ester protecting group of [51] was hydrolysed with lithium hydroxide at room temperature for 3 h to give the corresponding carboxylic acid, while the *N*-Boc protecting group of  $\gamma^4$ -*h*Leu was cleaved by treatment with an excess of TFA to give the

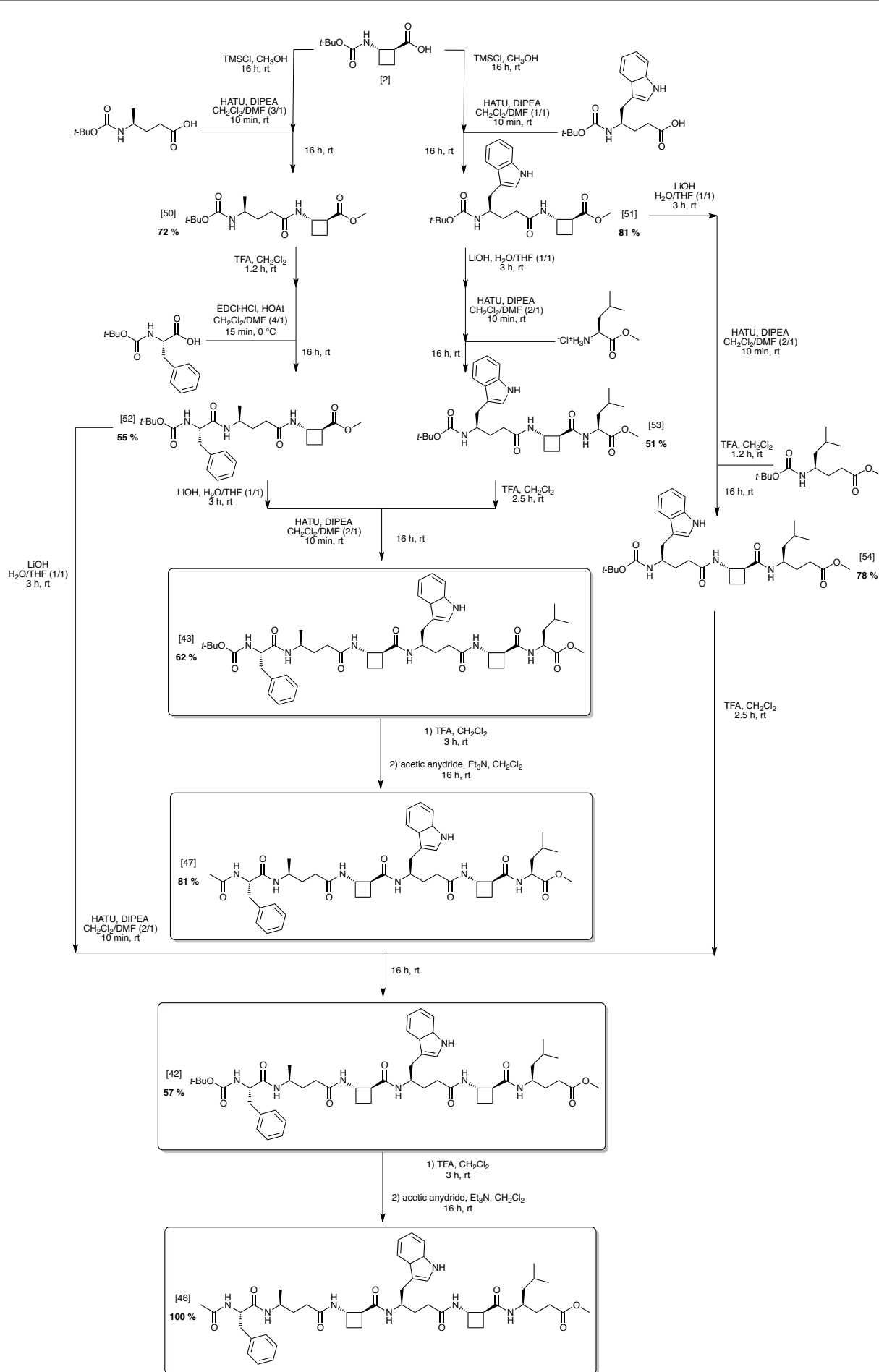


corresponding TFA salt. The carboxylate of [51] was coupled with the TFA salt using HATU in an overnight reaction to afford tripeptide [54] with a good yield of 78 %.

The *N*-Boc protecting group of tripeptide [54] was then cleaved with a large excess of TFA for 2.5 h while the methyl ester of tripeptide [52] was hydrolysed using lithium hydroxide at room temperature for 3 h. The two monoprotected tripeptides were coupled using HATU in an overnight reaction to afford the target hexapeptide [42] with a yield of 57 %.

The *N*-Boc protecting group of hexapeptide [42] was cleaved by treatment with a large excess of TFA during 3 h to give the corresponding TFA salt. The TFA salt was acetylated with acetic anhydride in an overnight reaction to give the hexapeptide [46] with a quantitative yield.

The four hexapeptides [42], [43], [46] and [47] were synthesised with yields of 23 %, 25 %, 23 % and 20 % in three and four steps respectively, from Boc-*trans*-ACBC [2].



*Scheme 16. Synthesis of  $\alpha/\beta/\gamma$ -peptides [42], [43], [46] and [47].*

### 3.2.2. Synthesis of $\alpha/\beta/\gamma$ -peptides bearing $\gamma^4$ -hPhe [44], [45], [48], [49]

The syntheses of hexapeptides Boc-FGaAGfAL-OMe [45], Boc-FGaAGfAGl-OMe [44], Ac-FGaAGfAL-OMe [49], Ac-FGaAGfAGl-OMe [48] were carried as shown in Scheme 17. The strategy was similar to that adopted for the preparation of the four hexapeptides [42], [43], [46] and [47] in order to make common use of the N-terminal tripeptide [52].

The benzyl ester of dipeptide [35] was removed by hydrogenolysis under a hydrogen atmosphere in the presence of Pd/C (10%) in 2 h to give the corresponding carboxylic acid, which was then activated using HATU and coupled in an overnight reaction with the hydrochloride salt of Leu-OMe (commercial) to afford tripeptide [55] with a good yield of 75 %.

The *N*-Boc protecting group of tripeptide [55] was then cleaved with a large excess of TFA for 2.5 h while the methyl ester of tripeptide [52] was hydrolysed with lithium hydroxide during 3 h at room temperature. The two deprotected tripeptides were coupled using HATU in an overnight reaction to afford the targeted hexapeptide [45] with a yield of 76 %.

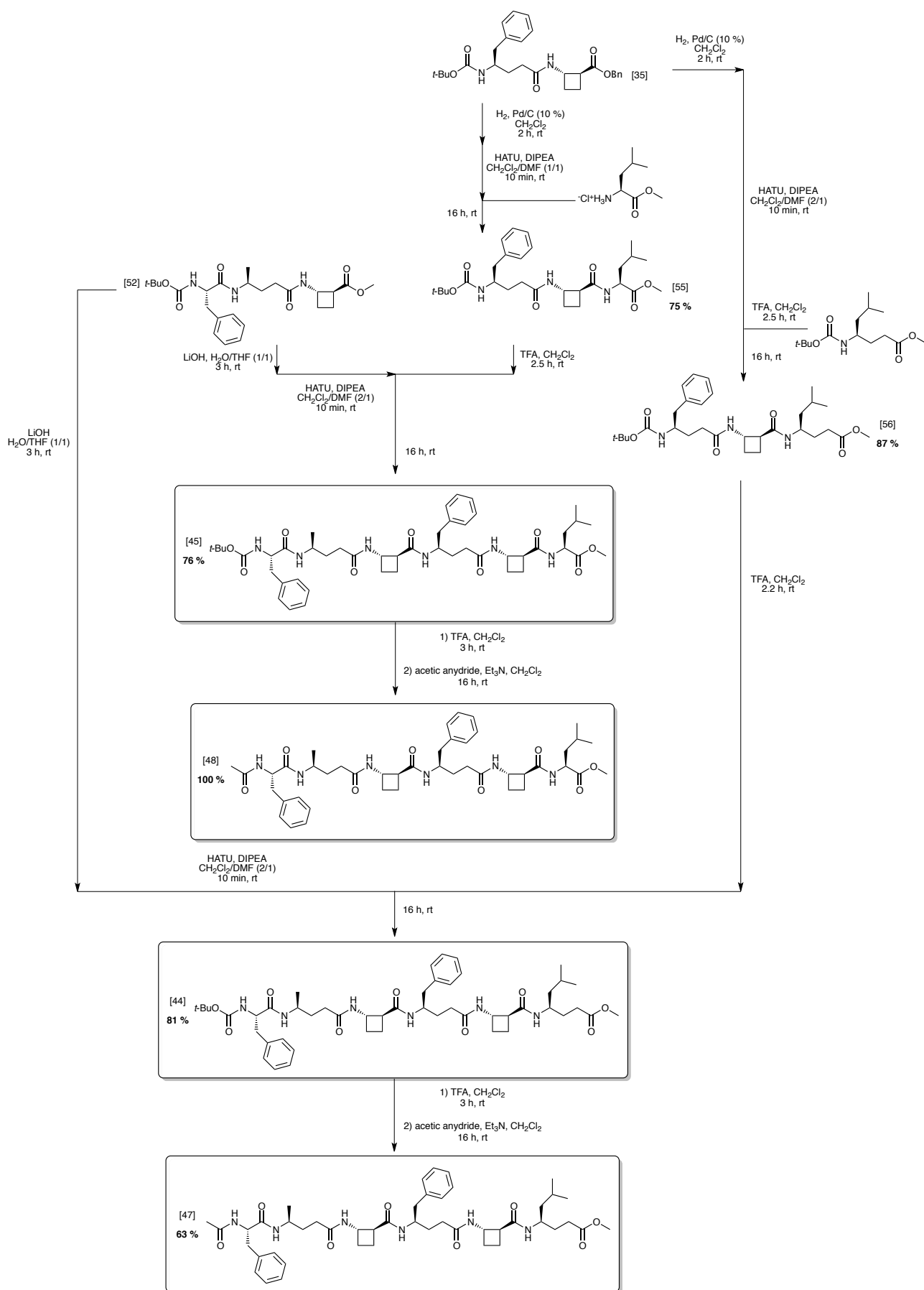
The *N*-Boc protecting group of hexapeptide [45] was cleaved by treatment with a large excess of TFA during 3 h to give the corresponding TFA salt. The TFA salt was acetylated with acetic anhydride in an overnight reaction to give the hexapeptide [49] with a quantitative yield.

In an analogous manner, the synthesis of hexapeptide [44] was carried out using the N-terminal tripeptide [52], and a C-terminal tripeptide bearing  $\gamma^4$ -hLeu instead of Leu. For the preparation of this fragment, the benzyl ester of dipeptide [35] was removed by hydrogenolysis in 2 h to give the corresponding carboxylic acid, while the *N*-Boc protecting group of  $\gamma^4$ -hLeu was cleaved by treatment with an excess of TFA to give the corresponding TFA salt. The carboxylate of [35] was coupled with the TFA salt using HATU in an overnight reaction to afford tripeptide [56] with a good yield of 87 %.

The *N*-Boc protecting group of tripeptide [56] was then cleaved with a large excess of TFA for 2.5 h while the methyl ester of tripeptide [52] was hydrolysed using lithium hydroxide at room temperature for 3 h. The two monoprotected tripeptides were coupled using HATU in an overnight reaction to afford the target hexapeptide [44] with a yield of 81 %.

The *N*-Boc protecting group of hexapeptide [44] was cleaved by treatment with a large excess of TFA during 3 h to give the corresponding TFA salt. The TFA salt was acetylated with acetic anhydride in an overnight reaction to give the hexapeptide [48] with a yield of 63 %.

The four hexapeptides [43], [44], [48] and [49] were synthesised with yields of 32 %, 30 %, 20 % and 30 % in three and four steps respectively, from *trans*-ACBC derivatives.

Scheme 17. Synthesis of  $\alpha/\beta/\gamma$ -peptides [44], [45], [47] and [48].

### 3.3 Structural studies of the $\alpha/\beta/\gamma$ -peptides

Differences in the solubilities of the eight peptides were observed in the NMR experiments. The four *N*-Boc protected peptides were soluble in chloroform while the four *N*-acetylated peptides were soluble in methanol. The conformational preferences of the  $\alpha/\beta/\gamma$ -peptides were investigated with Boc-FGaAGwAGI-OMe [42], Boc-FGaAGwAL-OMe [43], Boc-FGaAGfAGI-OMe [44] and Boc-FGaAGfAL-OMe [45].

#### 3.3.1. DMSO- $d_6$ titration

All  $^1\text{H}$  and  $^{13}\text{C}$  signals pertinent for conformational analyses of the four peptides [42]-[45] were unambiguously assigned, except for certain  $\text{H}\beta$ ,  $\text{C}\beta$ ,  $\text{H}\gamma$  and aromatic protons and carbons of  $\gamma^4$ -residues that could not be clearly assigned (see in PART III).

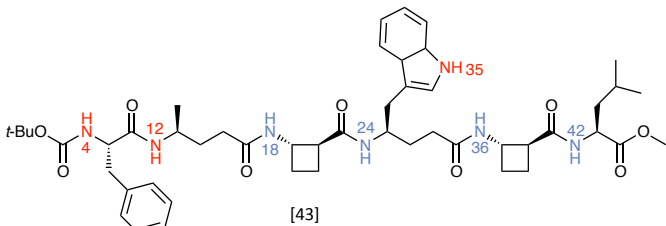
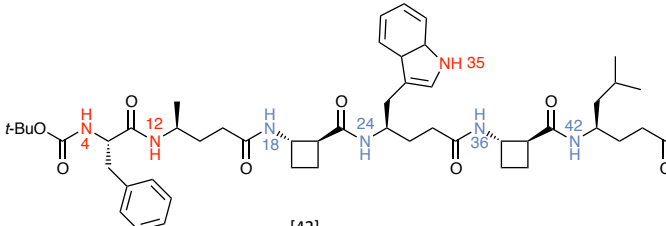
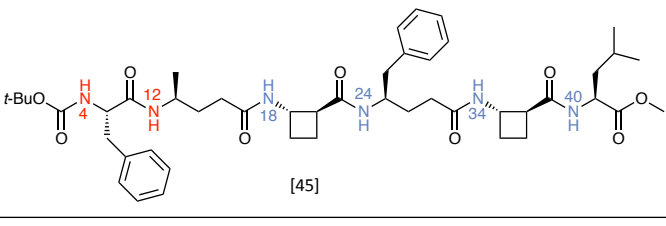
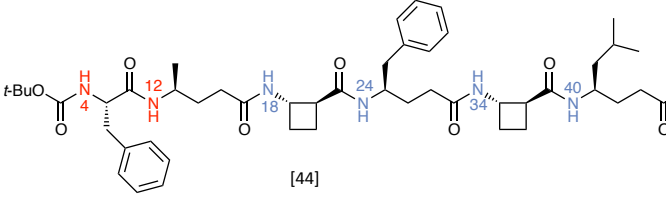
The titration of  $\text{CDCl}_3$  solutions by DMSO- $d_6$  was carried out for the four peptides [42]-[45]. The differences in the chemical shifts of the N-H between 0% and 50% of added DMSO- $d_6$  were determined and were classified by a colour code as: high (in red), medium (in green) and low (in blue) (see Table 13).

All of the  $\alpha/\beta/\gamma$ -peptides clearly possessed two N-H signals with a high DMSO- $d_6$  titration coefficient that is to say two free N-H (in red). The  $\alpha/\beta/\gamma$ -peptides possessing a  $\gamma^4$ -*h*Trp presented a third very high DMSO- $d_6$  titration coefficient corresponding to the free N-H of the indole ring.

The other N-H signals all showed low titration coefficients suggesting that they are not exposed to solvents and are engaged into a hydrogen bond (in blue).

These observations suggested that the folding behaviour for each of the four  $\alpha/\beta/\gamma$ -peptides was indeed the consistent **12/13-helix** suggested by theoretical calculations.

Table 13. DMSO-*d*<sub>6</sub> titration of the  $\alpha/\beta/\gamma$ -peptides [42]-[45].

$\Delta\delta(\text{NH}(4))$	1.39	
$\Delta\delta(\text{NH}(12))$	1.58	
$\Delta\delta(\text{NH}(18))$	0.52	
$\Delta\delta(\text{NH}(24))$	0.40	
$\Delta\delta(\text{NH}(35))$	2.19	
$\Delta\delta(\text{NH}(36))$	0.12	
$\Delta\delta(\text{NH}(42))$	-0.09	
$\Delta\delta(\text{NH}(4))$	1.10	
$\Delta\delta(\text{NH}(12))$	1.37	
$\Delta\delta(\text{NH}(18))$	0.36	
$\Delta\delta(\text{NH}(24))$	0.13	
$\Delta\delta(\text{NH}(35))$	1.84	
$\Delta\delta(\text{NH}(36))$	-0.12	
$\Delta\delta(\text{NH}(42))$	-0.09	
$\Delta\delta(\text{NH}(4))$	1.31	
$\Delta\delta(\text{NH}(12))$	1.59	
$\Delta\delta(\text{NH}(18))$	0.52	
$\Delta\delta(\text{NH}(24))$	0.26	
$\Delta\delta(\text{NH}(34))$	-0.08	
$\Delta\delta(\text{NH}(40))$	-0.02	
$\Delta\delta(\text{NH}(4))$	1.31	
$\Delta\delta(\text{NH}(12))$	1.59	
$\Delta\delta(\text{NH}(18))$	0.52	
$\Delta\delta(\text{NH}(24))$	0.26	
$\Delta\delta(\text{NH}(34))$	-0.08	
$\Delta\delta(\text{NH}(40))$	-0.02	

### 3.3.2. 2D $^1\text{H}$ - $^1\text{H}$ ROESY experiments

ROESY experiments of the four peptides [42]-[45] were recorded in  $\text{CDCl}_3$  solutions at a concentration of 10 mM (see Figure 103).

The four ROEs,  $\text{H}\beta(i)\text{-NH}(i+2)$ ,  $\text{H}\beta(i)\text{-H}\alpha(i+2)$ ,  $\text{H}\gamma(i)\text{-NH}(i+2)$  and  $\text{H}\gamma(i)\text{-NH}(i+3)$  (in pink), which were established in Chapter II as **diagnostic of 13-membered hydrogen-bonded rings** were found in alternating  $\beta/\gamma$ -segments of the four peptides.

Furthermore new long-distance ROEs,  $\text{H}\alpha(i)\text{-NH}(i+2)$  and  $\text{H}\alpha(i)\text{-H}\alpha(i+2)$  (in blue), which implicated the  $\alpha/\gamma/\beta$ -segments in each of four peptides, were detected.

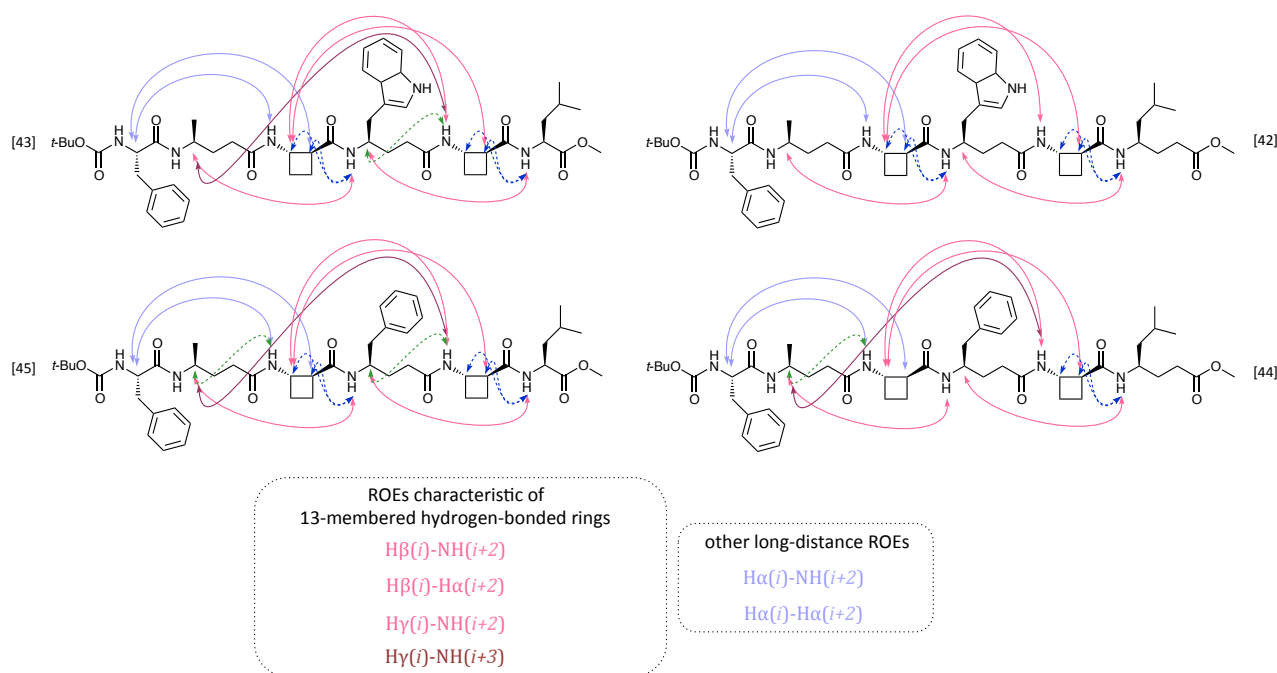


Figure 103. ROEs observed for  $\alpha/\beta/\gamma$ -peptides [42]-[45].

No ROE or NOE of  $\alpha/\beta/\gamma$ -peptides have been reported in the literature to date. There is no precedent for comparison for  $Ha(i)-NH(i+2)$  and  $Ha(i)-Ha(i+2)$  ROEs, but these correlations bear a clear analogy with those which arise from 13-membered hydrogen-bonded ring systems. These ROEs were therefore compatible with a 12-membered hydrogen-bonded ring, which was suggested by the two N-terminal N-H free determined by DMSO- $d_6$  titration experiments and theoretical calculations.

The proposed p53 mimetics accommodated a **12-membered hydrogen-bonded ring** formed by the concatenation of  $\alpha/\gamma/\beta$ -amino acids and **three successive 13-membered hydrogen-bonded rings** formed by the concatenation of  $\beta/\gamma$ -peptides (see Figure 104).

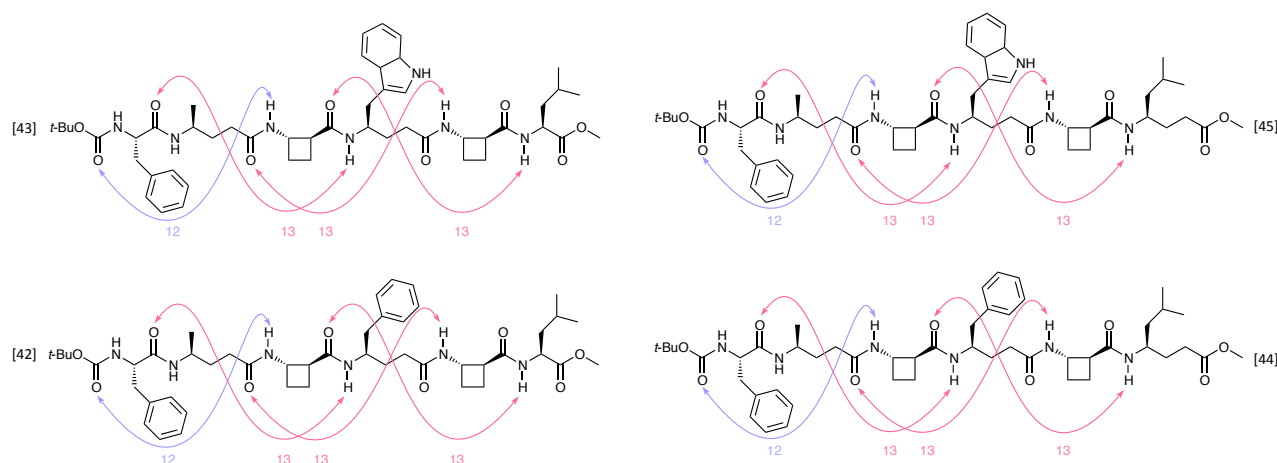


Figure 104. Deduced hydrogen-bonded patterns adopted by  $\alpha/\beta/\gamma$ -peptides [42]-[45].

### 3.3.1. Infrared analysis

IR spectra of the four  $\alpha/\beta/\gamma$ -peptides [42]-[45] were recorded in  $\text{CDCl}_3$  solutions at a concentration of 10 mM (see Figure 105).

The spectra of each of the four  $\alpha/\beta/\gamma$ -peptides presented two types of N-H stretch absorptions. In each case, sharp bands between 3410 and 3440  $\text{cm}^{-1}$  corresponded to free N-H while a broad band in the range of 3250-3350  $\text{cm}^{-1}$  corresponded to amide N-H engaged in intramolecular hydrogen bonds. For Boc-FGaAGwAGI-OMe [42] and Boc-FGaAGwAL-OMe [43], a third vibration band at 3490  $\text{cm}^{-1}$  was observed and corresponded to the free N-H of the indole ring of the Trp residue.

The lower frequency band presented a maximum at 3325  $\text{cm}^{-1}$  characteristic of amide N-Hs engaged in 13-membered hydrogen-bonded rings. It was reported that N-H engaged in 12-membered hydrogen-bonded rings featured an absorption at 3300  $\text{cm}^{-1}$ .<sup>111</sup> The absorption of N-H engaged in C12 might be overlaid with the absorption of N-H engaged in C13.

Furthermore, in each case, a small shoulder was noticed at 3250  $\text{cm}^{-1}$  which might indicate an amide N-H engaged in an 8-membered hydrogen-bonded ring as shown in Chapters 1 and 2. This confirmed the presence of a second conformer, suggested by the theoretical calculations as a 12-13-13-8 conformer family frayed at C-terminal.

The IR spectra were consistent with the proposed conformational preference of a 12/13-helix of the four  $\alpha/\beta/\gamma$ -peptides suggested in the previous sections by NMR experiments and by molecular modelling.

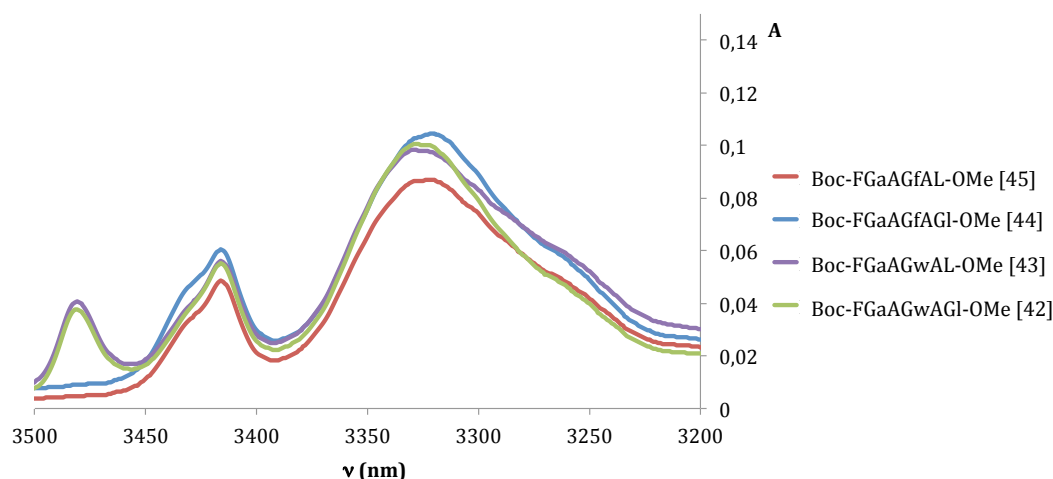


Figure 105. Infrared spectra of  $\alpha/\beta/\gamma$ -peptides [42]-[45].



### 3.3.2. Circular Dichroism

Far-UV CD spectra of the four  $\alpha/\beta/\gamma$ -peptides, [42]-[45], were recorded in methanol solutions at a concentration of 0.2 mM (see Figure 106). The CD curves showed a marked Cotton effect, which increased with increasing peptide length. Each spectrum displayed a minimum near 206 nm and a maximum near 224 nm.

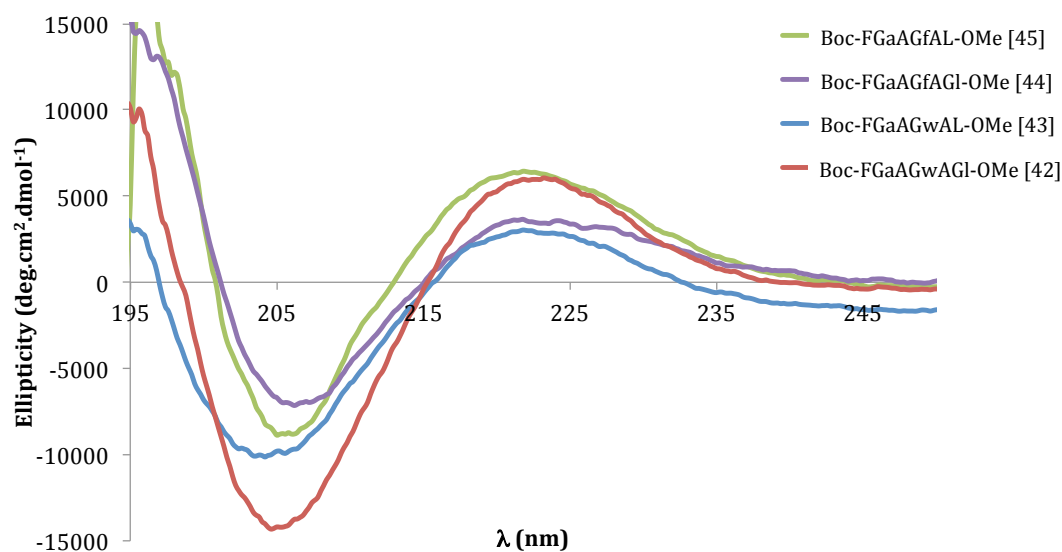


Figure 106. Circular Dichroism spectra of  $\alpha/\beta/\gamma$ -peptides [42]-[45].

CD data were compared with available CD spectra for related compounds (see Figure 107). The CD curve of Boc-FGaAGwAGI-OMe [42] showed very similar minimum and maximum Cotton effects to the signature of the 13-helix adopted by  $\beta/\gamma$ -peptide Boc-AGfAGfAGI-NHBn [34]. The curve of FGaAGwAGI-OMe [42] also resembled the signature of the 12-helix adopted by octamer of *trans*-ACBC. These similarities suggested that [42], as well as [43], [44] and [45] adopted a conformer similar to that of the 13- and 12-helices in methanol, which was again consistent with the 12/13-helical folding predicted by theoretical calculations.

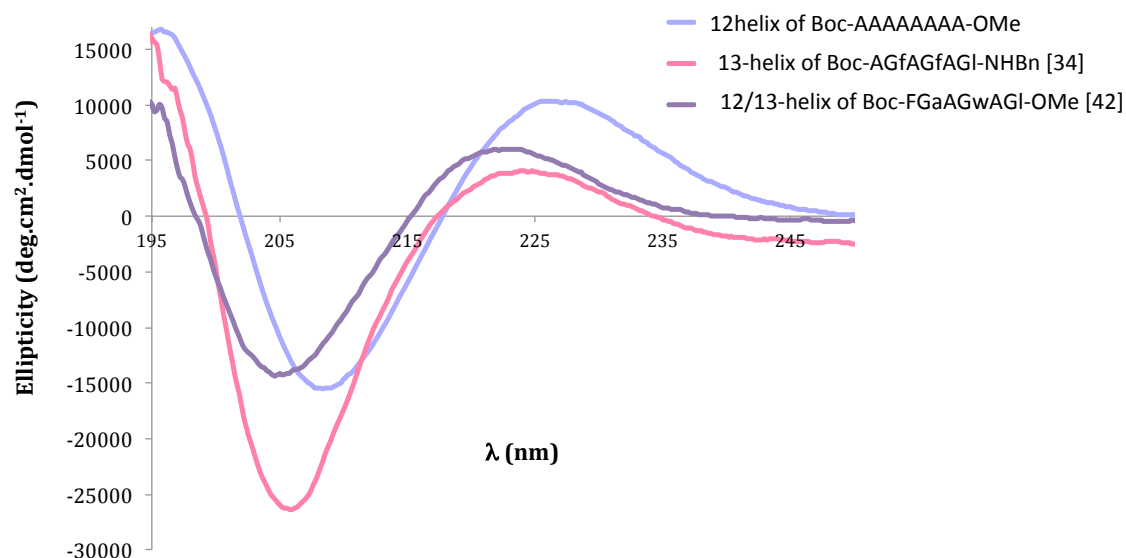


Figure 107. Comparison between the CD spectra of an  $\alpha/\beta/\gamma$ -peptide [42], a 12-helical  $\beta$ -peptide and a 13-helical  $\beta/\gamma$ -peptide [34].

### 3.4 Biophysical analyses of the $\alpha/\beta/\gamma$ -peptides proposed as $\alpha$ -helix mimetics

The biophysical analyses of the  $\alpha/\beta/\gamma$ -peptides were carried out during a Visiting Research Assistant placement in the research laboratory of Prof. A. J. Wilson, University of Leeds.

#### 3.4.1. Proteolytic studies

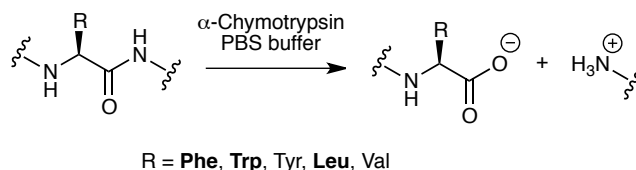
In the first instance, the resistance of the  $\alpha/\beta/\gamma$ -peptides to proteolytic degradation was tested. It is of crucial importance that peptides are not digested enzymatically if future pharmaceutical developments are intended.

It has been shown previously that  $\beta$ - and  $\gamma$ -peptides are resistant to proteolytic cleavage. However, the stability of  $\alpha/\beta/\gamma$ -peptides, related to the peptides studied here, has not been addressed to date. Indeed, the presence of an  $\alpha$ -amino acid residue might render these peptides more vulnerable to enzymatic degradation.

Proteolytic studies were performed on the eight  $\alpha/\beta/\gamma$ -peptides [42]-[49] and also on the p53(15-31) peptide<sup>xi</sup> for comparison.  $\alpha$ -Chymotrypsin was chosen for this study since this enzyme

<sup>xi</sup> p53(15-31) peptide corresponds to a synthetic  $\alpha$ -peptide reproducing the segment 15 to 31 of the related p53 protein.

selectively cleaves amide bonds adjacent to residues with hydrophobic side chains (see Scheme 18), such as Phe, Trp and Leu, which feature prominently in the peptides under study.



Scheme 18. Peptide degradation by  $\alpha$ -chymotrypsin.

Each peptide was treated with commercial  $\alpha$ -chymotrypsin (EC 3.4.21.1) (1:10,000 enzyme/substrate ratio) at room temperature and the degradation was followed using analytical HPLC. The extent of degradation was determined after 5, 12, 21, 45 and 90 minutes of incubation. The HPLC traces of the p53(15-31) peptide digestion are presented in Figure 108. After only 5 min of incubation, cleavage products of p53(15-31) peptide were already detected. After 12 min, p53(15-31) peptide was completely degraded.

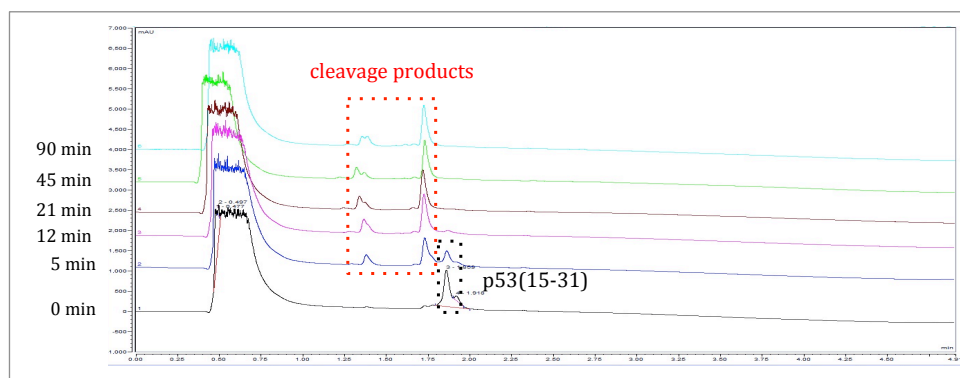


Figure 108. Analytic HPLC traces of the positive control, p53(15-29) peptide, incubated with  $\alpha$ -chymotrypsin.

The proteolytic activity of  $\alpha$ -chymotrypsin was considered to have been verified via this positive control before being tested on the four  $\alpha/\beta/\gamma$ -peptides [42]-[49]. The HPLC traces of  $\alpha/\beta/\gamma$ -peptides resulting from incubation with  $\alpha$ -chymotrypsin are presented in Figure 109.

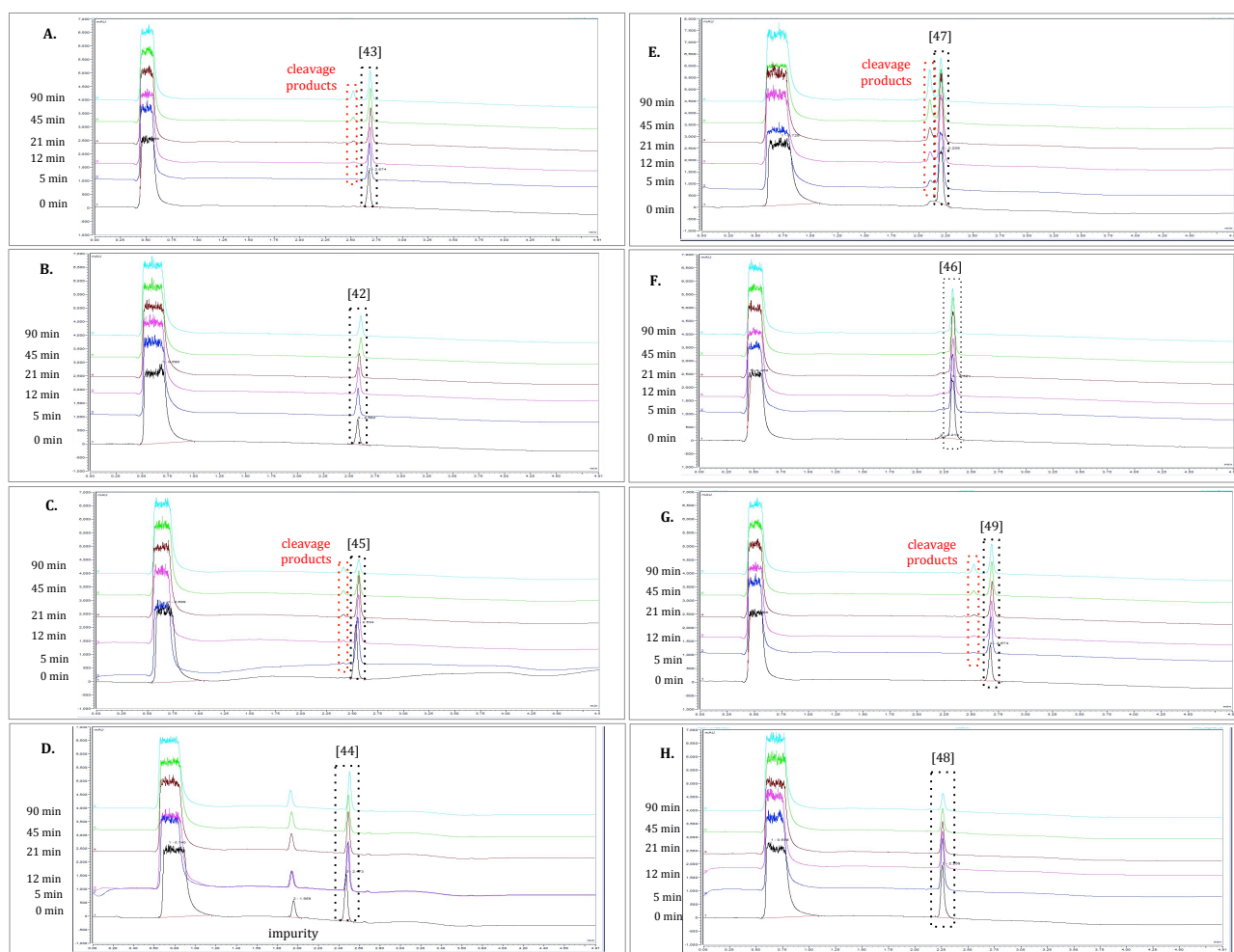


Figure 109. Analytic HPLC traces of  $\alpha/\beta/\gamma$ -peptides [42]-[49] incubated with  $\alpha$ -chymotrypsin.

The HPLC traces showed the intact hexapeptides [42], [44], [46] and [48] even after an incubation time of 90 minutes suggesting complete resistance to degradation by  $\alpha$ -chymotrypsin over the allotted time.

However, a new peak was detected after 5 min of incubation time for hexapeptides [43], [45], [47] and [49] indicating that these peptides were partially degraded by the enzyme. The four intact hexapeptides were still largely present after 90 min of incubation time, however.

The cleavage products were analysed by LCMS (see Figure 110). The data obtained in each case indicated that the cleavage product has lost only 14 Da from its molecular mass. This suggested that the transformation which had been affected by  $\alpha$ -chymotrypsin was methyl ester cleavage. There was no evidence of further degradation of the resulting carboxylic acid forms of the  $\alpha/\beta/\gamma$ -peptides.

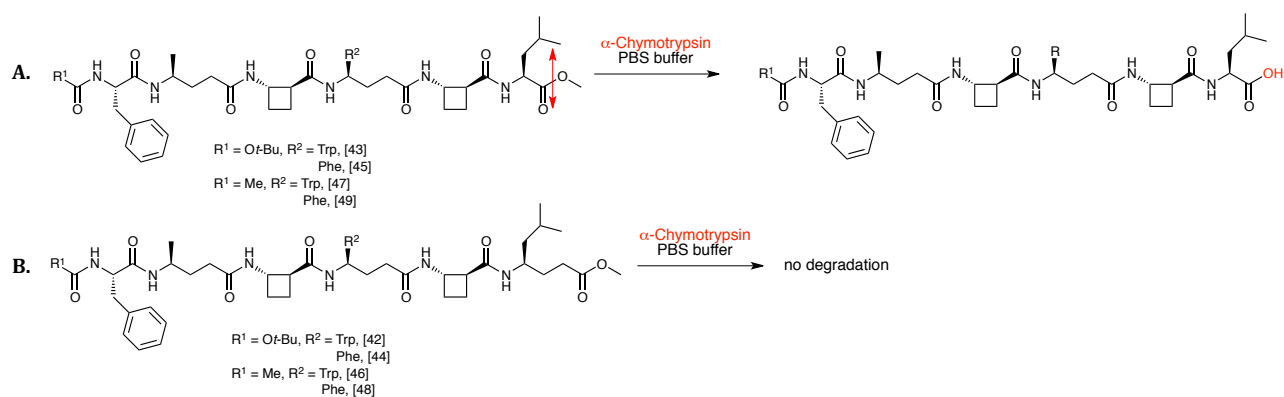
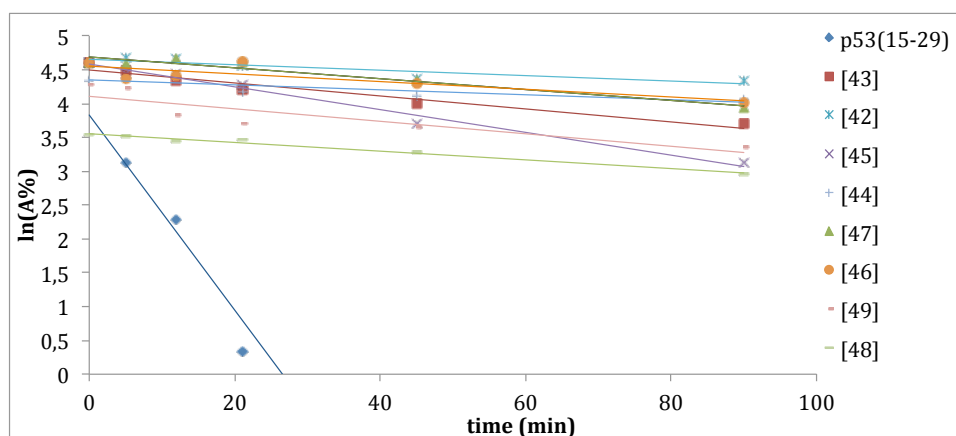


Figure 110. Reactivity of the  $\alpha/\beta/\gamma$ -peptides to  $\alpha$ -chymotrypsin suggested by LCMS analyses.

The HPLC data were further analysed to extract kinetic degradation profiles and to determine rate constants from a linear fit (see Figure 111), as well as the half-life times of proteolysis, using Equation 1.

$$\ln\left(\frac{A_t}{A_0}\right) = -kt$$

Equation 1.  $A_t$  = Areas of substrate at time  $t$ ;  $A_0$  = Substrate area at time zero;  $k$  = reaction rate coefficient.



	p53(15-29)	[43]	[42]	[45]	[46]	[47]	[46]	[49]	[48]
$t_{1/2}$ (min)	4.8	72.2	173.3	41.3	187.3	86.6	121.6	75.3	121.6

Figure 111. Kinetics of proteolytic degradation studies calculated half-lives time of degradation for p53(15-29) peptide and  $\alpha/\beta/\gamma$ -peptides [42]-[49].

The eight  $\alpha/\beta/\gamma$ -peptides displayed much greater resistance to  $\alpha$ -chymotrypsin than did p53(15-29)  $\alpha$ -peptide: at least 32-fold greater for [42], [44], [46] and [48] and at least greater 10-fold greater for [43], [45], [47] and [49]. Although methyl ester hydrolysis of the latter four compounds was observed, the hexapeptide core stayed intact.

The  $\alpha/\beta/\gamma$ -peptides under study presented sufficient **proteolytic resistance** to be employed with confidence in further biological studies.

### 3.4.2. Fluorescence anisotropy (FA) competition assays for inhibition of PPIs

The eight  $\alpha/\beta/\gamma$ -peptides [42]-[49] were tested for their ability to act as inhibitors of an  $\alpha$ -helix mediated PPI.

#### 3.4.2.1. Presentation of the technique

Fluorescence Anisotropy (FA) competition assays have been extensively developed in the group of Prof. A. J. Wilson to test libraries of compounds as inhibitors of particular PPIs, these being p53/hDM2, Bak/Bcl<sub>xL</sub> and NOXA B/Mcl-1 interactions.<sup>58,61,96,172,173</sup>

The technique is based on a competitive binding to the targeted protein of a tracer peptide (the fluorophore-labelled native peptide) and a competitor (the putative inhibitor) (see Figure 112). Following excitation of the tracer peptide with plane-polarized light, the anisotropy is measured from the intensity of the light emitted by the fluorophore. In the absence of a competitor, the tracer peptide binds to its protein preventing the tracer peptide from tumbling and results in a maximum of anisotropy. In the presence of a competitor, the interaction can be disrupted; the tracer peptide can be displaced into the solution, where it tumbles faster. This process results in the loss of the directionality of the polarized excitation light and in a decrease of anisotropy.

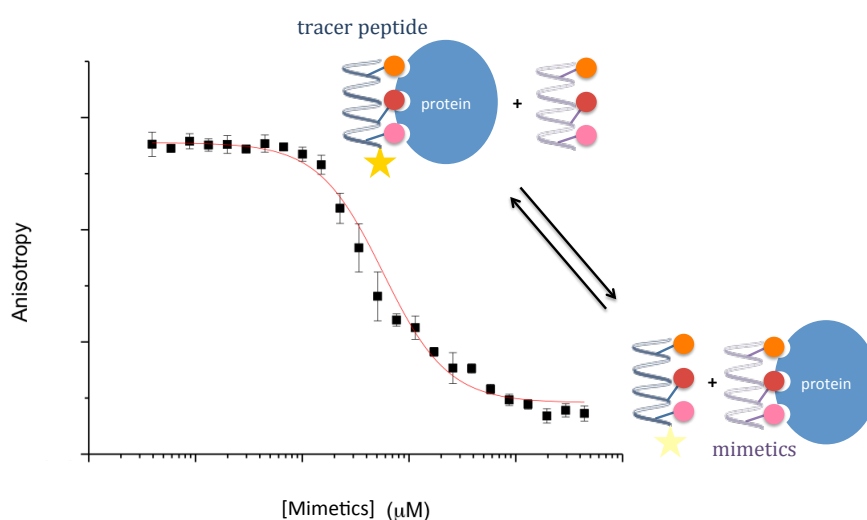


Figure 112. FA competition assay principle.

## 3.4.2.2. FA directed against p53/hDM2 interaction

As we stated above, hexapeptides [42]-[49] were designed as mimetics of the  $\alpha$ -helical segment 19-26 of the p53 protein.

Before testing these peptides for their ability to act as inhibitors of the p53/hDM2 interaction, a positive control experiment was conducted using a well-known inhibitor, Nutlin 3-a, of p53/hDM2 interaction (see PART I, Section 2.2). The tracer peptide was flu-p53(15-31) which corresponded to p53(15-31) peptide labelled with 2-(*N*-methylsuccinimide)fluorescein linked to its C-terminal. Into constant concentrations of protein and tracer peptide, serial dilution of the competitive inhibitor, Nutlin 3-a, gave the full competition curve of Nutlin 3-a shown in Figure 113. Nutlin 3-a showed an  $IC_{50}$  of  $0.434 \pm 0.024 \mu\text{M}$  in this assay. This value was consistent with previous studies carried out in the Wilson group.<sup>173</sup>

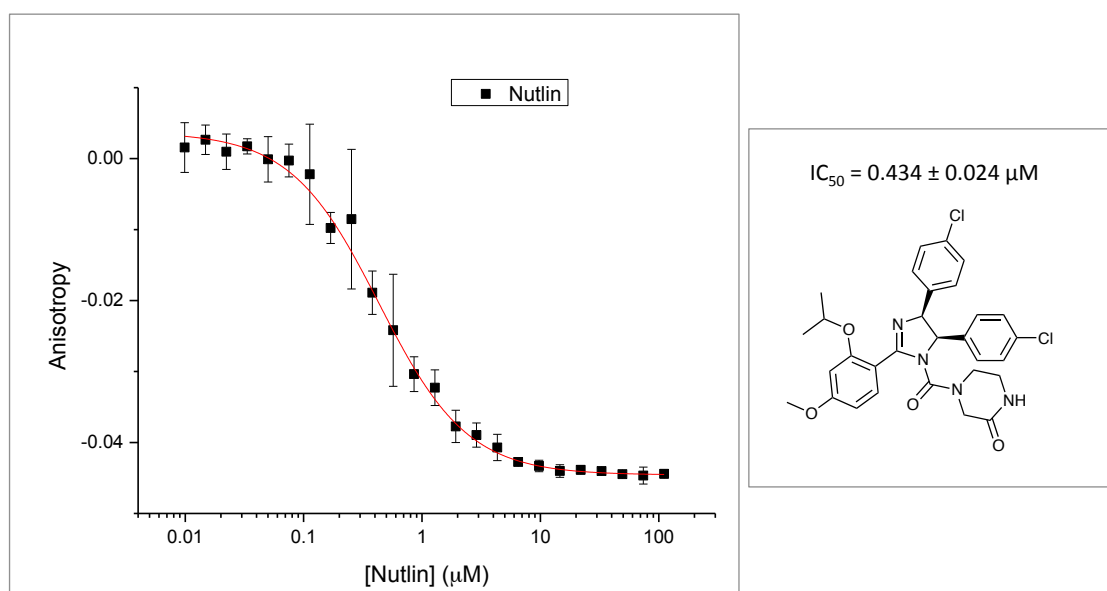


Figure 113: Dose response curves of Nutlin 3-a against flu-p53(15-29)/hDM2 interaction – Positive control

This positive control experiment allowed us to confirm the quality of the starting materials, the labelled peptide and the protein, which are sensitive to degradation. The activity of each of the eight  $\alpha/\beta/\gamma$ -peptides was tested in a FA competition assay against the flu-p53(15-29)/hDM2 interaction (see Figure 114).

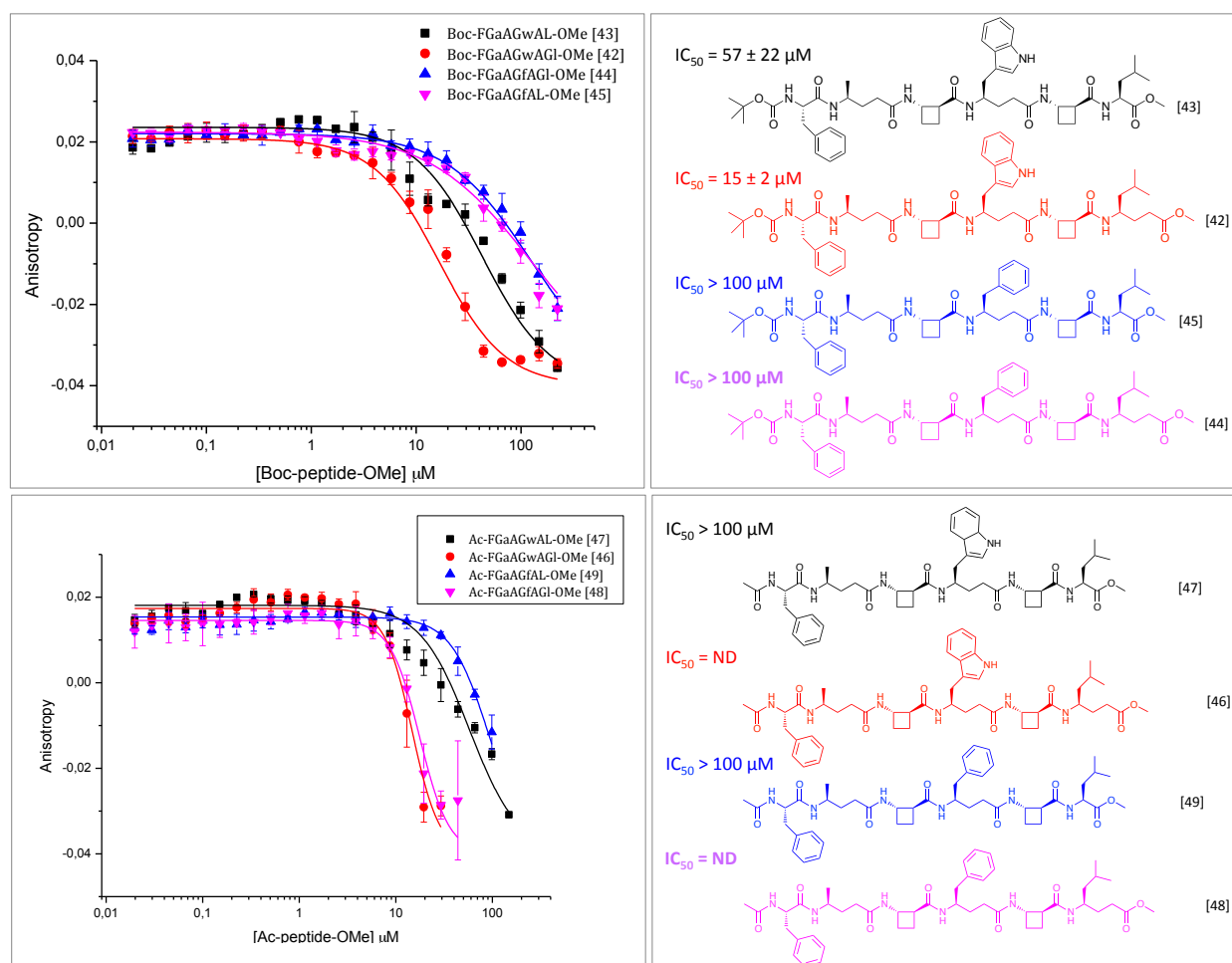


Figure 114. Dose response curves of [42]-[49] against flu-p53/hDM2 interaction.

The competitive curves showed that all of the four *N*-Boc protected peptides bound to *hDM2* while the behaviour of the four *N*-acetamide peptides was less clear.

Peptides [44], [45], [47], [49] whilst weakly binding to *hDM2*, were not sufficiently potent ligands to generate full competition curves. They displayed  $\text{IC}_{50}$  values superior to  $100 \mu\text{M}$ .

Peptides [46] and [48] did not generate full competition curves. For concentrations of peptides above  $40 \mu\text{M}$  (not shown), the curves presented an anisotropy maximum of 0.02 instead of an anisotropy minimum of  $-0.04$ , preventing the determination of the  $\text{IC}_{50}$  value.

Peptides [42] and [43] presented full competition curves, each with a similar anisotropy minimum of  $-0.04$  and anisotropy maximum of 0.02 to Nutlin 3-a. Very encouragingly, they presented impressive inhibitory activities, with a very good  **$\text{IC}_{50}$  value of  $15 \pm 2 \mu\text{M}$  for [42]** and a good  $\text{IC}_{50}$  value of  $57 \pm 22 \mu\text{M}$  for [43].

The difference in behaviour between the pair of peptides [42] and [43] and the pair of peptides [44] and [45] suggested that  $\gamma^4$ -*h*Trp played a significant role in binding to *hDM2*. Indeed it has been shown that Trp 21 of native p53 protein establishes a hydrogen bond with the carbonyl of Leu 54 of *hDM2* when located in the binding-pocket of the latter.<sup>128</sup>



### 3.4.2.3. Test of selectivity: FA directed against Bak/Bcl-x<sub>L</sub> and NOXA B/Mcl-1 interactions

It has been reported that potent inhibitors of p53/hDM2 sometimes present a drawback through a lack of selectivity, in that they are also able to inhibit other PPI based on the recognition of hydrophobic side chains. These PPIs include the Bak/Bcl-x<sub>L</sub> and NOXA B/Mcl-1 interactions.

We therefore tested the four *N*-Boc protected  $\alpha/\beta/\gamma$ -peptides [42]-[45] proposed as p53(19-26) mimetics in FA assays against (see Figure 115):

- BODIPY-Bak/Bcl-x<sub>L</sub> interaction, in which the tracer peptide Bak( ) was labelled with boron-dipyromethene (BODIPY). A known inhibitor of the Bak/Bcl-x<sub>L</sub> interaction, ABT-737, was used as a positive control.
- FITC-NOXA B/Mcl-1 interaction, in which the tracer peptide NOXA-B( ) was labelled with fluorescein isothiocyanate (FITC) and N-acetylated NOXA-B was used as a positive control.

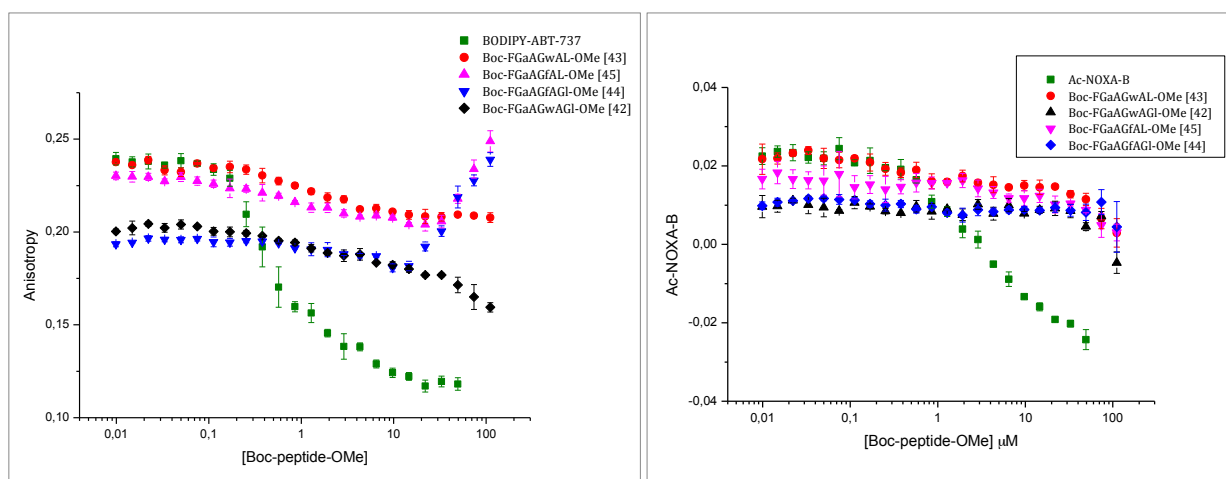


Figure 115. A: Dose response curves of p53 mimetics against BODIPY-BAK/Bcl-x<sub>L</sub>. B: Dose response curves of p53 mimetics against FITC-NOXA B/Mcl-1 interactions (the positive controls are shown for comparison in green)

None of the four peptides showed any sign of inhibitory activity or even binding to Mcl-1 or Bcl-x<sub>L</sub>. The peptides were therefore selective in targeting the p53/hDM2 interaction. This result illustrated the success of the rational design of the p53-mimetics, which was presented in Section 3.1.

Peptides [42] represented the **first example of  $\alpha/\beta/\gamma$ -peptides successfully designed type I  $\alpha$ -helix mimetics** to date. They provided reasonably potent yet selective inhibition against the  $\alpha$ -helix mediated PPI of p53/hDM2.

### 3.4.3. $^1\text{H}$ - $^{15}\text{N}$ HSQC NMR study of the $\alpha$ -helix p53 mimetics in complex with *hDM2*

The Wilson group has developed a  $^1\text{H}$ - $^{15}\text{N}$  HSQC NMR perturbation shift experimental protocol for the study of type II  $\alpha$ -helix mimetics.<sup>61,172,173</sup> This powerful technique was used to establish whether the Boc-FGaAGwAGI-OMe [42]  $\alpha$ -helix mimetics prepared in our work bound to *hDM2* at the p53 binding cleft. At the same time, the poor ligand for *hDM2*, Ac-FGaAGfAL-OMe [49] was evaluated as a negative control as it presented a low affinity for *hDM2* as suggested by the high  $\text{IC}_{50}$  determined by FA. The interaction between the peptide and the protein was estimated by measuring the protein amide N-H perturbation shifts by comparison of data for the protein alone with data for the protein in the presence of the peptide.

HSQC spectra were acquired for the  $^{15}\text{N}$ -labelled apoform of *hDM2* (at a concentration of 125  $\mu\text{M}$  in 100 mM of sodium phosphate buffer at pH 7.3 with 2.5 % of glycerol, 1 mM of DTT, 5 % of DMSO) and for the  $^{15}\text{N}$ -labelled apoform of *hDM2* in the presence of each specified  $\alpha/\beta/\gamma$ -peptides (at a concentration of 200  $\mu\text{M}$  after overnight incubation).

The spectra of labelled  $^{15}\text{N}$ -*hDM2* in the absence (in black) and in the presence (in red) of Boc-FGaAGwAGI-OMe [42] are superimposed in Figure 116 A. The perturbation shifts were calculated and displayed for each residue in Figure 116 B. The presence of peptide [42] resulted in significant shifts of certain crosspeaks in the  $^1\text{H}$ - $^{15}\text{N}$  HSQC spectrum.

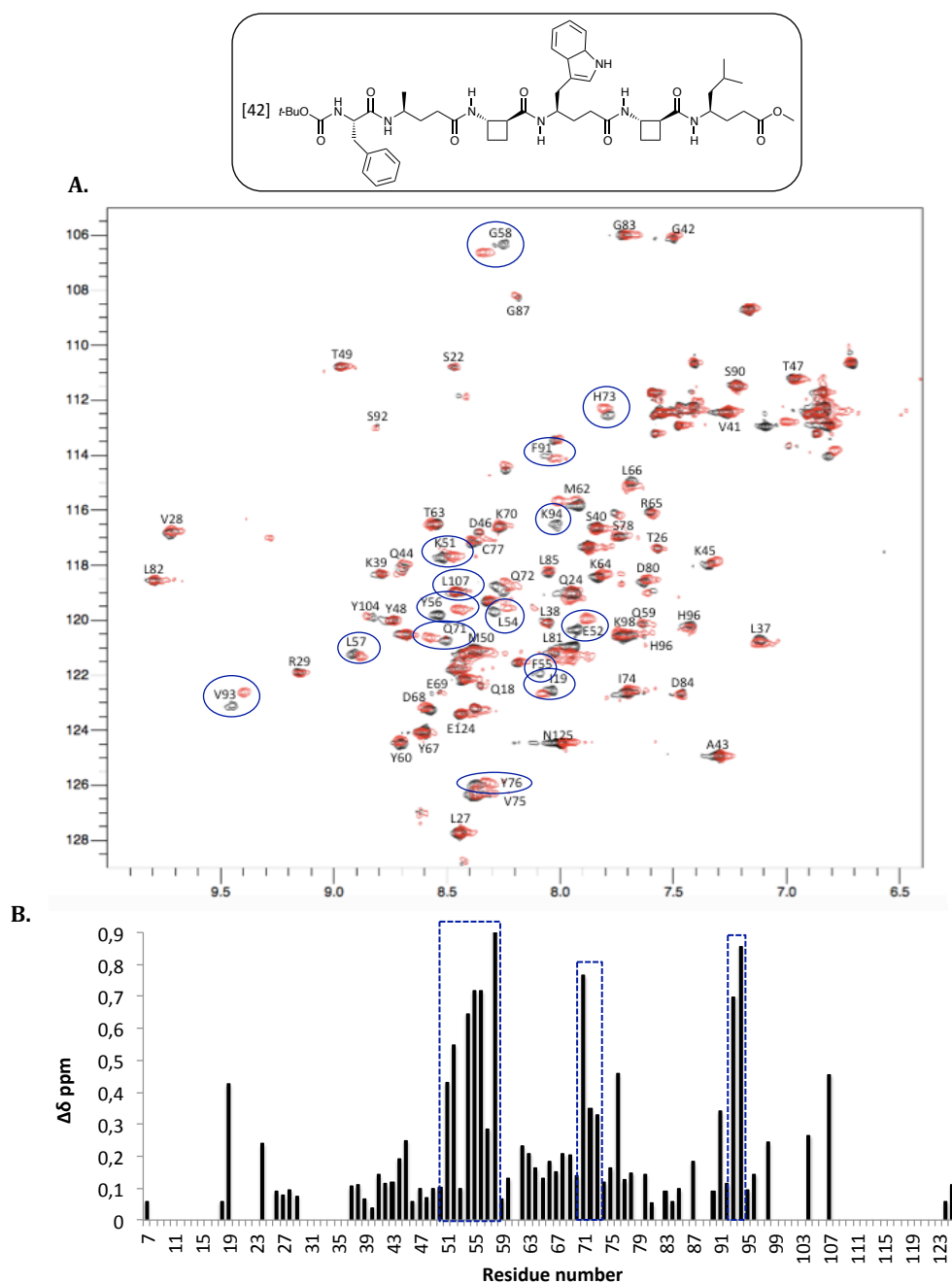
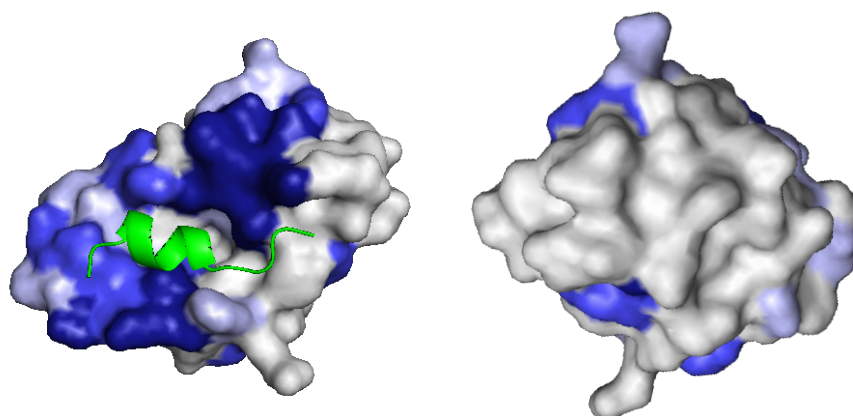


Figure 116. A: Superimposition of  $^1\text{H}$ - $^{15}\text{N}$  HSQC spectra of  $^{15}\text{N}$ -labelled hDM2 in absence (in black) and in presence (in red) of [42]. B: Perturbation shifts of amide NH of hDM2

The negative control experiment was performed in an analogous manner using peptide [49] (see Figure 117 A). The perturbation shifts were calculated and displayed for each residue in Figure 117 B. The perturbation shifts of crosspeaks in the  $^1\text{H}$ - $^{15}\text{N}$  HSQC spectrum were much smaller in magnitude than those found for [42].





Colours	Perturbation shifts (ppm)	residues
Dark blue	$0.4 > \delta$	19, 51, 52, 54, 55, 56, 58, 71, 76, 93, 94, 107
Blue	$0.2 < \delta < 0.4$	24, 45, 57, 61, 63, 68, 69, 72, 73, 91, 98, 104
Light blue	$0.1 < \delta < 0.2$	41, 42, 43, 44, 60, 64, 65, 66, 67, 70, 74, 75, 77, 78, 80, 87, 92, 96, 125
Grey	$\delta < 0.1$	7, 18, 26, 27, 28, 29, 37, 38, 39, 40, 46, 47, 48, 49, 50, 53, 59, 81, 83, 84, 85, 90, 95, 124

Figure 118.  $^1\text{H}$ - $^{15}\text{N}$  HSQC perturbations induced by [42] mapped onto the crystal structure of the p53/hDM2 complex (PDB ID: 1YCR).

The shift changes were induced throughout the protein and were comparable to those induced by p53(15-29) peptide in its interaction with hDM2, previously characterised by the Wilson group.<sup>61</sup> Significant movement, characterised by strong and medium perturbation shifts, were observed for amide N-H of Phe 55 and His 73, which are located at opposite edges of the hydrophobic cleft. This suggested that the p53(15-29) peptide cleft of hDM2 accommodated Boc-FGaAGwAGl-OMe [42], supporting the notion that **this  $\alpha/\beta/\gamma$ -peptide  $\alpha$ -helix mimetic bound in the p53 peptide binding site.**

### 3.5 Conclusion

In conclusion to this chapter, the objective of mimicking the native  $\alpha$ -helix with helical peptides incorporating  $\beta/\gamma$ -segments of *trans*-ACBC and  $\gamma^4$ -amino acids was reached.

Based on the results acquired from Chapter 1 and 2, we were able to successfully design and efficiently prepare helical  $\alpha/\beta/\gamma$ -peptides which displayed the appropriate side-chains at the right positions of the targeted helical segment (19-26) of p53 protein.

Proteolytic studies conducted on the hybrid  $\alpha/\beta/\gamma$ -peptides demonstrated their resistance to enzymatic degradation, which is advantageous with respect to  $\alpha$ -peptides.

As a proof of concept, the  $\alpha/\beta/\gamma$ -peptides were tested as inhibitors of the p53/hDM2 interaction in FA assays. Low micromolar inhibitors of this interaction were identified and a high level of selectivity was shown for these peptides towards hDM2. The most potent inhibitor was further

examined by  $^1\text{H}$ - $^{15}\text{N}$  HSQC NMR studies and appeared to bind in the p53 peptide binding cleft of *hDM2*, showing the success of our design strategy of **the type I  $\alpha$ -helix mimetics**.



## CONCLUSION

This thesis has addressed the questions of design, synthesis, structural characterisation, and biological evaluation of  $\beta/\gamma$ -peptides which were proposed to mimic the  $\alpha$ -helix, a secondary structure which is present in many native proteins. Following a bottom-up design strategy, the axiom which was chosen implicated a  $\beta$ -amino acid component (*trans*-ACBC) whose role was to impart severe conformational constraints, and a  $\gamma$ -amino acid component (GABA or a simple derivative) which was required to impose the lowest degree of constraint possible and thereby provide a versatile support for functional side chains.

The first Chapter was dedicated to the investigation of  $\beta/\gamma$ -peptides incorporating ***trans*-ACBC** and **GABA**, the latter being devoid of any side chain induced constraint. The solution-phase synthesis of a selected panel of relevant  $\beta/\gamma$ -peptides was successful: a convergent synthetic strategy was employed for  $\beta/\gamma$ -peptides with GABA at the N-terminal, whereas the atypical reactivity of C-terminal GABA peptide intermediates prompted the adoption of a linear synthetic strategy for  $\beta/\gamma$ -peptides in which *trans*-ACBC was the N-terminal residue.

The folding behaviour of these peptides was explored in solution in chloroform using an array of spectroscopic techniques (DMSO-*d*<sub>6</sub> titration, <sup>1</sup>H-<sup>1</sup>H ROESY NMR, IR, CD) and theoretical calculations (Monte Carlo Multiple Minima followed by DFT optimizations of low-energy conformers). These investigations led to the discovery of an **unprecedented 9/8-ribbon foldamer structure**. The local flexibility of the constituent GABA residues provides for the co-existence of several low-energy 9/8-ribbon conformers which are more or less curved, and for which the global molecular topology is governed by a unique combined configuration-conformation code.

In the second Chapter, a modified  $\beta/\gamma$ -peptide paradigm was proposed and examined, whereby the  $\beta/\gamma$ -peptide composition implicated ***trans*-ACBC** and a  **$\gamma^4$ -amino acid**. A set of oligopeptides with differing sequence lengths and compositions was prepared without difficulty, according to a convergent synthetic strategy using solution-state techniques.

Experimental and theoretical investigations of this series of oligopeptides were carried out using the same techniques as those used in the previous Chapter. The new series of  $\beta/\gamma$ -peptides showed a clear preference for **13-helix** folding behaviour in solution, which increased commensurately with the peptide chain length. In this way, the presence of a single substituent on the  $\gamma$ -amino acid components was shown to have a decisive influence on the conformational landscape: the predominant feature shifted from a 9/8-ribbon (no  $\gamma$ -amino acid substituent) to a 13-helix ( $\gamma^4$ -amino acid substituent). The 13-helix thus unveiled constitutes only the second example of this



category of foldamer and has the considerable advantage, when compared to the only other example, of being largely unchallenged from a steric point of view; this significant facet is the direct result of the bottom-up design strategy which was adopted.

The third Chapter was devoted to the design and evaluation of  **$\alpha/\beta/\gamma$ -peptides** which were conceived to reproduce, as closely as possible, the hot-spot residues of the known  $\alpha$ -helical (19-26) fragment of the p53 protein; molecular modelling was employed to assist the identification of appropriate target peptide structures. The requisite series of peptides was prepared without difficulty according to a convergent solution-phase synthetic strategy. Spectroscopic studies, carried out in an analogous fashion to those employed in the preceding Chapters, confirmed the anticipated folding of these peptides into an **unprecedented 12/13-helix**.

The helical  $\alpha/\beta/\gamma$ -peptides were investigated using biophysical assays in order to evaluate their ability to mimic native  $\alpha$ -helical secondary structure. A demonstrated advantage of the  $\alpha/\beta/\gamma$ -peptide motif, compared to native  $\alpha$ -peptides, was its resistance to proteolytic degradation. The  $\alpha/\beta/\gamma$ -peptides were tested as inhibitors of the p53/*hDM2* interaction using FA assays. Most of the studied  $\alpha/\beta/\gamma$ -peptides were able to bind to the target *hDM2* protein and **low micromolar inhibition** of this interaction was demonstrated for two of the  $\alpha/\beta/\gamma$ -peptides. The most potent inhibitor was shown through  $^1\text{H}$ - $^{15}\text{N}$  HSQC NMR studies to bind in the p53(15-29) peptide binding cleft of *hDM2*. This study provides a convincing proof-of-concept for the  $\alpha$ -helix mimetic design strategy proposed in this thesis.

These results open up the field of foldamers towards the programmable bottom-up design of mimetics of the native  $\alpha$ -helix. The monomer-level assessment of the possible folding propensities of short oligopeptides led to the prediction of a **minimum steric constraints** axiom for robust helical mimics of the native  $\alpha$ -helix. This foldamer design principle is sufficiently reliable for it to be applied successfully for the conception of hybrid peptides, which possess  $\alpha$ -,  $\beta$ -, and  $\gamma$ -amino acids, which fold reliably into requisite helical structures.

Attractive future developments will implicate other combinations of  $\alpha$ -,  $\beta$ -, and  $\gamma$ -amino acids, with specifically designated tasks for each residue which are defined as structural, functional, or perhaps combinations of both. Variation of the side-chain identities and diversification of the targeted side-chain hot-spot topology sets are likely to be significant objectives in the next-generation foldamer-based  $\alpha$ -helix mimetic developments.

## **PART III. EXPERIMENTAL PART**



All reagents and solvents were of commercial grade and were used without further purification, with the following exceptions: dichloromethane was dried over activated alumina, DMF, Et<sub>3</sub>N and DIPEA were dried and distilled from CaH<sub>2</sub> under argon and THF was distilled from sodium/benzophenone under argon. All  $\gamma^4$ -amino acids were purchased from PolyPeptide.

Flash chromatography was performed using Combiflash from Teledyne ISCO with columns of silica gel SI60 (15–40  $\mu$ m) from Merck Chimie SAS. Analytical thin-layer chromatography was performed with 0.25 mm coated commercial silica gel plates (EMD, Silica Gel 60F<sub>254</sub>). TLC plates were visualized by UV fluorescence at 254 nm, then revealed with a ninhydrin solution (14 mM in EtOH). Retention factors ( $R_f$ ) are given for such analyses.

Nuclear magnetic resonance (NMR) data were acquired on Bruker 250, 360, 400 and 600 MHz for <sup>1</sup>H and at 62.5, 90 and 100 MHz for <sup>13</sup>C spectrometers. Chemical shifts ( $\delta$ ) are reported in parts per million (ppm) from tetramethylsilane with the solvent resonance resulting from incomplete deuteration as the internal reference. Splitting patterns for H<sup>1</sup> NMR signals are designated as: s (singlet), d (doublet), t (triplet), m (multiplet) or bs (broad singlet). Coupling constants ( $J$ ) are reported in hertz.

All <sup>1</sup>H-<sup>15</sup>N HSQC experiments were performed on a Varian Inova spectrometer at 600MHz. A gradient filtered pulse sequence was used and the data was phased using NMRpipe and visualised using ccpnmr Analysis.

High resolution mass spectrometry data were recorded on a MicroTOF-Q (Bruker) spectrometer equipped with an electrospray source in positive or negative mode (HRMS+ or HRMS-).

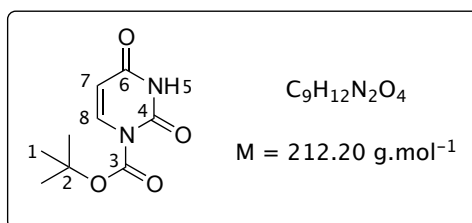
Melting points were obtained in open capillary tubes using a Büchi B-545 melting point apparatus and are uncorrected.

Samples for Fourier-transform infrared spectroscopy (IR) were obtained in a solution in CDCl<sub>3</sub> (10 mM) measured in a 0.2 mm length NaCl solution cell with a CDCl<sub>3</sub> background. Spectra were recorded on a Spectrum One (Perkin-Elmer) spectrometer. Maximum absorbances ( $\nu$ ) are given for significant bands in cm<sup>-1</sup>.

Optical rotations were measured on a Jasco P-1010 polarimeter, using a 10 cm quartz cell. Values for were obtained with the D-line of sodium at the indicated temperature  $T$ , using solutions of concentration ( $c$ ) in units of g·100 mL<sup>-1</sup>.

## 1. Synthesis of *trans*-ACBC

### 1-*t*-Butyloxycarbonyluracil - [5]



To a suspension of uracil (10.000 g, 89 mmol, 1.0 eq.) in  $CH_3CN$  (500 mL) were added  $Boc_2O$  (19.464 g, 89 mmol, 1.0 eq.) and DMAP (102 mg, 0.89 mmol, 0.01 eq.). The mixture was stirred overnight at room temperature, then the solvent was removed under reduced pressure to give the crude Boc-uracil (g, quant.) as a pale orange solid which was directly used in the next step without purification.

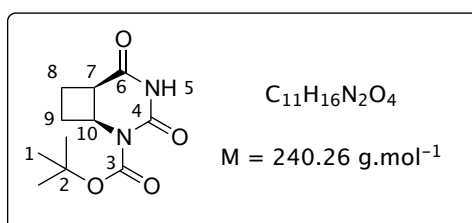
$R_f$  0.81 ( $Et_2O$ )

$^1H$  NMR (360 MHz,  $DMSO-d_6$ )  $\delta$  1.52 (s, 9H, 9H-1), 5.69 (d,  $J = 8.4$  Hz, 1H, H-8), 7.88 (d,  $J = 8.4$  Hz, 1H, H-7), 11.40 (s, 1H, H-5).

UV/Vis ( $CH_3CN$ ):  $\lambda$  ( $\epsilon.M^{-1}.cm^{-1}$ ) = 208 (11908), 250 (16021).

The spectral data were identical to those reported previously.<sup>165</sup>

### cis-2-(*t*-Butyloxycarbonyl)-2,4-diazabicyclo[4.2.0]octane-3,5-dione ( $\pm$ ) - [4]



A solution of crude Boc-uracil [5] (45 mmol) in acetone (1 L) placed in a cylindrical water-cooled reactor was degassed with an argon stream for 30 min, and then saturated with ethylene for 30 min. The solution was then irradiated for 5 h with a 400 W medium-pressure mercury lamp fitted with a

Pyrex filter while ethylene was bubbled through. The solution was then concentrated under reduced pressure. Flash chromatography of the residue (gradient from 10 / 90 to 30 / 70 : EtOAc / PE) gave the cycloadduct ( $\pm$ )-[4] (7.2 g, 67% yield over 2 steps) as a white solid.

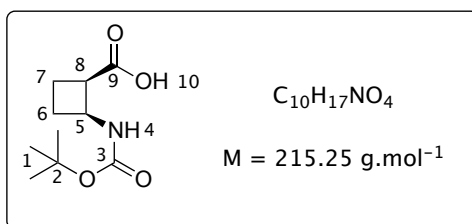
**R<sub>f</sub>** 0.26 (EtOAc / PE = 30 / 70)

**Mp:** 140 °C

**<sup>1</sup>H NMR** (250 MHz, CDCl<sub>3</sub>)  $\delta$  1.56 (s, 9H, 9H-1), 2.11-2.34 (m, 3H, 2H-8, H-9), 2.42-2.58 (m, 1H, H-9'), 3.33-3.39 (m, 1H, H-7), 4.70-4.81 (m, 1H, H-10), 8.03 (bs, 1H, H-5).

The spectral data were identical to those reported previously.<sup>165</sup>

**cis-2-(*t*-Butyloxycarbonylamino)cyclobutanecarboxylic acid ( $\pm$ )-[1]**



Cycloadduct [4] (14 g, 58 mmol, 1.0 eq.) was treated with a 0.5 M aqueous NaOH solution (583 mL) for 8 h at room temperature. The solution was cooled to 0 °C and solid NaOH (58 g, 1 450 mmol, 25 eq.) was added portionwise to increase the concentration to 3 M. The mixture was stirred for overnight at room temperature, then was cooled to 0 °C and acidified slowly with concentrated HCl to pH 3. The aqueous phase was extracted with EtOAc (3 × 150 mL). The organic phase was dried over Na<sub>2</sub>SO<sub>4</sub>, filtered and concentrated under reduced pressure to give [1] (9 g, 72%) as a white solid. The crude product was used for the next step without any purification.

**R<sub>f</sub>** 0.13 (EtOAc / PE = 50 / 50)

**Mp:** 159°C

**<sup>1</sup>H NMR** (360 MHz, DMSO-*d*<sub>6</sub>)  $\delta$  1.36 (s, 9H, 9H-1), 1.77-1.95 (m, 3H, 2H-7, H-6), 2.09 (m, 1H, H-6'), 3.31-3.39 (m, 1H, H-8), 4.22-4.29 (m, 1H, H-5), 7.75 (bs, 1H, H-4), 12.04 (bs, 1H, H-10).

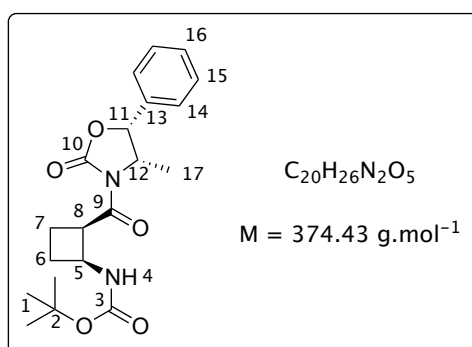
$^{13}\text{C}$  NMR (90 MHz,  $\text{DMSO}-d_6$ )  $\delta$  18.0 (C-7), 27.7 (C-6), 27.9 (C-1), 45.5 (C-5), 46.8 (C-8), 83.5 (C-2), 154.6 (C-3), 174.4 (C-9).

The spectral data were identical to those reported previously.<sup>165</sup>

### Chiral derivatization of ( $\pm$ )-[1] with (4*S*,5*R*)-4-methyl-5-phenyloxazolidin-2-one

To a cold ( $-78\text{ }^\circ\text{C}$ ) solution of Boc-amino acid ( $\pm$ )-[1] (6.00 g, 27.91 mmol, 1 eq.) and  $\text{Et}_3\text{N}$  (4.65 mL, 3.38 g, 33.49, 1.2 eq.) in dry THF (277 mL) was added dropwise pivaloyl chloride (3.60 mL, 29.30 mmol, 1.05 eq.) under argon atmosphere. The mixture was stirred for 1 h at  $-20\text{ }^\circ\text{C}$  to form the mixed anhydride, then cooled to  $-78\text{ }^\circ\text{C}$ . In a separate flask, a cold ( $-40\text{ }^\circ\text{C}$ ) solution of (4*S*,5*R*)-4-methyl-5-phenyloxazolidin-2-one (4.94 g, 27.91 mmol, 1 eq.) in THF (130 mL) was carefully treated with *n*-BuLi (1.6 M solution in hexane, 17 mL, 1 eq.) and stirred for 5 min. The resulting solution was added to the cooled ( $-78\text{ }^\circ\text{C}$ ) solution of the mixed anhydride. The resulting mixture was stirred for 1 h at  $-78\text{ }^\circ\text{C}$ . After warming to  $0\text{ }^\circ\text{C}$ , the mixture was treated with a saturated solution of  $\text{NaHCO}_3$  and THF was removed under reduced pressure. The aqueous layer was extracted with EtOAc. The combined organic layers were washed with a saturated solution of  $\text{NaHCO}_3$  and brine, dried over  $\text{Na}_2\text{SO}_4$  and filtered. After evaporation of the solvent under reduced pressure, the total separation of the two diastereomers was obtained with a succession of 5 crystallizations in cyclohexane to give pure [7] followed by a unique purification by flash chromatography (EtOAc / PE = 10 / 90) of the combined mother liquors in cyclohexane to give the diastereoisomers [6] (4.8 g, 48%) and [7] (4.7 g, 47%) as white foams.

### (4*S*,5*R*)-*N*-[(1*R*,2*S*)-2-(*t*-Butyloxycarbonylamino)cyclobutanecarbonyl]-4-methyl-5-phenyl-3-oxazolidin-2-one (-) - [6]



$R_f$  0.53 (EtOAc / PE = 30 / 70)

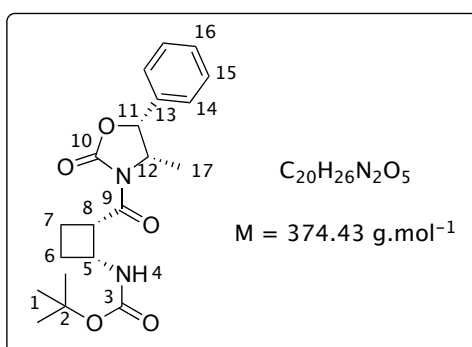
$[\alpha]_D^{25} = -65$  (c. 0.50 in  $\text{CHCl}_3$ )

**$^1\text{H}$  NMR** (360 MHz,  $\text{CDCl}_3$ )  $\delta$  0.77 (d,  $J = 6.6$  Hz, 3H, 3H-17), 1.28 (s, 9H, 9H-1), 1.89-2.04 (m, 3H, 2H-7, H-6), 2.27-2.31 (m, 1H, H-6'), 4.43 (m, 1H, H-8), 4.52 (m, 1H, H-5), 4.61-4.71 (m, 1H, H-12), 5.31 (bs, 1H, H-4), 5.53 (d,  $J = 7$  Hz, 1H, H-11), 7.18-7.31 (m, 5H, 2H-14, 2H-15, H-16).

**$^{13}\text{C}$  NMR** (90 MHz,  $\text{CDCl}_3$ )  $\delta$  14.5 (C-17), 18.4 (C-7), 28.2 (C-6), 28.9 (C-1), 44.7 (C-5), 47.2 (C-8), 54.4 (C-12), 78.6 (C-2), 78.9 (C-11), 125.5, 128.8, 128.9 (C-14, C-15, C-16), 133.3 (C-13), 152.1 (C-10), 154.3 (C-3), 173.1 (C-9).

The spectral data were identical to those reported previously.<sup>165</sup>

**(4*S*,5*R*)-*N*-[(1*S*,2*R*)-2-(*t*-Butyloxycarbonylamino)cyclobutanecarbonyl]-4-methyl-5-phenyl-3-oxazolidin-2-one (+) - [7]**



$R_f$  0.64 (EtOAc / EP = 30 / 70)

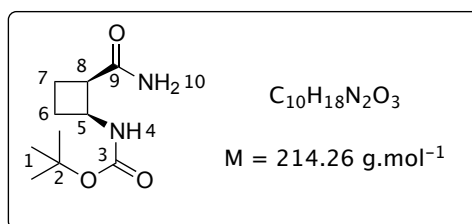
$[\alpha]_D^{25} = +52$  (c. 0.50 in  $\text{CHCl}_3$ )

**$^1\text{H}$  NMR** (360 MHz,  $\text{CDCl}_3$ )  $\delta$  0.77 (d,  $J = 6.8$  Hz, 3H, 3H-17), 1.32 (s, 9H, 9H-1), 1.84-2.07 (m, 3H, 2H-7, H-6), 2.28-2.30 (m, 1H, H-6'), 4.43 (bs, 2H, H-5, H-8), 4.59-4.71 (m, 1H, H-12), 5.23 (bs, 1H, H-4), 5.53 (d,  $J = 6.8$  Hz, 1H, H-11), 7.16-7.30 (m, 5H, 2H-14, 2H-15, H-16).

**$^{13}\text{C}$  NMR** (90 MHz,  $\text{CDCl}_3$ )  $\delta$  14.6 (C-17), 19.3 (C-7), 28.4 (C-6), 28.7 (C-1), 44.9 (C-5), 47.7 (C-8), 55.0 (C-12), 79.1 (C-2), 79.3 (C-11), 125.7, 128.8 (C-14, C-15, C-16), 133.5 (C-13), 152.6 (C-10), 155.0 (C-3), 173.1 (C-9).

The spectral data were identical to those reported previously.<sup>165</sup>



**(1*R*,2*S*)-2-(*t*-Butyloxycarbonylamino)cyclobutanecarboxamide (+) - [8]**

To a solution of [6] (3.40 g, 9.07 mmol, 1 eq.) in THF (156 mL) was added an excess of aqueous ammonia (25% w/w solution, 79 mL). The resulting mixture was stirred for 48 h at room temperature. Solvents were removed under reduced pressure. The crude residue was purified by flash chromatography (EtOAc / c.hexane = 50 / 50) to give [8] (1.76 g, 90%) as a white solid.

$R_f$  0.16 (EtOAc / PE = 50 / 50)

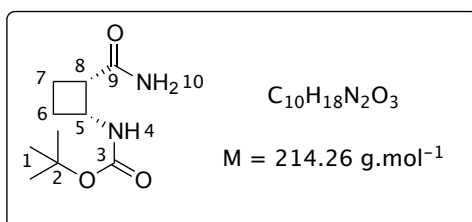
**Mp:** 170 °C

$[\alpha]_D^{23} = +117$  (c. 0.50 in  $CHCl_3$ )

**$^1H$  NMR** (250 MHz,  $CDCl_3$ )  $\delta$  1.37 (s, 9H, 9H-1), 2.08 (m, 1H, H-6), 2.13-2.36 (m, 3H, 2H-7, H-6'), 3.43 (m, 1H, H-8), 4.40 (m, 1H, H-5), 5.4 (bs, 1H, H-4), 5.6 (bd, 2H, H-10).

**$^{13}C$  NMR** (62.5 MHz,  $CDCl_3$ )  $\delta$  18.0 (C-7), 28.3 (C-6), 28.8 (C-1), 45.8, 46.4 (C-5, C-8), 79.5 (C-2), 155.3 (C-3), 175.21 (C-9).

The spectral data were identical to those reported previously.<sup>165</sup>

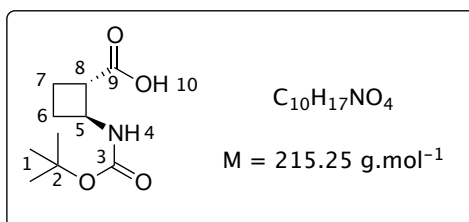
**(1*R*,2*S*)-2-(*t*-Butyloxycarbonylamino)cyclobutanecarboxamide (–) - [8']**

The enantiomer of [8] was prepared from [7], following the above-described sequences with comparable yields.

$$[\alpha]_D^{23} = -113 \text{ (c. 0.50 in CHCl}_3\text{)}$$

The spectral data were comparable to the enantiomer [8].

**(1*S*,2*S*)-2-(*t*-Butyloxycarbonylamino)cyclobutanecarboxylic acid (+) - [2]**



To a solution of [8] (1.45 g, 6.74 mmol, 1 eq.) in MeOH (92 mL) was added 6 M aqueous NaOH (273 mL). The resulting mixture was refluxed overnight. Methanol was removed under reduced pressure. The aqueous layer was then cooled to 0 °C and slowly acidified with concentrated HCl to pH 3. The aqueous layer was extracted with EtOAc (3 × 75 mL). The organic layer was dried over Na<sub>2</sub>SO<sub>4</sub>, filtered and concentrated under reduced pressure to give the Boc-amino acid [2] (875 mg, 60%) as a pale yellow solid.

$R_f$  0.26 (EtOAc / PE) = 70 / 30

**Mp:** 124 °C

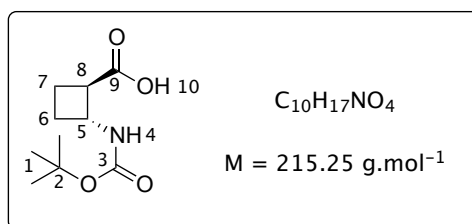
$$[\alpha]_D^{24} = +30 \text{ (c. 0.59 in EtOH)}$$

**<sup>1</sup>H NMR** (250 MHz, CDCl<sub>3</sub>) δ 1.44 (s, 9H, 9H-1), 1.78-1.82 (m, 1H, H-6), 2.15-2.20 (m, 3H, H-6', 2H-7), 2.96-3.00 (m, 1H, H-8), 4.06-4.13 (m, 1H, H-5) 4.91 (bs, 1H, H-4).

**<sup>13</sup>C NMR** (90 MHz, CDCl<sub>3</sub>) δ 18.6 (C-7), 23.7 (C-6), 28.2 (C-1), 47.8 (C-5), 48.7 (C-8), 82.0 (C-2), 157.3 (C-3), 174.3 (C-1).

**HRMS (ESI)** [M+Na]<sup>+</sup> found 238.1047, C<sub>10</sub>H<sub>18</sub>NNaO<sub>4</sub> calcd 238.1050.

The spectral data were identical to those reported previously.<sup>165</sup>

**(1*R*,2*R*)-2-(*t*-Butyloxycarbonylamino)cyclobutanecarboxylic acid (-) - [2']**

The enantiomer of [2] was prepared from [8'], following the above-described sequences with comparable yields.

$$[\alpha]_D^{24} = -27 \text{ (c. 0.59 in EtOH)}$$

The spectral data were comparable to the enantiomer [2].

## 2. Synthesis of peptides

### General procedure A for the hydrogenolysis of benzyl ester protecting group

To a solution of Boc-peptide-OBn (1 eq.) in  $CH_2Cl_2$  (40 mL / mmol) was added 10 % Pd-C (10 % (w/w) - 50 mg as the minimum required quantity). The black suspension was stirred under  $H_2$  atmosphere until the reaction was complete (TLC monitoring). The mixture was then filtered through a celite pad and  $CH_2Cl_2$  was concentrated under reduced pressure to afford Boc-peptide-OH which was directly used in the coupling reaction without further purification.

### General procedure B for the basic hydrolysis of methyl ester protecting group

To a solution of PG-peptide-OMe (1 eq.) in a 1 : 1 mixture of  $H_2O$  : THF (10 mL / mmol) was added LiOH· $H_2O$  (1.5 eq.). The white suspension was stirred for 3 h at room temperature. THF was then removed under reduced pressure. The aqueous solution was then slowly acidified at 0 °C with a solution of HCl (1 M) to reach pH 3. EtOAc was added to extract three times the desired acid. The combined organic layers were dried over  $Na_2SO_4$ , filtered and concentrated under reduced pressure to give the corresponding PG-peptide-OH carboxylic acid.

### General procedure C for the cleavage of *tert*-butoxycarbonyl protecting group

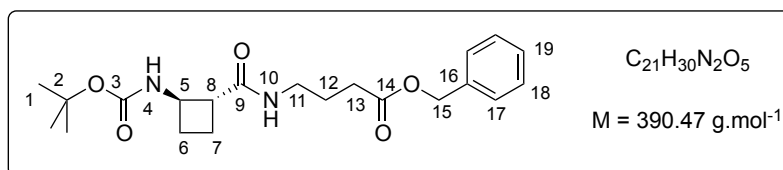
To a solution of Boc-peptide-OPG (1 eq.) in dry  $\text{CH}_2\text{Cl}_2$  (25 mL / mmol) was added TFA (30 eq.) at room temperature under argon atmosphere. The resulting yellowish mixture was stirred until the reaction was complete (TLC monitoring).  $\text{CH}_2\text{Cl}_2$  was then evaporated under reduced pressure. Toluene was added to co-evaporate the excess of TFA. The corresponding TFA salt was directly engaged to the coupling reaction without further purification.

#### General procedure D for coupling reaction

To a solution of Boc-peptide-OH (1 eq.) in a mixture of  $\text{CH}_2\text{Cl}_2$  and DMF (6 mL / mmol) was added DIPEA (2 eq.) followed by HATU (1.05 eq.). The resulting mixture was stirred for 10 min at room temperature and the solution became brownish. A solution of the TFA salt partner (1 eq.) and DIPEA (sufficient quantity to reach pH 9) in  $\text{CH}_2\text{Cl}_2$  (6 mL / mmol) was prepared and added to the reaction mixture which was stirred overnight. Solvents were removed under reduced pressure. The crude product was dissolved in EtOAc and successively washed by a saturated solution of  $\text{NaHCO}_3$ , brine, a 1 M solution of HCl and brine. The organic layer was dried over  $\text{Na}_2\text{SO}_4$ , filtered and concentrated under reduced pressure. The crude residue was well dried under vacuum then purified by flash chromatography.

### 2.1 Peptides alternating (1*R*,2*R*)-ACBC and GABA

#### Boc-(1*R*,2*R*)-ACBC-GABA-OBn (-) - [9]



According to the general procedure **D**, the coupling reaction was performed with Boc-(1*R*,2*R*)-ACBC-OH [2'] (430 mg, 2 mmol), DIPEA (629  $\mu\text{L}$ , 476 mg, 4 mmol) and HATU (788 mg, 2.1 mmol) in a mixture of  $\text{CH}_2\text{Cl}_2$  / DMF (4 mL / 1 mL), and  $\text{H}_2\text{N}$ -GABA-OBn (386 mg, 2 mmol), DIPEA (2.085 mL, 1.548 g, 12 mmol) overnight. The purification was carried out by flash chromatography (gradient from 10 / 90 to 100 / 0 : EtOAc / PE) to give Boc-(1*R*,2*R*)-ACBC-GABA-OBn [9] as a white solid (483 mg, 62%).

$R_f$  0.14 (EtOAc / PE = 50 / 50)

**Mp:** 116 °C

$$[\alpha]_D^{21} = -10 \text{ (c. 0.50 in CHCl}_3\text{)}$$

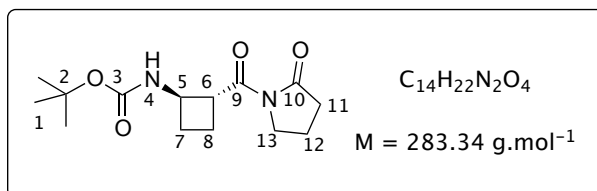
**<sup>1</sup>H NMR** (360 MHz, CDCl<sub>3</sub>) δ 1.42 (s, 9H, 9H-1), 1.70-1.78 (m, 1H, H-6), 1.85-1.92 (m, 3H, H-7, 2H-12), 2.08-2.22 (m, 2H, H-7', H-6'), 2.46 (t, 2H, J = 7.6 Hz, 2H-13), 2.85-2.92 (m, 1H, H-8), 3.22-3.27 (m, 1H, H-11), 3.34-3.39 (m, 1H, H-11'), 4.05-4.13 (m, 1H, H-5), 4.91 (bs, 1H, H-4), 5.12 (s, 2H, 2H-15), 7.32-7.36 (m, 5H, 2H-17, 2H-18, H-19), 8.12 (bs, 1H, H-10).

**<sup>13</sup>C NMR** (90 MHz, CDCl<sub>3</sub>) δ 18.6 (C-7), 24.7 (C-6, C-12), 28.3 (C-1), 31.2 (C-13), 38.6 (C-11), 48.8 (C-5), 50.1 (C-8), 66.2 (C-15), 80.5 (C-2), 128.2, 128.2, 128.5 (C-17, C-18, C-19), 136.0 (C-16), 156.3 (C-3), 173.1, 173.1 (C-9, C-14).

**IR** (10 mmol/L, in CDCl<sub>3</sub>)  $\nu_{\max}$  1499, 1562, 1649, 1692, 1730, 3297 (br), 3447 cm<sup>-1</sup>.

**HRMS (ESI):** [M+Na]<sup>+</sup>, theor. 413.2047 (calc. for C<sub>21</sub>H<sub>30</sub>N<sub>2</sub>NaO<sub>5</sub>), meas. 413.2065.

#### N-[(1*R*,2*R*)-2-(*t*-Butyloxycarbonylamino)cyclobutanecarbonyl]-2-oxopyrrolidine - [18]



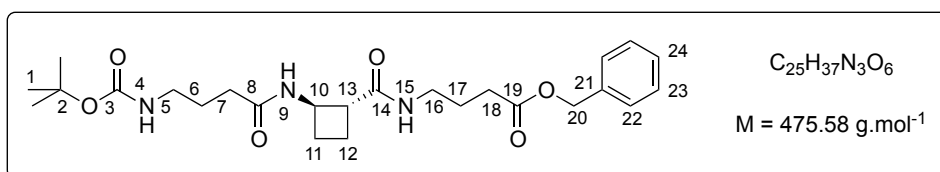
To a cold (−78 °C) solution of [2] (337 mg, 1.56 mmol, 1 eq.) and Et<sub>3</sub>N (421 μL, 316 mg, 3.13 mmol, 2 eq.) in dry THF (15 mL) was added dropwise pivaloyl chloride (202 μL, 1.64 mmol, 1.05 eq.) under argon atmosphere. The mixture was stirred for 30 min at −20 °C to form the mixed anhydride, then cooled to −78 °C. In a separate flask, a cold (−40 °C) solution of 2-pyrrolidinone (133 μg, 119 μL, 1.56 mmol, 1 eq.) in THF (7 mL) was carefully treated with *n*-BuLi (1.6 M solution in hexane, 961 μL, 1.56 mmol, 1 eq.) and stirred for 5 min. The resulting solution was added to the cooled (−78 °C) solution of the mixed anhydride. The resulting mixture was stirred for 1 h at −78 °C. After warming to 0 °C, the mixture was treated with a saturated solution of NaHCO<sub>3</sub> and THF was removed under reduced pressure. The aqueous layer was extracted with EtOAc. The combined organic layers were washed with a saturated solution of NaHCO<sub>3</sub> and brine, dried over Na<sub>2</sub>SO<sub>4</sub> and filtered. The solution was then concentrated under reduced pressure. Flash chromatography of the residue (20 / 80 : EtOAc / PE) gave [18] (432 mg, 98% yield) as a white solid.

$R_f$  0.10 (EtOAc / PE = 30 / 70)

$^1\text{H NMR}$  (250 MHz,  $\text{CDCl}_3$ )  $\delta$  1.28 (s, 9H, 9H-1), 1.91 (m, 4H, 1H-7, 2H-8, 2H-12), 2.23 (m, 1H, H-7'), 2.45 (m, 2H, 2H-11), 3.68 (m, 2H, 2H-13), 4.37 (m, 2H, H-5, H-6), 5.57 (bs, 1H, H-4).

**HRMS (ESI):**  $[\text{M}+\text{Na}]^+$ , theor. 305.1473 (calc. for  $\text{C}_{14}\text{H}_{22}\text{N}_2\text{NaO}_4$ ), meas. 305.1454.

**Boc-GABA-(1*R*,2*R*)-ACBC-GABA-OBn (-) - [20]**



According to the general procedure **C**, *tert*-butoxycarbonyl group of [9] (483 mg, 1.2 mmol) was fully removed in 3 h to give the corresponding TFA salt,  $\text{TFA} \cdot \text{H}_2\text{N-GABA-(1*R*,2*R*)-ACBC-OBn}$ .

According to the general procedure **D**, the coupling reaction was performed with Boc-GABA-OH (258 mg, 1.2 mmol), DIPEA (415  $\mu\text{L}$ , 309 mg, 2.4 mmol) and HATU (473 mg, 1.3 mmol) in a mixture of  $\text{CH}_2\text{Cl}_2$  / DMF (2 mL / 0.5 mL), and  $\text{TFA} \cdot \text{H}_2\text{N-GABA-(1*R*,2*R*)-ACBC-OBn}$ , DIPEA (1.252 mL, 929 mg, 7.2 mmol) in  $\text{CH}_2\text{Cl}_2$  (4 mL) overnight. The purification was carried out by flash chromatography (gradient from 10 / 90 to 100 / 0 : EtOAc / PE) to give [20] as a white sticky solid (435 mg, 76%).

$R_f$  0.57 (EtOAc = 100)

**Mp:** 85 °C

$[\alpha]_D^{23} = -15$  (c. 0.50 in  $\text{CHCl}_3$ )

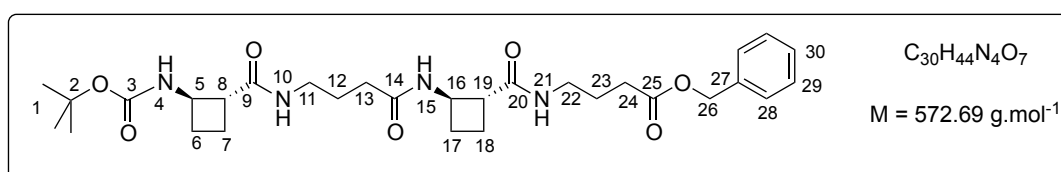
$^1\text{H NMR}$  (400 MHz,  $\text{CDCl}_3$ )  $\delta$  1.43 (s, 9H, 9H-1), 1.71-1.82 (m, 2H, 2H-6), 1.86-1.98 (m, 4H, H-11, H-12, 2H-17), 2.11-2.16 (m, 2H, H-11', H-12'), 2.23 (t, 2H,  $J = 6.5 \text{ Hz}$ , 2H-7), 2.44 (t, 1H,  $J = 7.5 \text{ Hz}$ , 2H-18), 2.94-3.01 (m, 1H, H-13), 3.12 (bs, 2H, 2H-5), 3.29 (dt, 2H,  $J = 6.3 \text{ Hz}$ ,  $J = 6.5 \text{ Hz}$ , H-16), 4.24-4.31 (m, 1H, H-10), 5.03 (bs, 1H, H-4), 5.11 (s, 2H, 2H-20), 7.34 (m, 5H, 2H-22, 2H-23, H-24), 7.59 (bs, 1H, H-9), 8.81 (bs, 1H, H-15).

**$^{13}\text{C}$  NMR** (100 MHz,  $\text{CDCl}_3$ )  $\delta$  18.9, 23.7 (C-11, C-12), 24.3 (C-17), 26.2 (C-6), 28.2 (C-1), 31.5 (C-18), 32.7 (C-7), 38.7 (C-16), 39.2 (C-5), 47.8 (C-10), 49.1 (C-13), 66.1 (C-20), 79.4 (C-2), 128.0, 128.1, 128.4 (C-22, C-23, C-24), 135.7 (C-21), 156.6 (C-3), 172.9 (C-8), 173.9 (C-14), 174.2 (C-19).

**IR** (10 mmol/L, in  $\text{CDCl}_3$ )  $\nu_{\text{max}}$  1514, 1565, 1647, 1697, 1729, 2980, 3280 (br), 3452  $\text{cm}^{-1}$ .

**HRMS (ESI):**  $[\text{M}+\text{Na}]^+$ , theor. 498.2575 (calc. for  $\text{C}_{25}\text{H}_{37}\text{N}_3\text{NaO}_6$ ), meas. 498.2581.

**Boc-[(1*R*,2*R*)-ACBC-GABA]<sub>2</sub>-OBn (-) - [10]**



According to the general procedure **C**, *tert*-butoxycarbonyl group of [20] (435 mg, 0.9 mmol) was fully removed in 2 h to give the corresponding TFA salt,  $\text{TFA} \cdot \text{H}_2\text{N-GABA-(1*R*,2*R*)-ACBC-GABA-OBn}$ .

According to the general procedure **D**, the coupling reaction was performed with Boc-(1*R*,2*R*)-ACBC-OH (194 mg, 0.9 mmol), DIPEA (310  $\mu\text{L}$ , 232 mg, 1.8 mmol) and HATU (356 mg, 1 mmol) in a mixture of  $\text{CH}_2\text{Cl}_2$  / DMF (1.5 mL / 0.5 mL), and  $\text{TFA} \cdot \text{H}_2\text{N-GABA-(1*R*,2*R*)-ACBC-OBn}$ , DIPEA (940  $\mu\text{L}$ , 697 mg, 5.4 mmol) in  $\text{CH}_2\text{Cl}_2$  (4 mL) overnight. The purification was carried out by flash chromatography (gradient from 10 / 90 to 100 / 0 : EtOAc / PE then from 0 / 100 to 10 / 90 :  $\text{CH}_3\text{OH}$  /  $\text{CH}_2\text{Cl}_2$ ) to give [10] as a white sticky solid (300 mg, 58%).

$R_f$  0.60 ( $\text{CH}_3\text{OH}$  /  $\text{CH}_2\text{Cl}_2$  = 10 / 90)

**Mp:** 197  $^\circ\text{C}$

$[\alpha]_D^{22} = -19$  (c. 0.50 in  $\text{CHCl}_3$ )

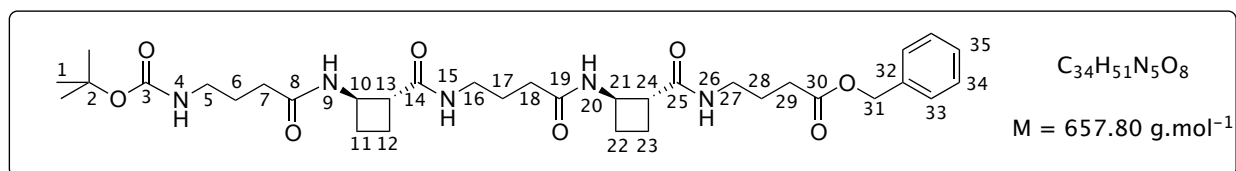
**$^1\text{H}$  NMR** (600 MHz,  $\text{CDCl}_3$ )  $\delta$  1.44 (s, 9H, 9H-1), 1.69-1.70 (m, 1H, H-12), 1.83-1.95 (m, 4H, H-6, H-12', 2H-23), 1.98-2.06 (m, 5H, 2H-7, H-17, 2H-18), 2.16-2.22 (m, 4H, H-6', 2H-13, H-17'), 2.46 (t, 2H,  $J = 7.5$  Hz, 2H-24), 2.84-2.87 (m, 1H, H-8), 3.00-3.05 (m, 1H, H-19), 3.11-3.14 (bs, 1H, H-11), 3.29-3.32 (m, 2H, 2H-22), 3.43-3.45 (bs, 1H, H-11'), 4.21-4.24 (m, 1H, H-5), 4.35-4.37 (m, 1H, H-16), 5.11 (s, 2H, 2H-26), 5.58 (d, 1H,  $J = 7.3$  Hz, H-4), 7.32-7.35 (m, 5H, 2H-28, 2H-29, H-30), 7.57 (bs, 1H, H-10), 7.91 (d, 1H,  $J = 6.7$  Hz, H-15), 8.63 (t, 1H,  $J = 5.2$  Hz, H-21).

**$^{13}\text{C}$  NMR** (90 MHz,  $\text{CDCl}_3$ )  $\delta$  18.2, 18.3 (C-7, C-18), 24.4 (C-17), 24.8 (C-23), 25.1 (C-6), 26.2 (C-12), 28.3 (C-1), 29.7, 31.8 (C-24), 32.3 (C-13), 37.2 (C-11), 38.5 (C-22), 48.1 (C-16), 48.9 (C-5), 49.6 (C-19), 50.2 (C-8), 66.1 (C-26), 80.4 (C-2), 128.1, 128.5 (C-28, C-29, C-30), 136.0 (C-27), 156.1 (C-3), 173.3, 173.1 (C-14, C-20), 173.4 (C-25), 173.7 (C-9).

**IR** (10 mmol/L, in  $\text{CDCl}_3$ )  $\nu_{\text{max}}$  1469, 1499, 1560, 1600, 1647, 1692, 1704, 1717, 1731, 1793, 1812, 2982, 3280 (br), 3349, 3444  $\text{cm}^{-1}$ .

**HRMS (ESI):**  $[\text{M}+\text{Na}]^+$ , theor. 595.3102 (calc. for  $\text{C}_{30}\text{H}_{44}\text{N}_4\text{NaO}_7$ ), meas. 595.3100.

**Boc-GABA-[(1*R*,2*R*)-ACBC-GABA]<sub>2</sub>-OBn (-) - [21]**



According to the general procedure **C**, *tert*-butoxycarbonyl group of [10] (220 mg, 0.38 mmol) was fully removed in 3 h to give the corresponding TFA salt,  $\text{TFA}\cdot\text{H}_2\text{N}-(1R,2R)\text{-ACBC-GABA-(1R,2R)-ACBC-GABA-OBn}$ .

According to the general procedure **D**, the coupling reaction was performed with Boc-GABA-OH (82 mg, 0.38 mmol), DIPEA (132  $\mu\text{L}$ , 98 mg, 0.76 mmol) and HATU (150 mg, 0.40 mmol) in a mixture of  $\text{CH}_2\text{Cl}_2$  / DMF (0.5 mL / 1 mL); and  $\text{TFA}\cdot\text{H}_2\text{N}-(1R,2R)\text{-ACBC-GABA-(1R,2R)-ACBC-GABA-OBn}$ , DIPEA (395  $\mu\text{L}$ , 294 mg, 2.28 mmol) in  $\text{CH}_2\text{Cl}_2$  (3 mL) overnight. The purification was carried out by flash chromatography (gradient from 10 / 90 to 100 / 0 : EtOAc / PE then from 0 / 100 to 20 / 80 :  $\text{CH}_3\text{OH}$  /  $\text{CH}_2\text{Cl}_2$ ) to give [21] as a white sticky solid (163 mg, 65%).

**$R_f$**  0.53 ( $\text{CH}_3\text{OH}$  /  $\text{CH}_2\text{Cl}_2$  = 10 / 90)

**Mp:** 185  $^\circ\text{C}$

**$[\alpha]_D^{23}$**  = - 23 (c. 0.50 in  $\text{CH}_3\text{OH}$ )

**$^1\text{H}$  NMR** (600 MHz,  $\text{CDCl}_3$ )  $\delta$  1.45 (s, 9H, 9H-1), 1.73-1.82 (m, 4H, 2H-6, 2H-17), 1.82-2.03 (m, 6H, 2H-28, H-11, H-12, H-22, H-23), 2.08-2.29 (m, 8H, 2H-7, H-11', H-12', 2H-18, H-22', H-23'), 2.91-2.96 (m,



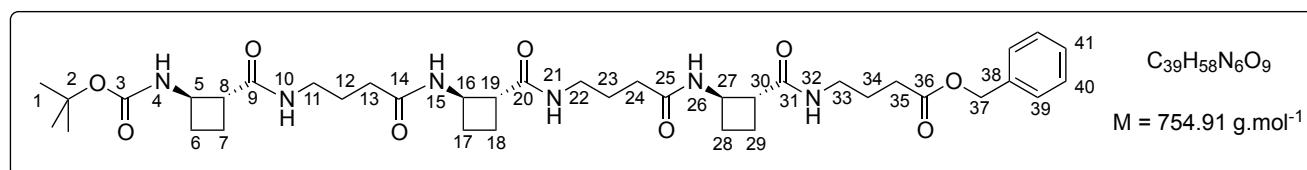
2H, H-13, H-24), 3.13-3.23 (m, 3H, 2H-5, H-16), 3.23-3.36 (m, 3H, H-16', 2H-27), 4.27-4.33 (m, 1H, H-21), 4.33-4.38 (m, 1H, H-10), 4.85 (m, 1H, H-4), 5.10 (s, 2H, 2H-31), 7.26-7.35 (m, 5H, 2H-33, 2H-34, H-35), 7.50 (m, 1H, H-9), 8.08 (m, 1H, H-20), 8.30 (m, 1H, H-15), 8.64 (m, 1H, H-26).

$^{13}\text{C}$  NMR (100 MHz,  $\text{CDCl}_3$ )  $\delta$  18.6, 18.7, 24.1, 24.2, 24.8 (C-11, C-12, C-22, C-23, C-28), 26.3, 26.7 (C-6, C-17), 28.4 (C-1), 31.8 (C-29), 32.8, 32.9 (C-18, C-7), 37.3, 39.1 (C-5, C-16), 38.6 (C-27), 48.1, 48.3 (C-10, C-21), 49.8, 49.9 (C-13, C-24), 66.2 (C-31), 79.9 (C-2), 128.2, 128.5 (C-32, C-33, C-34), 140.2 (C-31), 157.0 (C-3), 173.1 (C-30), 173.5, 173.7, (C-14, C-25), 173.9, 173.9 (C-8, C-19).

IR (10 mmol/L, in  $\text{CDCl}_3$ )  $\nu_{\text{max}}$  1447, 1515, 1567, 1647, 1695, 1731, 2879, 2939, 2980, 3073, 3278 (br), 3442  $\text{cm}^{-1}$ .

HRMS (ESI):  $[\text{M}+\text{Na}]^+$ , theor. 680.3630 (calc. for  $\text{C}_{34}\text{H}_{51}\text{N}_5\text{NaO}_8$ ), meas. 680.3625.

#### Boc-[(1*R*,2*R*)-ACBC-GABA]<sub>3</sub>-OBn (-) - [11]



According to the general procedure **C**, *tert*-butoxycarbonyl group of [21] (126 mg, 0.19 mmol) was fully removed in 3 h to give the corresponding TFA salt,  $\text{TFA} \cdot \text{H}_2\text{N-GABA-(1R,2R)-ACBC-GABA-(1R,2R)-ACBC-GABA-OBn}$ .

According to the general procedure **D**, the coupling reaction was performed with Boc-(1*R*,2*R*)-ACBC-OH (41 mg, 0.19 mmol), DIPEA (65  $\mu\text{L}$ , 49 mg, 0.38 mmol) and HATU (75 mg, 0.20 mmol) in a mixture of  $\text{CH}_2\text{Cl}_2$  / DMF (0.5 mL / 1 mL), and  $\text{TFA} \cdot \text{H}_2\text{N-GABA-(1R,2R)-ACBC-GABA-(1R,2R)-ACBC-GABA-OBn}$ , DIPEA (200  $\mu\text{L}$ , 147 mg, 1.14 mmol) in DMF (4 mL) overnight. The purification was carried out by flash chromatography (gradient from 10 / 90 to 100 / 0 : EtOAc / PE then from 0 / 100 to 20 / 80 :  $\text{CH}_3\text{OH}$  /  $\text{CH}_2\text{Cl}_2$ ) to give [11] as a white solid (104 mg, 75%).

$R_f$  0.51 ( $\text{CH}_3\text{OH}$  /  $\text{CH}_2\text{Cl}_2$  = 10/90)

**Mp**: 246  $^\circ\text{C}$

$[\alpha]_D^{23} = -16$  (c. 0.50 in  $\text{CH}_3\text{OH}$ )

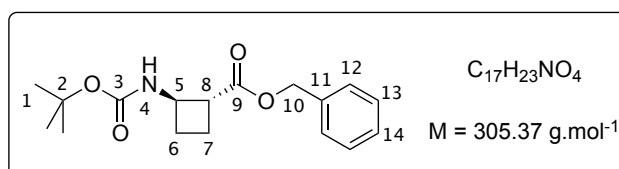
**<sup>1</sup>H NMR** (600 MHz, CDCl<sub>3</sub>) δ 1.47 (s, 9H, 9H-1), 1.65-1.71 (m, 4H, 2H-12, 2H-23), 1.78-1.88 (m, 4H, 2H-6, 2H-34), 1.91-2.04 (m, 8H, 2H-7, H-13, H-17, H-18, H-24, H-28, H-29), 2.08-2.29 (m, 7H, H-6', H-13', H-17', H-18', H-24', H-28', H-29'), 2.48 (t, 2H, J = 7.5 Hz, 2H-35), 2.76-2.80 (m, 1H, H-8), 2.96-3.04 (m, 2H, H-19, H-30), 3.07-3.11 (m, 2H, H-11, H-22), 3.28-3.36 (m, 2H, 2H-33), 3.55-3.59 (m, 2H, H-11', H-22'), 4.25-4.28 (m, 1H, H-5), 4.32-4.34 (m, 1H, H-27), 4.45-4.48 (m, 1H, H-16), 5.12 (d, 1H, J = 7.3 Hz, H-4), 5.13 (s, 2H, H-37), 6.81-6.83 (m, 1H, H-10), 7.33-7.38 (m, 5H, 2H-39, 2H-40, H-41), 8.02 (d, 1H, J = 7.7 Hz, H-15), 8.13 (t, 1H, J = 5.1 Hz, H-21), 8.24 (d, 1H, J = 6.9 Hz, H-26), 8.67 (t, 1H, J = 5.4 Hz, H-32).

**<sup>13</sup>C NMR** (100 MHz, CDCl<sub>3</sub>) δ 17.1, 18.1, 18.3 (C-7, C-18, C-29), 24.0, 24.8, 25.4, 25.5, 26.3, 32.6 (C-6, C-12, C-13, C-17, C-23, C-24, C-28, C-34), 28.3 (C-1), 31.2 (C-35), 36.6, 37.1 (C-11, C-22), 38.5 (C-33), 48.1 (C-16, C-27), 48.9 (C-5), 49.8 (C-19, C-30), 50.5 (C-8), 66.0 (C-37), 80.5 (C-2), 128.0, 128.0, 128.4 (C-39, C-40, C-41), 136.3 (C-38), 155.7 (C-3), 172.5, 173.3, 173.4, 173.9 (C-9, C-14, C-20, C-25, C-31, C-36)

**IR** (10 mmol/L, in CDCl<sub>3</sub>)  $\nu_{\max}$  1443, 1453, 1501, 1560, 1648, 1698, 1730, 2879, 2943, 2981, 3072, 3286, 3329 (br), 3443 cm<sup>-1</sup>.

**HRMS (ESI):** [M+Na]<sup>+</sup>, theor. 777.4157 (calc. for C<sub>39</sub>H<sub>58</sub>N<sub>6</sub>NaO<sub>9</sub>), meas. 777.4115.

#### Boc-(1*R*,2*R*)-ACBC-OBn (-) - [22]



To a solution of Boc-(1*R*,2*R*)-ACBC [2] (800 mg, 3.72 mmol, 1 eq.) in anhydrous DMF (12 mL) were added Cs<sub>2</sub>CO<sub>3</sub> (7.231 g, 22.32 mmol, 6 eq.) followed by BnBr (665 μL, 954 mg, 5.58 mmol, 1.5 eq.) under argon atmosphere. The resulting white suspension was stirred overnight at room temperature. Water (10 mL) and EtOAc (20 mL) were added to the reaction mixture. The organic layer was separated, dried over Na<sub>2</sub>SO<sub>4</sub>, filtered and concentrated under reduced pressure. The crude product was purified by flash chromatography (gradient from 0 / 100 to 30 / 70 : EtOAc / PE) to give Boc-(1*R*,2*R*)-ACBC-OBn [22] as a white solid (850 mg, 75%).

*R<sub>f</sub>* 0.8 (EtOAc / PE = 30 / 70)

**Mp:** 100 °C

$[\alpha]_D^{23} = -36$  (c. 0.50 in CHCl<sub>3</sub>)

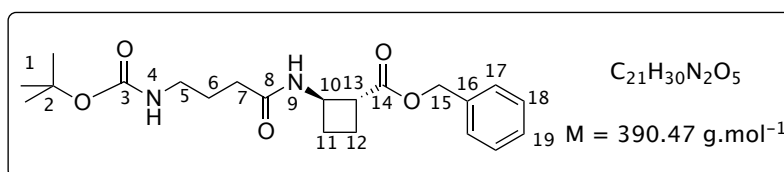
**<sup>1</sup>H NMR** (400 MHz, CDCl<sub>3</sub>)  $\delta$  1.4 (s, 9H, 9H-1), 1.94-2.00 (m, 3H, H-6, 2H-7), 2.26-2.28 (m, 1H, H-6'), 3.06 (bs, 1H, H-8), 4.30 (bs, 1H, H-5), 4.88 (bs, 1H, H-4), 5.15 (s, 2H, 2H-10), 7.36-7.37 (m, 5H, 2H-12, 2H-13, H-14).

**<sup>13</sup>C NMR** (100 MHz, CDCl<sub>3</sub>)  $\delta$  18.1 (C-7), 27.4 (C-6), 28.4 (C-1), 47.1 (C-8), 48.9 (C-5), 66.3 (C-10), 79.5 (C-2), 128.1, 128.1, 128.5 (C-12, C-13, C-14), 136.0 (C-11), 154.6 (C-3), 172.8 (C-9).

**IR** (10 mmol/L, in CDCl<sub>3</sub>)  $\nu_{\max}$  1456, 1504, 1713, 1725, 2871, 2932, 2982, 3003, 3446 cm<sup>-1</sup>.

**HRMS (ESI):** [M+Na]<sup>+</sup>, theor. 328.1519 (calc. for C<sub>17</sub>H<sub>23</sub>NaNO<sub>4</sub>), meas. 328.1521.

**Boc-GABA-(1*R*,2*R*)-ACBC-OBn (-) - [12]**



According to the general procedure **C**, *tert*-butoxycarbonyl group of [22] (160 mg, 0.52 mmol) was fully removed in 3 h to give the corresponding TFA salt, TFA·H<sub>2</sub>N-(1*R*,2*R*)-ACBC-OBn.

According to the general procedure **D**, the coupling reaction was performed with Boc-GABA-OH (112 mg, 0.52 mmol), DIPEA (180  $\mu$ L, 134 mg, 1.04 mmol) and HATU (206 mg, 0.55 mmol) in a mixture of CH<sub>2</sub>Cl<sub>2</sub> / DMF (2 mL / 0.5 mL); and TFA·H<sub>2</sub>N-(1*R*,2*R*)-ACBC-OBn, DIPEA (540  $\mu$ L, 402 mg, 3.12 mmol) in CH<sub>2</sub>Cl<sub>2</sub> (2 mL) overnight. The purification was carried out by flash chromatography (gradient from 10 / 90 to 50 / 50 : EtOAc / PE) to give [12] as a white sticky solid (155 mg, 76%).

**R<sub>f</sub>** 0.1 (EtOAc/ PE = 90 / 10)

**Mp:** 109 °C

$[\alpha]_D^{22} = -16$  (c. 0.50 in CHCl<sub>3</sub>)

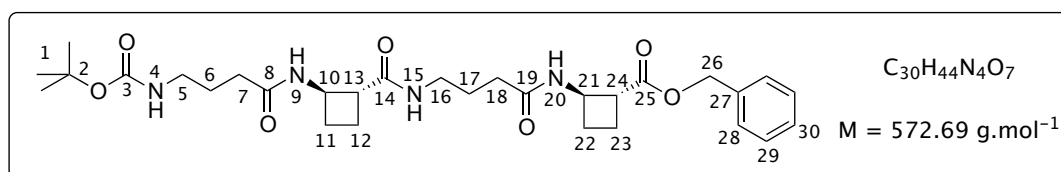
**<sup>1</sup>H NMR** (360 MHz, CDCl<sub>3</sub>) δ 1.45 (s, 9H, 9H-1), 1.71-1.80 (m, 2H, 2H-6), 1.93-2.05 (m, 3H, H-11, 2H-12), 2.15-2.31 (m, 3H, 2H-7, H-11'), 3.02-3.18 (m, 3H, 2H-5, H-13), 4.50-4.63 (m, 1H, H-10), 4.72-4.90 (m, 1H, H-4), 5.13 (s, 2H, 2H-15), 6.93 (bs, 1H, H-9), 7.29-7.37 (m, 5H, 2H-17, 2H-18, H-19)

**<sup>13</sup>C NMR** (90 MHz, CDCl<sub>3</sub>) δ 18.6 (C-12), 26.3 (C-6), 27.0 (C-11), 28.4 (C-1), 33.2 (C-7), 39.5 (C-5), 46.7 (C-13), 47.4 (C-10), 66.4 (C-15), 79.5 (C-2), 128.1, 128.1, 128.5 (C-17, C-18, C-19), 136.0 (C-16), 156.7 (C-3), 172.1 (C8), 172.8 (C-14)

**IR** (10 mmol/L, in CDCl<sub>3</sub>)  $\nu_{\max}$  1455, 1512, 1670, 1699, 1723, 2871, 2934, 2981, 3312 (br), 3451 cm<sup>-1</sup>

**HRMS (ESI):** [M+Na]<sup>+</sup>, theor. 413.2047 (calc. for C<sub>21</sub>H<sub>30</sub>N<sub>2</sub>NaO<sub>5</sub>), meas. 413.2032.

### Boc-[GABA-(1*R*,2*R*)-ACBC]<sub>2</sub>-OBn (-) - [13]



According to the general procedure **A**, benzyl ester of [12] (75 mg, 0.19 mmol) was hydrolysed in 2 h to give the corresponding carboxylic acid, Boc-GABA-(1*R*,2*R*)-ACBC-OH (57 mg, 100% crude yield).

According to the general procedure **C**, *tert*-butoxycarbonyl group of [12] (75 mg, 0.19 mmol) was fully removed in 2 h to give the corresponding TFA salt, TFA·H<sub>2</sub>N-GABA-(1*R*,2*R*)-ACBC-OBn.

According to the general procedure **D**, the coupling reaction was performed with Boc-GABA-(1*R*,2*R*)-ACBC-OH (57 mg, 0.19 mmol), DIPEA (66 μL, 49 mg, 0.38 mmol) and HATU (206 mg, 0.55 mmol) in a mixture of CH<sub>2</sub>Cl<sub>2</sub> / DMF (1 mL / 0.5 mL), and TFA·H<sub>2</sub>N-GABA-(1*R*,2*R*)-ACBC-OBn, DIPEA (198 μL, 147 mg, 1.14 mmol) in CH<sub>2</sub>Cl<sub>2</sub> (2 mL) overnight. The purification was carried out by flash chromatography (gradient from 10 / 90 to 100 / 0 : EtOAc / PE) to give [13] as a white solid (65 mg, 58%).

**R<sub>f</sub>** 0.45 (CH<sub>3</sub>OH / CH<sub>2</sub>Cl<sub>2</sub> = 10 / 90)

**Mp:** 141 °C

**[α]<sub>D</sub><sup>16</sup>** = - 32 (c. 0.50 in CHCl<sub>3</sub>)

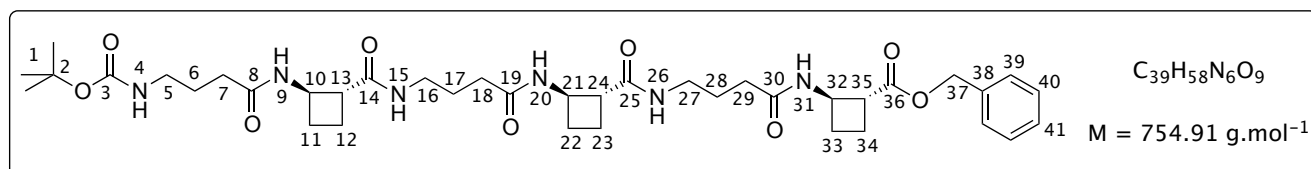
**<sup>1</sup>H NMR** (600 MHz, CDCl<sub>3</sub>) δ 1.42 (s, 9H, 9H-1), 1.73-1.79 (m, 5H, 2H-6, 2H-17, H-23), 1.93-2.00 (m, 4H, H-11, H-12, H-22, H-23'), 2.07-2.24 (m, 7H, 2H-7, H-11', H-12', 2H-18, H-22'), 2.89-2.94 (m, 1H, H-13), 3.11-3.14 (m, 4H, 2H-5, H-16, H-24), 3.19-3.24 (m, 1H, H-16'), 4.27-4.32 (m, 1H, H-10), 4.53-4.58 (m, 1H, H-21), 5.07-5.11 (m, 3H, H-4, 2H-26), 7.28-7.32 (m, 5H, 2H-28, 2H-29, H-30), 7.65 (d, *J* = 6.3 Hz, 1H, H-9), 7.81 (d, *J* = 8.1 Hz, 1H, H-20), 8.36 (t, *J* = 5.6 Hz, 1H, H-15).

**<sup>13</sup>C NMR** (90 MHz, CDCl<sub>3</sub>) δ 18.5, 18.7 (C-11, C-12), 24.1 (C-22), 26.2, 26.5, 26.9 (C-6, C-17, C-23), 28.4 (C-1), 33.0, 33.2 (C-7, C-18), 37.5 (C-16), 39.3 (C-5), 46.6 (C-21), 47.4 (C-24), 48.1 (C-10), 49.7 (C-13), 66.3 (C-26), 79.6 (C-2), 128.0, 128.1, 128.5 (C-28, C-29, C-30), 136.0 (C-27), 156.8 (C-3), 172.4, 173.1, 173.6 (C-8, C-14, C-19), 174.1 (C-25).

**IR** (10 mmol/L, in CDCl<sub>3</sub>)  $\nu_{\max}$  1470, 1515, 1560, 1603, 1646, 1695, 2902, 2984, 3072, 3155, 3283 (br), 3451 cm<sup>-1</sup>.

**HRMS (ESI):** [M+Na]<sup>+</sup>, theor. 595.3102 (calc. for C<sub>30</sub>H<sub>44</sub>N<sub>4</sub>NaO<sub>7</sub>), meas. 595.3081.

#### Boc-[GABA-(1*R*,2*R*)-ACBC]<sub>3</sub>-OBn (-) - [14]



According to the general procedure **A**, benzyl ester of [12] (60 mg, 0.15 mmol) was hydrolysed in 2 h to give the corresponding carboxylic acid, Boc-GABA-(1*R*,2*R*)-ACBC-OH (36 mg, 80% crude yield).

According to the general procedure **C**, *tert*-butoxycarbonyl group of [13] (60 mg, 0.10 mmol) was fully removed in 3 h to give the corresponding TFA salt, TFA·H<sub>2</sub>N-GABA-(1*R*,2*R*)-ACBC-GABA-(1*R*,2*R*)-ACBC-OBn.

According to the general procedure **D**, the coupling reaction was performed with Boc-GABA-(1*R*,2*R*)-ACBC-OH (36 mg, 0.12 mmol), DIPEA (40 μL, 31 mg, 0.24 mmol) and HATU (47 mg, 0.13 mmol) in a mixture of CH<sub>2</sub>Cl<sub>2</sub> / DMF (1 mL / 0.5 mL); and TFA·H<sub>2</sub>N-GABA-(1*R*,2*R*)-ACBC-GABA-(1*R*,2*R*)-ACBC-OBn, DIPEA (200 μL, 147 mg, 1.14 mmol) in CH<sub>2</sub>Cl<sub>2</sub> (2 mL) overnight. The purification was carried out by flash chromatography (gradient from 10 / 90 to 100 / 0 : EtOAc / PE then from 0 / 100 to 20 / 80 : CH<sub>3</sub>OH / CH<sub>2</sub>Cl<sub>2</sub>) to give [14] as a white solid (42 mg, 56%).

**R<sub>f</sub>** 0.5 (CH<sub>3</sub>OH / CH<sub>2</sub>Cl<sub>2</sub> = 10 / 90)

**Mp:** 215 °C

$[\alpha]_D^{21} = -25$  (c. 0.50 in CH<sub>3</sub>OH)

**<sup>1</sup>H NMR** (600 MHz, CDCl<sub>3</sub>)  $\delta$  1.47 (s, 9H, 9H-1), 1.76-1.92 (m, 7H, 2H-6, 2H-17, 2H-28, H-34), 1.92-2.03 (m, 6H, H-11, H-12, H-22, H-23, H-33, H-34'), 2.05-2.17 (m, 3H, H-12', H-22', H-23'), 2.19-2.27 (m, 8H, 2H-7, H-11', 2H-18, 2H-29, H-33'), 2.91-3.00 (m, 2H, H-13, H-24), 3.13-3.23 (m, 5H, 2H-5, H-16, H-27, H-35), 3.28 (bs, 1H, H-27'), 3.42 (bs, 1H, H-16'), 4.32-4.41 (m, 2H, H-10, H-21), 4.57-4.63 (m, 1H, H-32), 4.81 (bs, 1H, H-4), 5.13 (s, 2H, 2H-37), 7.31-7.36 (m, 5H, 2H-39, 2H-40, H-41), 7.92 (bs, 1H, H-31), 8.11 (bs, 1H, H-15), 8.25 (bs, 1H, H-20), 8.51 (bs, 1H, H-26).

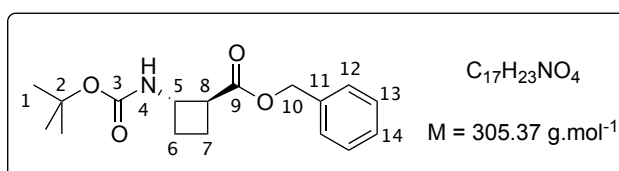
**<sup>13</sup>C NMR** (100 MHz, CDCl<sub>3</sub> / CD<sub>3</sub>OD : 1 / 1)  $\delta$  18.2, 18.3 (C-12, C-23), 24.0 (C-22), 25.5, 25.8, 25.8, 26.1 (C-6, C-17, C-28, C-34), 26.6 (C-11, C-33), 28.2 (C-1), 32.5, 32.8, 33.1 (C-7, C-18, C-29), 37.5 (C-16), 37.7 (C-27), 39.3 (C-5), 46.4 (C-35), 47.2 (C-32), 47.8 (C-10, C-21), 49.4 (C-24), 49.5 (C-13), 66.3 (C-37), 79.6 (C-2), 128.0, 128.0, 128.4 (C-39, C-40, C-41), 135.8 (C-38), 156.9 (C-3), 172.9, 173.1, 173.1, 174.1 (C-8, C-14, C-19, C-25, C-30, C-36).

**IR** (10 mmol/L, in CDCl<sub>3</sub>)  $\nu_{\max}$  1443, 1456, 1517, 1551, 1646, 1692, 1725, 2870, 2940, 2980, 3038, 3083, 3283 (br), 3442 cm<sup>-1</sup>.

**HRMS (ESI):** [M+Na]<sup>+</sup>, theor. 777.4163 (calc. for C<sub>39</sub>H<sub>58</sub>N<sub>6</sub>NaO<sub>9</sub>), meas. 777.4189.

## 2.2 Peptides alternating (1S,2S)-ACBC and (R)- $\gamma^4$ -homologous amino acids

### Boc-(1S,2S)-ACBC-OBn (+) – [22]

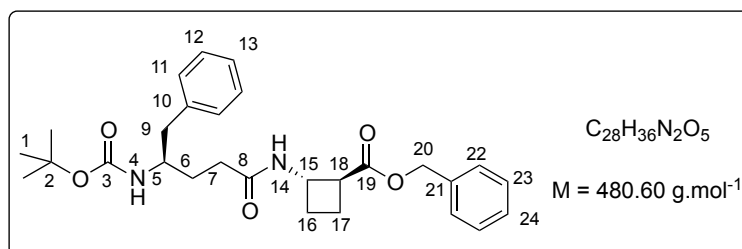


The enantiomer of [22] was prepared from [2], following the above-described sequences with comparable yields.

$[\alpha]_D^{24} = +34$  (c. 0.50 in CHCl<sub>3</sub>)

Data were identical to those described for (-)-[22].

**Boc-(*R*)- $\gamma^4$ -hPhe-(1*S*,2*S*)-ACBC-OBn (-) - [35]**



According to the general procedure **C**, *tert*-butoxycarbonyl group of Boc-(1*S*,2*S*)-ACBC-OBn [22] (252 mg, 1.17 mmol) was fully removed in 1.3 h to give the corresponding TFA salt, TFA·H<sub>2</sub>N-(1*S*,2*S*)-ACBC-OBn.

According to the general procedure **D**, the coupling reaction was performed with Boc-(*R*)- $\gamma^4$ -hPhe-OH (342 mg, 1.17 mmol), DIPEA (400  $\mu$ L, 302 mg, 2.34 mol) and HATU (461 mg, 1.23 mmol) in a mixture of CH<sub>2</sub>Cl<sub>2</sub> / DMF (5 mL / 2 mL), and TFA·H<sub>2</sub>N-(1*S*,2*S*)-ACBC-OBn, DIPEA (1.195 mL, 906 mg, 7.02 mmol) in CH<sub>2</sub>Cl<sub>2</sub> (2 mL) for 3 d. The purification was carried out by flash chromatography (gradient from 10 / 90 to 80 / 20 : EtOAc / PE) to give [35] as a white sticky solid (242 mg, 43%).

**R<sub>f</sub>** 0.15 (EtOAc / PE = 30 / 70)

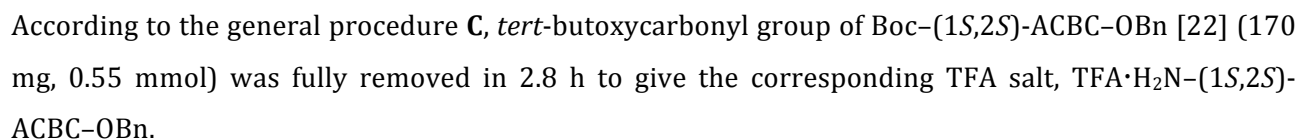
**[ $\alpha$ ]<sub>D</sub><sup>26</sup>** = - 115 (c. 0.10 in CHCl<sub>3</sub>)

**<sup>1</sup>H NMR** (360 MHz, CDCl<sub>3</sub>)  $\delta$  1.39 (s, 9H, 9H-1), 1.56-1.65 (m, 1H, H-6), 1.70-1.82 (m, 1H, H-6'), 1.95-1.99 (m, 3H, H-16, 2H-17), 2.15-2.20 (m, 3H, 2H-7, H-16'), 2.65 (m, 2H, 2H-9), 3.13-3.15 (m, 1H, H-18), 3.81 (m, 1H, H-5), 4.55-4.57 (m, 1H, H-15), 4.79 (d, 1H, J = 7.5 Hz, H-4), 5.11 (s, 2H, 2H-20), 7.15 (m, 1H, H-14), 7.12-7.32 (10H, m, 2H-11, 2H-12, H-13, 2H-22, 2H-23, H-24).

**<sup>13</sup>C NMR** (90 MHz, CDCl<sub>3</sub>)  $\delta$  18.5 (C-6), 26.9 (C-7), 28.3 (C-1), 30.8 (C-17), 33.2 (C-16), 41.6 (C-9), 46.7 (C-18), 47.5 (C-15), 51.3 (C-5), 66.3 (C-20), 79.3 (C-2), 126.4-129.3 (C-11, C-12, C-13, C-22, C-23, C-24), 136.0 (C-10), 137.9 (C-21), 156.3 (C-3), 172.4 (C-8), 173.0 (C-19).

**IR** (10 mmol/L, in CDCl<sub>3</sub>)  $\nu_{\max}$  1454, 1505, 1603, 1670, 1697, 1725, 2870, 2981, 3031, 3066, 3087, 3302 (br), 3436 cm<sup>-1</sup>.

**HRMS (ESI):** [M+Na]<sup>+</sup>, 503.2536 found, C<sub>28</sub>H<sub>36</sub>N<sub>2</sub>NaO<sub>5</sub> 503.2516 calcd.



According to the general procedure **D**, the coupling reaction was performed with Boc-(*R*)- $\gamma^4$ -*h*Leu-OH (161 mg, 0.62 mmol), DIPEA (185  $\mu$ L, 1.10 mol) and HATU (217 mg, 0.58 mmol) in a mixture of CH<sub>2</sub>Cl<sub>2</sub> / DMF (3 mL / 1 mL), and TFA·H<sub>2</sub>N-(1*S*,2*S*)-ACBC-OBn, DIPEA (560  $\mu$ L, 426 mg, 3.30 mmol) in CH<sub>2</sub>Cl<sub>2</sub> (2 mL) for 3 d. The purification was carried out by flash chromatography (gradient from 10 / 90 to 80 / 20 : EtOAc / PE) to give **[36]** as a white sticky solid (204 mg, 86%).

**$R_f$  0.20 (EtOAc / PE = 30 / 70)**

$$[\mathbf{a}]_D^{21} = +16 \text{ (c. 0.35 in CHCl}_3\text{)}, [\mathbf{a}]_D^{22} = +24 \text{ (c. 0.35 in CH}_3\text{OH)}$$

**<sup>1</sup>H NMR** (400 MHz, CDCl<sub>3</sub>) δ 0.80 (d, J = 6.9 Hz, 3H, 3H-11), 0.82 (d, J = 6.9 Hz, 3H, 3H-11'), 1.07 (m, 1H, H-9), 1.20 (m, 1H, H-9'), 1.43 (s, 9H, 9H-1), 1.56 (m, 3H, 2H-10, H-15), 1.69 (m, 1H, H-15'), 2.03 (m, 3H, 2H-6, H-7), 2.19 (m, 3H, H-7', 2H-14), 3.11 (m, 1H, H-16), 3.60 (m, 1H, H-5), 4.49 (d, J = 9.5 Hz, 1H, H-4), 4.56 (m, 1H, H-13), 5.09 (s, 2H, 2H-18), 7.31 (m, 5H, 2H-20, 2H-21, H-22), 7.41 (d, J = 7.9 Hz, 1H, H-12).

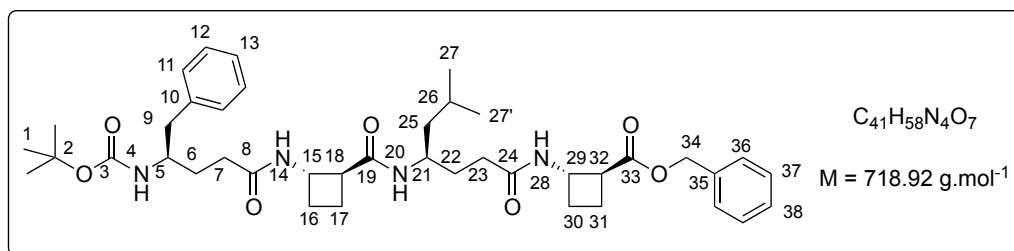
**<sup>13</sup>C NMR** (100 MHz, CDCl<sub>3</sub>) δ 18.5 (C-15), 21.8, 22.9 (C-11, C-11'), 24.8 (C-10), 26.5 (C-7), 28.4 (C-1), 32.7 (C-6), 32.9 (C-14), 44.7 (C-9), 46.9 (C-16), 47.1 (C-13), 48.2 (C-5), 66.4 (C-18), 79.5 (C-2), 128.1-128.4 (C-20, C-21, C-22), 135.8 (C-19), 156.8 (C-3), 172.9 (C-8), 173.5 (C-17).

**IR** (10 mmol/L, in CDCl<sub>3</sub>)  $\nu_{\text{max}}$  1457, 1468, 1507, 1664, 1693, 1726, 2871, 2960, 3154, 3300 (br), 3436 cm<sup>-1</sup>.

**HRMS (ESI):**  $[M+Na]^+$ , found 469.2714  $C_{25}H_{38}N_2NaO_5$ , 469.2673 calcd.

**Boc- $\gamma^4$ -*h*Phe-(1*S*,2*S*)-ACBC-(*R*)- $\gamma^4$ -*h*Leu-(1*S*,2*S*)-ACBC-OBn (+) - [23]**





According to the general procedure **A**, benzyl ester of [35] (245 mg, 0.51 mmol) was hydrolysed in 3.2 h to give the corresponding carboxylic acid, Boc-(*R*)- $\gamma^4$ -*h*Phe-(1*S*,2*S*)-ACBC-OH (175 mg, 88% crude yield).

According to the general procedure **C**, *tert*-butoxycarbonyl group of [36] (198 mg, 0.46 mmol) was fully removed in 2.4 h to give the corresponding TFA salt, TFA·H<sub>2</sub>N-(*R*)- $\gamma^4$ -*h*Leu-(1*S*,2*S*)-ACBC-OBn.

According to the general procedure **D**, the coupling reaction was performed with Boc-(*R*)- $\gamma^4$ -*h*Phe-(1*S*,2*S*)-ACBC-OH (245 mg, 0.45 mmol), DIPEA (155  $\mu$ L, 116 mg, 0.90 mmol) and HATU (176 mg, 0.47 mmol) in a mixture of CH<sub>2</sub>Cl<sub>2</sub> / DMF (2 mL / 1 mL); and TFA·H<sub>2</sub>N-(*R*)- $\gamma^4$ -*h*Leu-(1*S*,2*S*)-ACBC-OBn, DIPEA (1.350 mL, 859 mg, 4.5 mmol) in CH<sub>2</sub>Cl<sub>2</sub> (2 mL) overnight. The purification was carried out by flash chromatography (gradient from 10 / 90 to 100 / 0 : EtOAc / PE) to give [23] as a white sticky solid (225 mg, 71%).

*R<sub>f</sub>* 0.64 (EtOAc = 100)

$[\alpha]_D^{24} = +16$  (c. 0.50 in CH<sub>3</sub>OH)

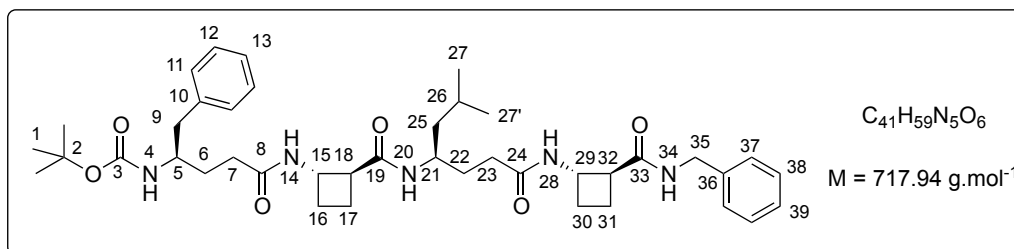
**<sup>1</sup>H NMR** (600 MHz, CDCl<sub>3</sub>)  $\delta$  0.76 (d, *J* = 6 Hz, 3H, 3H-27), 0.79 (d, *J* = 6 Hz, 3H, 3H-27'), 1.02-0.93 (m, 1H, H-26), 1.21-1.30 (m, 2H, 2H-25), 1.37-1.56 (m, 13H, 9H-1, 2H-6, 2H-22), 1.78-1.88 (m, 3H, H-16, 2H-23), 1.90-2.03 (m, 6H, 2H-7, H-17, H-30, 2H-31) 2.07-2.29 (m, 3H, H-16', H-17', H-30'), 2.64-2.69 (m, 1H, H-9), 2.76-2.89 (m, 2H, H-9', H-18), 3.17 (m, 1H, H-32), 3.8 (m, 1H, H-5), 3.9 (m, 1H, H-21), 4.41 (m, 1H, H-15), 4.52 (d, *J* = 7.7 Hz, 1H, H-4), 4.61 (m, 1H, H-29), 5.12 (s, 2H, 2H-34), 6.66 (d, *J* = 8.4 Hz, 1H, H-14), 7.11-7.37 (m, 10H, 2H-11, 2H-12, H-13, 2H-36, 2H-37, H-38), 7.52 (d, *J* = 8.4 Hz, 1H, H-20), 8.04 (d, *J* = 6.7 Hz, 1H, H-28).

**<sup>13</sup>C NMR** (100 MHz, CDCl<sub>3</sub>)  $\delta$  18.3 (C-6), 21.6, 22.6 (C-27, C27'), 24.8 (C-26), 25.3 (C-22), 26.5 (C-7), 28.2 (C-1), 30.7 (C-31), 32.5 (C-17), 33.3, 33.4 (C-16, C-30), 41.9 (C-9), 44.6 (C-25), 46.4 (C-21), 46.9 (C-32), 47.3 (C-29), 48.0 (C-15), 50.0 (C-5, C-18), 66.1 (C-34), 79.6 (C-2), 126.5, 127.8, 127.9, 128.3, 128.4, 129.1 (C-11, C-12, C-13, C-36, C-37, C-38), 135.1 (C-10), 135.9 (C-35), 156.1 (C-3), 172.5 (C-19), 172.7, 172.8 (C-8, C-24), 173.0 (C-33).

**IR** (10 mmol/L, in CDCl<sub>3</sub>)  $\nu_{\max}$  1507, 1545, 1658, 1700, 1725, 2870, 2958, 3031, 3067, 3279 (br), 3342 (br), 3434 cm<sup>-1</sup>.

**HRMS (ESI):** [M+Na]<sup>+</sup>, 741.4201 found, C<sub>41</sub>H<sub>58</sub>N<sub>4</sub>NaO<sub>7</sub> calcd 741.4203.

**Boc- $\gamma^4$ -hPhe-(1*S*,2*S*)-ACBC-(*R*)- $\gamma^4$ -hLeu-(1*S*,2*S*)-ACBC-NHBn (+) - [24]**



According to the general procedure **A**, benzyl ester of [23] (54 mg, 0.076 mmol) was hydrolysed in 3 h to give the corresponding carboxylic acid, Boc-(*R*)- $\gamma^4$ -hPhe-(1*S*,2*S*)-ACBC-(*R*)- $\gamma^4$ -hLeu-(1*S*,2*S*)-ACBC-OH (47 mg, 100% crude yield).

According to the general procedure **D**, the coupling reaction was performed with Boc-(*R*)- $\gamma^4$ -hPhe-(1*S*,2*S*)-ACBC-(*R*)- $\gamma^4$ -hLeu-(1*S*,2*S*)-ACBC-OH (47 mg, 0.076 mmol), DIPEA (25  $\mu$ L, 19 mg, 0.152 mmol) and HATU (30 mg, 0.079 mmol) in a mixture of CH<sub>2</sub>Cl<sub>2</sub> / DMF (1 mL / 0.5 mL), and benzylamine (12  $\mu$ L, 12 mg, 0.114 mmol), DIPEA (60  $\mu$ L, 44 mg, 0.342 mmol) for 3 d. The purification was carried out by flash chromatography (gradient from 10 / 90 to 100 / 0 : EtOAc / PE) to give [24] as a white sticky foam (35 mg, 64%).

**R<sub>f</sub>** 0.60 (EtOAc = 100)

**[ $\alpha$ ]<sub>D</sub><sup>24</sup>** = + 31 (c. 0.50 in CHCl<sub>3</sub>)

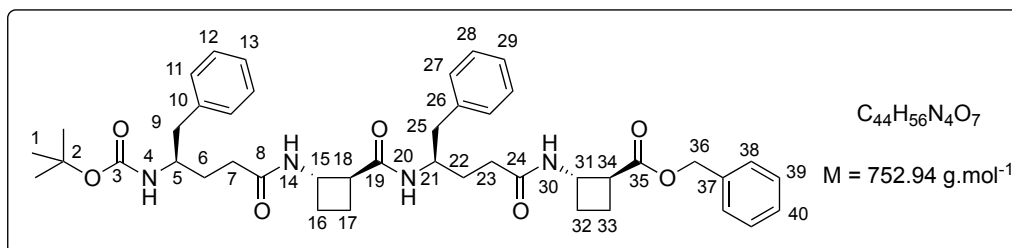
**<sup>1</sup>H NMR** (600 MHz, CDCl<sub>3</sub>)  $\delta$  0.77 (d, *J* = 6.2 Hz, 3H, 3H-27), 0.78 (d, *J* = 6.3 Hz, 3H, 3H-27'), 1.06-1.14 (m, 1H, H-25), 1.20-1.30 (m, 3H, 2H-22, H-25'), 1.36-1.44 (m, 12H, 9H-1, 2H-6, H-26), 1.85-2.19 (m, 10H, H-16, H-17, 2H-23, 2H-30, 2H-31, 2H-7), 2.20-2.25 (m, 2H, H-16', H-17'), 2.63-2.66 (m, 1H, H-9), 2.72-2.76 (m, 2H, H-9', H-18), 3.05-3.06 (m, 1H, H-32), 3.75-3.82 (m, 1H, H-5), 3.89-3.96 (m, 1H, H-21), 4.35-4.37 (m, 1H, H-29), 4.42-4.43 (m, 1H, H-15), 4.45-4.46 (m, 2H, 2H-35), 4.57 (d, *J* = 9.4 Hz, 1H, H-4), 6.7 (d, *J* = 7.0 Hz, 1H, 14H), 7.09-7.34 (m, 11H, 2H-11, 2H-12, H-13, H-20, 2H-37, 2H-38, H-39), 8.29 (d, *J* = 5.7 Hz, 1H, H-28), 9.04 (m, 1H, H-34).

**$^{13}\text{C}$  NMR** (100 MHz,  $\text{CDCl}_3$ )  $\delta$  16.9 (C-30), 18.4 (C-31), 22.1, 22.9 (C-27, C-27'), 24.4 (C-23), 24.9 (C-26), 25.7 (C-7), 28.4 (C-1), 29.1 (C-6), 29.7 (C-25), 30.6 (C-22), 32.5, 32.9 (C-16, C-17), 42.2 (C-9), 43.0 (C-35), 46.3 (C-21), 48.1, 48.2 (C-15, C-29), 49.7 (C-32), 50.0 (C-5), 50.2 (C-18), 79.8 (C-2), 126.7, 127.5, 128.4, 128.5, 129.3 (C-11, C-12, C-13, C-37, C-38, C-39), 137.2, 139.3 (C-10, C-36), 156.2 (C-3), 172.3, 172.5, 173.4 (C-8, C-19, C-24), 174.2 (C-33).

**IR** (10 mmol/L, in  $\text{CDCl}_3$ )  $\nu_{\text{max}}$  1442, 1455, 1467, 1509, 1548, 1648, 1699, 2870, 2930, 2959, 3031, 3067, 3281 (br), 3333 (br), 3434  $\text{cm}^{-1}$ .

**HRMS (ESI):**  $[\text{M}+\text{Na}]^+$ , 740.4361 found,  $\text{C}_{44}\text{H}_{59}\text{N}_5\text{NaO}_6$  calcd 740.4363.

**Boc- $\gamma^4$ -hPhe-(1*S*,2*S*)-ACBC-(*R*)- $\gamma^4$ -hPhe-(1*S*,2*S*)-ACBC-OBn (+) - [37]**



According to the general procedure **A**, benzyl ester of [35] (360 mg, 0.75 mmol) was hydrolysed in 2 h to give the corresponding carboxylic acid, Boc-(*R*)- $\gamma^4$ -hPhe-(1*S*,2*S*)-ACBC-OH (293 mg, 100% crude yield).

According to the general procedure **C**, *tert*-butoxycarbonyl group of [35] (335 mg, 0.69 mmol) was fully removed in 2 h to give the corresponding TFA salt,  $\text{TFA}\cdot\text{H}_2\text{N}-(\text{R})-\gamma^4\text{-hPhe}-(1\text{S},2\text{S})\text{-ACBC-OBn}$ .

According to the general procedure **D**, the coupling reaction was performed with Boc-(*R*)- $\gamma^4$ -hPhe-(1*S*,2*S*)-ACBC-OH (335 mg, 0.75 mmol), DIPEA (260  $\mu\text{L}$ , 193 mg, 1.5 mmol) and HATU (293 mg, 0.78 mmol) in a mixture of  $\text{CH}_2\text{Cl}_2$  / DMF (2 mL / 1 mL); and  $\text{TFA}\cdot\text{H}_2\text{N}-(\text{R})-\gamma^4\text{-hPhe}-(1\text{S},2\text{S})\text{-ACBC-OBn}$ , DIPEA (710  $\mu\text{L}$ , 536 mg, 4.15 mmol) in a mixture of  $\text{CH}_2\text{Cl}_2$  / DMF (2 mL / 2 mL) overnight. The purification was carried out by flash chromatography (gradient from 10 / 90 to 100 / 0 : EtOAc / PE) to give [37] as a white sticky solid (450 mg, 79%).

$R_f$  0.60 (EtOAc = 100)

$[\alpha]_D^{25} = +8$  (c. 0.50 in  $\text{CH}_3\text{OH}$ )

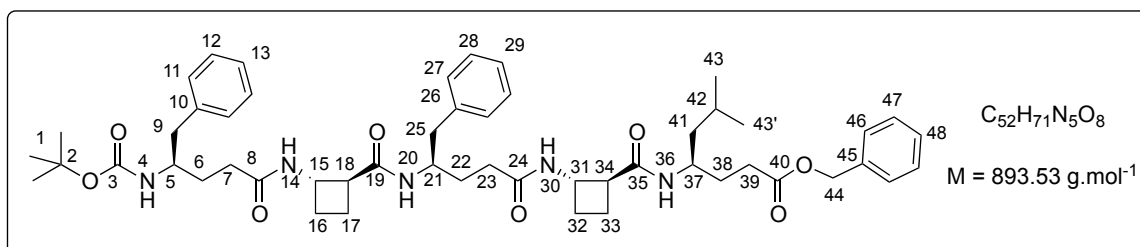
**<sup>1</sup>H NMR** (360 MHz, CDCl<sub>3</sub>) δ 1.40 (s, 9H, 9H-1), 1.49-1.53 (m, 4H, 2H-6, 2H-22), 1.82-2.08 (m, 6H, H-16, 2H-17, H-32, 2H-33), 2.08-2.29 (m, 6H, 2H-7, H-16', 2H-23, H-32'), 2.61-2.81 (m, 5H, H-9, H-9', H-25, H-25', H-18), 3.09-3.20 (m, 1H, H-34), 3.80 (bs, 1H, H-5), 4.15 (bs, 1H, H-21), 4.31-4.35 (m, 1H, H-15), 4.56-4.63 (m, 2H, H-4, H-31), 5.11 (s, 2H, 2H-36), 6.90 (bs, 1H, H-14), 7.08-7.38 (m, 15H, 2H-11, 2H-12, H-13, 2H-27, 2H-28, H-29, 2H-38, 2H-39, H-40), 7.6 (d, *J* = 7.2 Hz, 1H, H-20), 7.91 (d, *J* = 5.4 Hz, 1H, H-30).

**<sup>13</sup>C NMR** (90 MHz, CDCl<sub>3</sub>) δ 17.4, 18.7 (C-17, C-33), 25.0 (C-16), 26.6 (C-32), 28.4 (C-1), 30.6, 31.8 (C-6, C-22), 32.6, 33.1 (C-7, C-23), 41.1 (C-25), 42.0 (C-9), 46.8 (C-34), 47.4 (C-31), 48.1 (C-15), 49.8 (C-18, C-21), 50.4 (C-5), 66.4 (C-36), 79.8 (C-2), 126.2, 126.7, 128.1, 128.2, 128.5, 129.1, 129.4, (C-11, C-12, C-13, C-27, C-28, C-29, C-38, C-39, C-40), 136.1, 137.4, 138.4 (C-10, C-26, C-37), 156.3 (C-3), 173.0, 173.2, 173.3 (C-8, C-19, C-24, C-35).

**IR** (10 mmol/L, in CDCl<sub>3</sub>)  $\nu_{\max}$  1444, 1455, 1509, 1544, 1659, 1699, 1724, 2869, 2955, 2981, 3031, 3067, 3086, 3300 (br), 3335 (br), 3434 cm<sup>-1</sup>.

**HRMS (ESI):** [M+Na]<sup>+</sup>, 775.4035 found, C<sub>44</sub>H<sub>56</sub>N<sub>4</sub>NaO<sub>7</sub> calcd 775.4047.

**Boc- $\gamma^4$ -hPhe-(1*S*,2*S*)-ACBC-(*R*)- $\gamma^4$ -hPhe-(1*S*,2*S*)-ACBC-(*R*)- $\gamma^4$ -hLeu-OBn (+) - [25]**



According to the general procedure **A**, benzyl ester of [37] (86 mg, 0.13 mmol) was hydrolysed in 4.8 h to give the corresponding carboxylic acid, Boc-(*R*)- $\gamma^4$ -hPhe-(1*S*,2*S*)-ACBC-(*R*)- $\gamma^4$ -hPhe-(1*S*,2*S*)-ACBC-OH (90 mg, 88% crude yield).

According to the general procedure **C**, *tert*-butoxycarbonyl group of BocHN-(*R*)- $\gamma^4$ -hLeu-OBn (110 mg, 0.30 mmol) was fully removed in 6 h to give the corresponding TFA salt, TFA·H<sub>2</sub>N-(*R*)- $\gamma^4$ -hLeu-OBn.

According to the general procedure **D**, the coupling reaction was performed with Boc-(*R*)- $\gamma^4$ -hPhe-(1*S*,2*S*)-ACBC-(*R*)- $\gamma^4$ -hPhe-(1*S*,2*S*)-ACBC-OH (86 mg, 0.13 mmol), DIPEA (44  $\mu$ L, 33 mg, 0.26 mmol) and HATU (53 mg, 0.14 mmol) in a mixture of CH<sub>2</sub>Cl<sub>2</sub> / DMF (1 mL / 1 mL), and TFA·H<sub>2</sub>N-(*R*)- $\gamma^4$ -hLeu-OBn, DIPEA (135  $\mu$ L, 101 mg, 0.78 mmol) overnight. The purification was carried out by flash

chromatography (gradient from 0 / 100 to 10 / 90 : CH<sub>3</sub>OH / CH<sub>2</sub>Cl<sub>2</sub>) to give [25] as a white sticky solid (75 mg, 65%).

*R<sub>f</sub>* 0.48 (EtOAc = 100)

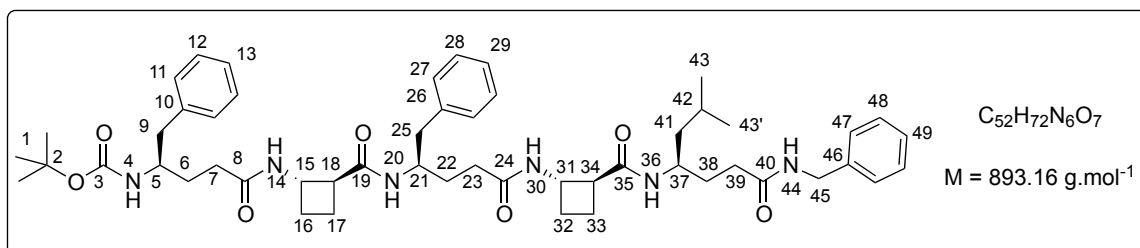
$[\alpha]_D^{18} = +24$  (c. 0.50 in CHCl<sub>3</sub>)

**<sup>1</sup>H NMR** (600 MHz, CDCl<sub>3</sub>)  $\delta$  0.85 (d, *J* = 4.6 Hz, 3H, 3H-43), 0.86 (d, *J* = 4.6 Hz, 3H, 3H-43'), 1.18-1.22 (m, 2H, 2H-41), 1.30-1.45 (m, 13H, 9H-1, 2H-22, 2H-38), 1.45-1.49 (m, 2H, 2H-6), 1.56-1.59 (m, 1H, H-42), 1.73-1.94 (m, 4H, H-7, H-17, H-23, H-32), 1.97-2.01 (m, 3H, H-32', 2H-33), 2.04-2.09 (m, 1H, H-17'), 2.14-2.20 (m, 3H, H-7', H-23', H-39), 2.22-2.31 (m, 3H, 2H-16, H-39'), 2.63-2.74 (m, 5H, 2H-9, H-18, 2H-25), 2.92-2.97 (m, 1H, H-34), 3.77-3.83 (m, 1H, H-5), 3.98-4.03 (m, 1H, H-37), 4.13-4.19 (m, 1H, H-21), 4.27-4.32 (m, 1H, H-31), 4.35-4.43 (m, 1H, H-15), 4.76 (d, *J* = 10.1 Hz, 1H, H-4), 5.11-5.12 (m, 2H, 2H-44), 6.86 (d, 1H, H-14), 7.07-7.36 (m, 16H, 2H-11, 2H-12, H-13, H-20, 2H-27, 2H-28, H-29, 2H-46, 2H-47, H-48), 8.2 (d, *J* = 7.3 Hz, 1H, H-30), 8.33 (d, *J* = 8.3 Hz, 1H, H-36).

**<sup>13</sup>C NMR** (100 MHz, CDCl<sub>3</sub>)  $\delta$  16.9 (C-39), 18.0 (C-33), 22.2, 23.2 (C-43, C-43'), 24.4, 25.3, 26.7 (C-23, C-17, C-7), 24.9 (C-42), 28.5 (C-1), 31.0 (C-6), 32.4 (C-32), 32.8 (C-16), 41.5, 42.1 (C-9, C-25), 43.9 (C-22, C-38), 46.5 (C-37), 48.0, 48.1 (C-15, C-31), 48.9 (C-21), 49.9 (C-34), 50.0 (C-18), 50.2 (C-5), 66.1 (C-44), 79.6 (C-2), 126.1, 126.2, 126.5, 128.0, 128.1, 128.1, 128.2, 128.4, 128.5, 129.1, 129.2, 129.4 (C-11, C-12, C-13, C-27, C-28, C-29, C-46, C-47, C-48), 136.1, 137.5, 138.2 (C-10, C-26, C-45), 156.1 (C-3), 172.3 (C-19), 172.4 (C-35), 173.0 (C-40), 173.6, 173.8 (C-8, C-24).

**IR** (10 mmol/L, in CDCl<sub>3</sub>)  $\nu_{\max}$  1443, 1454, 1509, 1546, 1602, 1653, 1697, 1727, 2869, 2930, 2958, 3031, 3067, 3259 (br), 3333 (br), 3434 cm<sup>-1</sup>.

**HRMS (ESI):** [M+Na]<sup>+</sup>, 916.5145 found, C<sub>52</sub>H<sub>71</sub>N<sub>5</sub>NaO<sub>8</sub> calcd 916.5200.

**Boc- $\gamma^4$ -hPhe-(1S,2S)-ACBC-(R)- $\gamma^4$ -hPhe-(1S,2S)-ACBC-(R)- $\gamma^4$ -hLeu-NHBn (+) - [26]**

According to the general procedure **A**, benzyl ester of [37] (141mg, 0.18 mmol) was hydrolysed in 6 h to give the corresponding carboxylic acid, Boc-(R)- $\gamma^4$ -hPhe-(1S,2S)-ACBC-(R)- $\gamma^4$ -hPhe-(1S,2S)-ACBC-OH (119 mg, 100% crude yield).

According to the general procedure **C**, *tert*-butoxycarbonyl group of BocHN-(R)- $\gamma^4$ -hLeu-NHBn (73 mg, 0.21 mmol) was fully removed in 6 h to give the corresponding TFA salt, TFA·H<sub>2</sub>N-(R)- $\gamma^4$ -hLeu-NHBn.

According to the general procedure **D**, the coupling reaction was performed with Boc-(R)- $\gamma^4$ -hPhe-(1S,2S)-ACBC-(R)- $\gamma^4$ -hPhe-(1S,2S)-ACBC-OH (119 mg, 0.18 mmol), DIPEA (60  $\mu$ L, 46 mg, 0.36 mmol) and HATU (71 mg, 0.19 mmol) in a mixture of CH<sub>2</sub>Cl<sub>2</sub> / DMF (1 mL / 0.5 mL), and TFA·H<sub>2</sub>N-(R)- $\gamma^4$ -hLeu-NHBn, DIPEA (185  $\mu$ L, 139 mg, 1.08 mmol) in CH<sub>2</sub>Cl<sub>2</sub> (1 mL) overnight. The purification was carried out by flash chromatography (gradient from 0 / 100 to 10 / 90 : CH<sub>3</sub>OH / CH<sub>2</sub>Cl<sub>2</sub>) to give [27] as a white sticky solid (60 mg, 45%).

$R_f$  0.67 (MeOH / CH<sub>2</sub>Cl<sub>2</sub> = 10 / 90)

$[\alpha]_D^{19} = +30$  (c. 0.50 in CHCl<sub>3</sub>)

**<sup>1</sup>H NMR** (600 MHz, CDCl<sub>3</sub>)  $\delta$  0.82 (d,  $J$  = 6.3 Hz, 3H, H-43), 0.86 (d,  $J$  = 6.4 Hz, 3H, H-43'), 1.12-1.19 (m, 4H, 2H-22, 2H-41), 1.28-1.34 (m, 1H, H-38), 1.43 (s, 9H, H-1), 1.46-1.48 (m, 3H, 2H-6, H-38'), 1.60-1.66 (m, 1H, H-42), 1.70-1.76 (m, 2H, H-17, H-33), 1.85-1.92 (m, 2H, H-16, H-32), 1.94-2.05 (m, 3H, H-7, H-17', H-23), 2.094-2.12 (m, 2H, H-23', H-32'), 2.18-2.23 (m, H-16', H-33'), 2.26-2.34 (m, 2H, H-7', H-39), 2.36-2.42 (m, 1H, H-25), 2.50-2.57 (m, 2H, H-25', H-39'), 2.61-2.69 (m, 1H, H-18), 2.71-2.78 (m, 1H, H-9), 2.74-2.78 (m, 1H, H-9'), 2.89-2.93 (m, 1H, H-34), 3.77-3.83 (m, 1H, H-5), 3.99-4.07 (m, 2H, H-37, H-21), 4.37-4.39 (m, 1H, H-15), 4.40-4.43 (m, 1H, H-31), 4.43-4.46 (m, 2H, H-45), 4.76 (d,  $J$  = 9.3 Hz, 1H, H-4), 6.59 (d,  $J$  = 9.5 Hz, 1H, H-20), 6.88 (d,  $J$  = 7.3 Hz, 1H, H-14), 7.00-7.37 (m, 15H, 2H-11, 2H-12, H-13, 2H-27, 2H-28, H-29, 2H-47, 2H-48, H-49), 7.85 (d,  $J$  = 9.4 Hz, 1H, H-36), 8.18 (d,  $J$  = 8.7 Hz, 1H, H-30), 8.5 (t,  $J$  = 5.0 Hz, 1H, H-44).

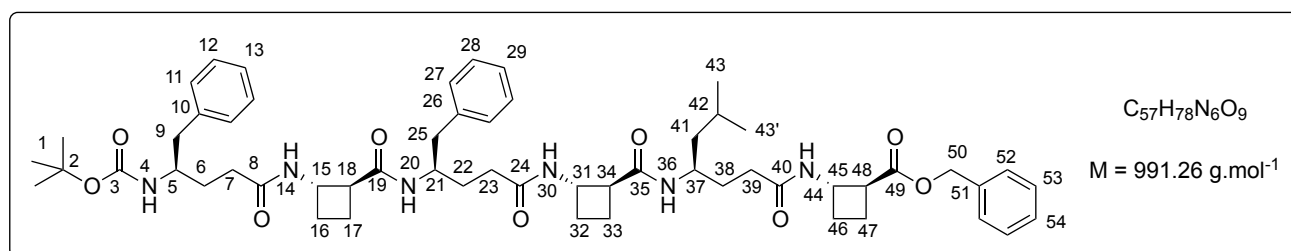
**<sup>13</sup>C NMR** (100 MHz, CDCl<sub>3</sub>)  $\delta$  15.7, 16.9 (C-33, C-17), 22.2, 23.2 (C-43, C-43'), 25.0 (C-42), 25.6, 26.0 (C-16, C-32), 28.5 (C-1), 29.7, 29.8, (C-22, C-41), 30.0 (C-38), 31.9 (C-23), 32.3 (C-7), 33.6 (C-39), 34.0 (C-

6), 42.1 (C-9), 42.2 (C-25), 43.4 (C-45), 46.8 (C-37), 47.4 (C-21), 47.7 (C-15), 48.2 (C-31), 49.8, 49.9 (C34, C-5), 50.0 (C-18), 79.8 (C-2), 126.3, 126.6, 127.0, 127.9, 128.1, 128.4, 128.4, 128.4, 129.4, 129.4 (C-11, C-12, C-13, C-27, C-28, C-29, C-47, C48, C-49), 137.4, 137.8, 139.2 (C-10, C-26, C-46), 156.1 (C-3), 171.7 (C-19), 171.9 (C-24), 172.0 (C-8), 172.5 (C-35), 174.5 (C-40).

**IR** (10 mmol/L, in CDCl<sub>3</sub>)  $\nu_{\max}$  1443, 1454, 1510, 1551, 1604, 1649, 1697, 2870, 2931, 2958, 3031, 3066, 3086, 3317, 3434 cm<sup>-1</sup>.

**HRMS (ESI):** [M+Na]<sup>+</sup>, 915.5312 found, C<sub>52</sub>H<sub>72</sub>N<sub>6</sub>NaO<sub>7</sub> calcd 915.5360.

**Boc-(R)- $\gamma^4$ -hPhe-(1S,2S)-ACBC-(R)- $\gamma^4$ -hPhe-(1S,2S)-ACBC-(R)- $\gamma^4$ -hLeu-(1S,2S)-ACBC-OBn (+) - [27]**



According to the general procedure **A**, benzyl ester of [35] (48 mg, 0.10 mmol) was hydrolysed in 4 h to give the corresponding carboxylic acid, Boc-(R)- $\gamma^4$ -hPhe-(1S,2S)-ACBC-OH (39 mg, 100% crude yield).

According to the general procedure **C**, *tert*-butoxycarbonyl group of [23] (65 mg, 0.09 mmol) was fully removed in 1.2 h to give the corresponding TFA salt, TFA·H<sub>2</sub>N-(R)- $\gamma^4$ -hPhe-(1S,2S)-ACBC-(R)- $\gamma^4$ -hLeu-(1S,2S)-ACBC-OBn.

According to the general procedure **D**, the coupling reaction was performed with Boc-(R)- $\gamma^4$ -hPhe-(1S,2S)-ACBC-OH (39mg, 0.10 mmol), DIPEA (65  $\mu$ L, 49 mg, 0.38 mmol) and HATU (39 mg, 0.11 mmol) in a mixture of CH<sub>2</sub>Cl<sub>2</sub> / DMF (1 mL / 1 mL), and TFA·H<sub>2</sub>N-(R)- $\gamma^4$ -hPhe-(1S,2S)-ACBC-(R)- $\gamma^4$ -hLeu-(1S,2S)-ACBC-OBn, DIPEA (200  $\mu$ L, 151 mg, 1.17 mmol) in CH<sub>2</sub>Cl<sub>2</sub> (2 mL) overnight. The purification was carried out by flash chromatography (gradient from 10 / 90 to 100 / 0 : EtOAc / PE then from 0 / 100 to 20 / 80) to give [27] as a white sticky solid (30 mg, 30%).

**R<sub>f</sub>** 0.50 (MeOH / CH<sub>2</sub>Cl<sub>2</sub> = 10 / 90)

**[ $\alpha$ ]<sub>D</sub><sup>16</sup>** = + 56 (c. 0.50 in CHCl<sub>3</sub>)

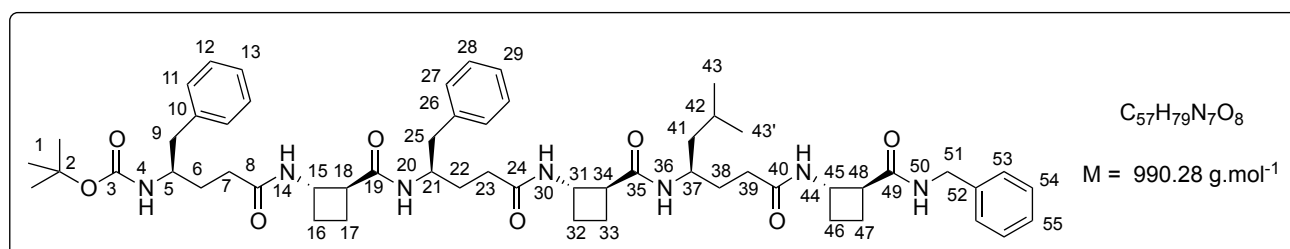
**<sup>1</sup>H NMR** (600 MHz, CDCl<sub>3</sub>) δ 0.81 (d, J = 6.7 Hz, 3H, 3H-43), 0.83 (d, J = 6.7 Hz, 3H, 3H-43'), 1.05-1.08 (m, 2H, 2H-41), 1.24-1.30 (m, 3H, H-22, H-22', H-38), 1.43 (m, 10H, 9H-1, H-38'), 1.49-1.54 (m, 2H, 2H-6), 1.57-1.61 (m, 1H, H-42), 1.74-1.76 (m, 2H, H-17, H-33), 1.89-1.96 (m, 4H, H-16, H-32, H-46, H-47), 1.97-2.04 (m, 4H, H-7, H-17', H-23, H-47'), 2.11-2.19 (m, 4H, H-16', H-32', H-33', H-46'), 2.26-2.28 (m, 1H, H-7'), 2.55 (dd, J = 14.3 Hz, J = 7.9 Hz, 1H, H-25), 2.67-2.69 (m, 3H, H-9, H-18, H-25'), 2.75-2.77 (dd, J = 12.7 Hz, J = 5.7 Hz, 1H, H-9)', 2.90-2.94 (m, 1H, H-34), 3.16-3.21 (m, 1H, H-48), 3.82-3.85 (m, 1H, H-5), 4.00-4.02 (m, 1H, H-37), 4.10-4.14 (m, 1H, H-21), 4.38-4.44 (m, 2H, H-15, H-31), 4.60-4.64 (m, 1H, H-45), 4.71-4.73 (d, 1H, H-4), 5.12 (d, J = 12.4 Hz, 1H, H-50), 5.16 (d, J = 12.4 Hz, 1H, H-50'), 6.64 (d, J = 10 Hz, 1H, H-20), 6.73 (d, J = 8.2 Hz, 1H, H-14), 7.86 (d, J = 7.4 Hz, 1H, H-36), 8.24 (d, J = 8.9 Hz, 1H, H-30), 8.39 (d, J = 6.7 Hz, 1H, H-44).

**<sup>13</sup>C NMR** (100 MHz, CDCl<sub>3</sub>) δ 15.9 (C-33), 16.9 (C-17), 18.7 (C-47), 22.0, 23.2 (C-43, C-43'), 24.9 (C-42), 25.9 (C-6), 26.5 (C-46), 28.4 (C-1), 29.7, 30.1 (C-38, C-23), 32.1, 32.4 (C-7, C-39), 33.5, 33.8 (C-16, C-32), 42.1 (C-9), 42.4 (C-25), 43.9 (C-41), 46.6 (C-37), 46.9 (C-48), 47.4 (C-45), 47.8 (C-15, C-21), 48.2 (C-31), 49.9, 50.0 (C-5, C-18, C-34), 66.2 (C-50), 79.8 (C-2), 126.4, 127.9, 128.1, 128.2, 128.4, 128.5, 129.4 (C-11, C-12, C-13, C-27, C-28, C-29, C-52, C-53, C-54), 136.0, 137.3, 137.7 (C-10, C-26, C-51), 156.2 (C-3), 171.8 (C-24), 172.0 (C-35), 172.1 (C-19), 172.7 (C-8), 173.4 (C-40), 173.6 (C-49).

**IR** (10 mmol/L, in CDCl<sub>3</sub>)  $\nu_{\max}$  1443, 1455, 1568, 1509, 1549, 1602, 1649 1651, 1697, 1724, 2869, 2957, 3030, 3066, 3318 (br), 3433 cm<sup>-1</sup>.

**HRMS (ESI):** [M+Na]<sup>+</sup>, 1013.5722 found, C<sub>57</sub>H<sub>78</sub>N<sub>6</sub>NaO<sub>9</sub> 1013.5727 calcd.

**Boc-(R)- $\gamma^4$ -hPhe-(1S,2S)-ACBC-(R)- $\gamma^4$ -hPhe-(1S,2S)-ACBC-(R)- $\gamma^4$ -hLeu-(1S,2S)-ACBC-NHBn (+) - [28]**



According to the general procedure A, benzyl ester of [27] (70 mg, 0.070 mmol) was hydrolysed in 24 h to give the corresponding carboxylic acid, Boc-(R)- $\gamma^4$ -hPhe-(1S,2S)-ACBC-(R)- $\gamma^4$ -hPhe-(1S,2S)-ACBC-(R)- $\gamma^4$ -hLeu-(1S,2S)-ACBC-OH (50 mg, 79% crude yield).



According to the general procedure **D**, the coupling reaction was performed with Boc-(*R*)- $\gamma^4$ -hPhe-(1*S*,2*S*)-ACBC-(*R*)- $\gamma^4$ -hPhe-(1*S*,2*S*)-ACBC-(*R*)- $\gamma^4$ -hLeu-(1*S*,2*S*)-ACBC-OH (50 mg, 0.056 mmol), DIPEA (20  $\mu$ L, 13 mg, 0.112 mmol) and HATU (22 mg, 0.058 mmol) in a mixture of CH<sub>2</sub>Cl<sub>2</sub> / DMF (1 mL / 1 mL), and benzylamine (9  $\mu$ L, 9 mg, 0.084 mmol), DIPEA (22  $\mu$ L, 16 mg, 0.140 mmol) overnight. The purification was carried out by flash chromatography (gradient from 10 / 90 to 100 / 0 : EtOAc / PE then from 0 / 100 to 10 / 90 : CH<sub>3</sub>OH / CH<sub>2</sub>Cl<sub>2</sub>) to give [28] as a yellow sticky foam (25 mg, 50%).

$R_f$  0.42 (MeOH / CH<sub>2</sub>Cl<sub>2</sub> = 10 / 90)

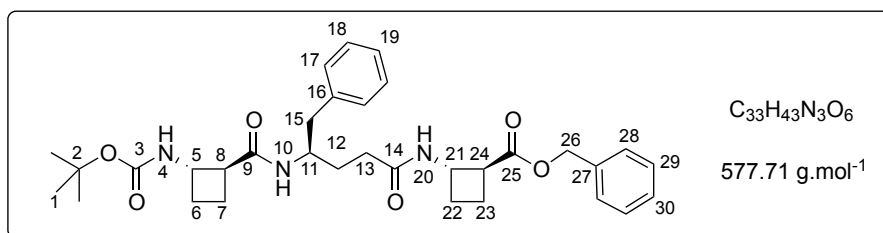
$[\alpha]_D^{18} = +46$  (c. 0.50 in CHCl<sub>3</sub>)

**<sup>1</sup>H NMR** (600 MHz, CDCl<sub>3</sub>)  $\delta$  0.82 (d, *J* = 6.4 Hz, 3H, 3H-43), 0.82 (d, *J* = 6.4 Hz, 3H, 3H-43'), 1.13-1.17 (m, 1H, H-38), 1.28-1.32 (m, 2H, H-22, H-38'), 1.38-1.43 (m, 13H, 9H-1, 2H-6, 2H-41), 1.57-1.64 (m, 1H, H-42), 1.73-1.79 (m, 2H, H-17, H-33), 1.90-1.93 (m, 2H, H-16, H-32), 2.01-2.13 (m, 5H, H-17', H-23, H-39, H-46, H-47), 2.17-2.25 (m, 6H, H-7, H-16', H-23', H-32', H-33', H-39'), 2.29-2.31 (m, 3H, H-7', H-46', H-47'), 2.57-2.60 (m, 2H, 2H-25), 2.64-2.69 (m, 2H, H-9, H-18), 2.77 (dd, *J* = 13.9 Hz, 5.4 Hz, 1H, H-9'), 2.88-2.93 (m, 1H, H-34), 3.09-3.13 (m, 1H, H-48), 3.81-3.87 (m, 1H, H-5), 3.98-4.04 (m, 1H, H-37), 4.10-4.16 (m, 1H, H-21), 4.30-4.35 (m, 1H, H-45), 4.40-4.44 (m, 1H, H-15), 4.46-4.49 (m, 1H, H-31), 4.50-4.54 (m, 2H, 2H-51), 4.68 (d, *J* = 10.2 Hz, H-4), 6.72 (d, *J* = 9.8 Hz, 1H, H-20), 6.8 (d, *J* = 8.1 Hz, 1H, H-14), 7.04-7.37 (m, 15H, 2H-11, 2H-12, H-13, 2H-27, 2H-28, H-29, 2H-53, 2H-54, H-55), 7.64 (d, *J* = 9.3 Hz, 1H, H-36), 8.29 (d, *J* = 7.6 Hz, 1H, H-30), 8.54 (d, *J* = 6.5 Hz, 1H, H-44), 9.15 (t, *J* = 5.3 Hz, 1H, H-50).

**<sup>13</sup>C NMR** (100 MHz, CDCl<sub>3</sub>)  $\delta$  15.8 (C-33), 16.9 (C-17), 18.3, 24.3 (C-23, C-39), 22.4, 23.0 (C-43, C-43'), 25.0 (C-42), 25.8, 26.0 (C-16, C-32), 28.5 (C-1), 29.4 (C-22), 30.0 (C-6), 31.9 (C-7), 32.3 (C-41), 32.5, 32.8 (C-46, C-47), 42.1 (C-9), 42.7 (C-25), 43.0 (C-51), 44.8 (C-38), 46.0 (C-37), 47.8 (C-21), 48.1 (C-15), 48.1, 48.1 (C-31, C-45), 49.7 (C-47), 49.9, 49.9 (C-5, C-34), 50.1 (C-18), 79.8 (C-2), 126.4, 126.7, 126.7, 127.4, 128.2, 128.3, 128.4, 129.4, 129.4 (C-11, C-12, C-13, C-27, C-28, C-29, C-53, C-54, C-55), 137.3, 137.6 (C-10, C-26), 139.4 (C-52), 156.2 (C-3), 171.2 (C-19), 171.8 (C-24), 172.0 (C-8), 172.2 (C-35), 173.7 (C-49), 174.4 (C-40).

**IR** (10 mmol/L, in CDCl<sub>3</sub>)  $\nu_{\max}$  1443, 1455, 1509, 1554, 1603, 1648, 1696, 2870, 2930, 2958, 3032, 3067, 3086, 3310 (br), 3433 cm<sup>-1</sup>.

**HRMS (ESI):** [M+Na]<sup>+</sup>, 1012.5820 found, 1012.5882 C<sub>57</sub>H<sub>79</sub>N<sub>7</sub>NaO<sub>8</sub> calcd.

**Boc-(1*S*,2*S*)-ACBC-(*R*)- $\gamma^4$ -*h*Phe-(1*S*,2*S*)-ACBC-OBn (+) - [39]**

According to the general procedure **C**, *tert*-butoxycarbonyl group of [35] (240 mg, 0.50 mmol) was fully removed in 4 h to give the corresponding TFA salt, TFA·H<sub>2</sub>N-(*R*)- $\gamma^4$ -*h*Phe-(1*S*,2*S*)-ACBC-OBn.

According to the general procedure **D**, the coupling reaction was performed with Boc-(1*S*,2*S*)-ACBC-OH [2] (108 mg, 0.50 mmol), DIPEA (170  $\mu$ L, 129 mg, 1.00 mmol) and HATU (197 mg, 0.53 mmol) in a mixture of CH<sub>2</sub>Cl<sub>2</sub> / DMF (2 mL / 1 mL), and TFA·H<sub>2</sub>N-(*R*)- $\gamma^4$ -*h*Phe-(1*S*,2*S*)-ACBC-OBn, DIPEA (515  $\mu$ L, 387 mg, 3.00 mmol) in CH<sub>2</sub>Cl<sub>2</sub> (2 mL) overnight. The purification was carried out by flash chromatography (gradient from 0 / 100 to 10 / 90 : CH<sub>3</sub>OH / CH<sub>2</sub>Cl<sub>2</sub>) to give [38] as a pale yellow sticky solid (125 mg, 43%).

$R_f$  0.77 (CH<sub>3</sub>OH / CH<sub>2</sub>Cl<sub>2</sub> = 10 / 90)

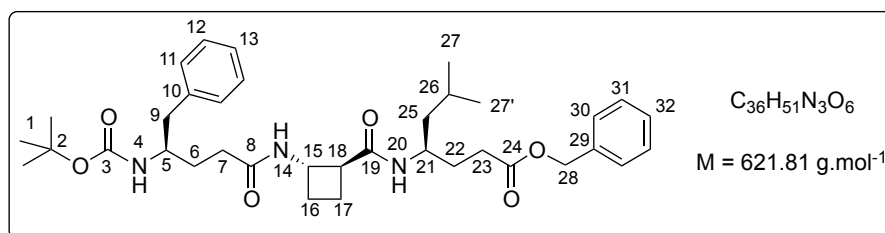
$[\alpha]_D^{29} = +30$  (c. 0.50 in CHCl<sub>3</sub>)

**<sup>1</sup>H NMR** (250 MHz, CDCl<sub>3</sub>)  $\delta$  1.44 (s, 9H, 9H-1), 1.63-1.89 (m, 5H, 2H-6, H-7, 2H-12), 1.97-2.07 (m, 3H, H-7', H-22, H-23), 2.15-2.28 (m, 4H, H-22', H-23', 2H-13), 2.54-2.57 (m, 2H, 2H-15), 2.70-2.82 (m, 1H, H-8), 3.13-3.24 (m, 1H, H-24), 4.08-4.17 (m, 2H, H-5, H-11), 4.55-4.68 (m, 1H, H-21), 5.08 (d,  $J$  = 12.8 Hz, 1H, H-26), 5.17 (d,  $J$  = 12.8 Hz, 1H, H-26'), 5.19 (d,  $J$  = 5.6 Hz, 1H, H-4), 7.03-7.33 (m, 10H, 2H-17, 2H-18, H-19, 2H-28, 2H-29, H-30), 7.55 (d,  $J$  = 8.8 Hz, 1H, H-10), 7.77 (d,  $J$  = 8.1 Hz, 1H, H-20).

**<sup>13</sup>C NMR** (62.5 MHz, CDCl<sub>3</sub>)  $\delta$  18.3 (C-12), 24.9, 26.7 (C-22, C-23), 28.4 (C-1), 31.8, (C-6, C-7), 33.1 (C-13), 41.2 (C-15), 46.9 (C-24), 47.6 (C-21), 48.9, 49.6 (C-5, C-11), 50.0 (C-8), 66.3 (C-26), 80.4 (C-2), 126.2, 128.0, 128.1, 128.2, 128.5, 129.0, 129.3 (C-17, C-18, C-19, C-28, C-29, C-30), 136.1 (C-16), 138.1 (C-27), 156.1 (C-3), 172.6 (C-14), 173.1 (C-9), 173.8 (C-25).

**IR** (10 mmol/L, in CDCl<sub>3</sub>)  $\nu_{\max}$  1456, 1499, 1552, 1664, 1691, 1727, 2875, 2953, 2982, 3032, 3068, 3090, 3276 (br), 3355 (br), 3445 cm<sup>-1</sup>.

**HRMS (ESI):** [M+Na]<sup>+</sup>, 600.3038 found, C<sub>33</sub>H<sub>43</sub>N<sub>3</sub>NaO<sub>6</sub> 600.3044 calcd.

**Boc-(*R*)- $\gamma^4$ -*h*Phe-(1*S*,2*S*)-ACBC-(*R*)- $\gamma^4$ -*h*Leu-OBn (-) - [39]**

According to the general procedure **A**, benzyl ester of [35] (399 mg, 0.83 mmol) was hydrolysed in 5.5 h to give the corresponding carboxylic acid, Boc-(1*S*,2*S*)-ACBC-(*R*)- $\gamma^4$ -*h*Phe-OH (307 mg, 95%).

According to the general procedure **C**, *tert*-butoxycarbonyl group of BocHN-(*R*)- $\gamma^4$ -*h*Leu-OBn (275 mg, 0.79 mmol) was fully removed in 5 h to give the corresponding TFA salt, TFA·H<sub>2</sub>N-(*R*)- $\gamma^4$ -*h*Leu-OBn.

According to the general procedure **D**, the coupling reaction was performed with , Boc-(1*S*,2*S*)-ACBC-(*R*)- $\gamma^4$ -*h*Phe-OH (307 mg, 0.79 mmol), DIPEA (270  $\mu$ L, 204 mg, 1.58 mmol) and HATU (311 mg, 0.83 mmol) in a mixture of CH<sub>2</sub>Cl<sub>2</sub> / DMF (5 mL / 1 mL), and TFA·H<sub>2</sub>N-(*R*)- $\gamma^4$ -*h*Leu-OBn, DIPEA (810  $\mu$ L, 611 mg, 4.74 mmol) in CH<sub>2</sub>Cl<sub>2</sub> (2 mL) overnight. The purification was carried out by flash chromatography (gradient from 10 / 90 to 100 / 0 : EtOAc / PE) to give [39] as a white sticky solid (340 mg, 69%).

*R<sub>f</sub>* 0.70 (CH<sub>3</sub>OH / CH<sub>2</sub>Cl<sub>2</sub> = 10 / 90)

$[\alpha]_D^{20} = -9$  (c. 0.50 in CH<sub>3</sub>OH)

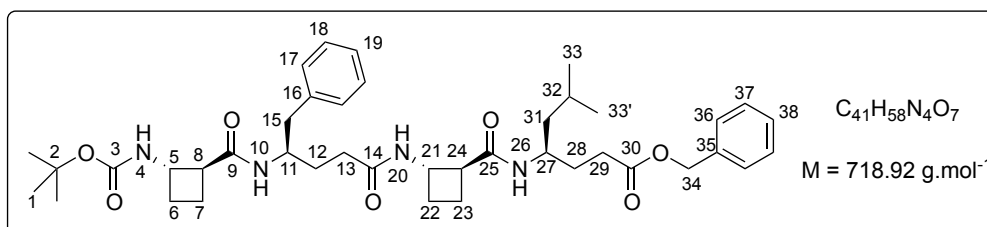
**<sup>1</sup>H NMR** (250 MHz, CDCl<sub>3</sub>)  $\delta$  0.74 (d, *J* = 2.9 Hz, 3H, 3H-27), 0.77 (d, *J* = 3.0 Hz, 3H, 3H-27'), 1.11-1.13 (m, 11H, 9H-1, 2H-22), 1.41-1.51 (m, 4H, 2H-6, 2H-25), 1.57-1.66 (m, 1H, H-26), 1.73-1.85 (m, 4H, H-7, H-16, H-17, H-25'), 1.93-2.14 (m, 3H, H-7', H-16', H17'), 2.27-2.39 (m, 2H, 2H-23), 2.63-2.65 (m, 2H, 2H-9), 2.77-2.86 (m, 1H, H-18), 3.71 (bs, 1H, H-5), 3.81-3.91 (m, 1H, H-21), 4.18-4.25 (m, 1H, H-15), 4.58 (d, *J* = 9.3 Hz, 1H, H-4), 5.02 (m, 2H, 2H-28), 6.98 (d, *J* = 7.2 Hz, 1H, H-14), 7.03-7.28 (m, 10H, 2H-11, 2H-12, H-13, 2H-30, 2H-31, H-32), 7.78 (d, *J* = 8.7 Hz, 1H, H-20).

**<sup>13</sup>C NMR** (62.5 MHz, CDCl<sub>3</sub>)  $\delta$  18.6, 24.5 (C-16, C-17), 22.1, 23.1 (C-27, C-27'), 24.9 (C-26), 28.3 (C-1), 30.8, 31.0 (C-6, C-23, C-25), 32.6 (C-7), 41.7 (C-9), 43.9 (C-22), 46.7 (C-21), 47.8 (C-15), 49.7 (C-18), 50.7 (C-5), 66.3 (C-28), 79.6 (C-2), 126.4, 126.9, 127.4, 128.1, 128.4, 128.4, 129.0, 129.2 (C-11, C-12, C-13, C-30, C-31, C-32), 135.8, 137.5 (C-10, C-29), 156.2 (C-3), 173.1, 173.7, 173.9 (C-8, C-19, C-24).

**IR** (10 mmol/L, in CDCl<sub>3</sub>)  $\nu_{\max}$  1455, 1506, 1563, 1603, 1645, 1694, 1727, 2839, 2870, 1946, 3031, 3067, 3267 (br), 3435 cm<sup>-1</sup>.

**HRMS (ESI):**  $[M+Na]^+$ , 644.3680 found,  $C_{36}H_{51}N_3NaO_6$  644.3670 calcd.

**Boc-(1*S*,2*S*)-ACBC-(*R*)- $\gamma^4$ -*h*Phe-(1*S*,2*S*)-ACBC-(*R*)- $\gamma^4$ -*h*Leu-OBn (+) - [29]**



According to the general procedure **A**, benzyl ester of [38] (92 mg, 0.16 mmol) was hydrolysed in 2.8 h to give the corresponding carboxylic acid, Boc-(1*S*,2*S*)-ACBC-(*R*)- $\gamma^4$ -*h*Phe-(1*S*,2*S*)-ACBC-OH (70 mg, 88%).

According to the general procedure **C**, *tert*-butoxycarbonyl group of BocHN-(*R*)- $\gamma^4$ -*h*Leu-OBn (70 mg, 0.20 mmol) was fully removed in 1.2 h to give the corresponding TFA salt, TFA·H<sub>2</sub>N-(*R*)- $\gamma^4$ -*h*Leu-OBn. According to the general procedure **D**, the coupling reaction was performed with Boc-(1*S*,2*S*)-ACBC-(*R*)- $\gamma^4$ -*h*Phe-(1*S*,2*S*)-ACBC-OH (70 mg, 0.14 mmol), DIPEA (45  $\mu$ L, 33 mg, 0.28 mmol) and HATU (56 mg, 0.15 mmol) in a mixture of CH<sub>2</sub>Cl<sub>2</sub> / DMF (2 mL / 0.5 mL), and TFA·H<sub>2</sub>N-(*R*)- $\gamma^4$ -*h*Leu-OBn, DIPEA (135  $\mu$ L, 100 mg, 0.84 mmol) in CH<sub>2</sub>Cl<sub>2</sub> (1 mL) overnight. The purification was carried out by flash chromatography (gradient from 10 / 90 to 100 / 0 : EtOAc / PE) to give [29] as a white sticky solid (70 mg, 70%).

***R*<sub>f</sub>** 0.64 (CH<sub>3</sub>OH / CH<sub>2</sub>Cl<sub>2</sub> = 10 / 90)

**$[\alpha]_D^{18}$**  = + 18 (c. 0.50 in CHCl<sub>3</sub>)

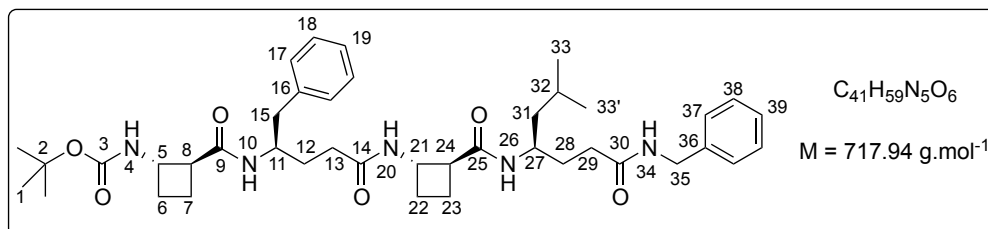
**<sup>1</sup>H NMR** (600 MHz, CDCl<sub>3</sub>)  $\delta$  0.86 (d, *J* = 6.3 Hz, 3H, 3H-33), 0.88 (d, *J* = 6.3 Hz, 3H, 3H-33'), 1.19-1.23 (m, 1H, H-31), 1.37-1.42 (m, 10H, 9H-1, H-31'), 1.48-1.55 (m, 2H, 2H-12), 1.57-1.62 (m, 1H, H-32), 1.71-1.78 (m, 3H, H-6, 2H-28), 1.84-1.97 (m, 6H, 2H-7, H-22, 2H-23, H-13), 2.10-2.21 (m, 3H, H-6', H-22', H-13'), 2.50-2.55 (m, 2H, 2H-29), 2.65-2.69 (m, 2H, H-8, H-15), 2.78 (dd, *J* = 13.8 Hz, 5.3 Hz, 1H, H-15'), 3.03-3.008 (m, 1H, H-24), 4.00-4.06 (m, 1H, H-27), 4.13-4.19 (m, 1H, H-11), 4.19-4.24 (m, 1H, H-5), 4.32-4.37 (m, 1H, H-21), 5.12-5.14 (m, 2H, 2H-34), 5.2 (d, *J* = 6.6 Hz, 1H, H-4), 6.75 (d, *J* = 9.0 Hz, 1H, H-10), 7.10-7.39 (m, 10H, 2H-17, 2H-18, H-19, 2H-36, 2H-37, H-38), 7.88-7.89 (m, 1H, H-20), 8.25 (d, *J* = 8.3 Hz, 1H, H-26).

**$^{13}\text{C}$  NMR** (100 MHz,  $\text{CDCl}_3$ )  $\delta$  18.1, 18.1 (C-7, C-23), 22.1, 23.2 (C-33, C-33'), 24.4 (C-22), 25.0 (C-32), 25.3 (C-6), 28.3 (C-1), 30.9, 31.0 (C-28, C-29), 31.3 (C-12), 32.1 (C-13), 41.6 (C-15), 43.8 (C-31), 47.0 (C-27), 48.2 (C-21), 48.5, 48.7 (C-5, C-11), 49.4 (C-24), 50.2 (C-8), 66.2 (C-34), 80.3 (C-2), 126.4, 128.1, 128.2, 128.3, 128.5, 129.2, (C-17, C-18, C-19, C-36, C-37, C-38), 136.2, 137.8 (C-16, C-35), 155.8 (C-3), 172.9, 173.4, 173.6, 173.7 (C-9, C-14, C-25, C-30).

**IR** (10 mmol/L, in  $\text{CDCl}_3$ )  $\nu_{\text{max}}$  1455, 1499, 1564, 1649, 1693, 1729, 2871, 2959, 3032, 3068, 3265 (br), 3348 (br), 3445  $\text{cm}^{-1}$ .

**HRMS (ESI):**  $[\text{M}+\text{Na}]^+$ , 741.4203 found,  $\text{C}_{41}\text{H}_{58}\text{N}_4\text{NaO}_7$  741.4211 calcd.

**Boc-(1*S*,2*S*)-ACBC-(*R*)- $\gamma^4$ -*h*Phe-(1*S*,2*S*)-ACBC-(*R*)- $\gamma^4$ -*h*Leu-NHBn - [30]**



According to the general procedure **A**, benzyl ester of [29] (21 mg, 0.030 mmol) was hydrolysed in 8 h to give the corresponding carboxylic acid, Boc-(1*S*,2*S*)-ACBC-(*R*)- $\gamma^4$ -*h*Phe-(1*S*,2*S*)-ACBC-(*R*)- $\gamma^4$ -*h*Leu-OH (16 mg, 83%).

According to the general procedure **D**, the coupling reaction was performed with Boc-(1*S*,2*S*)-ACBC-(*R*)- $\gamma^4$ -*h*Phe-(1*S*,2*S*)-ACBC-(*R*)- $\gamma^4$ -*h*Leu-OH (16 mg, 0.025 mmol), DIPEA (8  $\mu\text{L}$ , 6 mg, 0.052 mmol) and HATU (10 mg, 0.026 mmol) in a mixture of  $\text{CH}_2\text{Cl}_2$  / DMF (1 mL / 0.5 mL); and benzylamine (7  $\mu\text{L}$ , 7 mg, 0.063 mmol), DIPEA (23  $\mu\text{L}$ , 18 mg, 0.150 mmol) overnight. The purification was carried out by flash chromatography (gradient from 10 / 90 to 100 / 0 : EtOAc / PE then from 0 / 100 to 10 / 90 :  $\text{CH}_3\text{OH}$  /  $\text{CH}_2\text{Cl}_2$ ) to give [30] as a yellow sticky foam (7 mg, 39%).

$R_f$  0.68 ( $\text{CH}_3\text{OH}$  /  $\text{CH}_2\text{Cl}_2$  = 10 / 90)

$[\alpha]_D^{27}$ : not enough soluble

**$^1\text{H}$  NMR** (600MHz,  $\text{CDCl}_3$ )  $\delta$  0.84 (d,  $J$  = 6.6 Hz, 3H, 3H-33), 0.86 (d,  $J$  = 6.6 Hz, 3H, 3H-33'), 1.11-1.15 (m, 4H, 2H-12, 2H-28), 1.18-1.31 (m, 1H, H-31), 1.42-1.45 (m, 10H, 9H-1, H-31'), 1.62-1.69 (m, 1H, H-32), 1.74-1.80 (m, 4H, H-6, H-7, H-13, H-23), 1.83-1.91 (m, 2H, H-7', H-22), 1.94-2.07 (m, 2H, H-13', H-

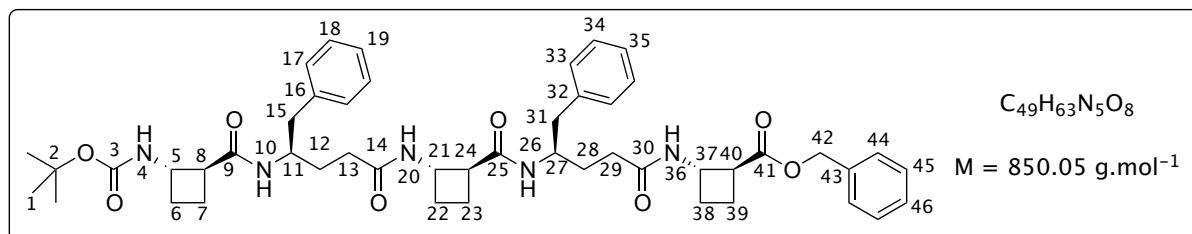
22'), 2.10-2.14 (m, 1H, H-23'), 2.21-2.53 (m, 1H, H-6'), 2.31-2.36 (m, 1H, H-29), 2.42 (dd,  $J = 13.8$  Hz, 7.0 Hz, 1H, H-15), 2.45-2.50 (m, 1H, H-29'), 2.52-2.56 (m, 1H, H-8), 2.62 (dd,  $J = 13.6$  Hz, 4.1 Hz, 1H, H-15'), 2.93-2.97 (m, 1H, H-24), 4.06 (bs, 2H, H-11, H-27), 4.23-4.28 (m, 1H, H-5), 4.44-4.52 (m, 3H, H-21, 2H-35), 5.06 (d,  $J = 6.8$  Hz, 1H, H-4), 5.54 (d,  $J = 10.3$  Hz, 1H, H-10), 6.99-7.40 (m, 10H, 2H-17, 2H-18, H-19, 2H-37, 2H-38, H-39), 7.65 (d,  $J = 9.2$  Hz, 1H, H-26), 7.81 (d,  $J = 9.5$  Hz, 1H, H-20), 8.29 (t,  $J = 5.6$  Hz, 1H, H-34).

$^{13}\text{C}$  NMR (100 MHz,  $\text{CDCl}_3$ )  $\delta$  15.7, 26.0 (C-13, C-23), 17.9 (C-7), 22.2, 23.2 (C-33, C-33'), 25.0 (C-32), 25.9 (C-6), 28.4 (C-1), 29.7, 30.0 (C-12, C-28), 31.7 (C-22), 33.6 (C-29), 41.6 (C-15), 43.4 (C-35), 44.3 (C-31), 46.7 (C-27), 47.3 (C-11), 48.2 (C-21), 48.8 (C-5), 49.7 (C-24), 50.7 (C-8), 80.4 (C-2), 126.6, 126.9, 128.1, 128.3, 128.4, 129.5 (C-17, C-18, C-19, C-37, C-38, C-39), 137.1, 139.4 (C-16, C-36), 155.3 (C-3), 171.4, 171.8, 172.4 (C-9, C-14, C-25), 174.1 (C-30).

IR (10 mmol/L, in  $\text{CDCl}_3$ )  $\nu_{\text{max}}$  1443, 1455, 1499, 1511, 1554, 1603, 1650, 1699, 2869, 2929, 2958, 3030, 3065, 3260, 3332 (br), 3431, 3443  $\text{cm}^{-1}$ .

HRMS (ESI):  $[\text{M}+\text{Na}]^+$ , 740.4350 found,  $\text{C}_{41}\text{H}_{59}\text{N}_5\text{NaO}_6$  740.4358 calcd.

#### Boc-(1*S*,2*S*)-ACBC-(*R*)- $\gamma^4$ -*h*Phe-(1*S*,2*S*)-ACBC-(*R*)- $\gamma^4$ -*h*Phe-(1*S*,2*S*)-ACBC-OBn (+) - [31]



According to the general procedure **C**, *tert*-butoxycarbonyl group of [37] (175 mg, 0.23 mmol) was fully removed in 2.5 h to give the corresponding TFA salt,  $\text{TFA} \cdot \text{H}_2\text{N}-(R)-\gamma^4$ -*h*Phe-(1*S*,2*S*)-ACBC-(*R*)- $\gamma^4$ -*h*Phe-(1*S*,2*S*)-ACBC-OBn.

According to the general procedure **D**, the coupling reaction was performed with Boc-(1*S*,2*S*)-ACBC-OH [2] (50 mg, 0.23 mmol), DIPEA (75  $\mu\text{L}$ , 53 mg, 0.46 mmol) and HATU (91 mg, 0.24 mmol) in a mixture of  $\text{CH}_2\text{Cl}_2$  / DMF (1 mL / 0.5 mL), and  $\text{TFA} \cdot \text{H}_2\text{N}-(R)-\gamma^4$ -*h*Phe-(1*S*,2*S*)-ACBC-(*R*)- $\gamma^4$ -*h*Phe-(1*S*,2*S*)-ACBC-OBn, DIPEA (215  $\mu\text{L}$ , 164 mg, 1.38 mmol) in  $\text{CH}_2\text{Cl}_2$  (1 mL) for 3 d. The purification was carried out by flash chromatography (gradient from 0 / 100 to 10 / 90 :  $\text{CH}_3\text{OH}$  /  $\text{CH}_2\text{Cl}_2$ ) to give [31] as a pale yellow sticky solid (85 mg, 44%).

$R_f$  0.65 (CH<sub>3</sub>OH / CH<sub>2</sub>Cl<sub>2</sub> = 10 / 90)

$[\alpha]_D^{22} = +32$  (c. 0.50 in CH<sub>3</sub>OH)

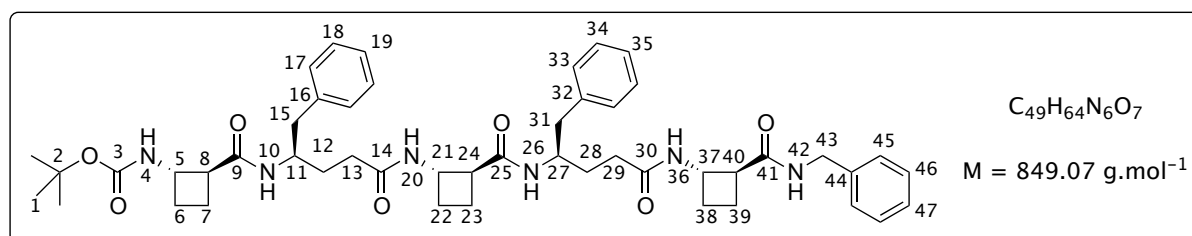
**<sup>1</sup>H NMR** (600 MHz, CDCl<sub>3</sub>)  $\delta$  1.36-1.44 (m, 13H, 9H-1, 2H-12, 2H-28), 1.68-1.71 (m, 1H, H-23), 1.81-1.84 (m, 1H, H-7), 1.87-1.94 (m, 3H, H-6, H-7', H-22), 1.99-2.07 (m, 4H, H-29, 2H-38, H-39), 2.08-2.25 (m, 6H, H-6', 2H-13, H-22', H-23', H-29'), 2.37-2.41 (m, 1H, H-38'), 2.56-2.62 (m, 3H, H-8, H-15, H-31), 2.69-2.74 (m, 2H, H-15', H-31'), 2.94-2.99 (m, 1H, H-24), 3.18-3.22 (m, 1H, H-40), 4.15 (bs, 1H, H-11), 4.20-4.23 (m, 1H, H-27), 4.29-4.32 (m, 1H, H-5), 4.49-4.52 (m, 1H, H-21), 4.60-4.62 (m, 1H, H-37), 5.12 (d,  $J = 12.8$  Hz, 1H, H-42), 5.16 (d,  $J = 12.6$  Hz, 1H, H-42'), 5.8 (d,  $J = 7.5$  Hz, 1H, H-4), 6.28 (d,  $J = 9.4$  Hz, 1H, H-10), 7.08-7.36 (m, 15H, 2H-17, 2H-18, H-19, 2H-33, 2H-34, H-35, 2H-44, 2H-45, H-46), 7.88 (d,  $J = 9.3$  Hz, 1H, H-26), 7.99 (d,  $J = 9.6$  Hz, 1H, H-20), 8.33 (d,  $J = 7.3$  Hz, 1H, H-36).

**<sup>13</sup>C NMR** (100 MHz, CDCl<sub>3</sub>)  $\delta$  14.3 (C-23), 16.8 (C-7), 17.9 (C-39), 24.7 (C-6), 25.2 (C-22), 25.7 (C-29), 27.7 (C-1), 29.3 (C-12, C-28), 31.0 (C-13), 32.3 (C-6, C-22), 32.7 (C-38), 40.1 (C-32), 41.2 (C-15), 46.1 (C-40), 46.8 (C-37), 46.7 (C-11), 47.2 (C-21), 47.9 (C-5), 48.3 (C-24), 48.9 (C-8), 49.0 (C-27), 65.1 (C-42), 78.5 (C-2), 125.1, 125.4, 127.0, 127.1, 127.2, 127.3, 127.6, 128.5, 128.7 (C-17, C-18, C-19, C-33, C-34, C-35, C-44, C-45, C-46), 135.4, 137.2, 138.4 (C-16, C-32, C-43), 156.8 (C-3), 170.6 (C-14), 171.3 (C-25), 171.4 (C-9), 172.3 (C-30, C-41).

**IR** (10 mmol/L, in CDCl<sub>3</sub>)  $\nu_{\max}$  1443, 1455, 1497, 1512, 1555, 1603, 1650, 1698, 1724, 2870, 2980, 3031, 367, 3086, 3329 (br), 3428, 3443 cm<sup>-1</sup>.

**HRMS (ESI):** [M+Na]<sup>+</sup>, 872.4528 found, C<sub>49</sub>H<sub>63</sub>N<sub>5</sub>NaO<sub>8</sub> 872.4574 calcd.

**Boc-(1*S*,2*S*)-ACBC-(*R*)- $\gamma^4$ -hPhe-(1*S*,2*S*)-ACBC-(*R*)- $\gamma^4$ -hPhe-(1*S*,2*S*)-ACBC-NHBn (+) - [32]**



According to the general procedure A, benzyl ester of [31] (26 mg, 0.030 mmol) was hydrolysed in 24 h to give the corresponding carboxylic acid, Boc-(1*S*,2*S*)-ACBC-(*R*)- $\gamma^4$ -hPhe-(1*S*,2*S*)-ACBC-(*R*)- $\gamma^4$ -hPhe-(1*S*,2*S*)-ACBC-OH (21 mg, 92% crude yield).

According to the general procedure **D**, the coupling reaction was performed with Boc-(1*S*,2*S*)-ACBC-(*R*)- $\gamma^4$ -*h*Phe-(1*S*,2*S*)-ACBC-(*R*)- $\gamma^4$ -*h*Phe-(1*S*,2*S*)-ACBC-OH (21 mg, 0.027 mmol), DIPEA (8  $\mu$ L, 6 mg, 0.054 mmol) and HATU (11 mg, 0.029 mmol) in a mixture of CH<sub>2</sub>Cl<sub>2</sub> / DMF (1 mL / 0.5 mL), and benzylamine (7  $\mu$ L, 7 mg, 0.068 mmol), DIPEA (25  $\mu$ L, 19 mg, 0.162 mmol) for 3 d. The purification was carried out by flash chromatography (gradient from 10 / 90 to 100 / 0 : EtOAc / PE then from 0 / 100 to 10 / 90 : CH<sub>3</sub>OH / CH<sub>2</sub>Cl<sub>2</sub>) to give [32] as a yellow sticky solid (17 mg, 74%).

**R<sub>f</sub>** 0.63 (CH<sub>3</sub>OH / CH<sub>2</sub>Cl<sub>2</sub> = 10 / 90)

**[ $\alpha$ ]<sub>D</sub><sup>27</sup>** = + 20 (c. 0.50 in CH<sub>3</sub>OH)

**<sup>1</sup>H NMR** (600 MHz, CDCl<sub>3</sub>)  $\delta$  1.27-1.43 (m, 13H, 9H-1, 2H-12, 2H-28), 1.67-1.72 (m, 1H, H-7), 1.83-1.90 (m, 2H, H-6, H-7'), 1.98-2.32 (m, 13H, H-6', H-13, H-13', H-22, H-22', 2H-23, H-29, H-29', H-38, H-38', H-39, H-39'), 2.47 (dd, *J* = 13.8 Hz, *J* = 7.3 Hz, 1H, H-32), 2.56 (dd, *J* = 13.6 Hz, *J* = 5.5 Hz, 1H, H-32'), 2.63-2.77 (m, 3H, H-8, 2H-15), 2.93-2.97 (m, 1H, H-24), 3.12-3.16 (m, 1H, H-40), 4.15 (m, 2H, H-11, H-27), 4.26-4.30 (m, 1H, H-5), 4.37-4.38 (m, 1H, H-43), 4.40-4.41 (m, 1H, H-37), 4.43-4.46 (m, 1H, H-21), 4.63 (dd, *J* = 15.3 Hz, *J* = 5.9 Hz, 1H, H-43'), 5.88 (bs, 1H, H-4), 6.42 (bs, 1H, H-10), 7.01-7.38 (m, 15H, 2H-17, 2H-18, H-19, 2H-34, 2H-35, H-36, 2H-45, 2H-46, H-47), 7.8 (d, *J* = 6.5 Hz, 1H, H-26), 8.06 (d, *J* = 8.9 Hz, 1H, H-20), 8.56 (bs, 1H, H-31), 9.16 (bs, 1H, H-42).

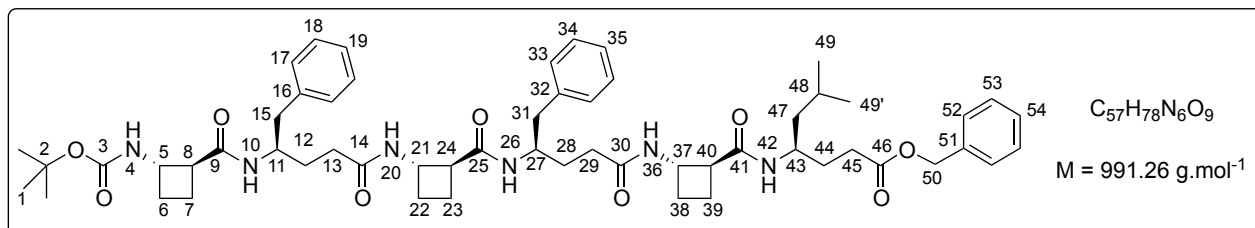
**<sup>13</sup>C NMR** (100 MHz, CDCl<sub>3</sub>)  $\delta$  15.7 (C-23), 17.6 (C-7), 18.0 (C-39), 24.6 (C-6), 25.8 (C-22), 26.1 (C-29), 28.4 (C-1), 28.5 (C-12), 29.7 (C-28), 29.7 (C-13), 30 (C-6), 31.2 (C-22), 32.7 (C-38), 41.7 (C-32), 42.0 (C-15), 43.0 (C-46), 47.4 (C-37), 48.1 (C-11), 48.2 (C-21), 48.5 (C-5), 48.9 (C-24), 49.5 (C-8), 49.7 (C-27), 70.5 (C-43), 80 (C-2), 126.0, 126.5, 126.8, 127.4, 128.0, 128.3, 128.4, 129.4, (C-17, C-18, C-19, C-33, C-34, C-35, C-45, C-46, C-47), 137.5, 138.5, 139.2 (C-16, C-32, C-44), 155.6 (C-3), 171.6, 172.1, 172.4, 173.8, 173.9 (C-9, C-14, C-25, C-30, C-41).

**IR** (10 mmol/L, in CDCl<sub>3</sub>)  $\nu_{\max}$  1443, 1455, 1497, 1512, 1554, 1603, 1650, 1698, 2858, 2930, 2956, 3031, 3066, 3320 (br), 3429, 3443 cm<sup>-1</sup>.

**HRMS (ESI)**: [M+Na]<sup>+</sup>, 871.4577 found, C<sub>49</sub>H<sub>64</sub>N<sub>6</sub>NaO<sub>7</sub> 871.4729 calcd.



**Boc-(1*S*,2*S*)-ACBC-(*R*)- $\gamma^4$ -*h*Phe-(1*S*,2*S*)-ACBC-(*R*)- $\gamma^4$ -*h*Phe-(1*S*,2*S*)-ACBC-(*R*)- $\gamma^4$ -*h*Leu-OBn (+) - [33]**



According to the general procedure **A**, benzyl ester of [35] (125 mg, 0.22 mmol) was hydrolysed in 3 h to give the corresponding carboxylic acid, Boc-(1*S*,2*S*)-ACBC-(*R*)- $\gamma^4$ -*h*Phe-(1*S*,2*S*)-ACBC-OH (107 mg, 100% crude yield).

According to the general procedure **C**, *tert*-butoxycarbonyl group of [23] (186 mg, 0.30 mmol) was fully removed in 1.2 h to give the corresponding TFA salt, TFA·H<sub>2</sub>N-(*R*)- $\gamma^4$ -*h*Phe-(1*S*,2*S*)-ACBC-(*R*)- $\gamma^4$ -*h*Leu-OBn.

According to the general procedure **D**, the coupling reaction was performed with Boc-(1*S*,2*S*)-ACBC-(*R*)- $\gamma^4$ -*h*Phe-(1*S*,2*S*)-ACBC-OH (107 mg, 0.22 mmol), DIPEA (75  $\mu$ L, 57 mg, 0.44 mmol) and HATU (87 mg, 0.23 mmol) in a mixture of CH<sub>2</sub>Cl<sub>2</sub> / DMF (2 mL / 1 mL), and TFA·H<sub>2</sub>N-(*R*)- $\gamma^4$ -*h*Phe-(1*S*,2*S*)-ACBC-(*R*)- $\gamma^4$ -*h*Leu-OBn, DIPEA (375  $\mu$ L, 234 mg, 2.20 mmol) in CH<sub>2</sub>Cl<sub>2</sub> (2 mL) overnight. The purification was carried out by flash chromatography (gradient from 10 / 90 to 100 / 0 : EtOAc / PE) to give [33] as a white sticky solid (114 mg, 52%).

**R<sub>f</sub>** 0.56 (CH<sub>3</sub>OH / CH<sub>2</sub>Cl<sub>2</sub> = 10 / 90)

**[ $\alpha$ ]<sub>D</sub><sup>27</sup>** = + 36 (c. 0.50 in CHCl<sub>3</sub>)

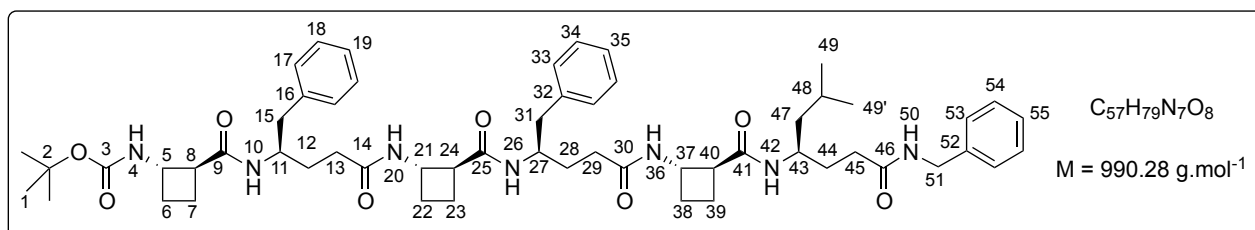
**<sup>1</sup>H NMR** (600 MHz, CDCl<sub>3</sub>)  $\delta$  0.79 (d, J = 6.1 Hz, 6H, 3H-49, 3H-49'), 1.11-1.16 (m, 1H, H-47), 1.29-1.37 (m, 14H, 9H-1, 2H-12, 2H-28, H-47'), 1.51-1.60 (m, 2H, H-23, H-48), 1.65-1.85 (m, 6H, H-6, 2H-7, H-38, 2H-44), 1.87-1.94 (m, 3H, H-22, H-38', H-39), 1.98-2.18 (m, 8H, H-6', 2H-13, H-22', H-23', 2H-29, H-39'), 2.44-2.51 (m, 3H, H-31, 2H-45), 2.55-2.62 (m, 3H, 2H-15, H-31'), 2.67-2.71 (m, 1H, H-8), 2.84-2.89 (m, 2H, H-24, H-40), 3.90 (bs, 1H, H-43), 4.00 (bs, 1H, H-11), 4.09 (bs, 1H, H-27), 4.16-4.22 (m, 2H, H-5, H-37), 4.33-4.38 (m, 1H, H-21), 5.04 (m, 2H, H-50), 6.40 (d, J = 7.9 Hz, 1H, H-4), 6.91 (d, J = 9.4 Hz, 1H, H-10), 6.98-7.28 (m, 15H, 2H-17, 2H-18, H-19, 2H-33, 2H-34, H-35, 2H-52, 2H-53, H-54), 7.74 (d, J = 9.9 Hz, 1H, H-26), 8.04 (d, J = 9.9 Hz, 1H, H-20), 8.29 (d, J = 8.8 Hz, 1H, H-42), 8.39 (d, J = 6.6 Hz, 1H, H-36).

**$^{13}\text{C}$  NMR** (100 MHz,  $\text{CDCl}_3$ )  $\delta$  15.2 (C-23), 17.4 (C-7), 18.1 (C-39), 22.1, 23.1 (C-49, C-49'), 24.1 (C-22), 24.8 (C-48), 25.7 (C-6), 28.4 (C-1), 29.7 (C-12 or C-28, C-38), 30.8, 30.9 (C-44 or C-28, C-45), 31.5 (C-24), 31.7 (C-29), 32.7 (C-13), 41.4 (C-31), 42.0 (C-15), 43.8 (C-47), 46.4 (C-43), 47.2 (C-11), 47.8 (C-37), 47.9 (C-21), 48.6 (C-27), 48.7 (C-5), 49.2 (C-8), 49.9 (C-40), 66.0 (C-50), 79.6 (C-2), 125.8, 126.2, 127.9, 128.0, 128.1, 128.4, 129.2, 129.3 (C-17, C-18, C-19, C-33, C-34, C-35, C-52, C-53, C-54), 136.0, 137.6, 138.7 (C-16, C-32, C-51), 155.5 (C-3), 171.5 (C-14), 172.0 (C-9, C-25), 173.1 (C-41), 173.7 (C-30), 173.9 (C-46).

**IR** (10 mmol/L, in  $\text{CDCl}_3$ )  $\nu_{\text{max}}$  1455, 1498, 1514, 1558, 1602, 1649, 1698, 1735, 2876, 2932, 2959, 3028, 3068, 3330 (br), 3429, 3446  $\text{cm}^{-1}$ .

**HRMS (ESI):**  $[\text{M}+\text{Na}]^+$ , 1013.5743 found,  $\text{C}_{57}\text{H}_{78}\text{N}_6\text{NaO}_9$  1013.5722 calcd.

**Boc-(1*S*,2*S*)-ACBC-(*R*)- $\gamma^4$ -*h*Phe-(1*S*,2*S*)-ACBC-(*R*)- $\gamma^4$ -*h*Phe-(1*S*,2*S*)-ACBC-(*R*)- $\gamma^4$ -*h*Leu-NHBn (+) - [34]**



According to the general procedure **A**, benzyl ester of [33] (70 mg, 0.07 mmol) was hydrolysed in 24 h to give the corresponding carboxylic acid, Boc-(1*S*,2*S*)-ACBC-(*R*)- $\gamma^4$ -*h*Phe-(1*S*,2*S*)-ACBC-(*R*)- $\gamma^4$ -*h*Phe-(1*S*,2*S*)-ACBC-(*R*)- $\gamma^4$ -*h*Leu-OH (40 mg, 63% crude yield).

According to the general procedure **D**, the coupling reaction was performed with Boc-(1*S*,2*S*)-ACBC-(*R*)- $\gamma^4$ -*h*Phe-(1*S*,2*S*)-ACBC-(*R*)- $\gamma^4$ -*h*Phe-(1*S*,2*S*)-ACBC-(*R*)- $\gamma^4$ -*h*Leu-OH (40 mg, 0.044 mmol), DIPEA (15  $\mu\text{L}$ , 11 mg, 0.088 mmol) and HATU (17 mg, 0.046 mmol) in a mixture of  $\text{CH}_2\text{Cl}_2$  / DMF (1 mL / 1 mL), and benzylamine (5  $\mu\text{L}$ , 5 mg, 0.046 mmol, 1.05 eq), DIPEA (15  $\mu\text{L}$ , 11 mg, 0.88 mmol) overnight. The purification was carried out by flash chromatography (gradient from 10 / 90 to 100 / 0 : EtOAc / PE then from 0 / 100 to 10 / 90 :  $\text{CH}_3\text{OH}$  /  $\text{CH}_2\text{Cl}_2$ ) to give [34] as a pale yellow sticky solid (17 mg, 38%).

**$R_f$**  0.43 ( $\text{CH}_3\text{OH}$  /  $\text{CH}_2\text{Cl}_2$  = 10 / 90)

**$[\alpha]_D^{20}$**  = + 44 (c. 0.50 in  $\text{CHCl}_3$ )

**<sup>1</sup>H NMR** (600MHz, CDCl<sub>3</sub>/DMSO-d<sub>6</sub> (5/1)) δ 0.76 (d, J = 6.4 Hz, 3H, 3H-49), 0.79 (d, J = 6.4 Hz, 3H, 3H-49'), 1.06-1.13 (m, 3H, 2H-28, H-47), 1.24-1.31 (m, 3H, 2H-12, H-47'), 1.35 (s, 9H, 9H-1), 1.43-1.50 (m, 1H, H-44), 1.53-1.79 (m, 5H, H-6, H-7, H-23, H-39, H-48), 1.80-2.12 (m, 12H\*, H-6', H-7', 2H-13, 2H-22, H-23', 2H-29, 2H-38, 2H-39), 2.37 (dd, J = 13.5 Hz, 7.7 Hz, 1H, H-31), 2.44-2.51 (m, 4H, H-15, H-31', 2H-45), 2.59-2.65 (m, 2H, H-8, H-15'), 2.79-2.84 (m, 2H, H-24, H-40), 3.94 (bs, 1H, H-43), 4.03 (bs, 2H, H-11, H-27), 4.12-4.17 (m, 1H, H-5), 4.29-4.36 (m, 4H, H-21, H-37, 2H-51), 5.90 (d, J = 8.0 Hz, 1H, H-4), 6.29 (d, J = 9.9 Hz, 1H H-10), 6.95-7.29 (m, 15H, 2H-16, 2H-17, H-18, 2H-33, 2H-34, H-35, 2H-53, 2H-54, H-55), 7.49 (d, J = 9.8 Hz, 1H, H-26), 7.83 (d, J = 9.0 Hz, 1H, H-42), 7.99 (d, J = 9.6 Hz, 1H, H-20), 8.26 (d, J = 8.7 Hz, 1H, H-36), 8.41 (t, J = 5.7 Hz, 1H, H-50).

\*H-44 '

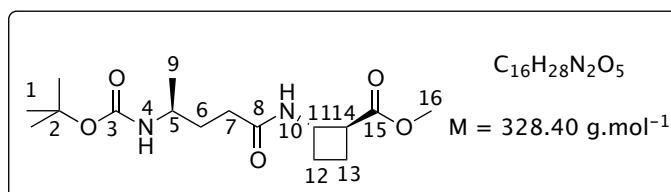
**<sup>13</sup>C NMR** (100 MHz, CDCl<sub>3</sub>/DMSO-d<sub>6</sub> (5/1)) δ 15.6, 15.9 (C-23, C-39), 17.4 (C-7), 22.3, 23.1 (C-49, C-49'), 24.8 (C-48), 25.6, 25.6 (C-22, C-38), 28.4 (C-1), 29.5, 29.5, 29.6 (C-6, C-12, C-28), 31.6, 31.8 (C-13, C-29), 33.4 (C-45), 33.6 (C-44), 41.7 (C-15), 42.1 (C-31), 43.2 (C-51), 44.0 (C-47), 46.7 (C-43), 46.9 (C-11), 47.5 (C-27), 47.8 (C-21, C-37), 48.0 (C-5), 48.9, 49.3 (C-24, C-40), 50.1 (C-8), 79.9 (C-2), 126.0, 126.4, 126.8, 127.8, 127.9, 128.1, 128.3, 129.4 (C-17, C-18, C-19, C-33, C-34, C-35, C-53, C-54, C-55), 137.3, 138.2, 139.2 (C-16, C-32, C-52), 155.5 (C-3), 171.5 (C-14), 171.6 (C-25), 172.0 (C-9), 172.1 (C-30), 172.4 (C-41), 174.3 (C-46).

**IR** (10 mmol/L, in CDCl<sub>3</sub>) ν<sub>max</sub> 1443, 1455, 1497, 1512, 1557, 1647, 1698, 2870, 2930, 2958, 3030, 3067, 3086, 3311 (br), 3429, 3443 cm<sup>-1</sup>.

**HRMS (ESI):** [M+Na]<sup>+</sup>, 1012.5841 found, C<sub>57</sub>H<sub>79</sub>N<sub>7</sub>NaO<sub>8</sub> 1012.5882 calcd.

## 2.3 Peptides containing (1*S*,2*S*)-ACBC, (*R*)- $\gamma^4$ -homologous amino acids and $\alpha$ -amino acids

### Boc-(*R*)- $\gamma^4$ -*h*Ala-(1*S*,2*S*)-ACBC-OMe (+) - [50]



To a solution of Boc-(1*S*,2*S*)-ACBC-OH [2] (150 mg, 0.70 mmol, 1 eq.) in CH<sub>3</sub>OH (5 mL) was slowly added an excess of TMSCl (267  $\mu$ L, 227 mg, 2.1 mmol, 3 eq.) under inert atmosphere. The reaction mixture was stirred overnight at room temperature. CH<sub>3</sub>OH and TMSCl were evaporated under reduced pressure to give a pale yellow solid, HCl·H<sub>2</sub>N-(1*S*,2*S*)-ACBC-OMe which was directly used in the coupling reaction.

According to the general procedure **D**, the coupling reaction was performed with Boc-(*R*)- $\gamma^4$ -*h*Ala-OH (152 mg, 0.70 mmol), DIPEA (245  $\mu$ L, 180 mg, 1.40 mmol) and HATU (276 mg, 0.70 mmol) in a mixture of CH<sub>2</sub>Cl<sub>2</sub> / DMF (3 mL / 1 mL); and HCl·H<sub>2</sub>N-(1*S*,2*S*)-ACBC-OMe, DIPEA (485  $\mu$ L, 361 mg, 2.80 mmol) in DMF (2 mL) for 3 d. The purification was carried out by flash chromatography (gradient from 10 / 90 to 80 / 20 : EtOAc / PE) to give [50] as a white sticky solid (166 mg, 72%).

$R_f$  0.53 (CH<sub>3</sub>OH / CH<sub>2</sub>Cl<sub>2</sub> = 10 / 90)

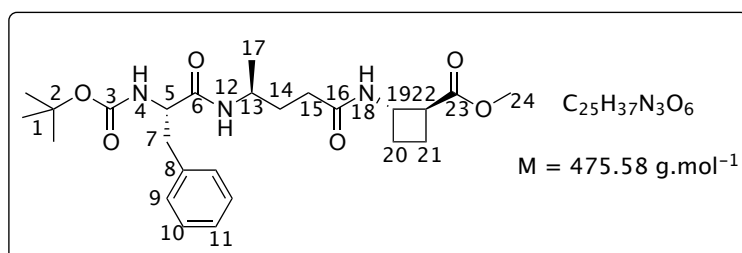
$[\alpha]_D^{25} = +16$  (c. 0.50 in CH<sub>3</sub>OH)

**<sup>1</sup>H NMR** (400 MHz, CDCl<sub>3</sub>)  $\delta$  1.10 (d,  $J = 6.4$  Hz, 3H, 3H-9), 1.40 (s, 9H, 9H-1), 1.68 (bs, 2H, 2H-6), 1.86-2.02 (m, 3H, 2H-13, H-12), 2.14-2.22 (m, 3H, 2H-7, H-12'), 3.03.09 (m, 1H, H-14), 3.64 (s, 4H, H-5, 3H-16), 4.47-4.55 (m, 1H, H-11), 4.59 (d,  $J = 8.4$  Hz, 1H, H-4), 7.09 (d,  $J = 4.9$  Hz, 1H, H-10).

**<sup>13</sup>C NMR** (100 MHz, CDCl<sub>3</sub>)  $\delta$  18.8 (C-13), 21.0 (C-9), 26.4 (C-12), 28.3 (C-1), 32.8 (C-7), 33.1 (C-6), 45.8 (C-5), 46.5 (C-14), 47.0 (C-11), 51.8 (C-16), 79.4 (C-2), 156.1 (C-3), 172.8 (C-8), 174.2 (C-15).

**IR** (10 mmol/L, in CDCl<sub>3</sub>)  $\nu_{\max}$  1438, 1453, 1508, 1669, 1695, 1727, 2874, 2955, 2981, 3307 (br), 3439 cm<sup>-1</sup>.

**HRMS (ESI):** [M+Na]<sup>+</sup>, 351.1908 found, C<sub>16</sub>H<sub>28</sub>N<sub>2</sub>NaO<sub>5</sub> 351.1890 calcd.

**Boc-Phe-(R)- $\gamma^4$ -hAla-(1S,2S)-ACBC-OMe - [52]**

According to the general procedure **C**, *tert*-butoxycarbonyl group of [50] (94 mg, 0.29 mmol) was fully removed in 1.2 h to give the corresponding TFA salt, TFA·H<sub>2</sub>N- $\gamma^4$ -hAla-(1S,2S)-ACBC-OMe.

To a solution of Boc-Phe-OH (77 mg, 0.29 mmol, 1 eq.) in CH<sub>2</sub>Cl<sub>2</sub> (1.5 mL) were added HOAt (39 mg, 0.29 mmol, 1 eq.) followed by EDCI·HCl (61 mg, 0.32 mmol, 1.1 eq.) at 0 °C under inert atmosphere. After 15 min of activation, a solution of TFA·H<sub>2</sub>N- $\gamma^4$ -hAla-(1S,2S)-ACBC-OMe and DIPEA (182  $\mu$ L, 138 mg, 1.16 mmol, 4 eq.) in a mixture of CH<sub>2</sub>Cl<sub>2</sub> / DMF (2 / 0.5 mL) was added to the reaction mixture. The reaction was stirred overnight at room temperature. After such time, the reaction mixture was washed with a saturated solution of NaHCO<sub>3</sub>, HCl (1 M) and H<sub>2</sub>O, dried over Na<sub>2</sub>SO<sub>4</sub> and filtered. Solvents were evaporated under reduced pressure. The crude residue was purified by flash chromatography (gradient from 10 / 90 to 60 / 40 : EtOAc / PE) to give [52] (80 mg, 55%).

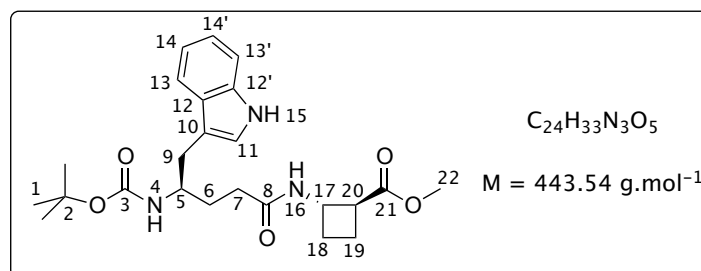
**R<sub>f</sub>** 0.59 (CH<sub>3</sub>OH / CH<sub>2</sub>Cl<sub>2</sub> = 10 / 90)

**<sup>1</sup>H NMR** (250 MHz, CDCl<sub>3</sub>)  $\delta$  1.08 (d, *J* = 6.4 Hz, 3H, 3H-17), 1.42 (s, 9H, 9H-1), 1.50-1.58 (m, 2H, 2H-14), 1.68-2.03 (m, 5H, H-15, H-15', H-20, 2H-21), 2.18-2.32 (m, 1H, H-20'), 3.06 (d, *J* = 6.8 Hz, 2H, 2H-7), 2.11-2.18 (m, 1H, H-22), 3.67 (s, 3H, 3H-24), 3.86 (bs, 1H, H-13), 4.29 (td, *J* = 7.1 Hz, *J* = 6.8 Hz, 1H, H-5), 4.44-4.57 (m, 1H, H-19), 5.14 (d, *J* = 7.1 Hz, 1H, H-4), 6.12 (d, *J* = 6.5 Hz, 1H, H-12), 7.11 (bs, 1H, H-18), 7.21-7.34 (m, 5H, 2H-9, 2H-10, H-11).

**<sup>13</sup>C NMR** (62.5 MHz, CDCl<sub>3</sub>)  $\delta$  18.4 (C-21), 21.0 (C-17), 27.0 (C-20), 28.3 (C-1), 32.8, 32.9 (C-14, C-15), 38.2 (C-7), 44.8 (C-13), 46.6 (C-22), 47.6 (C-19), 51.8 (C-24), 56.3 (C-5), 80.6 (C-2), 127.1, 128.7, 129.3 (C-9, C-10, C-11), 136.5 (C-8), 155.6 (C-3), 171.2, 172.0 (C-6, C-16), 173.5 (C-23).

**IR** (10 mmol/L, in CDCl<sub>3</sub>)  $\nu_{\text{max}}$  1495, 1522, 1669, 1715, 1723, 2878, 2951, 2982, 3069, 3304, 3353 (br), 3424 cm<sup>-1</sup>.

**HRMS (ESI):** [M+Na]<sup>+</sup>, 498.2594 found, C<sub>25</sub>H<sub>37</sub>N<sub>3</sub>NaO<sub>6</sub> 498.2575 calcd.

**Boc-(*R*)- $\gamma^4$ -*h*Trp-(1*S*,2*S*)-ACBC-OMe (+) - [51]**

To a solution of Boc-(1*S*,2*S*)-ACBC-OH [2] (150 mg, 0.70 mmol, 1 eq.) in CH<sub>3</sub>OH (5 mL) was slowly added an excess of TMSCl (267  $\mu$ L, 227 mg, 2.1 mmol, 3 eq.) under inert atmosphere. The reaction mixture was stirred overnight at room temperature. CH<sub>3</sub>OH and TMSCl were evaporated under reduced pressure to give a pale yellow solid, HCl·H<sub>2</sub>N-(1*S*,2*S*)-ACBC-OMe which was directly used in the coupling reaction.

According to the general procedure **D**, the coupling reaction was performed with Boc-(*R*)- $\gamma^4$ -*h*Trp-OH (156 mg, 0.47 mmol), DIPEA (165  $\mu$ L, 121 mg, 0.94 mmol) and HATU (185 mg, 0.49 mmol) in a mixture of CH<sub>2</sub>Cl<sub>2</sub> / DMF (1 mL / 1 mL); and HCl·H<sub>2</sub>N-(1*S*,2*S*)-ACBC-OMe, DIPEA (165  $\mu$ L, 121 mg, 0.94 mmol) in DMF (2 mL) overnight. The purification was carried out by flash chromatography (gradient from 10 / 90 to 80 / 20 : EtOAc / PE) to give [51] as a white sticky solid (170 mg, 81%).

$R_f$  0.55 (CH<sub>3</sub>OH / CH<sub>2</sub>Cl<sub>2</sub> = 10 / 90)

$[\alpha]_D^{26} = +14$  (c. 0.50 in CH<sub>3</sub>OH)

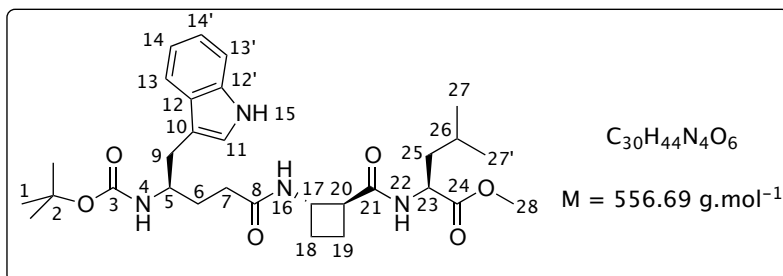
**<sup>1</sup>H NMR** (360 MHz, CDCl<sub>3</sub>)  $\delta$  1.43 (s, 9H, 9H-1), 1.62 (bs, 2H, 2H-6), 1.86-2.20 (m, 6H, 2H-7, 2H-18, 2H-19), 2.89 (d,  $J = 6.6$  Hz, 2H, 2H-9), 3.00-3.04 (m, 1H, H-20), 3.62 (s, 3H, 3H-22), 3.92 (bs, 1H, H-5), 4.45-4.54 (m, 1H, H-17), 4.72 (d,  $J = 9.6$  Hz, 1H, H-4), 6.88 (d,  $J = 7.1$  Hz, 1H, H-16), 6.96 (s, 1H, H-11), 7.10 (t,  $J = 7.7$  Hz, 1H, H-14), 7.17 (t,  $J = 7.2$  Hz, 1H, H-14'), 7.35 (d,  $J = 7.8$  Hz, 1H, H-13), 7.59 (d,  $J = 7.8$  Hz, 1H, H-13'), 8.67 (bs, 1H, H-15).

**<sup>13</sup>C NMR** (90 MHz, CDCl<sub>3</sub>)  $\delta$  18.8 (C-7), 26.5 (C-18), 28.4 (C-1), 30.7, 31.1 (C-6, C-9), 33.1 (C-19), 46.6 (C-20), 47.2 (C-17), 50.4 (C-5), 51.9 (C-22), 79.5 (C-2), 111.2 (C-12), 111.3 (C-13), 118.8 (C-13'), 119.3 (C-14), 121.8 (C-14'), 123.0 (C-11), 127.8, 136.3 (C-10, C-12'), 156.5 (C-3), 172.9 (C-8), 174.0 (C-21).

**IR** (10 mmol/L, in CDCl<sub>3</sub>)  $\nu_{\max}$  1439, 1457, 1505, 1669, 1696, 1725, 2869, 2954, 2981, 3058, 3310 (br), 3436, 3480 cm<sup>-1</sup>.

**HRMS (ESI):**  $[M+Na]^+$ , 466.2309 found,  $C_{24}H_{33}N_3NaO_5$  466.2312 calcd.

**Boc-(*R*)- $\gamma^4$ -*h*Trp-(1*S*,2*S*)-ACBC-Leu-OMe (+) - [53]**



According to the general procedure **B**, methyl ester of [51] (193 mg, 0.44 mmol) was hydrolysed to give the corresponding carboxylic acid, Boc-(*R*)- $\gamma^4$ -*h*Trp-(1*S*,2*S*)-ACBC-OH (176 mg, 94 % crude yield).

According to the general procedure **D**, the coupling reaction was performed with Boc-(*R*)- $\gamma^4$ -*h*Trp-(1*S*,2*S*)-ACBC-OH (176 mg, 0.41 mmol), DIPEA (144  $\mu$ L, 107 mg, 0.83 mmol) and HATU (161 mg, 0.43 mmol) in a mixture of  $CH_2Cl_2$  / DMF (2 mL / 1 mL), and  $H_2N$ -Leu-OMe (98 mg, 0.50 mmol), DIPEA (85  $\mu$ L, 63 mg, 0.49 mmol) overnight. The purification was carried out by flash chromatography (gradient from 10 / 90 to 100 / 0 : EtOAc / PE) to give [53] as a white foam (123 mg, 54%).

$R_f$  0.53 ( $CH_3OH$  /  $CH_2Cl_2$  = 10 / 90)

$[\alpha]_D^{25} = +5$  (c. 0.50 in  $CH_3OH$ )

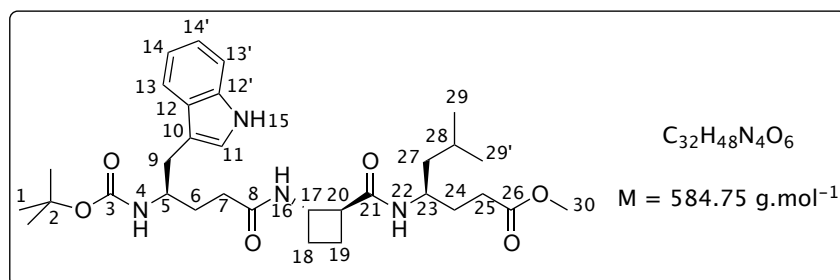
**$^1H$  NMR** (250 MHz,  $CDCl_3$ )  $\delta$  0.90 (d,  $J = 5.7$  Hz, 3H, 3H-27), 0.93 (d,  $J = 6.1$  Hz, 3H, H-27'), 1.45 (s, 9H, 9H-1), 1.62-1.65 (m, 4H, 2H-6, H-25, H-26), 1.82-2.08 (m, 5H, H-7, H-18, 2H-19, H-25'), 2.13-2.27 (m, 2H, H-7', H-18'), 2.89-2.96 (m, 3H, 2H-9, H-20), 3.71 (s, 3H, 3H-28), 3.95 (bs, 1H, H-5), 4.35-4.41 (m, 1H, H-17), 4.47-4.55 (m, 1H, H-23), 4.78 (d,  $J = 8.7$  Hz, 1H, H-4), 6.99 (s, 1H, H-11), 7.07-7.24 (m, 3H, H-14, H-14', H-16), 7.36 (d,  $J = 8.6$  Hz, 1H, H-13), 7.57 (d,  $J = 7.9$  Hz, 1H, H-13'), 8.72 (d,  $J = 6.5$  Hz, H-22), 8.88 (s, 1H, H-15)

**$^{13}C$  NMR** (62.5 MHz,  $CDCl_3$ )  $\delta$  18.4 (C-19), 21.8, 22.9 (C-27, C-27'), 24.4 (C-18), 24.9 (C-26), 28.4 (C-1), 31.1, 31.3 (C-9, C-25), 32.9 (C-7), 40.5 (C-6), 48.0 (C-17), 49.2 (C-20), 50.2 (C-5), 51.0 (C-23), 52.2 (C-28), 79.7 (C-2), 111.0 (C-12), 111.4 (C-13), 118.7 (C-13'), 119.3 (C-14), 121.9 (C-14'), 123.0 (C-11), 127.8, 136.4 (C-10, C-12'), 156.6 (C-3), 173.5, 173.8, 173.9 (C-8, C-21, C-24)

**IR** (10 mmol/L, in CDCl<sub>3</sub>)  $\nu_{\max}$  1440, 1456, 1506, 1552, 1657, 1692, 1741, 2873, 2932, 2959, 3208, 3267 (br), 3435, 3479 cm<sup>-1</sup>.

**HRMS (ESI):** [M+Na]<sup>+</sup>, 579.3154 found, C<sub>30</sub>H<sub>44</sub>N<sub>4</sub>NaO<sub>6</sub> 579.3153 calcd.

**Boc-(R)- $\gamma^4$ -*h*Trp-(1*S*,2*S*)-ACBC-(R)- $\gamma^4$ -*h*Leu-OMe (+) - [54]**



According to the general procedure **B**, methyl ester of [51] (144 mg, 0.33 mmol) was hydrolysed to give the corresponding carboxylic acid, Boc-(R)- $\gamma^4$ -*h*Trp-(1*S*,2*S*)-ACBC-OH (142 mg, 100% crude yield).

According to the general procedure **D**, the coupling reaction was performed with Boc-(R)- $\gamma^4$ -*h*Trp-(1*S*,2*S*)-ACBC-OH (142 mg, 0.33 mmol), DIPEA (115  $\mu$ L, 85 mg, 0.66 mmol) and HATU (130 mg, 0.35 mmol) in a mixture of CH<sub>2</sub>Cl<sub>2</sub> / DMF (2 mL / 1 mL), and H<sub>2</sub>N-(R)- $\gamma^4$ -*h*Leu-OMe (98 mg, 0.50 mmol), DIPEA (170  $\mu$ L, 127 mg, 0.99 mmol) in DMF (2 mL) overnight. The purification was carried out by flash chromatography (gradient from 10 / 90 to 100 / 0 : EtOAc / PE) to give [54] as a white foam (150 mg, 78%).

$R_f$  0.50 (CH<sub>3</sub>OH / CH<sub>2</sub>Cl<sub>2</sub> = 10 / 90)

$[\alpha]_D^{26} = +5$  (c. 0.50 in CH<sub>3</sub>OH)

**<sup>1</sup>H NMR** (600 MHz, CDCl<sub>3</sub>)  $\delta$  0.85 (d,  $J = 6.4$  Hz, 3H, 3H-29), 0.87 (d,  $J = 6.7$  Hz, 3H, 3H-29'), 1.19-1.23 (m, 1H, H-27), 1.33-1.39 (m, 1H, H-27'), 1.43 (s, 9H, 9H-1), 1.51-1.55 (m, 1H, H-28), 1.58-1.62 (m, 2H, 2H-6), 1.68-1.72 (m, 1H, H-24), 1.84-1.96 (m, 3H, H-18, H-19, H-24'), 2.01-2.06 (m, 1H, H-19'), 2.12-2.17 (m, 2H, H-7, H-18'), 2.20-2.24 (m, 1H, H-7'), 2.37-2.40 (m, 2H, 2H-25), 2.81-2.86 (m, 1H, H-20), 2.91-2.92 (m, 2H, 2H-9), 3.65 (s, 3H, 3H-30), 3.92-3.97 (m, 2H, H-5, H-23), 4.28-4.33 (m, 1H, H-17), 4.69 (d,  $J = 9.2$  Hz, 1H, H-4), 7.02 (s, 1H, H-11), 7.08 (d,  $J = 7.4$  Hz, 1H, H-16), 7.11, 7.18 (2t,  $J = 6.9$  Hz,  $J = 8.0$  Hz, 2H, H-14, H-14'), 7.37, 7.57 (2d,  $J = 8.5$  Hz,  $d = 7.57$ , 2H, H-13, H-13'), 7.72 (d,  $J = 8.7$  Hz, 1H, H-22), 8.62 (s, 1H, H-15).

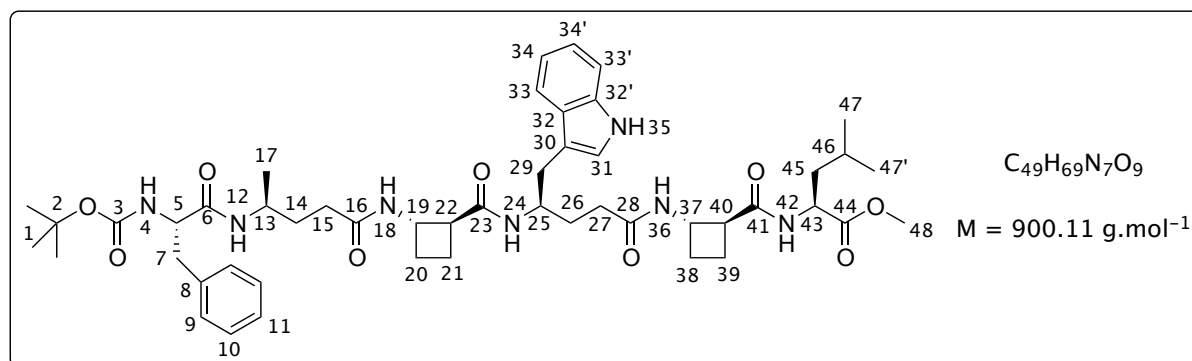


**$^{13}\text{C}$  NMR** (62.5 MHz,  $\text{CDCl}_3$ )  $\delta$  18.6 (C-19), 22.2, 23.1 (C-29, C-29'), 24.5 (C-6), 25.0 (C-28), 28.4 (C-1), 30.8, 30.9, 31.0 (C-9, C-18, C-24, C-25), 32.8 (C-7), 43.9 (C-27), 46.6 (C-23), 47.6 (C-17), 49.7 (C-20), 50.1 (C-5), 51.7 (C-30), 79.6 (C-2), 111.0 (C-10), 111.4, 118.7 (C-13, C-13'), 119.3, 121.8 (C-14, C-14'), 123.1 (C-11), 127.8, 136.4 (C-12, C-12'), 156.5 (C-3), 173.1, 173.9, 174.7 (C-8, C-21, C-26).

**IR** (10 mmol/L, in  $\text{CDCl}_3$ )  $\nu_{\text{max}}$  1439, 1456, 1505, 1556, 1649, 1693, 1729, 2868, 2937, 2957, 3065, 3268 (br), 3434, 3480  $\text{cm}^{-1}$ .

**HRMS (ESI):**  $[\text{M}+\text{Na}]^+$ , 607.3486 found,  $\text{C}_{32}\text{H}_{48}\text{N}_4\text{NaO}_6$  607.3466 calcd.

**Boc-Phe-(*R*)- $\gamma^4$ -*h*Ala-(1*S*,2*S*)-ACBC-(*R*)- $\gamma^4$ -*h*Trp-(1*S*,2*S*)-ACBC-Leu-OMe (+) - [43]**



According to the general procedure **B**, methyl ester of [52] (109 mg, 0.23 mmol) was hydrolysed to give the corresponding carboxylic acid, Boc-Phe-(*R*)- $\gamma^4$ -*h*Ala-(1*S*,2*S*)-ACBC-OH (100 mg, 91% crude yield).

According to the general procedure **C**, *tert*-butoxycarbonyl group of [53] (115 mg, 0.21 mmol) was fully removed in 2.5 h to give the corresponding TFA salt,  $\text{TFA}\cdot\text{H}_2\text{N}$ -(*R*)- $\gamma^4$ -*h*Trp-(1*S*,2*S*)-ACBC-Leu-OMe.

According to the general procedure **D**, the coupling reaction was performed with Boc-Phe-(*R*)- $\gamma^4$ -*h*Ala-(1*S*,2*S*)-ACBC-OH (100 mg, 0.21 mmol), DIPEA (73  $\mu\text{L}$ , 54 mg, 0.42 mmol) and HATU (83 mg, 0.22 mmol) in a mixture of  $\text{CH}_2\text{Cl}_2$  / DMF (2 mL / 1 mL), and  $\text{TFA}\cdot\text{H}_2\text{N}$ -(*R*)- $\gamma^4$ -*h*Trp-(1*S*,2*S*)-ACBC-Leu-OMe, DIPEA (145  $\mu\text{L}$ , 108 mg, 0.84 mmol) in DMF (2 mL) overnight. The purification was carried out by flash chromatography (gradient from 10 / 90 to 100 / 0 : EtOAc / PE then from 0 / 100 to 20 / 80 :  $\text{CH}_3\text{OH}$  /  $\text{CH}_2\text{Cl}_2$ ) to give [43] as an orange sticky solid (122 mg, 68%).

The compound was further purified using mass directed preparative HPLC (gradient from 5/95 to 95/5 of 0.1% formic acid water/methanol) to afford [43] with purity higher than 99%.

$R_f$  0.47 (CH<sub>3</sub>OH / CH<sub>2</sub>Cl<sub>2</sub> = 10 / 90)

$[\alpha]_D^{26} = +24$  (c. 0.50 in CH<sub>3</sub>OH)

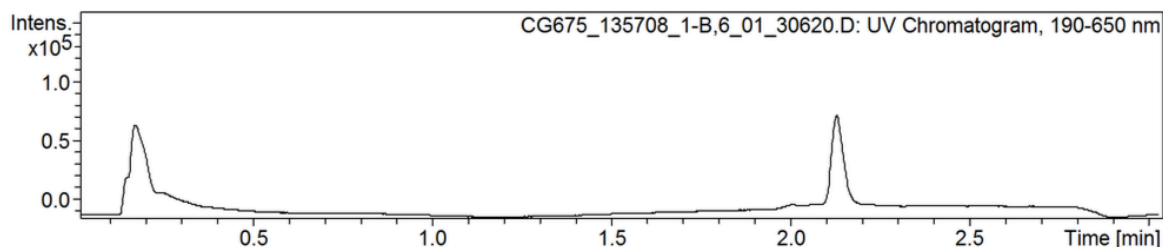
**<sup>1</sup>H NMR** (600 MHz, CDCl<sub>3</sub>)  $\delta$  0.87 (d,  $J$  = 6.4 Hz, 3H, 3H-47), 0.88 (d,  $J$  = 6.5 Hz, 3H, 3H-47'), 1.03 (d,  $J$  = 6.2 Hz, 3H, 3H-17), 1.37-1.45 (m, 2H, 2H-14), 1.46 (s, 9H, 9H-1), 1.49-1.70 (m, 7H, 2H-26, H-21, H-39, 2H-45, H-46), 1.86-1.92 (m, 2H, H-15, H-20), 1.99-2.17 (m, 6H, H-15', H-20', H-21', 2H-38, H-39'), 2.21-2.26 (m, 2H, 2H-27), 2.74-2.79 (m, 1H, H-22), 2.93 (dd,  $J$  = 5.6 Hz,  $J$  = 5.4 Hz, 2H, 2H-29), 3.06-3.13 (m, 3H, 2H-7, H-40), 3.71 (s, 3H, 3H-48), 3.85 (bs, 1H, H-13), 4.24-4.27 (m, 1H, H-5), 4.54-4.39 (m, 1H, H-25), 4.42-4.53 (m, 3H, H-19, H-37, H-43), 5.15 (d,  $J$  = 4.1 Hz, 1H, H-4), 6.02 (d,  $J$  = 10.4 Hz, 1H, H-12), 7.05-7.38 (m, 10H, 2H-9, 2H-10, H-11, H-18, H-33, H-33', H-34, H-34'), 7.45 (d,  $J$  = 8.1 Hz, 1H, H-24), 7.62 (d,  $J$  = 7.8 Hz, 1H, H-31), 8.17 (d,  $J$  = 6.5, 1H, H-36), 8.24 (s, 1H, H-35), 9.03 (d,  $J$  = 8.1 Hz, 1H, H-42).

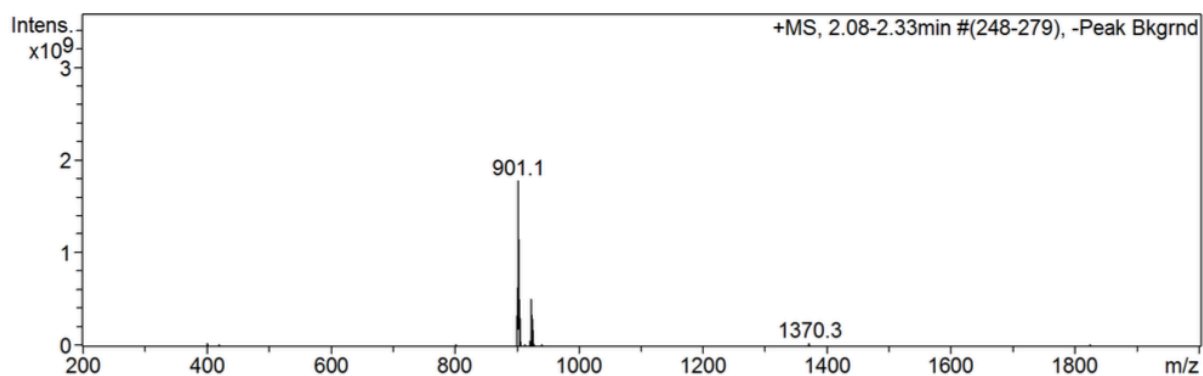
**<sup>13</sup>C NMR** (100 MHz, CDCl<sub>3</sub>)  $\delta$  16.0 (C-21), 17.8 (C-39), 21.5 (C-17), 21.7, 23.0 (C-47, C-47'), 24.5 (C-38), 24.9 (C-46), 26.0 (C-20), 28.4 (C-1), 31.4 (C-14, C-29), 31.9 (C-26), 32.6 (C-15, C-27), 37.3 (C-7), 40.3 (C-45), 43.3 (C-13), 48.0 (C-19, C-37), 48.2 (C-25), 49.4 (C-40), 49.9 (C-22), 51.1 (C-43), 52.0 (C-48), 56.9 (C-5), 81.6 (C-2), 111.1, 112.4, 118.9, 119.0, 121.6, , 127.5, 128.1, 129.0, 135.7 (C-9, C-10, C-11, C-31, C-33, C-33', C-34, C-34'), 122.7, 129.2 (C-30, C-32), 136.2 (C-8, C-32'), 156.5 (C-3), 171.3, 172.1, 173.6, 173.8 (C-6, C-16, C-23, C-28, C-41, C-44).

**IR** (10 mmol/L, in CDCl<sub>3</sub>)  $\nu_{\max}$  1456, 1484, 1552, 1655, 1703, 1742, 2872, 2935, 2960, 3063, 3260 (br), 3329 (br), 3416, 3481 cm<sup>-1</sup>.

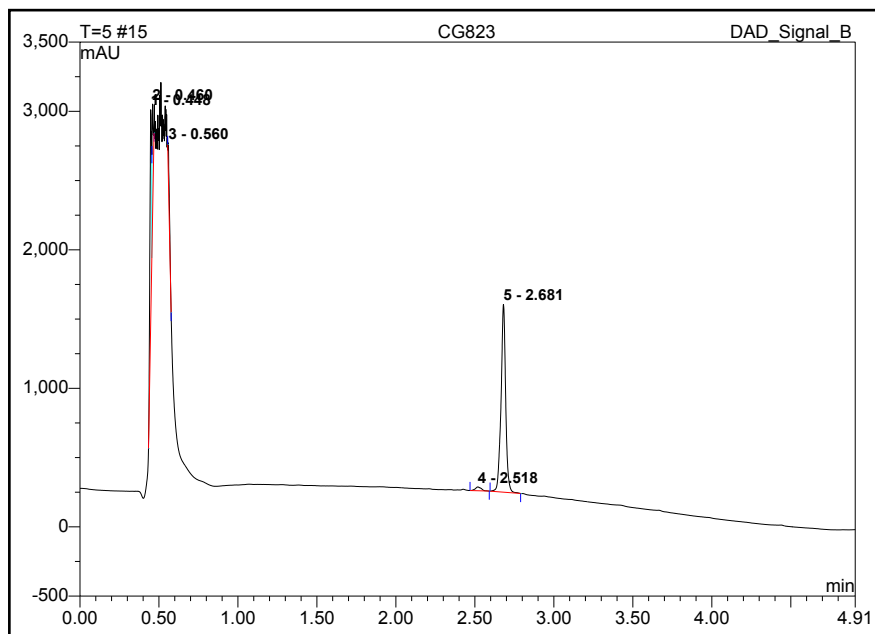
**HRMS (ESI):** [M+Na]<sup>+</sup>, 922.5042 found, C<sub>49</sub>H<sub>69</sub>N<sub>7</sub>NaO<sub>9</sub> 922.5049 calcd.

#### LCMS:

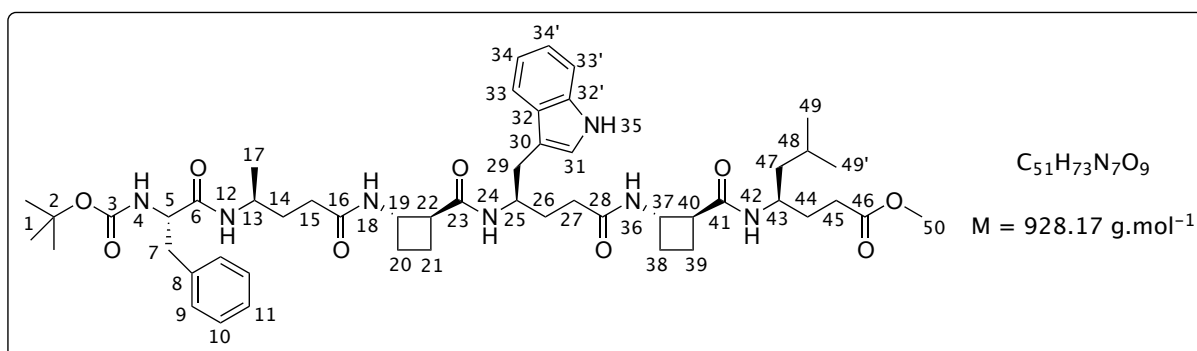




HPLC:



**Boc-Phe-(*R*)- $\gamma^4$ -hAla-(1*S*,2*S*)-ACBC-(*R*)- $\gamma^4$ -hTrp-(1*S*,2*S*)-ACBC-(*R*)- $\gamma^4$ -hLeu-OMe (+) - [42]**



According to the general procedure **B**, methyl ester of [52] (119 mg, 0.25 mmol) was hydrolysed to give the corresponding carboxylic acid, Boc-Phe-(*R*)- $\gamma^4$ -hAla-(1*S*,2*S*)-ACBC-OH (112 mg, 97% crude yield).

According to the general procedure **C**, *tert*-butoxycarbonyl group of [54] (150 mg, 0.26 mmol) was fully removed in 2.5 h to give the corresponding TFA salt, TFA·H<sub>2</sub>N-(*R*)-γ<sup>4</sup>-*h*Trp-(1*S*,2*S*)-ACBC-(*R*)-γ<sup>4</sup>-*h*Leu-OMe.

According to the general procedure **D**, the coupling reaction was performed with Boc-Phe-(*R*)-γ<sup>4</sup>-*h*Ala-(1*S*,2*S*)-ACBC-OH (112 mg, 0.24 mmol), DIPEA (83 μL, 62 mg, 0.48 mmol) and HATU (95 mg, 0.25 mmol) in a mixture of CH<sub>2</sub>Cl<sub>2</sub> / DMF (2 mL / 1 mL), and TFA·H<sub>2</sub>N-(*R*)-γ<sup>4</sup>-*h*Trp-(1*S*,2*S*)-ACBC-(*R*)-γ<sup>4</sup>-*h*Leu-OMe, DIPEA (250 μL, 186 mg, 1.44 mmol) in DMF (2 mL) overnight. The purification was carried out by flash chromatography (gradient from 10 / 90 to 100 / 0 : EtOAc / PE then from 0 / 100 to 20 / 80 : CH<sub>3</sub>OH / CH<sub>2</sub>Cl<sub>2</sub>) to give [42] as a yellow sticky solid (132 mg, 59%).

The compound was further purified using mass directed preparative HPLC (gradient from 5/95 to 95/5 of 0.1% formic acid water/methanol) to afford [42] with purity higher than 99%.

**R<sub>f</sub>** 0.50 (CH<sub>3</sub>OH / CH<sub>2</sub>Cl<sub>2</sub> = 10 / 90)

[α]<sub>D</sub><sup>27</sup> = + 30 (c. 0.50 in CH<sub>3</sub>OH)

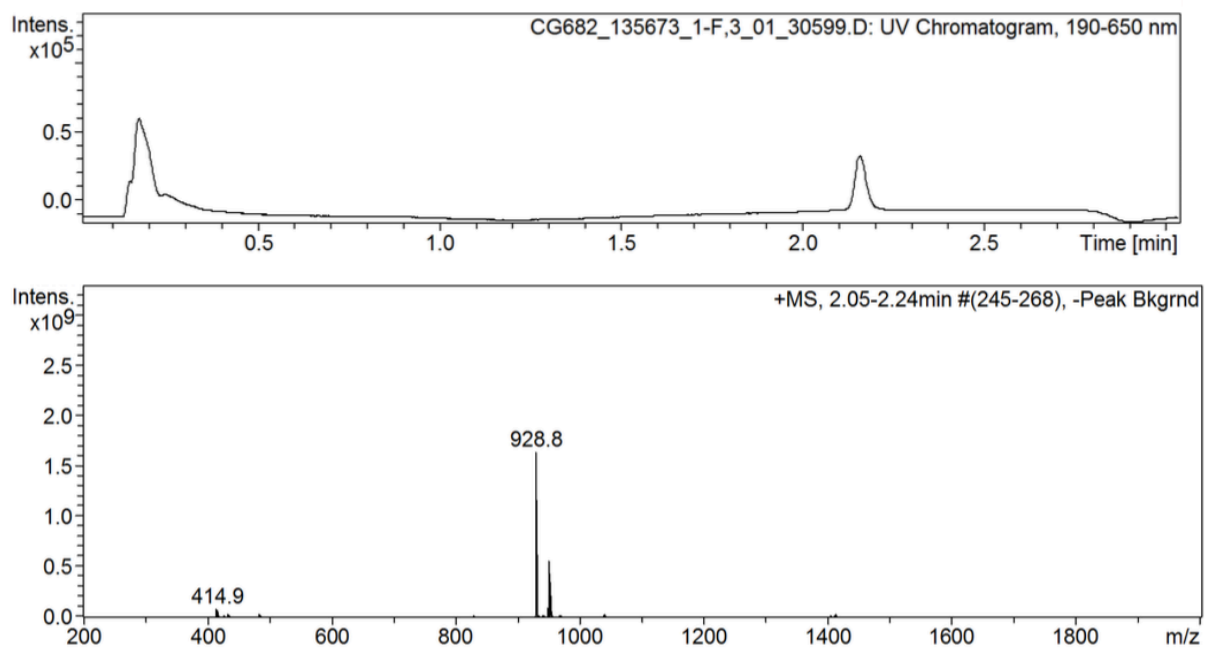
**<sup>1</sup>H NMR** (600 MHz, CDCl<sub>3</sub>) δ 0.83 (d, *J* = 6.8 Hz, 3H, 3H-49), 0.84 (d, *J* = 6.7 Hz, 3H, 3H-49'), 1.01 (d, *J* = 5.9 Hz, 3H, 3H-17), 1.15-1.20 (m, 1H, H-47), 1.36-1.46 (m, 14H, 9H-1, 2H-14, 2H-26, H-47'), 1.59-1.64 (m, 1H, H-48), 1.66-1.71 (m, 1H, H-21), 1.71-1.76 (m, 2H, 2H-44), 1.84-1.98 (m, 3H, H-20, H-38, H-39), 2.02-2.23 (m, 7H, 2H-15, H-20', H-21', H-27, H-38', H-39'), 2.29-2.32 (m, 1H, H-27'), 2.43-2.56 (m, 2H, 2H-45), 2.76-2.80 (m, 1H, H-22), 2.92-2.93 (m, 2H, 2H-29), 3.01-3.06 (m, 3H, 2H-7, H-40), 3.65 (s, 3H, 3H-50), 3.84 (bs, 1H, H-13), 3.99 (bs, 1H, H-43), 4.24-4.28 (m, 1H H-5), 4.32-4.39 (m, 2H, H-25, H-37), 4.43-4.49 (m, 1H, H-19), 5.30 (bs, 1H, H-4), 6.15 (d, *J* = 8.6 Hz, 1H, H-12), 7.01-7.37 (m, 10H, 2H-9, 2H-10, H-11, H-18, H-33, H-33', H-34, H-34'), 7.48 (d, *J* = 8.9 Hz, 1H, H-24), 7.62 (d, *J* = 7.5 Hz, 1H, H-31), 8.17 (d, *J* = 6.1 Hz, 1H, H-36), 8.28 (d, *J* = 7.9 Hz, 1H, H-42), 8.44 (bs, 1H, H-35).

**<sup>13</sup>C NMR** (100 MHz, CDCl<sub>3</sub>) δ 16.0 (C-21), 18.0 (C-15), 21.4 (C-17), 22.2, 23.1 (C-49, C-49'), 24.9 (C-48), 24.5, 26.0 (C-38, C-39), 28.4 (C-1), 29.9 (C-45), 30.8 (C-29), 31.3, 31.4 (C-14, C-26, C-44), 32.2 (C-27), 32.6 (C-20), 37.3 (C-7), 43.2 (C-13), 43.9 (C-47), 47.1 (C-43), 47.9, 48.0, 48.1 (C-19, C-25, C-37), 49.6, 49.7 (C-22, C-40), 51.5 (C-50), 57.1 (C-5), 81.5 (C-2), 111.1, 118.9, 120.0, 121.6, 122.7, 127.5, 129.0, 129.2 (C-9, C-10, C-11, C-31, C-33, C-33', C-34, C-34'), 112.3 (C-30), 128.1, 135.8, 136.2 (C-8, C-32, C-32'), 156.6 (C-3), 171.4, 172.1, 173.4, 173.6, 174.5 (C-6, C-16, C-23, C-28, C-41, C-46).

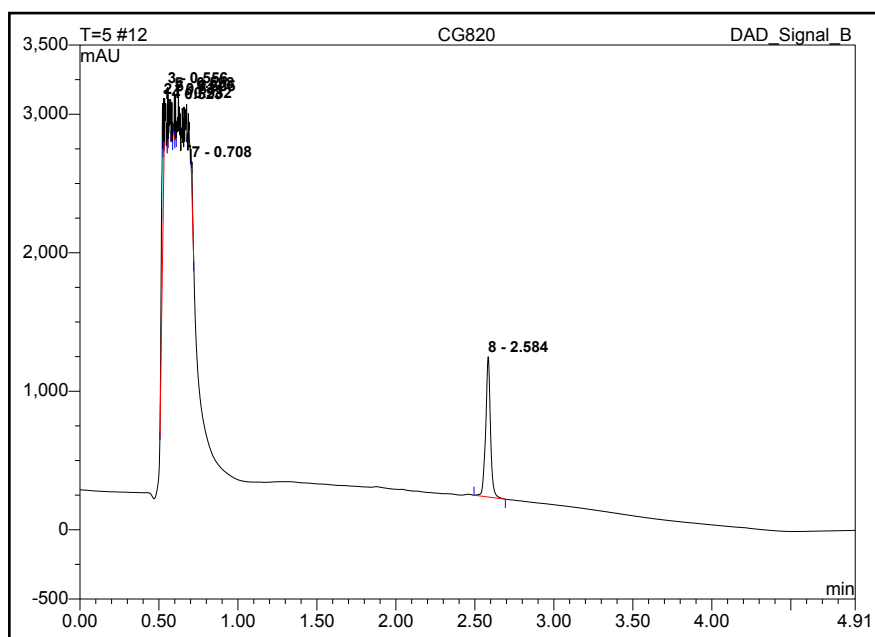
**IR** (10 mmol/L, in CDCl<sub>3</sub>) ν<sub>max</sub> 1455, 1484, 1552, 1655, 1704, 1726, 2872, 2930, 2957, 3065, 3265 (br), 3328 (br), 3416, 3481 cm<sup>-1</sup>.

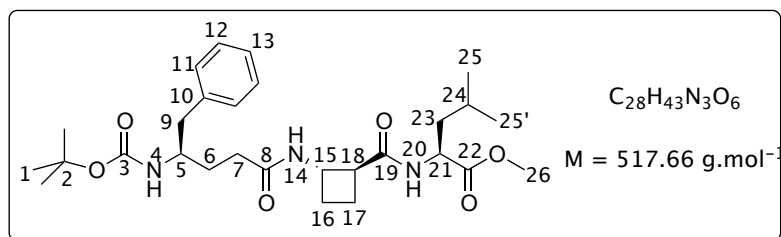
**HRMS (ESI):** [M+Na]<sup>+</sup>, 950.5366 found, C<sub>51</sub>H<sub>73</sub>N<sub>7</sub>NaO<sub>9</sub> 950.5362 calcd.

## LCMS:



## HPLC:



**Boc-(*R*)- $\gamma^4$ -hPhe-(1*S*,2*S*)-ACBC-Leu-OMe (+) - [55]**

According to the general procedure **A**, benzyl ester of [35] (105 mg, 0.26 mmol) was hydrolysed to give the corresponding carboxylic acid, Boc-Phe-(*R*)- $\gamma^4$ -hPhe-(1*S*,2*S*)-ACBC-OH (95 mg, 92% crude yield).

According to the general procedure **D**, the coupling reaction was performed with Boc-Phe-(*R*)- $\gamma^4$ -hPhe-(1*S*,2*S*)-ACBC-OH (95 mg, 0.24 mmol), DIPEA (83  $\mu$ L, 62 mg, 0.48 mmol) and HATU (96 mg, 0.26 mmol) in a mixture of  $CH_2Cl_2$  / DMF (1 mL / 1 mL), and  $H_2N$ -Leu-OMe (47 mg, 0.26 mmol), DIPEA (83  $\mu$ L, 62 mg, 0.48 mmol) in  $CH_2Cl_2$  (2 mL) overnight. The purification was carried out by flash chromatography (gradient from 10 / 90 to 80 / 20 : EtOAc / PE) to give [55] as a white sticky solid (102 mg, 82%).

$R_f$  0.60 ( $CH_3OH$  /  $CH_2Cl_2$  = 10 / 90)

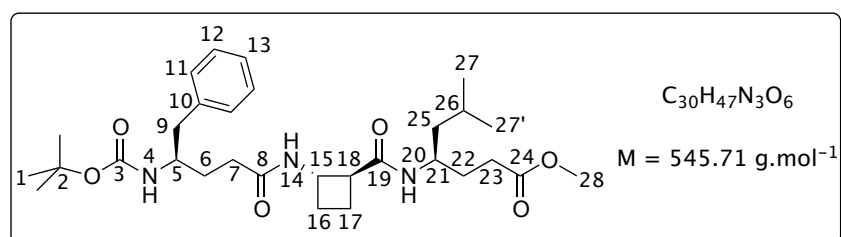
$[\alpha]_D^{24} = +19$  (c. 0.50 in  $CHCl_3$ )

**$^1H$  NMR** (360 MHz,  $CDCl_3$ )  $\delta$  0.89 (d,  $J = 6.0$  Hz, 3H, 3H-25), 0.91 (d,  $J = 6.9$  Hz, 3H, 3H-25'), 1.40 (s, 9H, 9H-1), 1.55-1.64 (m, 4H, H-6, 2H-23, H-24), 1.84-2.07 (m, 5H, H-6', H-7, H-16, 2H-17), 2.17-2.24 (m, 2H, H-7', H-16'), 2.76 (d,  $J = 6.4$  Hz, 2H, 2H-9), 2.92-2.99 (m, 1H, H-18), 3.72 (s, 3H, 3H-26), 3.85 (bs, 1H, H-5), 4.34-4.42 (m, 1H, H-15), 4.46-4.52 (m, 1H, H-21), 4.64 (d,  $J = 9.5$  Hz, 1H, H-4), 7.10 (d,  $J = 6.2$  Hz, 1H, H-14), 7.13-7.29 (m, 5H, 2H-11, 2H-12, H-13), 8.60 (d,  $J = 7.5$  Hz, 1H, H-20).

**$^{13}C$  NMR** (90 MHz,  $CDCl_3$ )  $\delta$  18.3 (C-17), 21.7, 22.9 (C-25, C-25'), 24.4 (C-16), 24.9 (C-24), 28.4 (C-1), 31.1 (C-6), 32.7 (C-7), 40.5 (C-23), 41.8 (C-9), 48.0 (C-15), 49.3 (C-18), 50.7 (C-5), 50.9 (C-21), 52.2 (C-26), 79.7 (C-2), 126.6, 128.5, 129.3 (C-11, C-12, C-13), 137.5 (C-10), 156.4 (C-3), 173.3 (C-19), 173.7 (C-8), 173.8 (C-22).

**IR** (10 mmol/L, in  $CDCl_3$ )  $\nu_{max}$  1453, 1469, 1508, 1552, 1603, 1657, 1694, 1741, 2872, 2935, 2959, 3033, 3067, 3211, 3266 (br), 3436  $cm^{-1}$ .

**HRMS (ESI):**  $[M+Na]^+$ , 540.3040 found,  $C_{28}H_{43}N_3NaO_6$  540.3044 calcd.

**Boc-(*R*)- $\gamma^4$ -*h*Phe-(1*S*,2*S*)-ACBC-(*R*)- $\gamma^4$ -*h*Leu-OMe (+) - [56]**

According to the general procedure **A**, benzyl ester of [35] (105 mg, 0.26 mmol) was hydrolysed to give the corresponding carboxylic acid, Boc-Phe-(*R*)- $\gamma^4$ -*h*Phe-(1*S*,2*S*)-ACBC-OH (100 mg, 95% crude yield).

According to the general procedure **D**, the coupling reaction was performed with Boc-Phe-(*R*)- $\gamma^4$ -*h*Phe-(1*S*,2*S*)-ACBC-OH (100 mg, 0.25 mmol), DIPEA (87  $\mu$ L, 65 mg, 0.50 mmol) and HATU (98 mg, 0.26 mmol) in a mixture of  $CH_2Cl_2$  / DMF (2 mL / 1 mL), and  $H_2N$ -(*R*)- $\gamma^4$ -*h*Leu-OMe (59 mg, 0.30 mmol), DIPEA (175  $\mu$ L, 129 mg, 1.00 mmol) in  $CH_2Cl_2$  (2 mL) overnight. The purification was carried out by flash chromatography (gradient from 10 / 90 to 80 / 20 : EtOAc / PE) to give [56] as a white sticky solid (125 mg, 92%).

$R_f$  0.55 ( $CH_3OH$  /  $CH_2Cl_2$  = 10 / 90)

$[\alpha]_D^{24} = +1.8$  (c. 0.50 in  $CH_3OH$ )

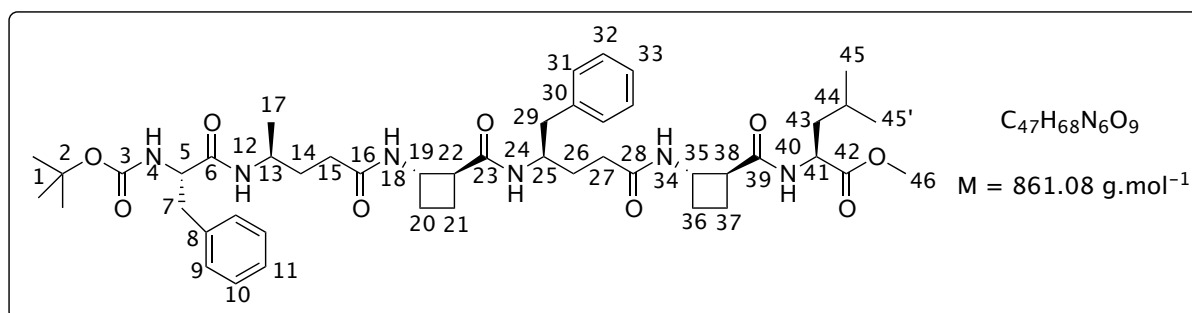
**$^1H$  NMR** (250 MHz,  $CDCl_3$ )  $\delta$  0.85 (d,  $J = 6.4$  Hz, 3H, 3H-27), 0.86 (d,  $J = 6.1$  Hz, 3H, 3H-27'), 1.22-1.27 (m, 1H, H-25), 1.39 (s, 10H, 9H-1, H-25'), 1.48-1.75 (m, 4H, 2H-6, H-22, H-26), 1.82-1.98 (m, 3H, H-16, H-17, H-22'), 2.06-2.31 (m, 4H, 2H-7, H-16', H-17'), 2.41 (t,  $J = 7.3$  Hz, 2H, 2H-23), 2.76 (d,  $J = 5.6$  Hz, 2H, 2H-9), 2.89-2.98 (m, 1H, H-18), 3.67 (s, 3H, 3H-28), 3.82 (bs, 1H, H-5), 3.91-3.98 (m, 1H, H-21), 4.24-4.36 (m, 1H, H-15), 4.65 (d,  $J = 9.1$  Hz, 1H, H-4), 7.14-7.32 (m, 6H, 2H-11, 2H-12, H-13, H-14), 8.04 (d,  $J = 8.8$  Hz, 1H, H-20).

**$^{13}C$  NMR** (62.5 MHz,  $CDCl_3$ )  $\delta$  18.6 (C-17), 22.1, 23.1 (C-27, C-27'), 24.4 (C-16), 25.0 (C-26), 28.3 (C-1), 30.8, 30.9 (C-6, C-22, C-23), 32.7 (C-7), 41.8 (C-9), 43.9 (C-25), 46.9 (C-21), 47.9 (C-15), 49.7 (C-18), 50.7 (C-5), 51.7 (C-28), 79.7 (C-2), 126.6, 128.5, 129.3 (C-11, C-12, C-13), 137.5 (C-10), 156.3 (C-3), 173.3, 173.9, 174.5 (C-8, C-19, C-24).

**IR** (10 mmol/L, in  $CDCl_3$ )  $\nu_{max}$  1440, 1451, 1507, 1555, 1564, 1649, 1699, 1730, 2872, 2957, 3030, 3070, 3194, 3267, 3340 (br), 3435  $cm^{-1}$ .

**HRMS (ESI):**  $[M+Na]^+$ , 568.3383 found,  $C_{30}H_{47}N_3NaO_6$  568.3357 calcd.

**Boc-Phe-(*R*)- $\gamma^4$ -hAla-(1*S*,2*S*)-ACBC-(*R*)- $\gamma^4$ -hPhe-(1*S*,2*S*)-ACBC-Leu-OMe (+) - [46]**



According to the general procedure **B**, methyl ester of [52] (67 mg, 0.14 mmol) was hydrolysed to give the corresponding carboxylic acid, Boc-Phe-(*R*)- $\gamma^4$ -hAla-(1*S*,2*S*)-ACBC-OH (66 mg, 98% crude yield). According to the general procedure **C**, *tert*-butoxycarbonyl group of [55] (70 mg, 0.14 mmol) was fully removed in 2.5 h to give the corresponding TFA salt, TFA·H<sub>2</sub>N-(*R*)- $\gamma^4$ -hPhe-(1*S*,2*S*)-ACBC-Leu-OMe. According to the general procedure **D**, the coupling reaction was performed with Boc-Phe-(*R*)- $\gamma^4$ -hAla-(1*S*,2*S*)-ACBC-OH (66 mg, 0.14 mmol), DIPEA (48  $\mu$ L, 36 mg, 0.28 mmol) and HATU (55 mg, 0.15 mmol) in a mixture of CH<sub>2</sub>Cl<sub>2</sub> / DMF (2 mL / 1 mL), and TFA·H<sub>2</sub>N-(*R*)- $\gamma^4$ -hPhe-(1*S*,2*S*)-ACBC-Leu-OMe, DIPEA (146  $\mu$ L, 108 mg, 0.84 mmol) in a mixture of CH<sub>2</sub>Cl<sub>2</sub> / DMF (2 mL / 1 mL) overnight. The purification was carried out by flash chromatography (gradient from 0 / 100 to 10 / 90 : CH<sub>3</sub>OH / CH<sub>2</sub>Cl<sub>2</sub>) to give [46] as a white sticky solid (94 mg, 78%).

The compound was further purified using mass directed preparative HPLC (gradient from 5/95 to 95/5 of 0.1% formic acid water/methanol) to afford the [46] with purity higher than 95%.

$R_f$  0.58 (CH<sub>3</sub>OH / CH<sub>2</sub>Cl<sub>2</sub> = 10 / 90)

$[\alpha]_D^{26} = +17$  (c. 0.50 in CHCl<sub>3</sub>)

**<sup>1</sup>H NMR** (600 MHz, CDCl<sub>3</sub>)  $\delta$  0.91 (d,  $J$  = 6.4 Hz, 6H, 6H-45), 1.05 (d,  $J$  = 6.5 Hz, 3H, 3H-17), 1.36-1.43 (m, 4H, 2H-14, 2H-26), 1.46 (s, 9H, 9H-1), 1.62-1.73 (m, 4H, H-21, 2H-43, H-44), 1.88-2.08 (m, 6H, H-15, H-20, H-27, H-36, 2H-37), 2.12-2.26 (m, 5H, H-15', H-20', H-21', H-27', H-36'), 2.77-2.79 (m, 3H, H-22, 2H-29), 3.04-3.08 (m, 1H, H-38), 3.13- 3.14 (m, 2H, 2H-7), 3.73 (s, 3H, 3H-46), 3.85 (bs, 1H, H-13), 4.23-4.32 (m, 2H, H-5, H-25), 4.41-4.44 (m, 1H, H-35), 4.47-4.50 (m, 1H, H-19), 4.50-4.54 (m, 1H, H-41), 5.10 (d,  $J$  = 3.8 Hz, 1H, H-4), 5.96 (d,  $J$  = 8.9 Hz, 1H, H-12), 7.15-7.40 (m, 11H, 2H-9, 2H-10, H-11, H-



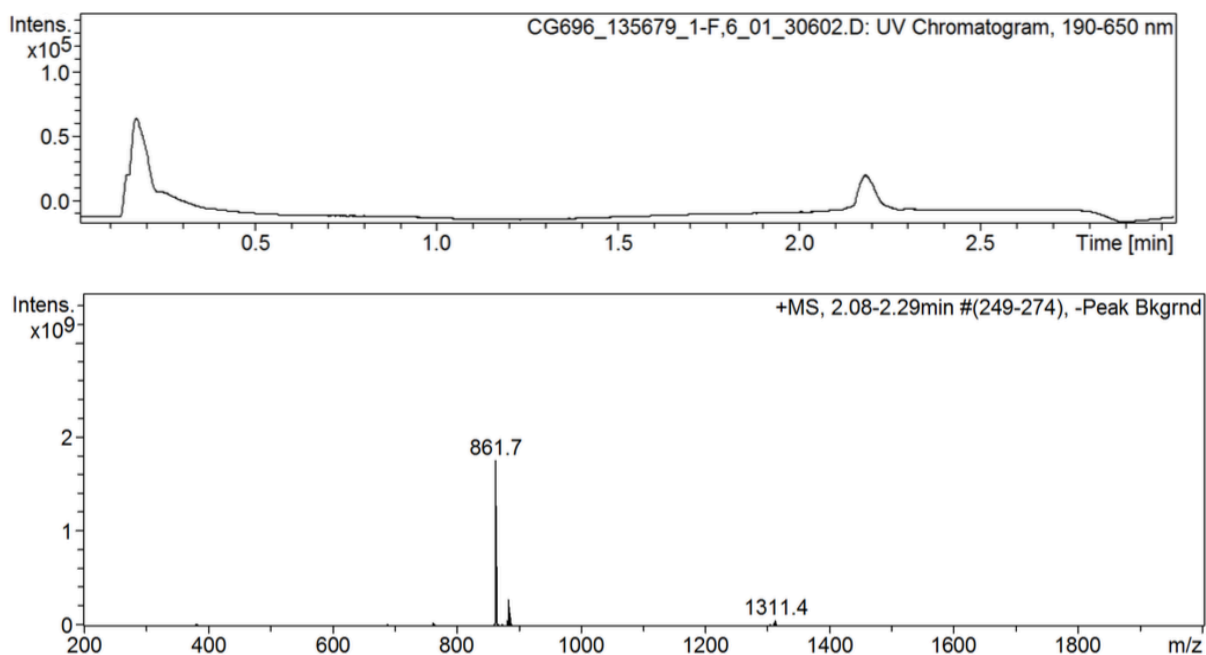
18, 2H-31, 2H-32, H-33), 7.47 (d,  $J = 9.5$  Hz, 1H, H-24), 8.17 (d,  $J = 6.5$  Hz, 1H, H-34), 8.98 (d,  $J = 7.7$  Hz, 1H, H-40).

**$^{13}\text{C}$  NMR** (100 MHz,  $\text{CDCl}_3$ )  $\delta$  15.9 (C-21), 17.8 (C-37), 21.5 (C-17), 21.7, 23.0 (C-45, C-45'), 24.4 (C-36), 24.9 (C-44), 26.1 (C-20), 28.3 (C-1), 31.4 (C-14, C-26), 31.8, 32.6 (C-15, C-27), 37.4 (C-7), 40.4 (C-43), 42.0 (C-29), 43.3 (C-13), 48.0 (C-19, C-35), 48.7 (C-25), 49.4 (C-38), 49.8 (C-22), 51.1 (C-41), 52.0 (C-5), 81.7 (C-2), 126.1, 127.6, 128.2, 129.1, 129.2, 129.4 (C-9, C-10, C-11, C-31, C-32, C-33), 135.6, 138.4 (C-8, C-30), 156.5 (C-3), 171.2, 171.3, 171.9, 173.5, 173.8 (C-6, C-16, C-23, C-28, C-39, C-42).

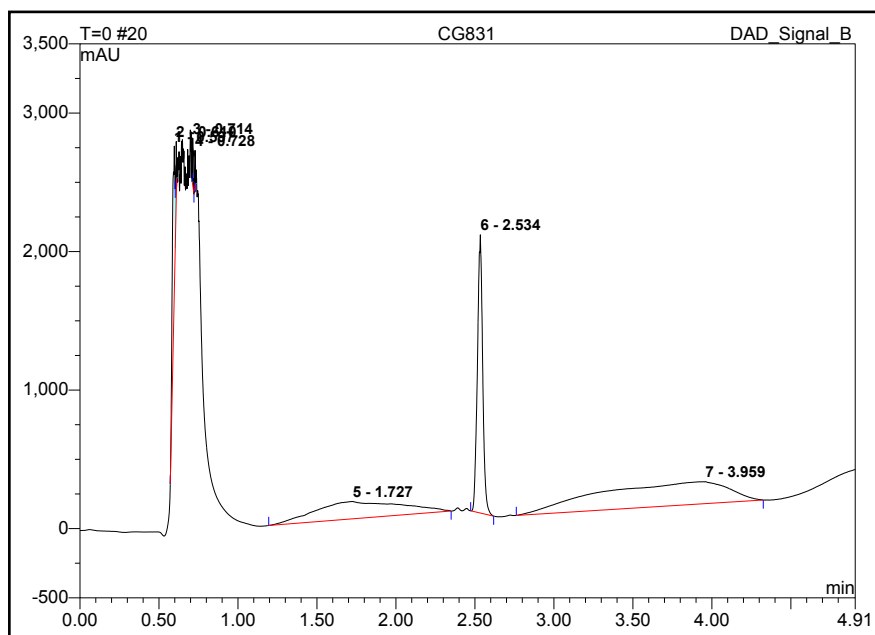
**IR** (10 mmol/L, in  $\text{CDCl}_3$ )  $\nu_{\text{max}}$  1454, 1483, 1550, 1654, 1703, 1743, 2871, 2960, 3030, 3067, 3263 (br), 3322 (br), 3416  $\text{cm}^{-1}$ .

**HRMS (ESI):**  $[\text{M}+\text{Na}]^+$ , 883.4936 found,  $\text{C}_{47}\text{H}_{68}\text{N}_6\text{NaO}_9$  883.4940 calcd.

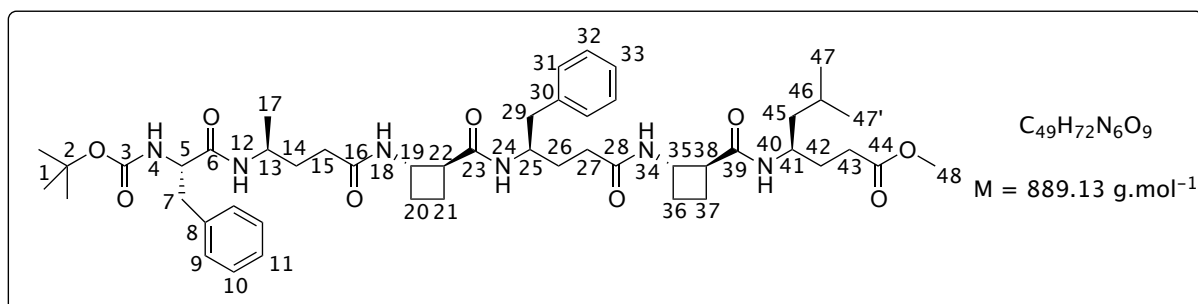
#### LCMS:



## HPLC:



**Boc-Phe-(*R*)- $\gamma^4$ -hAla-(1*S*,2*S*)-ACBC-(*R*)- $\gamma^4$ -hPhe-(1*S*,2*S*)-ACBC-(*R*)- $\gamma^4$ -hLeu-OMe (+) - [45]**



According to the general procedure **B**, methyl ester of [52] (57 mg, 0.12 mmol) was hydrolysed to give the corresponding carboxylic acid, Boc-Phe-(*R*)- $\gamma^4$ -hAla-(1*S*,2*S*)-ACBC-OH (55 mg, 96% crude yield).

According to the general procedure **C**, *tert*-butoxycarbonyl group of [56] (105 mg, 0.19 mmol) was fully removed in 2.2 h to give the corresponding TFA salt, TFA·H<sub>2</sub>N-(*R*)- $\gamma^4$ -hPhe-(1*S*,2*S*)-ACBC-(*R*)- $\gamma^4$ -hLeu-OMe.

According to the general procedure **D**, the coupling reaction was performed with Boc-Phe-(*R*)- $\gamma^4$ -hAla-(1*S*,2*S*)-ACBC-OH (55 mg, 0.12 mmol), DIPEA (41  $\mu$ L, 30 mg, 0.24 mmol) and HATU (49 mg, 0.13 mmol) in a mixture of CH<sub>2</sub>Cl<sub>2</sub> / DMF (2 mL / 1 mL); and TFA·H<sub>2</sub>N-(*R*)- $\gamma^4$ -hPhe-(1*S*,2*S*)-ACBC-(*R*)- $\gamma^4$ -hLeu-OMe, DIPEA (195  $\mu$ L, 144 mg, 1.15 mmol) in a mixture of CH<sub>2</sub>Cl<sub>2</sub> / DMF (2 mL / 1 mL) overnight. The purification was carried out by flash chromatography (gradient from 0 / 100 to 10 / 90 : CH<sub>3</sub>OH / CH<sub>2</sub>Cl<sub>2</sub>) to give [45] as a white sticky solid (90 mg, 84%).

## EXPERIMENTAL PART

The compound was further purified using mass directed preparative HPLC (gradient from 5/95 to 95/5 of 0.1% formic acid water/methanol) to afford the [45] with purity higher than 95%.

$R_f$  0.63 (CH<sub>3</sub>OH / CH<sub>2</sub>Cl<sub>2</sub> = 10 / 90)

$[\alpha]_D^{26} = +12$  (c. 0.50 in CH<sub>3</sub>OH)

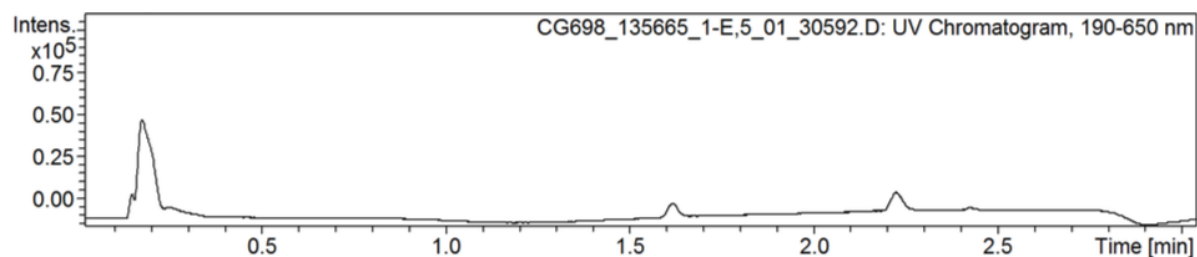
**<sup>1</sup>H NMR** (600 MHz, CDCl<sub>3</sub>)  $\delta$  0.85 (d,  $J$  = 6.8 Hz, 3H, 3H-47), 0.87 (d,  $J$  = 6.0 Hz, 3H, 3H-47'), 1.04 (d,  $J$  = 6.0 Hz, 3H, 3H-17), 1.18-1.22 (m, 1H, H-45), 1.36-1.43 (m, 5H, 2H-14, 2H-26, H-45'), 1.46 (s, 9H, 9H-1), 1.58-1.62 (m, 1H, H-46), 1.69-1.74 (m, 3H, H-21, 2H-42), 1.87-2.03 (m, 7H, H-20, 2H-16, H-27, H-36, 2H-37), 2.09-2.18 (m, 4H, H-20', H-21', H-27', H-36'), 2.44-2.52 (m, 2H, 2H-43), 2.76-2.81 (m, 3H, H-22, 2H-29), 2.96-3.00 (m, 1H, H-38), 3.12 (d,  $J$  = 6.3 Hz, 2H, 2H-7), 3.67 (s, 3H, 3H-48), 3.84 (bs, 1H, H-13), 3.99 (bs, 1H, H-41), 4.25 (bs, 1H, H-25), 4.28-4.31 (m, 1H, H-5), 4.33-4.36 (m, 1H, H-35), 4.44-4.47 (m, 1H, H-19), 5.18 (bs, 1H, H-4), 6.05 (d,  $J$  = 9.2 Hz, 1H, H-12), 7.14-7.39 (m, 11H, 2H-9, 2H-10, H-11, H-18, 2H-31, 2H-32, H-33), 7.48 (d,  $J$  = 8.8 Hz, 1H, H-24), 8.17 (d,  $J$  = 7.3 Hz, 1H, H-34), 8.23 (d,  $J$  = 8.5 Hz, 1H, H-40).

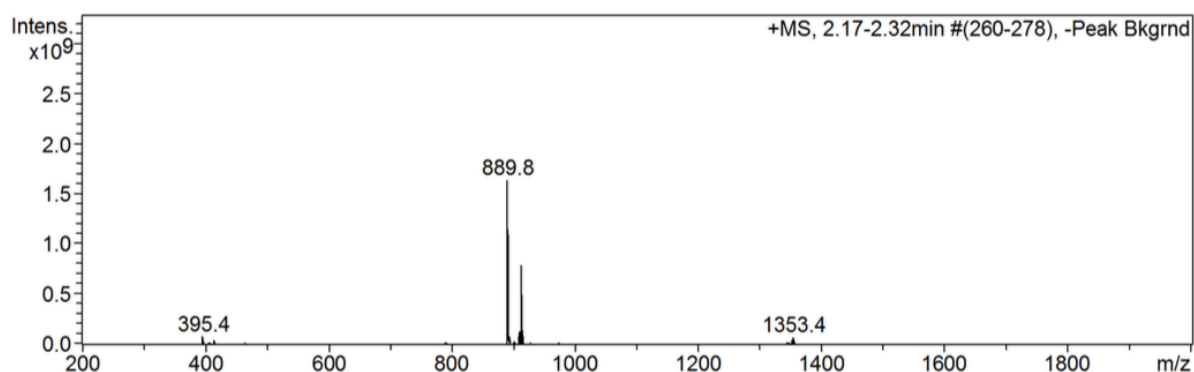
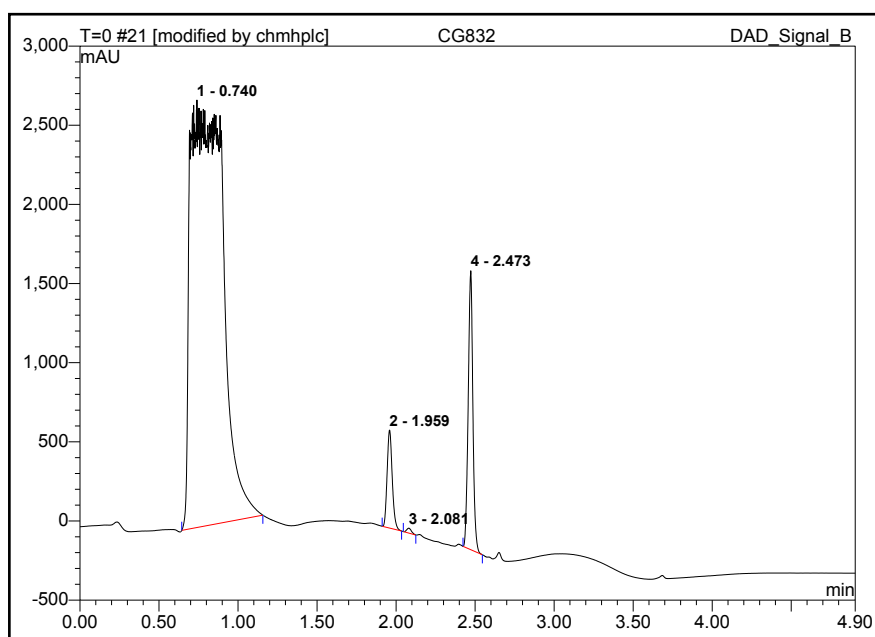
**<sup>13</sup>C NMR** (100 MHz, CDCl<sub>3</sub>)  $\delta$  15.7 (C-21), 17.6 (C-37), 21.3 (C-17), 22.2, 23.0 (C-47, C-47'), 24.4 (C-36), 24.8 (C-46), 26.0 (C-20), 28.2 (C-1), 30.6, 30.8 (C-42, C-43), 31.1, 31.4, 32.2, 32.5 (C-14, C-15, C-26, C-27), 37.2 (C-7), 41.7 (C-29), 43.1 (C-13), 43.9 (C-45), 46.5 (C-41), 47.8, 47.9 (C-19, C-35), 48.4 (C-25), 49.5 (C-22), 49.9 (C-38), 51.3 (C-48), 57.0 (C-5), 81.5 (C-2), 126.0, 127.4, 128.0, 128.9, 129.1, 129.3 (C-9, C-10, C-11, C-31, C-32, C-33), 135.4, 138.2 (C-8, C-30), 156.4 (C-3), 171.1, 171.3, 171.7 (C-6, C-16, C-23), 172.9 (C-39), 173.1 (C-28), 174.4 (C-44).

**IR** (10 mmol/L, in CDCl<sub>3</sub>)  $\nu_{\max}$  1454, 1484, 1494, 1522, 1552, 1654, 1703, 1727, 2870, 2930, 2957, 3027, 3066, 3260 (br), 3321 (br), 3416 cm<sup>-1</sup>.

**HRMS (ESI):** [M+Na]<sup>+</sup>, 911.5271 found, C<sub>49</sub>H<sub>72</sub>N<sub>6</sub>NaO<sub>9</sub> 911.5253 calcd.

### LCMS:



**HPLC:**

### 3. Biological assays

#### 3.1 Protein expression

The pET14b vector containing *hDM2* (17-126) L33E was expressed in *E. coli* BL21 (DE3) GOLD and purified by Dr. Jennifer Miles (University of Leeds). The purified *hDM2* (17-126) L33E was concentrated (typically to ~ 150  $\mu$ M) and stored at -80 °C.

The pet28a His-SUMO Mcl-1 (172-327) construct was over-expressed in the *E. coli* strain Rosetta and purified by Dr. Jennifer Miles (University of Leeds). The purified Mcl-1 (172- 327) was concentrated (typically to ~ 200 mM) and stored at -80 °C.

The pGEX Bcl-x<sub>L</sub> 'no loop' was over-expressed in the *E. coli* strain Rosetta 2 and purified by Dr. Jennifer Miles. The purified Bcl-x<sub>L</sub> 'no loop' was concentrated (typically to ~ 500 mM) and stored at -80 °C.

### 3.2 Fluorescence anisotropy

p53(15-31) transactivation domain peptide and its fluorescein-labelled analogue FITC-p53(15-31) were purchased from Peptide Protein Research Ltd and used without further purification. NOXA B(68-87) and its fluorescein-labelled analogue FITC-NOXA B(68-87) were synthesized and purified by Dr. Silvia Rodriguez Marin. Fluorescence anisotropy assays were performed in 384-well plates (Greiner Bio-one). Each experiment was run in triplicate and the fluorescence anisotropy measured using a Perkin Elmer EnVision™ 2103 MultiLabel plate reader, with excitation at 480 nm (30 nm bandwidth), polarised dichroic mirror at 505 nm and emission at 535 nm (40 nm bandwidth, S and P polarised).

All experiments were performed in assay buffer: 40 mM phosphate buffer at pH 7.50, containing 200 mM NaCl and 0.02 mg mL<sup>-1</sup> bovine serum albumin (BSA) and data analysed following previously published methods.

20 µL of buffer were first added to each well. 40 µL of a solution of α-helix mimetics (1 mM in 90:10 (v/v) assay buffer: DMSO) were added to the first column. The solution was well mixed and 40 µL was taken out and added to the next column and so on. This operation consists on serial dilution of the peptides across the plate (starting point: 222 µM; 18-points, 3/4 serial dilution). For the p53/hDM2 FA competition assay, 20 µL of FITC-p53(15-31) Flu and 20 µL of hDM2(17-126) L33E were added to each well to give a final concentration of 50 nM and 150 nM, respectively. For the NOXA B/Mcl-1 FA competition assay, FITC-NOXA B(68-87) and Mcl-1(172-327) were added to each well to give a final concentration of 50 nM and 150 nM, respectively. For the Bak/Bcl-x<sub>L</sub> FA competition assay, 20 µL of BODIPY-Bak and 20 µL of Bcl-x<sub>L</sub> were added to each well to give a final concentration of 50 nM and 150 nM, respectively. For control wells, the tracer peptide was replaced with an identical volume of assay buffer. The total volume in each well was 60 µL. Plates were read after 1 h of incubation at room temperature.

The data for both the P (perpendicular intensity) and S (parallel (same) intensity) channels, resulting from this measurement and corrected by subtracting the corresponding control wells, were used to calculate the intensity and anisotropy for each well following Equations 2 and 3:

$$I = (2PG) + S \text{ (Equation 2)}$$

$$r = \frac{S - PG}{I} \text{ (Equation 3)}$$

Where I is the total intensity, G is an instrument factor which was set to 1 for all experiments and r is the anisotropy. The average anisotropy (across three experimental replicates) and the standard

deviation of these values were then calculated and fit to a sigmoidal logistic model (Equation 4) using OriginPro 9.0 which provided the IC50 and error values.

$$y = r_{max} + \frac{r_{min} - r_{max}}{1 + \left(\frac{x}{x_0}\right)^p} \text{ (Equation 4)}$$

### 3.3 Proteolytic studies

$\alpha$ -Chymotrypsin Type II from bovine pancreas (lyophilized powder, MW = 25 kDa,  $\geq 40$  units/mg protein) was purchased from Sigma-Aldrich and used without further purification.

$\alpha/\beta/\gamma$ -Peptides and p53(15-31) peptide (200  $\mu$ M stock in PBS buffer pH 7.50, 2% DMSO) were treated with  $\alpha$ -Chymotrypsin Type II from bovine pancreas (0.02  $\mu$ M stock solutions in PBS buffer pH 7.50) in a 1:10000 enzyme/substrate ratio. The degradation was followed with analytical HPLC (Ascentis® Express Peptide Column, injection volume: 20  $\mu$ L, acetonitrile/water (0.1% TFA) 5-95% gradient) and the data was analysed to extract kinetic values.

### 3.4 $^1\text{H}$ - $^{15}\text{N}$ HSQC studies

*hDM2* (17-126) L33E was overexpressed in minimal media enriched with  $^{15}\text{N}$  Ammonium Chloride to produce isotopically labelled protein by Dr. Jennifer Miles (University of Leeds).

Each  $^1\text{H}$ - $^{15}\text{N}$  HSQC was obtained using 87  $\mu$ M protein that had been incubated in the absence or presence of 200  $\mu$ M compound overnight at 4°C. The buffer used for *hDM2* spectra contained 100 mM Sodium Phosphate at pH 7.3, 2.5% of glycerol, 1 mM of DTT and 5% of DMSO. Sample volumes of 330  $\mu$ L were placed in Shigemi BMS-005V tubes and included 10%  $\text{D}_2\text{O}$  v/v. All NMR datasets were acquired at 25 °C.

The crosspeaks were assigned from published structures, with BMRB entry 6621 used for *hDM2*.

The difference in chemical shift was calculated (Equation 5) where  $\Delta\delta_{\text{overall}}$  is the overall change in chemical shift  $\Delta\delta_{\text{N}}$  is the change in the nitrogen dimension and  $\Delta\delta_{\text{H}}$  is the change in the hydrogen dimension. The change in hydrogen dimension is scaled by the ratio of the magnetogyric radius of Nitrogen and Hydrogen to account for the larger chemical shift range of Nitrogen.

$$\Delta\delta_{\text{overall}} = \sqrt{(\Delta\delta_{\text{N}})^2 + \left(\frac{\gamma_{\text{H}}}{\gamma_{\text{N}}}\right)^2 (\Delta\delta_{\text{H}})^2} \text{ (Equation 5)}$$



## **BIBLIOGRAPHY**





## BIBLIOGRAPHY

1. Barlow, D. J. & Thornton, J. M. Helix geometry in proteins. *J. Mol. Biol.* **201**, 601–619 (1988).
2. Creighton, T. E. *Proteins: Structures and Molecular Properties*. (W.H.Freeman & Co Ltd, 1992).
3. Pauling, L., Corey, R. B. & Branson, H. R. The structure of proteins: Two hydrogen-bonded helical configurations of the polypeptide chain. *Proc. Natl. Acad. Sci.* **37**, 205–211 (1951).
4. Fodje, M. N. & Al-Karadaghi, S. Occurrence, conformational features and amino acid propensities for the  $\pi$ -helix. *Protein Eng.* **15**, 353–358 (2002).
5. Donohue, J. Hydrogen bonded helical configurations of the polypeptide chain. *Proc. Natl. Acad. Sci. U. S. A.* **39**, 470 (1953).
6. Kilosanidze, G. T., Kutsenko, A. S., Esipova, N. G. & Tumanyan, V. G. Analysis of forces that determine helix formation in  $\alpha$ -proteins. *Protein Sci.* **13**, 351–357 (2004).
7. Bullock, B. N., Jochim, A. L. & Arora, P. S. Assessing helical protein interfaces for inhibitor design. *J. Am. Chem. Soc.* **133**, 14220–14223 (2011).
8. Stites, W. E. Protein–Protein Interactions: Interface structure, binding thermodynamics, and mutational analysis. *Chem. Rev.* **97**, 1233–1250 (1997).
9. Fairlie, D. P., West, M. L. & Wong, A. K. Towards protein surface mimetics. *Curr. Med. Chem.* **5**, 29–62 (1998).
10. Hammami, R. & Fliss, I. Current trends in antimicrobial agent research: chemo- and bioinformatics approaches. *Drug Discov. Today* **15**, 540–546 (2010).
11. Fahs, S., Patil-Sen, Y. & Snape, T. J. Foldamers as anticancer therapeutics: targeting Protein-Protein Interactions and the cell membrane. *Chembiochem Eur. J. Chem. Biol.* (2015).
12. Eiríksdóttir, E., Konate, K., Langel, Ü., Divita, G. & Deshayes, S. Secondary structure of cell-penetrating peptides controls membrane interaction and insertion. *Biochim. Biophys. Acta BBA - Biomembr.* **1798**, 1119–1128 (2010).
13. Oren, M. Decision making by p53: life, death and cancer. *Cell Death Differ.* **10**, 431–442 (2003).
14. Böttger, A. *et al.* Molecular characterization of the hdm2-p53 interaction1. *J. Mol. Biol.* **269**, 744–756 (1997).

15. Moll, U. M. & Petrenko, O. The MDM2-p53 interaction. *Mol. Cancer Res.* **1**, 1001–1008 (2003).
16. Kussie, P. H. *et al.* Structure of the MDM2 oncoprotein bound to the p53 tumor suppressor transactivation domain. *Science* **274**, 948–953 (1996).
17. Fang, S., Jensen, J. P., Ludwig, R. L., Vousden, K. H. & Weissman, A. M. Mdm2 Is a RING Finger-dependent Ubiquitin Protein Ligase for Itself and p53. *J. Biol. Chem.* **275**, 8945–8951 (2000).
18. Marshall, S. A., Lazar, G. A., Chirino, A. J. & Desjarlais, J. R. Rational design and engineering of therapeutic proteins. *Drug Discov. Today* **8**, 212–221 (2003).
19. Sonnichsen, F. D., Van Eyk, J. E., Hodges, R. S. & Sykes, B. D. Effect of trifluoroethanol on protein secondary structure: an NMR and CD study using a synthetic actin peptide. *Biochem.* **31**, 8790–8798 (1992).
20. Fairlie, D. P., West, M. L. & Wong, A. M. Current Medicinal Chemistry. (Bentham Science Publishers, 1998).
21. Yun, R. H., Anderson, A. & Hermans, J. Proline in alpha-helix: stability and conformation studied by dynamics simulation. *Proteins* **10**, 219–228 (1991).
22. Takei, T. *et al.* The effects of the side chains of hydrophobic aliphatic amino acid residues in an amphipathic polypeptide on the formation of alpha helix and its association. *J. Biochem.* **139**, 271–278 (2006).
23. Doig, A. J. & Baldwin, R. L. N- and C-capping preferences for all 20 amino acids in alpha-helical peptides. *Protein Sci. Publ. Protein Soc.* **4**, 1325–1336 (1995).
24. Gradišar, H. & Jerala, R. De novo design of orthogonal peptide pairs forming parallel coiled-coil heterodimers. *J. Pept. Sci.* **17**, 100–106 (2011).
25. Zhou, H. X., Lyu, P. C., Wemmer, D. E. & Kallenbach, N. R. Structure of a C-Terminal .alpha.-Helix Cap in a Synthetic Peptide. *J. Am. Chem. Soc.* **116**, 1139–1140 (1994).
26. Lyu, P. C., Wemmer, D. E., Zhou, H. X., Pinker, R. J. & Kallenbach, N. R. Capping interactions in isolated .alpha. helices: position-dependent substitution effects and structure of a serine-capped peptide helix. *Biochem.* **32**, 421–425 (1993).
27. Scholtz, J. M., Qian, H., Robbins, V. H. & Baldwin, R. L. The energetics of ion-pair and hydrogen-bonding interactions in a helical peptide. *Biochem.* **32**, 9668–9676 (1993).
28. Smith, J. S. & Scholtz, J. M. Energetics of Polar Side-Chain Interactions in Helical Peptides: Salt Effects on Ion Pairs and Hydrogen Bonds. *Biochem.* **37**, 33–40 (1998).
29. Khan, N., Graslund, A., Ehrenberg, A. & Shriver, J. Sequence-specific proton NMR assignments and secondary structure of porcine motilin. *Biochem.* **29**, 5743–5751 (1990).

30. Olson, C. A., Shi, Z. & Kallenbach, N. R. Polar Interactions with Aromatic Side Chains in  $\alpha$ -Helical Peptides:  $\text{CH}\cdots\text{O}$  H-Bonding and Cation- $\pi$  Interactions. *J. Am. Chem. Soc.* **123**, 6451–6452 (2001).
31. Tsou, L. K., Tatko, C. D. & Waters, M. L. Simple Cation- $\pi$  Interaction between a Phenyl Ring and a Protonated Amine Stabilizes an  $\alpha$ -Helix in Water. *J. Am. Chem. Soc.* **124**, 14917–14921 (2002).
32. Albert, J. S. & Hamilton, A. D. Stabilization of Helical Domains in Short Peptides Using Hydrophobic Interactions. *Biochem.* **34**, 984–990 (1995).
33. Hunter, C. A., Singh, J. & Thornton, J. M.  $\pi$ - $\pi$  interactions: the geometry and energetics of phenylalanine-phenylalanine interactions in proteins. *J. Mol. Biol.* **218**, 837–846 (1991).
34. Ghadiri, M. R. & Choi, C. Secondary structure nucleation in peptides. Transition metal ion stabilized  $\alpha$ -helices. *J. Am. Chem. Soc.* **112**, 1630–1632 (1990).
35. Ghadiri, M. R. & Fernholz, A. K. Peptide architecture. Design of stable  $\alpha$ -helical metallopeptides via a novel exchange-inert ruthenium(III) complex. *J. Am. Chem. Soc.* **112**, 9633–9635 (1990).
36. Macarron, R. Critical review of the role of HTS in drug discovery. *Drug Discov. Today* **11**, 277–279 (2006).
37. Hajduk, P. J. & Greer, J. A decade of fragment-based drug design: strategic advances and lessons learned. *Nat. Rev. Drug Discov.* **6**, 211–219 (2007).
38. Vassilev, L. T. *et al.* In vivo activation of the p53 pathway by small-molecule antagonists of MDM2. *Science* **303**, 844–848 (2003).
39. Grasberger, B. L. *et al.* Discovery and cocrystal structure of benzodiazepinedione MDM2 antagonists that activate p53 in cells. *J. Med. Chem.* **48**, 909–912 (2005).
40. Shangary, S. *et al.* Temporal activation of p53 by a specific MDM2 inhibitor is selectively toxic to tumors and leads to complete tumor growth inhibition. *Proc. Natl. Acad. Sci.* **105**, 3933–3938 (2008).
41. Rew, Y. *et al.* Structure-Based Design of Novel Inhibitors of the MDM2-p53 Interaction. *J. Med. Chem.* **55**, 4936–4954 (2012).
42. Azzarito, V., Long, K., Murphy, N. S. & Wilson, A. J. Inhibition of  $\alpha$ -helix-mediated protein-protein interactions using designed molecules. *Nat. Chem.* **5**, 161–173 (2013).
43. Horwell, D. C., Howson, W., Ratcliffe, G. S. & Willems, H. M. The design of dipeptide helical mimetics: the synthesis, tachykinin receptor affinity and conformational analysis of 1,1,6-trisubstituted indanes. *Bioorg. Med. Chem.* **4**, 33–42 (1996).
44. Orner, B. P., Ernst, J. T. & Hamilton, A. D. Toward Proteomimetics: Terphenyl

Derivatives as Structural and Functional Mimics of Extended Regions of an  $\alpha$ -Helix. *J. Am. Chem. Soc.* **123**, 5382–5383 (2001).

45. Yin, H., Lee, G.-I. & Hamilton, A. D.  $\alpha$ -Helix mimetics in drug discovery. (John Wiley & Sons Inc.) (2007).

46. Kutzki, O. *et al.* Development of a Potent Bcl-xL Antagonist Based on  $\alpha$ -Helix Mimicry. *J. Am. Chem. Soc.* **124**, 11838–11839 (2002).

47. Kazi, A. *et al.* The BH3 -Helical Mimic BH3-M6 Disrupts Bcl-XL, Bcl-2, and MCL-1 Protein-Protein Interactions with Bax, Bak, Bad, or Bim and Induces Apoptosis in a Bax- and Bim-dependent Manner. *J. Biol. Chem.* **286**, 9382–9392 (2011).

48. Yin, H. & Hamilton, A. D. Terephthalamide derivatives as mimetics of the helical region of Bak peptide target Bcl-xL protein. *Bioorg. Med. Chem. Lett.* **14**, 1375–1379 (2004).

49. Rodriguez, J. M., Nevola, L., Ross, N. T., Lee, G. & Hamilton, A. D. Synthetic Inhibitors of Extended Helix-Protein Interactions Based on a Biphenyl 4,4'-Dicarboxamide Scaffold. *ChemBioChem* **10**, 829–833 (2009).

50. Rodriguez, J. M. & Hamilton, A. D. Benzoylurea Oligomers: Synthetic Foldamers That Mimic Extended  $\alpha$  Helices. *Angew. Chem. Int. Ed.* **46**, 8614–8617 (2007).

51. Rodriguez, J. M. & Hamilton, A. D. Intramolecular hydrogen bonding allows simple enaminones to structurally mimic the  $i$ ,  $i + 4$ , and  $i + 7$  residues of an  $\alpha$ -helix. *Tetrahedron Lett.* **47**, 7443–7446 (2006).

52. Rodriguez, J. M. *et al.* Structure and Function of Benzoylurea-Derived  $\alpha$ -Helix Mimetics Targeting the Bcl-xL/Bak Binding Interface. *ChemMedChem* **4**, 649–656 (2009).

53. Biros, S. M. *et al.* Heterocyclic  $\alpha$ -helix mimetics for targeting protein-protein interactions. *Bioorg. Med. Chem. Lett.* **17**, 4641–4645 (2007).

54. Cummings, C. G., Ross, N. T., Katt, W. P. & Hamilton, A. D. Synthesis and biological evaluation of a 5-6-5 imidazole-phenyl-thiazole based alpha-helix mimetic. *Org. Lett.* **11**, 25–28 (2009).

55. Huc, I. Aromatic Oligoamide Foldamers. *Eur. J. Org. Chem.* **2004**, 17–29 (2004).

56. Berl, V., Huc, I., Khoury, R. G. & Lehn, J.-M. Helical Molecular Programming: Folding of Oligopyridine-dicarboxamides into Molecular Single Helices. *Chem. Eur. J.* **7**, 2798–2809 (2001).

57. Ernst, J. T., Becerril, J., Park, H. S., Yin, H. & Hamilton, A. D. Design and Application of an  $\alpha$ -Helix-Mimetic Scaffold Based on an Oligoamide-Foldamer Strategy: Antagonism of the Bak BH3/Bcl-xL Complex. *Angew. Chem. Int. Ed.* **42**, 535–539 (2003).

58. Plante, J. P. *et al.* Oligobenzamide proteomimetic inhibitors of the p53-hDM2 protein–

- protein interaction. *Chem. Commun.* 5091–5093 (2009).
59. Azzarito, V. *et al.* 2-O-Alkylated para-benzamide  $\alpha$ -helix mimetics: the role of scaffold curvature. *Org. Biomol. Chem.* **10**, 6469–6472 (2012).
60. Long, K., Edwards, T. A. & Wilson, A. J. Microwave assisted solid phase synthesis of highly functionalized N-alkylated oligobenzamide  $\alpha$ -helix mimetics. *Bioorg. Med. Chem.* **21**, 4034–4040 (2013).
61. Campbell, F., Plante, J. P., Edwards, T. A., Warriner, S. L. & Wilson, A. J. N-alkylated oligoamide alpha-helical proteomimetics. *Org. Biomol. Chem.* **8**, 2344–2351 (2010).
62. Lu, F. *et al.* Proteomimetic Libraries: Design, Synthesis, and Evaluation of p53–MDM2 Interaction Inhibitors. *J. Comb. Chem.* **8**, 315–325 (2006).
63. Lee, J. H. *et al.* Novel Pyrrolopyrimidine-Based  $\alpha$ -Helix Mimetics: Cell-Permeable Inhibitors of Protein–Protein Interactions. *J. Am. Chem. Soc.* **133**, 676–679 (2011).
64. Marimnganti, S., Cheemala, M. N. & Ahn, J.-M. Novel Amphiphilic  $\alpha$ -Helix Mimetics Based on a Bis-benzamide Scaffold. *Org. Lett.* **11**, 4418–4421 (2009).
65. Thompson, S. & Hamilton, A. D. Amphiphilic  $\alpha$ -helix mimetics based on a benzoylurea scaffold. *Org. Biomol. Chem.* **10**, 5780–5782 (2012).
66. Kim, I. C. & Hamilton, A. D. Diphenylindane-Based Proteomimetics Reproduce the Projection of the i, i+3, i+4, and i+7 Residues on an  $\alpha$ -Helix. *Org. Lett.* **8**, 1751–1754 (2006).
67. Petros, A. M. *et al.* Rationale for Bcl-xL/Bad peptide complex formation from structure, mutagenesis, and biophysical studies. *Protein Sci. Publ. Protein Soc.* **9**, 2528–2534 (2000).
68. Becerril, J. & Hamilton, A. D. Helix Mimetics as Inhibitors of the Interaction of the Estrogen Receptor with Coactivator Peptides. *Angew. Chem. Int. Ed.* **46**, 4471–4473 (2007).
69. Xuereb, H., Maletic, M., Gildersleeve, J., Pelczer, I. & Kahne, D. Design of an Oligosaccharide Scaffold That Binds in the Minor Groove of DNA. *J. Am. Chem. Soc.* **122**, 1883–1890 (2000).
70. Gellman, S. H. Foldamers: a manifesto. *Acc. Chem. Res.* **31**, 173–180 (1998).
71. Hill, D. J., Mio, M. J., Prince, R. B., Hughes, T. S. & Moore, J. S. A field guide to foldamers. *Chem. Rev.* **101**, 3893–4012 (2001).
72. Lyu, P. C., Sherman, J. C., Chen, A. & Kallenbach, N. R. Alpha-helix stabilization by natural and unnatural amino acids with alkyl side chains. *Proc. Natl. Acad. Sci.* **88**, 5317–5320 (1991).
73. Toniolo, C. *et al.* Preferred conformations of peptides containing  $\alpha,\alpha$ -disubstituted  $\alpha$ -amino acids. *Biopol.* **22**, 205–215 (1983).
74. Solà, J., Helliwell, M. & Clayden, J. Interruption of a 310-helix by a single Gly residue in a

poly-Aib motif: A crystallographic study. *Biopolymers* **95**, 62–69 (2011).

75. Karle, I. L. & Balaram, P. Structural characteristics of .alpha.-helical peptide molecules containing Aib residues. *Biochem.* **29**, 6747–6756 (1990).

76. Marshall, G. R. *et al.* Factors governing helical preference of peptides containing multiple alpha,alpha-dialkyl amino acids. *Proc. Natl. Acad. Sci.* **87**, 487–491 (1990).

77. Banerjee, R., Basu, G., Chène, P. & Roy, S. Aib-based peptide backbone as scaffolds for helical peptide mimics. *J. Pept. Res. Off. J. Am. Pept. Soc.* **60**, 88–94 (2002).

78. Kahn, M. Alpha-helix mimetics and methods relating thereto. WO1997015589A1 (1997).

79. Kemp, D. S., Rothman, J. H., Curran, T. C. & Blanchard, D. E. A macrocyclic triproline-derived template for helix nucleation. *Tetrahedron Lett.* **36**, 3809–3812 (1995).

80. Lewis, A., Ryan, M. D. & Gani, D. Design, construction and properties of peptide N-terminal cap templates devised to initiate  $\alpha$ -helices. Part 1. Caps derived from N-(4-chlorobutyryl)-(2S)-Pro-(2S)-Pro-(2S)-Ala-OMe and N-[(2S)-2-chloropropionyl]-(2S)-Pro-(2S)-Pro-(2S,4S)-4-hydroxyPro-OMe. *J. Chem. Soc.* 3767–3776 (1998).

81. Lewis, A., Wilkie, J., Rutherford, T. J. & Gani, D. Design, construction and properties of peptide N-terminal cap templates devised to initiate  $\alpha$ -helices. Part 2.† Caps derived from N-[(2S)-2-chloropropionyl]-(2S)-Pro-(2S)-Pro-(2S,4S)-4-thioPro-OMe. *J. Chem. Soc.* 3777–3794 (1998).

82. Lewis, A., Rutherford, T. J., Wilkie, J., Jenn, T. & Gani, D. Design, construction and properties of peptide N-terminal cap templates devised to initiate  $\alpha$ -helices. Part 3.† Caps derived from N-[(2S)-2-chloropropionyl]-(2S)-Pro-(2R)-Ala-(2S,4S)-4-thioPro-OMe. *J. Chem. Soc. [Perkin 1]* 3795–3806 (1998).

83. Muller, K., Obrecht, D. & Knierzinger, A. *Perspect Med Chem* 513 (1993).

84. Arrhenius, T. & Satterthwait, A. C. *Peptides - Chemistry, Structure and Biology (Jean E. Rivier / Springer)* (1990).

85. Austin, R. E. *et al.* A Template for Stabilization of a Peptide  $\alpha$ -Helix: Synthesis and Evaluation of Conformational Effects by Circular Dichroism and NMR. *J. Am. Chem. Soc.* **119**, 6461–6472 (1997).

86. Jackson, D. Y., King, D. S., Chmielewski, J., Singh, S. & Schultz, P. G. General approach to the synthesis of short .alpha.-helical peptides. *J. Am. Chem. Soc.* **113**, 9391–9392 (1991).

87. Leduc, A.-M. *et al.* Helix-stabilized cyclic peptides as selective inhibitors of steroid receptor–coactivator interactions. *Proc. Natl. Acad. Sci.* **100**, 11273–11278 (2003).

88. Pellegrini, M., Royo, M., Chorev, M. & Mierke, D. F. Conformational consequences of i, i +

- 3 cystine linkages: nucleation for  $\alpha$ -helicity? *J. Pept. Res.* **49**, 404–414 (1997).
89. Galande, A. K. *et al.* Potent Inhibitors of LXXLL-Based Protein–Protein Interactions. *ChemBioChem* **6**, 1991–1998 (2005).
90. Galande, A. K., Bramlett, K. S., Burris, T. P., Wittliff, J. L. & Spatola, A. F. Thioether side chain cyclization for helical peptide formation: inhibitors of estrogen receptor-coactivator interactions. *J. Pept. Res. Off. J. Am. Pept. Soc.* **63**, 297–302 (2004).
91. Chorev, M. *et al.* Cyclic parathyroid hormone-related protein antagonists: lysine 13 to aspartic acid 17 [i to (i + 4)] side chain to side chain lactamization. *Biochemistry (Mosc.)* **30**, 5968–5974 (1991).
92. Geistlinger, T. R. & Guy, R. K. Novel Selective Inhibitors of the Interaction of Individual Nuclear Hormone Receptors with a Mutually Shared Steroid Receptor Coactivator 2. *J. Am. Chem. Soc.* **125**, 6852–6853 (2003).
93. Sia, S. K., Carr, P. A., Cochran, A. G., Malashkevich, V. N. & Kim, P. S. Short constrained peptides that inhibit HIV-1 entry. *Proc. Natl. Acad. Sci.* **99**, 14664–14669 (2002).
94. Blackwell, H. E. & Grubbs, R. H. Highly Efficient Synthesis of Covalently Cross-Linked Peptide Helices by Ring-Closing Metathesis. *Angew. Chem. Int. Ed.* **37**, 3281–3284 (1998).
95. Schafmeister, C. E., Po, J. & Verdine, G. L. An All-Hydrocarbon Cross-Linking System for Enhancing the Helicity and Metabolic Stability of Peptides. *J. Am. Chem. Soc.* **122**, 5891–5892 (2000).
96. Yeo, D. J., Warriner, S. L. & Wilson, A. J. Monosubstituted alkenyl amino acids for peptide ‘stapling’. *Chem. Commun.* **49**, 9131–9133 (2013).
97. Chang, Y. *et al.* 226 ATSP-7041, a Dual MDM2 and MDMX Targeting Stapled A-helical Peptide Exhibits Potent in Vitro and in Vivo Efficacy in Xenograft Models of Human Cancer. *Eur. J. Cancer* **48**, 68–69 (2012).
98. Baek, S. *et al.* Structure of the stapled p53 peptide bound to Mdm2. *J. Am. Chem. Soc.* **134**, 103–106 (2011).
99. Cabezas, E. & Satterthwait, A. C. The Hydrogen Bond Mimic Approach: Solid-Phase Synthesis of a Peptide Stabilized as an  $\alpha$ -Helix with a Hydrazone Link. *J. Am. Chem. Soc.* **121**, 3862–3875 (1999).
100. Chapman, R. N., Dimartino, G. & Arora, P. S. A Highly Stable Short  $\alpha$ -Helix Constrained by a Main-Chain Hydrogen-Bond Surrogate. *J. Am. Chem. Soc.* **126**, 12252–12253 (2004).
101. Wang, D., Liao, W. & Arora, P. S. Enhanced Metabolic Stability and Protein-Binding Properties of Artificial  $\alpha$  Helices Derived from a Hydrogen-Bond Surrogate: Application to Bcl-xL. *Angew. Chem. Int. Ed.* **44**, 6525–6529 (2005).



102. Yang, B., Liu, D. & Huang, Z. Synthesis and helical structure of lactam bridged BH3 peptides derived from pro-apoptotic Bcl-2 family proteins. *Bioorg. Med. Chem. Lett.* **14**, 1403–1406 (2004).
103. Henchey, L. K., Porter, J. R., Ghosh, I. & Arora, P. S. High Specificity in Protein Recognition by Hydrogen-Bond-Surrogate  $\alpha$ -Helices: Selective Inhibition of the p53/MDM2 Complex. *ChemBioChem* **11**, 2104–2107 (2010).
104. Wysoczanski, P. *et al.* NMR solution structure of a photoswitchable apoptosis activating Bak peptide bound to Bcl-xL. *J. Am. Chem. Soc.* **134**, 7644–7647 (2012).
105. Geier III, G. R. & Sasaki, T. The design, synthesis and characterization of a porphyrin-peptide conjugate. *Tetrahedron Lett.* **38**, 3821–3824 (1997).
106. Fasan, R. *et al.* Using a  $\beta$ -Hairpin To Mimic an  $\alpha$ -Helix: Cyclic Peptidomimetic Inhibitors of the p53–HDM2 Protein–Protein Interaction. *Angew. Chem. Int. Ed.* **43**, 2109–2112 (2004).
107. Günther, R., Hofmann, H.-J. & Kuczera, K. Searching for periodic structures in  $\beta$ -peptides. *J. Phys. Chem. B* **105**, 5559–5567 (2001).
108. Abele, S., Seiler, P. & Seebach, D. Synthesis, crystal structures, and modelling of  $\beta$ -oligopeptides consisting of 1-(aminomethyl)cyclopropanecarboxylic acid): ribbon-type arrangement of eight-membered H-bonded rings. *Helv. Chim. Acta* **82**, 1559–1571 (1999).
109. Threlfall, R., Davies, A., Howarth, N. M., Fisher, J. & Cosstick, R. Peptides derived from nucleoside  $\beta$ -amino acids form an unusual 8-helix. *Chem. Commun.* 585–587 (2008).
110. Gorrea, E. *et al.* Secondary Structure of Short  $\beta$ -Peptides as the Chiral Expression of Monomeric Building Units: A Rational and Predictive Model. *J. Org. Chem.* **77**, 9795–9806 (2012).
111. Altmayer-Henzien, A. *et al.* Fine Tuning of  $\beta$ -Peptide Foldamers: a Single Atom Replacement Holds Back the Switch from an 8-Helix to a 12-Helix. *Angew. Chem. Int. Ed.* n/a–n/a (2015).
112. Hetényi, A., Mándity, I. M., Martinek, T. A., Tóth, G. K. & Fülöp, F. Chain-length-dependent helical motifs and self-association of  $\beta$ -peptides with constrained side chains. *J. Am. Chem. Soc.* **127**, 547–553 (2005).
113. Claridge, T. D. W. *et al.* 10-Helical conformations in oxetane  $\beta$ -amino acid hexamers. *Tetrahedron Lett.* **42**, 4251–4255 (2001).
114. Izquierdo, S. *et al.* (+)- and (–)-2-Aminocyclobutane-1-carboxylic acids and their incorporation into highly rigid  $\beta$ -peptides: Stereoselective synthesis and a structural study. *J. Org. Chem.* **70**, 10890–10890 (2005).
115. Martinek, T. A. *et al.* Effects of the Alternating Backbone Configuration on the

- Secondary Structure and Self-Assembly of  $\beta$ -Peptides. *J. Am. Chem. Soc.* **128**, 13539–13544 (2006).
116. Szolnoki, É., Hetényi, A., Mándity, I. M., Fülöp, F. & Martinek, T. A. Foldameric  $\beta$ -H18/20P Mixed Helix Stabilized by Head-to-Tail Contacts: A Way to Higher-Order Structures. *Eur. J. Org. Chem.* **2013**, 3555–3559 (2013).
117. Rueping, M., Schreiber, J. V., Lelais, G., Jaun, B. & Seebach, D. Mixed  $\beta$ 2/ $\beta$ 3-Hexapeptides and  $\beta$ 2/ $\beta$ 3-Nonapeptides Folding to (P)-Helices with Alternating Twelve- and Ten-Membered Hydrogen-Bonded Rings. *Helv. Chim. Acta* **85**, 2577–2593 (2002).
118. Appella, D. H., Christianson, L. A., Karle, I. L., Powell, D. R. & Gellman, S. H. Synthesis and Characterization of *trans*-2-Aminocyclohexanecarboxylic Acid Oligomers: An Unnatural Helical Secondary Structure and Implications for  $\beta$ -Peptide Tertiary Structure. *J. Am. Chem. Soc.* **121**, 6206–6212 (1999).
119. Fernandes, C. *et al.* 12-Helix Folding of Cyclobutane  $\beta$ -Amino Acid Oligomers. *Org. Lett.* **12**, 3606–3609 (2010).
120. Torres, E. *et al.* Prevalence of Eight-Membered Hydrogen-Bonded Rings in Some Bis(cyclobutane)  $\beta$ -Dipeptides Including Residues with Trans Stereochemistry†. *Org. Lett.* **11**, 2301–2304 (2009).
121. Seebach, D. *et al.*  $\beta$ 2- and  $\beta$ 3-Peptides with Proteinaceous Side Chains: Synthesis and solution structures of constitutional isomers, a novel helical secondary structure and the influence of solvation and hydrophobic interactions on folding. *Helv. Chim. Acta* **81**, 932–982 (1998).
122. Seebach, D., Abele, S., Gademann, K. & Jaun, B. Pleated Sheets and Turns of  $\beta$ -Peptides with Proteinogenic Side Chains. *Angew. Chem. Int. Ed.* **38**, 1595–1597 (1999).
123. Applequist, J., Bode, K. A., Appella, D. H., Christianson, L. A. & Gellman, S. H. Theoretical and Experimental Circular Dichroic Spectra of the Novel Helical Foldamer Poly[(1R,2R)-*trans*-2-aminocyclopentanecarboxylic acid]. *J. Am. Chem. Soc.* **120**, 4891–4892 (1998).
124. Appella, D. H., Barchi, Joseph J., Durell, S. R. & Gellman, S. H. Formation of Short, Stable Helices in Aqueous Solution by  $\beta$ -Amino Acid Hexamers. *J. Am. Chem. Soc.* **121**, 2309–2310 (1999).
125. Celis, S., Gorrea, E., Nolis, P., Illa, O. & Ortuño, R. M. Designing hybrid foldamers: the effect on the peptide conformational bias of  $\beta$ - versus  $\alpha$ - and  $\gamma$ -linear residues in alternation with (1R,2S)-2-aminocyclobutane-1-carboxylic acid. *Org. Biomol. Chem.* **10**, 861–868 (2012).
126. Seebach, D., Beck, A. K. & Bierbaum, D. J. The world of  $\beta$ - and  $\gamma$ -peptides comprised of homologated proteinogenic amino acids and other components. *Chem. Biodivers.* **1**, 1111–

1239 (2004).

127. Porter, E. A., Weisblum, B. & Gellman, S. H. Mimicry of Host-Defense Peptides by Unnatural Oligomers: Antimicrobial  $\beta$ -Peptides. *J. Am. Chem. Soc.* **124**, 7324–7330 (2002).

128. Murray, J. K. & Gellman, S. H. Targeting protein–protein interactions: Lessons from p53/mDM2. *Biopolymers* **88**, 657–686 (2007).

129. Kritzer, J. A., Hodsdon, M. E. & Schepartz, A. Solution Structure of a  $\beta$ -Peptide Ligand for hDM2. *J. Am. Chem. Soc.* **127**, 4118–4119 (2005).

130. Kritzer, J. A., Lear, J. D., Hodsdon, M. E. & Schepartz, A. Helical  $\beta$ -Peptide Inhibitors of the p53-hDM2 Interaction. *J. Am. Chem. Soc.* **126**, 9468–9469 (2004).

131. Baldauf, C., Günther, R. & Hofmann, H.-J. Helix formation and folding in  $\gamma$ -peptides and their vinylogues. *Helv. Chim. Acta* **86**, 2573–2588 (2003).

132. Kothari, A., Qureshi, M. K. N., Beck, E. M. & Smith, M. D. Bend-ribbon forming  $\gamma$ -peptides. *Chem. Commun.* 2814–2816 (2007).

133. Sharma, G. V. M. *et al.* A left-handed 9-helix in  $\gamma$ -peptides: Synthesis and conformational studies of oligomers with dipeptide repeats of C-linked carbo- $\gamma$ 4-amino acids and  $\gamma$ -aminobutyric acid. *Angew. Chem. Int. Ed.* **45**, 2944–2947 (2006).

134. Hanessian, S., Luo, X., Schaum, R. & Michnick, S. Design of secondary structures in unnatural peptides: stable helical  $\gamma$ -tetra-, hexa-, and octapeptides and consequences of  $\alpha$ -substitution. *J. Am. Chem. Soc.* **120**, 8569–8570 (1998).

135. Hintermann, T., Gademann, K., Jaun, B. & Seebach, D.  $\gamma$ -peptides forming more stable secondary structures than  $\alpha$ -peptides: Synthesis and helical NMR-solution structure of the  $\gamma$ -hexapeptide analog of H-(Val-Ala-Leu)2-OH. *Helv. Chim. Acta* **81**, 983–1002 (1998).

136. Seebach, D., Brenner, M., Rueping, M. & Jaun, B.  $\gamma$ 2-,  $\gamma$ 3-, and  $\gamma$ 2,3,4-Amino acids, coupling to  $\gamma$ -hexapeptides: CD spectra, NMR solution and X-ray crystal structures of  $\gamma$ -peptides. *Chem. – Eur. J.* **8**, 573–584 (2002).

137. Seebach, D., Brenner, M., Rueping, M., Schweizer, B. & Jaun, B. Preparation and determination of X-ray-crystal and NMR-solution structures of  $\gamma$ 2,3,4-peptides. *Chem. Commun.* 207–208 (2001).

138. Seebach, D., Hook, D. F. & Glättli, A. Helices and other secondary structures of  $\beta$ - and  $\gamma$ -peptides. *Biopolymers* **84**, 23–37 (2006).

139. Frackenhohl, J., Arvidsson, P. I., Schreiber, J. V. & Seebach, D. The outstanding biological stability of  $\beta$ - and  $\gamma$ -peptides toward proteolytic enzymes: an in vitro investigation with fifteen peptidases. *Chembiochem Eur. J. Chem. Biol.* **2**, 445–455 (2001).

140. Baldauf, C., Günther, R. & Hofmann, H.-J. Theoretical prediction of the basic helix types

in  $\alpha/\beta$ -hybrid peptides. *Pept. Sci.* **84**, 408–413 (2006).

141. Srinivasulu, G., Kumar, S. K., Sharma, G. V. M. & Kunwar, A. C. 11/9-Mixed helices in the  $\alpha/\beta$ -peptides derived from alternating  $\alpha$ - and  $\beta$ -amino acids with proteinogenic side chains. *J. Org. Chem.* **71**, 8395–8400 (2006).

142. De Pol, S., Zorn, C., Klein, C. D., Zerbe, O. & Reiser, O. Surprisingly stable helical conformations in  $\alpha/\beta$ -peptides by incorporation of cis- $\beta$ -Aminocyclopropane carboxylic acids. *Angew. Chem. Int. Ed.* **43**, 511–514 (2004).

143. Jagadeesh, B. *et al.* Formation of left-handed helices in hybrid peptide oligomers with cis  $\beta$ -sugar amino acid and L-Ala as building blocks. *Chem. Commun.* 371–373 (2007).

144. Schmitt, M. A., Choi, S. H., Guzei, I. A. & Gellman, S. H. Residue requirements for helical folding in short  $\alpha/\beta$ -peptides: Crystallographic characterization of the 11-helix in an optimized sequence. *J. Am. Chem. Soc.* **127**, 13130–13131 (2005).

145. Choi, S. H., Guzei, I. A. & Gellman, S. H. Crystallographic Characterization of the  $\alpha/\beta$ -Peptide 14/15-Helix. *J. Am. Chem. Soc.* **129**, 13780–13781 (2007).

146. Sadowsky, J. D. *et al.* ( $\alpha/\beta+\alpha$ )-peptide antagonists of BH3 domain/Bcl-x(L) recognition: toward general strategies for foldamer-based inhibition of protein-protein interactions. *J. Am. Chem. Soc.* **129**, 139–154 (2007).

147. Lee, E. F. *et al.* High-Resolution structural characterization of a helical  $\alpha/\beta$ -peptide foldamer bound to the anti-apoptotic protein Bcl-x<sub>L</sub>. *Angew. Chem. Int. Ed.* **48**, 4318–4322 (2009).

148. Peterson-Kaufman, K. J. *et al.* Residue-based preorganization of BH3-derived  $\alpha/\beta$ -peptides: modulating affinity, selectivity and proteolytic susceptibility in  $\alpha$ -helix mimics. *ACS Chem. Biol.* **10**, 1667–1675 (2015).

149. Lee, E. F. *et al.* Structural basis of Bcl-x<sub>L</sub> recognition by a BH3-mimetic  $\alpha/\beta$ -peptide generated by sequence-based design. *Chembiochem Eur. J. Chem. Biol.* **12**, 2025–2032 (2011).

150. Baldauf, C., Günther, R. & Hofmann, H.-J. Helix formation in  $\alpha/\gamma$ - and  $\beta,\gamma$ -hybrid peptides: theoretical insights into mimicry of  $\alpha$ - and  $\beta$ -peptides. *J. Org. Chem.* **71**, 1200–1208 (2006).

151. Balaram, P. Hybrid polypeptides: Gabapentin as a stereochemically constrained  $\gamma$ -amino acid residue. *Pept. Sci.* **94**, 733–741 (2010).

152. Chatterjee, S. *et al.* Multiple conformational states in crystals and in solution in  $\alpha/\gamma$ -hybrid peptides. Fragility of the C12 helix in short sequences. *J. Org. Chem.* **73**, 6595–6606 (2008).

153. Bandyopadhyay, A., Jadhav, S. V. & Gopi, H. N.  $\alpha/\gamma$ 4-Hybrid peptide helices: synthesis,

- crystal conformations and analogy with the  $\alpha$ -helix. *Chem. Commun.* **48**, 7170–7172 (2012).
154. Sharma, G. V. M. *et al.* 12/10- and 11/13-mixed helices in  $\alpha/\gamma$ - and  $\beta/\gamma$ -hybrid peptides containing C-linked carbo- $\gamma$ -amino acids with alternating  $\alpha$ - and  $\beta$ -amino acids. *J. Am. Chem. Soc.* **128**, 14657–14668 (2006).
155. Giuliano, M. W. *et al.* A  $\gamma$ -amino acid that favors 12/10-helical secondary structure in  $\alpha/\gamma$ -peptides. *J. Am. Chem. Soc.* **136**, 15046–15053 (2014).
156. Guo, L. *et al.* Helix formation in preorganized  $\beta/\gamma$ -peptide foldamers: hydrogen-bond analogy to the  $\alpha$ -helix without  $\alpha$ -amino acid residues. *J. Am. Chem. Soc.* **132**, 7868–7869 (2010).
157. Sawada, T. & Gellman, S. H. Structural mimicry of the  $\alpha$ -helix in aqueous solution with an isoatomic  $\alpha/\beta/\gamma$ -peptide backbone. *J. Am. Chem. Soc.* **133**, 7336–7339 (2011).
158. Hernvann, F., Rasore, G., Declerck, V. & Aitken, D. J. Stereoselective intermolecular [2 + 2]-photocycloaddition reactions of maleic anhydride: stereocontrolled and regiocontrolled access to 1,2,3-trifunctionalized cyclobutanes. *Org. Biomol. Chem.* **12**, 8212–8222 (2014).
159. Aitken, D. J., Gauzy, C. & Pereira, E. Studies on the stability of the cyclobutane  $\beta$ -aminoacid skeleton: a cautionary tale. *Tetrahedron Lett.* **45**, 2359–2361 (2004).
160. Cannon, J. G., Rege, A. B., Gruen, T. L. & Long, J. P. 1, 2-Disubstituted cyclopropane and cyclobutane derivatives related to acetylcholine. *J. Med. Chem.* **15**, 71–75 (1972).
161. Kennewell, P. D., Matharu, S. S., Taylor, J. B., Westwood, R. & Sammes, P. G. Synthesis of  $\gamma$ -aminobutyric acid analogues of restricted conformation. Part 2. The 2-(aminomethyl) cycloalkanecarboxylic acids. *J. Chem. Soc.* 2563–2570 (1982).
162. Martín-Vilà, M. *et al.* Enantioselective synthetic approaches to cyclopropane and cyclobutane  $\beta$ -amino acids: synthesis and structural study of a conformationally constrained  $\beta$ -dipeptide. *Tetrahedron Asymm.* **11**, 3569–3584 (2000).
163. Aitken, D. J., Gauzy, C. & Pereira, E. A short synthesis of the cis-cyclobutane  $\beta$ -aminoacid skeleton using a [2+2] cycloaddition strategy. *Tetrahedron Lett.* **43**, 6177–6179 (2002).
164. Fernandes, C., Pereira, E., Faure, S. & Aitken, D. J. Expedient preparation of all isomers of 2-aminocyclobutanecarboxylic acid in enantiomerically pure form. *J. Org. Chem.* **74**, 3217–3220 (2009).
165. Declerck, V. & Aitken, D. J. A refined synthesis of enantiomerically pure 2-aminocyclobutanecarboxylic acids. *Amino Acids* **41**, 587–595 (2011).
166. de Meijere, A., Limbach, M., Janssen, A., Lygin, A. & Korotkov, V. S. Versatile access to 2-aminocyclobutene-1-carboxylic acid derivatives and their incorporation into small peptides. *Eur. J. Org. Chem.* **2010**, 3665–3671 (2010).

167. Jaime-Figueroa, S., Zamilpa, A., Guzmán, A. & Morgans, D. J. N-3-Alkylation of Uracil and Derivatives Via N-1-Boc Protection. *Synth. Commun.* **31**, 3739–3746 (2001).
168. Altmayer-Henzien, A. *et al.* Solution state conformational preferences of dipeptides derived from *N*-aminoazetidinecarboxylic acid: an assessment of the hydrazino turn. *J. Org. Chem.* **78**, 6031–6039 (2013).
169. Rao, C. P., Nagaraj, R., Rao, C. N. R. & Balaram, P. Infrared studies on the conformation of synthetic alamethicin fragments and model peptides containing .alpha.-aminoisobutyric acid. *Biochem.* **19**, 425–431 (1980).
170. Grison, C. M., Robin, S. & Aitken, D. J. The discovery of 9/8-ribbons,  $\beta/\gamma$ -peptides with curved shapes governed by a combined configuration-conformation code. *Chem. Commun.* (2015).
171. Lühr, S., Holz, J., Zayas, O., Wendisch, V. & Börner, A. Synthesis of chiral  $\beta$ 2-amino acids by asymmetric hydrogenation. *Tetrahedron Asymmetry* **23**, 1301–1319 (2012).
172. Barnard, A. *et al.* Selective and potent proteomimetic inhibitors of intracellular Protein–Protein Interactions. *Angew. Chem. Int. Ed.* **54**, 2960–2965 (2015).
173. Azzarito, V. *et al.* Stereocontrolled protein surface recognition using chiral oligoamide proteomimetic foldamers. *Chem. Sci.* **6**, 2434–2443 (2015).
174. Uhrinova, S. *et al.* Structure of free mDM2 N-terminal domain reveals conformational adjustments that accompany p53-binding. *J. Mol. Biol.* **350**, 587–598 (2005).







## RESUME SUBSTANTIEL EN FRANÇAIS

Cette thèse est consacrée à la synthèse et à l'étude structurale de peptides- $\beta/\gamma$ , contenant en alternance des acides aminés- $\beta$  et - $\gamma$ , conçus pour mimer l'hélice- $\alpha$  (ou hélice-13), structure secondaire des protéines. Ainsi, nous avons élaboré une stratégie de design « bottom-up » pour des peptides- $\beta/\gamma$  devant se replier sous forme d'hélice-13.

Ces peptides comportent ainsi un acide aminé- $\beta$ , le (1*S*,2*S*)-*trans*-2-aminocyclobutanecarboxylique, qui joue un rôle clé de brique constitutive en apportant des contraintes conformationnelles. Cet acide aminé- $\beta$  de configuration *trans* a été astucieusement choisi car il présente un angle de torsion  $\theta$  de 90° idéal pour inciter un peptide- $\beta/\gamma$  à adopter une structuration sous forme d'hélice-13.

Dans un premier chapitre, la synthèse énantiomériquement pure du *trans*-ACBC est basée sur une étape clé de photocycloaddition [2+2] entre l'uracile convenablement protégé et l'éthylène, conduisant à la formation du cycle à quatre chaînons. L'optimisation de chaque étape de cette synthèse a permis d'accéder à des quantités suffisantes en produit final pour la synthèse peptidique. Il a donc été possible de synthétiser deux séries de trois di-, tetra- et hexapeptides- $\beta/\gamma$  incorporant en alternance le *trans*-ACBC et le GABA, qui est un acide aminé- $\gamma$  dépourvu de toute contrainte. La synthèse d'un premier dipeptide a été optimisée afin de déterminer le meilleur agent de couplage activant le *trans*-ACBC. La synthèse des tetrapeptide et hexapeptide possédant le GABA comme acide aminé C-terminal s'est avérée complexe en adoptant une stratégie de synthèse convergente basée sur un fragment dipeptidique terminant par le GABA. L'activation du GABA lors du couplage peptidique n'a pas ou peu conduit au peptide désiré. Ainsi la séquence peptidique a été prolongée par une stratégie de synthèse linéaire évitant l'activation problématique du GABA. La synthèse des di-, tetra- et hexapeptides possédant le *trans*-ACBC comme acide aminé C-terminal a été réalisée sans difficulté en suivant une stratégie de synthèse convergente. Un protocole alliant études expérimentales (RMN, IR, CD) et théoriques fines (MCMM, DFT) ont permis d'étudier de façon systématique les préférences conformationnelles des peptides- $\beta/\gamma$ . Ces analyses structurales ont révélé une structuration inédite sous forme de ruban-9/8, en solution. Il a été démontré par modélisation moléculaire que ces nouveaux foldamères adoptent une forme plus ou moins courbe, gouvernée par un code combinant configuration du *trans*-ACBC et conformation du GABA.

Dans un deuxième chapitre, des contraintes sur l'acide aminé- $\gamma$  ont ensuite été introduites par la synthèse de deux séries de tetra-, penta- et hexapeptides- $\beta/\gamma$  alternant le *trans*-ACBC et des acides aminés- $\gamma^4$ . Ces deux séries de trois peptides chacune ont été dédoublées par l'introduction de protections C-terminales sous forme d'ester benzylique et d'amide benzylique. Des études expérimentales et théoriques de ces peptides- $\beta/\gamma$  en solution, suivant le protocole développé dans le premier chapitre, ont révélé une préférence conformationnelle sous forme d'hélice-13. L'introduction d'un simple substituant en position

4 de l'acide aminé- $\gamma$  a permis d'induire un changement de préférences conformationnelles des peptides- $\beta/\gamma$  se repliant sous forme d'un ruban-9/8 au profit de l'hélice-13 ciblée. La stabilité de cette structure hélicoïdale augmente avec la longueur de la chaîne peptidique. En effet, la co-existence de boucles à 9, 8 et 13 chaînons est observée au sein des tetra- et pentapeptides alors qu'une majorité voire une exclusivité de boucles à 13 chaînons est observée au sein des hexapeptides. Ces hélices-13 sont en effet fortement stabilisées à partir de 5 liaisons hydrogènes inter-résidus.

Enfin dans un troisième chapitre, forst des résultats obtenus dans les deux chapitres précédents, des peptides- $\alpha/\beta/\gamma$  capables de mimer l'hélice- $\alpha$  du segment (19-26) de la protéine p53 ont été conçus et synthétisés. Leur hélicité prédite par modélisation moléculaire a été vérifiée expérimentalement en suivant le protocole développé dans le premier chapitre. Une fois leur résistance à la dégradation protéolytique démontrée, ces peptides- $\alpha/\beta/\gamma$  ont été testés comme inhibiteur de l'interaction p53/hDM2 à travers des expériences biophysiques basées sur de la fluorescence anisotropie. Un candidat a particulièrement été capable d'inhiber cette interaction en se liant au site naturel de fixation avec la protéine hDM2 marquée à l'azote 15, ce qui a pu être mis en évidence par des expériences RMN HSQC  $^{15}\text{N}$ - $^1\text{H}$ . Ce résultat illustre la réussite de notre stratégie de construction de mimes de l'hélice- $\alpha$ .



**Titre :** Peptides- $\beta/\gamma$  mixtes : nouveaux édifices foldamères pour mimer l'hélice- $\alpha$

**Mots clés :** acide aminé- $\beta$  cyclique; acide aminé- $\gamma$ ; peptides- $\beta/\gamma$ ; foldamères; mimes de l'hélice- $\alpha$ ; inhibiteurs d'interactions protéine-protéine.

Cette thèse est consacrée à la synthèse et à l'étude structurale de peptides- $\beta/\gamma$ , contenant en alternance des acides aminés- $\beta$  et - $\gamma$ , conçus pour mimer l'hélice- $\alpha$  (ou hélice-13), structure secondaire des protéines. Ainsi, nous avons élaboré une stratégie de design « bottom-up » pour des peptides- $\beta/\gamma$  devant se replier sous forme d'hélice-13. Ces peptides comportent ainsi un acide aminé- $\beta$ , le (1*S*,2*S*)-*trans*-2-aminocyclobutanecarboxylique, qui joue un rôle clé de brique constitutive en apportant des contraintes conformationnelles. Dans un premier temps, la synthèse énantiomériquement pure du *trans*-ACBC basée sur une étape clé de photocycloaddition [2+2] a été optimisée. Il a alors été possible de synthétiser des peptides- $\beta/\gamma$  incorporant en alternance le *trans*-ACBC et le GABA, qui est un acide aminé- $\gamma$  dépourvu de toute contrainte. Des études expérimentales et théoriques fines de ces peptides- $\beta/\gamma$  ont révélé une structuration inédite sous forme de ruban-9/8, en solution. Il a été démontré que ces nouveaux foldamères adoptent une forme plus ou moins courbe gouvernée par un code combinant configuration et conformation des acides aminés constitutifs de ces peptides. Dans un deuxième temps, des contraintes sur l'acide aminé- $\gamma$  ont ensuite été introduites par la préparation de peptides- $\beta/\gamma$  alternant le *trans*-ACBC et des acides aminés- $\gamma^4$ . Des études expérimentales et théoriques de ces peptides- $\beta/\gamma$  en solution ont révélé une préférence conformationnelle sous forme d'hélice-13. La stabilité de cette structure hélicoïdale augmente avec la longueur de la chaîne peptidique. Ces hélices-13 sont en effet fortement stabilisées à partir de 5 liaisons hydrogènes inter-résidus. Enfin, des peptides- $\alpha/\beta/\gamma$  capables de mimer l'hélice- $\alpha$  du segment (19-26) de la protéine p53 ont été conçus et synthétisés, afin de vérifier expérimentalement leur hélicité prédite par modélisation moléculaire. Une fois leur résistance à la dégradation protéolytique démontrée, ces peptides- $\alpha/\beta/\gamma$  ont été testés comme inhibiteur de l'interaction p53/hDM2. Un candidat a particulièrement été capable d'inhiber cette interaction en se liant au site naturel de fixation avec la protéine hDM2. Ce résultat illustre la réussite de notre stratégie de construction de mimes de l'hélice- $\alpha$ .

**Title :**  $\beta/\gamma$ -Peptide manifolds designed as  $\alpha$ -helix mimetics

**Keywords :** cyclic  $\beta$ -amino acid;  $\gamma$ -amino acid;  $\beta/\gamma$ -peptides; foldamers;  $\alpha$ -helix mimetics; protein-protein interaction inhibitors.

This thesis is devoted to the synthesis and the structural characterisation of  $\beta/\gamma$ -peptides, constructed from  $\beta$ - and  $\gamma$ -amino acids in alternation, designed to mimic the  $\alpha$ -helix secondary structure which is present in many native proteins. The  $\alpha$ -helix can be defined as a 13-helix and a bottom-up foldamer design strategy to target a 13-helical structure was examined, whereby  $\beta/\gamma$ -peptides were proposed in which (1*S*,2*S*)-*trans*-2-aminocyclobutanecarboxylic acid (*trans*-ACBC) was incorporated as a conformationally-restricted  $\beta$ -amino acid component. The scalable synthesis of enantiomerically pure *trans*-ACBC using a [2+2] photocycloaddition strategy was successfully optimized.  $\beta/\gamma$ -Peptides incorporating *trans*-ACBC and GABA, the latter being the  $\gamma$ -amino acid component devoid of any constraint, were then synthesised. Experimental and theoretical investigations of their solution-state folding behaviour revealed an unprecedented 9/8-ribbon foldamer structure that adopts curved shapes governed by a combined configuration-conformation code. Additional constraints on the  $\gamma$ -amino acid component were then considered and  $\beta/\gamma$ -peptides incorporating *trans*-ACBC and  $\gamma^4$ -amino acids were synthesised. Experimental and theoretical investigations of these  $\beta/\gamma$ -peptides in solution unveiled a preference for 13-helix folding behaviour, which increased commensurately with the peptide chain length; robust 13-helices were stabilised by a minimum of five intramolecular hydrogen bonds. In the last part of this thesis, molecular modelling was used to design helical  $\alpha/\beta/\gamma$ -peptides intended to reproduce as closely as possible the hot-spot residues of the known  $\alpha$ -helical segment (19-36) of the p53 protein. These peptides were synthesised and their predicted helical folding was verified experimentally along with their resistance to proteolytic enzymes. The  $\alpha/\beta/\gamma$ -peptides were tested as inhibitors of the p53/*h*DM2 interaction. One peptide was found to behave as potent inhibitor and to bind to the native peptide binding pocket of the *h*DM2 protein, providing a successful proof of concept of the  $\alpha$ -helix mimetic design strategy.

